3-2006

Forward-Looking Radar Clutter Suppression Using Frequency Diverse Arrays

Piotr Baizert

Forward-looking Radar Clutter Suppression using Frequency Diverse Arrays

THESIS

Piotr Baizert, Flight Lieutenant, RAAF

AFIT/GE/ENG/06-05

DEPARTMENT OF THE AIR FORCE
AIR UNIVERSITY

AIR FORCE INSTITUTE OF TECHNOLOGY

Wright-Patterson Air Force Base, Ohio

The views expressed in this thesis are those of the author and do not reflect the official policy or position of the United States Air Force, Department of Defense, the United States Government, Royal Australian Air Force, Australian Department of Defence, or Government of the Commonwealth of Australia.

AFIT/GE/ENG/06-05

Forward-looking Radar Clutter Suppression using Frequency Diverse Arrays

THESIS

Presented to the Faculty

Department of Electrical and Computer Engineering

Graduate School of Engineering and Management

Air Force Institute of Technology

Air University

Air Education and Training Command

In Partial Fulfillment of the Requirements for the

Degree of Master of Science in Electrical Engineering

Piotr Baizert, B.E. (Hons), M.Mgt.

Flight Lieutenant, RAAF

March 2006

AFIT/GE/ENG/06-05

Forward-looking Radar Clutter Suppression using Frequency Diverse Arrays

Piotr Baizert, B.E. (Hons), M.Mgt.
Flight Lieutenant, RAAF

Approved:

/signed/	20 Feb 2006
Maj. Todd B. Hale, PhD (Chairman)	date
/signed/	20 Feb 2006
Dr. Michael A. Temple (Member)	date
/signed/	20 Feb 2006
Lt Col. Stewart L. DeVilbiss (Member)	date

AFIT/GE/ENG/06-05

Abstract

Forward-Looking Airborne Radar (FLAR) Space-Time Adaptive Processing (STAP) has not achieved the same level of radar performance improvement as side-looking radar, because the ground clutter doppler-range dependence destroys the Independent and Identically Distributed (iid) assumption key to the STAP foundation.

This thesis examines the Frequency Diverse Array (FDA), where each channel transmits and receives at a different frequency. The resulting range-dependent FDA antenna pattern is proposed to improve FLAR STAP performance. The planar FDA radar data model is derived and analytically verified to be equivalent to the constant frequency data model when each element frequency is set to the same value.

The linear FDA at high platform altitude provides significant benefits by reducing the range ambiguous clutter contribution, improving target detection by 10 dB at the range ambiguous clutter notch. Additionally, the linear FDA achieved a consistent performance improvement of 1 to 2 dB at the lower platform altitude, independent of range ambiguous clutter and attributed to sample support data homogeneity.

The planar FDA showed up to a 20 dB detection improvement for a high altitude platform with an airborne target, where elevation adaptivity is unable to suppress range ambiguous clutter due to the co-altitude target. For three other engagement scenarios, the planar FDA performance did not show regularized sample support data benefits for targets at array boresight due to an increased clutter spectrum.

The simulation results show the FDA provides considerable benefit for low relative velocity targets, improving ground target detection for platforms such as Joint Surveillance and Target Attack Radar System (JSTARS) and Unmanned Aerial Vehicles (UAV). FDAs are not a radar panacea as the performance improvements are not realized across the range of potential target velocities.

Acknowledgements

If you tilt your head and squint hard enough, anything becomes as simple or complex as you'd like–regardless of whether it is or not.

Anonymous

Thank you to all the people associated with the Royal Australian Air Force and United States Air Force for making the opportunity to study at AFIT a reality, without your joint efforts none of this would be possible.

I extend my sincerest appreciation to Maj. Todd Hale for acting as my thesis advisor, providing great direction and support throughout both my thesis and study at AFIT. Thanks also to Dr. Michael Temple and Lt Col. Stewart DeVilbiss for agreeing to be part of my thesis committee and offering valuable comments.

To my new American friends, thank you for the company and helping me make the most of this experience. Last, but by no means least, thank you to my friends and family back in Australia, you helped keep the important things in focus.

Piotr Baizert

Table of Contents

Page

Page

List of Figures

List of Tables

List of Symbols

Symbol		Page
$\mathbf{R}$	Interference Covariance Matrix	8
$\boldsymbol{\chi}$	Space-Time Snapshot	8
$\mathbf{w}$	Weighting Vector	8
$\mathbf{v}$	Target Steering Vector	8
$\hat{\mathbf{R}}$	Estimated Interference Covariance Matrix	9
N	Number of Array Horizontal Channels	9
P	Number of Array Vertical Channels	9
M	Number of Pulses Integrated	9
η_a	JDL Azimuth Angular DOF	11
η_b	JDL Doppler DOF	11
η_e	JDL Elevation Angular DOF	11
γ	Clutter Strength in Constant Gamma Clutter Model	12
P_N	Thermal Noise Power	13
P_C	Ground Clutter Interference Power	13
P_{Sig}	Output Signal Power	13
ϕ	Azimuth Angle	13
θ	Elevation Angle	13
$\bar{\omega}$	Normalized Doppler	13
f_d	Target Doppler Frequency	13
f_r	Pulse Repetition Frequency	13
K	Required Sample Support Vectors	14
$\hat{\mathbf{R}}_K$	NHD Initial Interference Covariance Matrix Estimate	14
z_k	Non Homogeneity Detector Test Statistic	14
L	Available Sample Support Vectors	14
P_d	Probability of Detection	16

Symbol		Page
$\bar{\mathbf{\Omega}}$	Normalized Target Doppler Frequency Matrix	45
α_t	Complex Signal Amplitude	45
$\otimes$	Kronecker Product	46
$\odot$	Hadamard Product	46
VEC	Vector Operator: Reshape matrix into a column vector	46
$\mathbf{a}(\mathbf{\Psi}_{\boldsymbol{x}})$	Azimuth Steering Vector	46
$\mathbf{e}(\mathbf{\Psi}_{\boldsymbol{z}})$	Elevation Steering Vector	46
$\mathbf{b}(\bar{\mathbf{\Omega}})$	Temporal Steering Vector	46
$\mathbf{c}(\mathbf{F}, T_R)$	Target Range Dependent Steering Vector	47
$\mathbf{\Delta}\bar{\mathbf{\Omega}}$	Incremental Normalized Doppler Frequency Matrix	51
$\mathbf{\Delta\Psi}_{\boldsymbol{z}}$	Incremental Vertical Spatial Frequency Matrix	51
$\mathbf{\Delta\Psi}_{\boldsymbol{x}}$	Incremental Horizontal Spatial Frequency Matrix	54
Δf	Frequency Progression between Successive Channels	61
Δf_x	Frequency Progression between Horizontal Channels	61
Δf_z	Frequency Progression between Vertical Channels	61
β	Inter-channels crossed per Pulse Repetition Interval	72
R_{eff}	Effective Earth Radius	76
N_r	Number of Range Ambiguous Clutter Rings	86

List of Abbreviations

Abbreviation		Page
STAP	Space-Time Adaptive Processing	1
SLAR	Side-Looking Airborne Radar	1
ECM	Electronic Counter Measures	2
FDA	Frequency Diverse Array	2
AFRL	Air Force Research Laboratory	2
iid	Independent and Identically Distributed	2
FLAR	Forward-Looking Airborne Radar	3
JSTARS	Joint Surveillance and Target Attack Radar System	3
GMTI	Ground Moving Target Indication	3
UAV	Unmanned Aerial Vehicles	3
FL-FDA	Forward-Looking Frequency Diverse Array	5
AEWAC	Airborne Early Warning And Control	5
NHD	Non-Homogeneity Detector	5
DPCA	Displaced Phase Center Array	7
DOF	Degrees of Freedom	8
MF	Matched Filter	8
OAP	Optimal Adaptive Processor	8
SINR	Signal to Noise plus Interference Ratio	8
AMF	Adaptive Matched Filter	9
MCARM	Multiple-Channel Airborne Radar Measurements	9
CPI	Coherent Processing Interval	9
CSM	Cross Spectral Metric	10
FTS	Factored Time Space	10
DFT	Discrete Fourier Transform	11
MDV	Minimum Discernable Velocity	11

Abbreviation		Page
JDL	Joint Domain Localized	11
NA	Non-Adaptive	11
PRF	Pulse Repetition Frequency	13
GIP	Generalized Inner Product	14
FFT	Fast Fourier Transform	32
SAR	Synthetic Aperture Radar	32
LO	Local Oscillator	33
LPF	Low Pass Filter	33
PRI	Pulse Repetition Interval	41
TFACF	Time-Frequency Auto-Correlation Function	44
MUR	Maximum Unambiguous Range	60
BW	Bandwidth	60
MVE	Minimum Variance Estimator	67
IF	Improvement Factor	67

Forward-looking Radar Clutter Suppression using Frequency Diverse Arrays

I. Introduction

The past few decades have produced large increases in radar system performance, particularly in high clutter environments where clutter returns are many orders of magnitude larger than targets. One of the main reasons for the performance improvements is Space-Time Adaptive Processing (STAP), exploiting a number of assumptions closely met in Side-Looking Airborne Radar (SLAR) at and near array boresight.

1.1 Radar Arrays

An antenna array is defined as a combination of individual antennas, each of these individual antennas referred to as antenna channels, configured to interact and produce an overall radiation pattern. Whilst early antenna arrays utilized mechanical scanning, scanning is now commonly implemented electronically. The ability to electronically scan the array provides a benefit over mechanical scanned radars, as the switching of beam positions occurs at a faster rate and with greater flexibility.

A significant benefit of using arrays is the ability to perform multiple functions, often simultaneously. Additionally, having a large number of channels allows more graceful degradation of performance with individual channel failure, and often a higher peak and average total power transmitted, as the limits on each channel are reduced. The use of arrays is fundamental for this thesis, since multiple array channels, either physical or synthetic, are required to enable spatial processing and hence STAP.

One of the popular early methods to enable array steering was through frequency-scanning, where the beam is steered by changes in the transmit frequency. It is impor-

tant to note that whilst different frequencies were used, all array channels transmitted the same frequency. Unfortunately the use of frequency as a steering mechanism created bandwidth limitations [23] and also restricted the ability to use frequency diversity for other benefits.

Increases in digital technology combined with mass production of high-precision components have since led to an influx of phased array radar implementation, where the antenna beam is steered by phase delays at each channel. Advantages gained from the phased array radar include increased slew rates, better control and the ability to use frequency diversity for other purposes such as Electronic Counter Measures (ECM). Phased arrays are now the common baseline used when investigating STAP performance [15].

The concept of a Frequency Diverse Array (FDA) is radically different to both frequency-scanned and standard phased-arrays, with each channel transmitting and receiving a different frequency. The potentially unique frequencies at each channel produce an antenna pattern dependent on the target range since the number of wavelengths travelled varies across array channels.

Dr. M.C. Wicks, Senior Scientist for Sensor Signal Processing, Air Force Research Laboratory (AFRL) Rome NY, presented the FDA concept during his Keynote Address at the 2005 Waveform Diversity Workshop in Huntsville, Alabama. FDA work was recently authored by Antonik at the 2006 Waveform Diversity Conference [1] at the end of this thesis work.

1.2 Research Motivation

STAP is primarily used for SLAR because of a number of useful characteristics that exist. One of these characteristics is a constant doppler frequency along array boresight, producing data close to Independent and Identically Distributed (iid) over small ranges. The iid data assumption is typically applied to SLAR even when the beam is steered off array boresight for small angles as the deviation from iid is low.

For the Forward-Looking Airborne Radar (FLAR), the simple doppler sine-azimuth relationship no longer exists and there becomes a significant range-doppler dependence. This range-doppler dependence destroys the iid data assumption required for ideal STAP performance.

The use of FDA and its range-dependent antenna pattern is proposed to mitigate the doppler-range relationship, by reducing the amount of isodops the forward-looking beam intersects [14]. The FDA antenna pattern can be thought of as a type of doppler compensation, reducing the level of heterogeneous sample support data. The decrease in deviation from the ideal iid assumption, i.e. making sample support data more homogeneous, decreases the STAP degradation associated with interference covariance matrix estimation.

Additionally, the FDA is proposed as a method to provide range ambiguous clutter suppression for linear arrays. Suppression is achieved by the range-dependent FDA antenna pattern illuminating the range ambiguous clutter rings different than the target range clutter.

The reduction of range ambiguous clutter is especially useful for improving detection of ground targets, characterized by a low relative velocity. FDA performance benefits at the clutter notches are applicable for the Joint Surveillance and Target Attack Radar System (JSTARS) mission, allowing target detection in situations where previously it was not possible. Increasingly the Ground Moving Target Indication (GMTI) role is also being expanded to Unmanned Aerial Vehicles (UAV) and both platform types are used to guide simulation engagement parameters.

In order to explore the FDA concept, it is necessary to develop a method to implement and assess its performance. The foundation is based on deriving an appropriate radar data model based on STAP work completed by Jaffar [13], Ward [27] and extended by Hale [10].

1.3 Research Scope

This thesis focuses on exploration of FDA performance and its particular benefit in the improvement of FLAR STAP performance. Specific areas addressed in this thesis include:

- The development and analytic verification of the STAP radar data model as it applies for a generic planar FDA.
- An investigation into the impact of using a FDA, focusing on the effect the FDA antenna pattern has on clutter spectrum and clutter rank for both linear and planar arrays.
- Introduction of two approaches to assess channel frequency allocation selections, their impact on the antenna pattern and benefit to FLAR sample support data homogeneity.
- The comparison of FLAR STAP performance when using FDA compared to constant frequency arrays. The comparison is based on four distinct physically realistic engagement scenarios, combining high and low altitude platforms with airborne and ground targets, using both linear and planar arrays.

Due to the number of parameters affecting FDA performance, this thesis is not focused on optimization of a particular scenario using FDA. The focus is on developing a mathematical foundation and initial analysis of benefits provided by FDA use. *Therefore, the magnitude of improvements within this thesis may not be indicative of benefits achievable with different channel frequency selection.*

1.4 Organization

Chapter II provides a more detailed introduction of STAP and the problems encountered using STAP for forward-looking arrays. Additionally Chapter II overviews the performance metrics selected to accurately assess the performance benefits.

Chapter III develops the radar data model for the generic planar FDA. Based on the generic model, Chapter IV generates the simplifying cases of constant horizontal and vertical frequency arrays, leading to generic linear FDAs. Chapter IV additionally provides analytical verification for the linear and planar FDA radar data models by setting all channel frequencies to a single value and confirming the result is equivalent to the constant frequency radar data model.

Using the verified radar data model, Chapter V investigates the new array structure impact based on simple channel frequency allocations and resulting antenna patterns for both linear and planar arrays. The analysis includes the ground clutter spectrum within the azimuth-doppler space and the clutter rank, both important considerations in the ability to suppress clutter interference.

Armed with the radar data model and an overview of the problems of forward-looking STAP, Chapter VI implements the linear Forward-Looking FDA (FL-FDA). Results compare linear FDA performance to the constant frequency linear array using four physically realistic engagement scenarios that differ in platform operating altitude for both airborne and ground-based targets. The two platform altitudes correspond to potential mission parameters for JSTARS or Airborne Early Warning And Control (AEWAC) aircraft and UAV, two key radar platforms.

Chapter VII extends the FL-FDA results to a planar array, using the same performance metrics and engagement scenarios. Based on initial planar FDA results, partial planar frequency diversity, where array channels vary in frequency only across one array dimension, is also investigated.

A summary of results achieved and conclusions drawn from the simulations is presented in Chapter VIII, along with highlighted areas for further research. Following the conclusion, Appendix A introduces two approaches to *assess* channel frequency selection, firstly qualitatively comparing the antenna pattern to the forward-looking isodops and secondly through the Non-Homogeneity Detector (NHD) statistics. The

two approaches only assess the choice of a set of channel frequencies and are not techniques for determining frequency selection.

II. Current Forward-Looking STAP Overview

Space-Time Adaptive Processing (STAP) is a processing methodology allowing the detection of targets of much smaller magnitude than competing ground clutter. The basis of STAP is discriminating the target from competing ground clutter using azimuth, doppler and elevation. Therefore, all STAP techniques suffer degradation when the target approaches the mainbeam clutter in all three dimensions.

This chapter provides a brief overview of STAP, including its background and common classifications within the field. The next section introduces a range of different applicable performance metrics used to characterize Frequency Diverse Array (FDA) performance. After reviewing STAP and the performance metrics, the forward-looking array is examined with particular attention to the ground clutter doppler equation and the isodops generated. Isodop examination highlights the problems associated with STAP for forward-looking arrays. The final section briefly reviews two current approaches to forward-looking STAP.

2.1 STAP Background

The origin of STAP can be traced back to the 1970's with work by Brennan and Reed [2] and furthered by Klemm [16]. STAP was introduced as an alternative to cascaded processing where temporal (doppler filtering) and spatial (antenna beamforming) processing are performed separately in a cascade. The foundation of STAP is based on the relationship existing between the spatial and temporal domains; this relationship can be exploited to improve clutter rejection.

One of the most important STAP characteristics is adaptivity, thus differentiating it from Displaced Phase Center Array (DPCA) processing, where clutter rejection is achieved through compensation for platform motion. The compensation is in the form of a DPCA-condition, where the phase advance between two array positions is equal to the phase between two adjacent sensors. Whilst DPCA is designed for a set of specific parameters, STAP changes its clutter suppression properties based on the clutter environment.

There are many different ways to classify STAP techniques, however one important separation for comparison purposes is fully versus partially adaptive. The latter class can be further split into joint and factored processes. The classification scheme detailed is neither exclusive nor exhaustive, however it defines the approach taken in this thesis.

2.1.1 Fully Adaptive STAP. Fully adaptive STAP can be derived using several different methods [6]. A popular development uses the maximum likelihood or optimum detector. The term fully-adaptive provides an upper STAP performance limit and is based on processing using all available Degrees of Freedom (DOF), the product of number of channels and number of pulses individually phased. Each DOF is a point that can be weighted to modify the response from that particular channel or pulse. This STAP technique is generally referred to as the Matched Filter (MF) or the Optimal Adaptive Processor (OAP) and is based on the known interference covariance matrix $\mathbf{R}$. The covariance matrix is defined as the expected value of the outer product of the space-time snapshot $\boldsymbol{\chi}$ under the H_0 (no target) hypothesis

$$\mathbf{R} = \mathcal{E}\{\boldsymbol{\chi}\boldsymbol{\chi}^H\}. \tag{2.1}$$

The MF is optimal in terms of maximizing the Output Signal to Noise plus Interference Ratio (SINR) [3]. The MF weighting vector $\mathbf{w}$ is

$$\mathbf{w} = \mathbf{R}^{-1}\mathbf{v}, \tag{2.2}$$

where $\mathbf{v}$ is the target steering vector. The target steering vector encapsulates the phase progression from element to element and pulse to pulse corresponding to the target location.

This MF is not realistic for real-world performance since it assumes perfect clutter environment knowledge. In the real world, clutter statistics must be estimated from appropriate sample support data vectors, resulting in an estimated interference

covariance matrix $\hat{\mathbf{R}}$ [4]. Using the estimated clutter covariance matrix to generate the weighting vector, the fully adaptive technique is called the Adaptive Matched Filter (AMF) [4].

As mentioned above, clutter statistics need to be estimated and hence the number of sample support vectors used has a direct impact on STAP performance. In order to be within 3 dB of known covariance performance, the number of data support vectors required is twice the DOF, known as Reed's Rule [4].

Since the DOF available is based on radar parameters, specifically the number of channels and pulses individually phased, it is important to examine simulation parameters to evaluate whether fully adaptive STAP can theoretically be supported based on Reed's Rule. Using Multiple-Channel Airborne Radar Measurements (MCARM) [24] data as an example, the number of horizontal array channels N, the number of vertical array channels P, and the number of pulses integrated M, mean the DOF or total Coherent Processing Interval (CPI) gain is 2816 and required sample support is $2NMP = 5632$. Since only 630 range cells are available in MCARM data with the target at one range cell and assuming a guard cell on either side, only 627 available sample support vectors exist, showing the implementation limitation of fully adaptive STAP. Whilst there are 627 available sample support vectors, such a broad range swath would likely considerably degrade the approximate iid assumption.

2.1.2 Partially Adaptive STAP. As shown above for MCARM data, having sufficient sample support data for the AMF is often not physically realizable. However, the use of STAP techniques utilizing reduced DOF, i.e. partial adaptivity, can lead to significantly reduced support restrictions with only small performance degradation. Additionally, when using planar arrays, often more DOF are available than necessary to suppress the interference [9], increasing the benefit of partial STAP. As mentioned, two different types of partial STAP include joint and factored techniques, both types of techniques will be briefly examined.

By definition factored approaches are sub-optimal because clutter suppression is achieved through null placement at a particular azimuth, doppler *or* elevation. Alternatively, joint techniques can direct nulls in azimuth, doppler *and* elevation, enabling greater clutter cancellation within the three domains available for target discrimination.

It is important to note not all reduced DOF techniques have reduced sample support requirements. For example, the Cross Spectral Metric (CSM) requires $2(NMP-1)$ sample support approximately same as AMF despite being able to use reduced DOF because the CSM technique involves an eigenvalue decomposition when the signal space is of size $NMP-1$. Sample support requirement reduction is dependent on the signal space size rather than the actual DOF used in the technique, a minor but vital distinction.

2.1.2.1 Factored STAP. Factored techniques, as their name suggests, provide adaptivity in only one of the available dimensions, spatial or temporal. The basis of using factored STAP is the ability to fully factor the impact of spatial and temporal domains, an important distinction when the radar data model for the FDA is derived.

Factored Time Space (FTS) is an example of a factored STAP technique where the data is firstly non-adaptively doppler filtered and then adaptivity is constrained to the spatial domain. By doppler filtering the data of a linear array, the signal space is effectively reduced to size N at the expense of adaptivity over the doppler domain. Whilst FTS has performance benefits over cascaded processing because of spatial adaptivity within each doppler filter's return, the performance is considerably lower than the MF. This limited FTS performance is due to adaptivity in only one domain precluding the ability to fully exploit the azimuth-doppler relationship of ground clutter.

One technique to improve the performance of factored STAP is the use of amplitude tapers, also known as windowing. Windowing is used to reduce spectral leakage

effects caused by the finite Discrete Fourier Transform (DFT) extent [11]. The choice of window is a compromise between side-lobe level reduction, which improves spectral leakage, and main-lobe widening, which degrades performance near the clutter notch and hence increases the Minimum Discernable Velocity (MDV), the target velocity corresponding to the normalized doppler of the defined clutter notch.

2.1.2.2 Joint STAP. Conversely, joint techniques provide adaptivity over both domains but at a reduced DOF and signal space. In general, joint techniques outperform factored techniques for the same DOF. The strength of joint techniques is the ability to trade-off DOF in each domain, which is important as additional DOF in each domain typically has diminishing returns. The use of windows applied to joint STAP is not generally beneficial [25], since adaptivity in both domains results in the interference sources being nulled, and hence side-lobe reductions having negligible effect.

An example joint STAP technique is Joint Domain Localized (JDL) [26], which operates on the angular-doppler space and is adaptive in a Local Processing Region (LPR) over both temporal and spatial (albeit transformed) domains. The benefit of JDL is it allows trade-off between the DOF in both angular η_a and doppler η_b domains, where the total DOF is the product of the two, $\eta_a\eta_b$. For a planar array, there is an additional elevation angular DOF η_e.

2.1.3 Non-Adaptive Processing. Whilst the focus of this thesis is the performance of various STAP techniques, it is also important to consider Non-Adaptive (NA) processing. The NA weighting vector is based on the steering vector to the target location $\mathbf{v}$,

$$\mathbf{w} = \mathbf{v}, \tag{2.3}$$

in words 'undoing' the phase associated with the target location. NA is critical because it provides a performance baseline as to whether the additional computation required

for various STAP techniques is beneficial. It is noted the NA and MF weight vectors use the same symbol $\mathbf{w}$, but the contents of the weight vector depend on the STAP technique and are explicitly defined whenever the vector is used.

2.1.4 STAP Assumptions. Due to the popularity of STAP, there is a rich depth of current research. Whilst this research breadth has led to both large and small improvements in the field, it is also increases the importance to specify the assumptions used for particular results in order to ensure fair comparison.

Unless specifically stated, the results presented in this thesis:

- Include returns from range ambiguous clutter rings [9, 27],
- Assume Gaussian distributed clutter using a constant gamma model [23] with γ = -3 dB and
- Include no decorrelation effects such as Internal Clutter Motion, System Bandwidth and Range Walk [15].

2.2 Performance Metrics

Many different metrics can be used to characterize system performance. Since each metric provides slightly different information, it is beneficial to use multiple metrics and therefore vital to understand the implicit assumptions of each. The following metrics are introduced and used within this thesis: Output SINR, Antenna Pattern, Probability of Detection and Non-Homogeneity Detector (NHD).

2.2.1 Output SINR. Output SINR is one of the most common radar processing performance metrics and as the name suggests, is a ratio of output signal power to output interference power,

$$\text{Output SINR} = \frac{P_{\text{Sig}}}{P_N + P_C}. \tag{2.4}$$

Hence, Output SINR is a dimensionless quantity. One reason why Output SINR is so prevalent is because it has been shown maximizing Output SINR also maximizes Probability of Detection [2].

The total interference is a combination of thermal noise power P_N and ground clutter power P_C. However, if a barrage noise jammer is present, it is also included as an interference source. The total per-channel, per-pulse interference power can be found from any diagonal element within the interference covariance matrix $\mathbf{R}$.

The output signal power P_{Sig} can be calculated as the inner product between the space-time snapshot $\boldsymbol{\chi}$ and appropriate weighting vector $\mathbf{w}$,

$$P_{\text{Sig}} = |\mathbf{w}^H \boldsymbol{\chi}|^2. \tag{2.5}$$

The space-time snapshot encapsulates the return from a single point in space and time, in terms of its azimuth ϕ, elevation θ, and normalized doppler $\bar{\omega}$. Since the space-time snapshot contains per-element, per-pulse voltages, the power level requires squaring these voltages. The above definition is instantaneous signal power. Since the interference power is an average power, the average signal power must be calculated by taking the expected value across all snapshots,

$$\begin{aligned} P_{\text{Sig}} &= \mathcal{E}\{|\mathbf{w}^H \boldsymbol{\chi}|^2\} = \mathcal{E}\{\mathbf{w}^H \boldsymbol{\chi}\boldsymbol{\chi}^H \mathbf{w}\} \\ &= \mathbf{w}^H \mathcal{E}\{\boldsymbol{\chi}\boldsymbol{\chi}^H\}\mathbf{w} = \mathbf{w}^H \mathbf{R}\mathbf{w}. \end{aligned} \tag{2.6}$$

In order to allow target detection across Doppler bins, it does not make sense to change the transmit azimuth and elevation angle during a CPI. Since the transmit angle is not changed, Output SINR is plotted against the remaining variable, normalized doppler $\bar{\omega}$. Normalized doppler is the target doppler frequency f_d divided by the Pulse Repetition Frequency (PRF) f_r.

It is important to remember the Output SINR metric is defined for a known interference covariance matrix $\mathbf{R}$ and does not take into account losses associated with clutter covariance matrix estimation. Therefore, comparison between Output SINR and Probability of Detection must be analyzed with care since the latter incorporates the estimated covariance matrix $\hat{\mathbf{R}}$.

2.2.2 Antenna Pattern Performance Metric. The use of an antenna pattern is not a normal performance metric. However, for the FDA it provides beneficial insight into results of other metrics. The antenna pattern indicates the illumination of contributing clutter rings and is particularly important for the FDA where the antenna pattern is range dependent, as shown in Chapter III.

2.2.3 Non-Homogeneity Detector. As discussed previously in Section 1.2, the assumption of sample support data being Independent and Identically Distributed (iid) is not met for forward-looking arrays due to range-doppler dependence. Logical data selection methods can be a way to minimize the degradation caused by available non-iid sample support vectors. One such method is the Non-Homogeneity Detector [28].

NHD provides a structured way to improve the choice of sample support vectors and involves using K sample support vectors to form an initial interference covariance matrix estimate $\hat{\mathbf{R}}_K$. The next step of NHD is to use the Generalized Inner Product (GIP) to generate test statistics z_k,

$$z_k^K = \boldsymbol{\chi}_k^H \hat{\mathbf{R}}_K^{-1} \boldsymbol{\chi}_k, \qquad k : \{1 : L\} \tag{2.7}$$

for all L available sample support vectors $\boldsymbol{\chi}_k$ and determine the most homogenous K vectors, where $K < L$. The GIP results are then ordered, and the K most-homogenous vectors are selected by taking $\frac{K}{2}$ vectors on either side of the median test statistic, i.e. selecting vectors having minimum range amongst themselves. The K vectors selected are then used to generate an updated covariance matrix estimate $\hat{\mathbf{R}}$.

One fundamental NHD assumption is iid sample data with the exception of certain outliers or heterogeneities, such as multiple targets for a side-looking array. Under an iid assumption, NHD is most important for partial STAP, where fewer vectors are used to estimate the covariance matrix and the impact of a single heterogeneous sample vector is proportionally larger.

To re-emphasize, the underlying iid assumption for NHD is problematic when implemented for a forward-looking array due to the range-dependence of ground clutter. Therefore, for forward-looking arrays, NHD has the largest benefit for techniques with large DOF, due to the greater level of sample support required and hence greater heterogeneity across the sample data.

2.2.3.1 GIP as a Performance Measure. In addition to being a method to logically select sample support data and improve performance, NHD can also be used to assess data homogeneity. Different sample data can be compared by measuring the GIP range and variance across each set of sample vectors, disregarding the actual GIP magnitude. A reduced dynamic range in the GIP indicates more homogeneous sample support data, however a direct link to matrix estimation improvement has not been established.

2.2.3.2 Limitation of NHD for Forward-Looking Arrays. As mentioned above, NHD assumes underlying iid. Therefore, there is no step in the NHD procedure to ensure the sample support vectors chosen have statistics *matching the target range-cell*. A problem arises for close targets and forward-looking arrays when all possible range-cells are used for NHD and the NHD selects the furthest range cells as the most homogeneous because they have the least range-doppler dependence. However, the selected range-cells are *not representative of target location clutter statistics* and when the covariance matrix is used to generate the weighting vector, performance degrades. This thesis overcomes the NHD limitation by generating the initial covariance matrix estimate using multiple snapshots artificially generated from the known covariance matrix for the range-cell of interest.

2.2.4 Probability of Detection. Monte Carlo simulation is a common procedure to generate experimental data over multiple trials. For this particular application the goal is to determine the Probability of Detection P_d for a given set of target characteristics. The number of runs required for each target input SINR is determined by the Probability of False Alarm P_{fa}. P_{fa} defines the probability of an incorrect decision, i.e. a target is present when no target is there, equivalently the number of times the detection threshold is exceeded when no target is present for a given number of observations. The number of runs required is equal to $\frac{10}{P_{fa}}$ and is based on getting sufficient number of false alarms to be statistically significant [18].

Arguably, P_d curves are the most applicable performance measure since detection is a primary role of radar and the performance can be tested in the real world, albeit with experimental error. A potential P_d disadvantage is each detection curve is valid only for a particular target location and doppler, rather than a sweep of target dopplers. Therefore, the selection of target doppler is important and is linked to the radar role and also radar parameters. Output SINR can also be helpful in determining which doppler values should be utilized since Output SINR curves cover all normalized doppler values.

As explained before, a differentiation is that the Output SINR is based on known covariance matrix, whilst P_d uses actual sample support vectors to estimate the interference matrix, where the known and estimated interference matrices are considerably different for forward-looking arrays with close target ranges. Since P_d curves use estimated covariance matrices, the effect of changes of sample support data homogeneity can be evaluated using this metric.

2.3 Forward-Looking Arrays

A forward-looking array is orientated so the array boresight is aligned with the platform motion. The simulation of a forward-looking array is achieved through addition of a 90° crab angle ϕ_c, the angle between the aircraft motion and array boresight, to the azimuth of a side-looking array model.

2.3.1 Forward-Looking Doppler. The inclusion of azimuth crab angle flows through the entire radar data model and produces the requisite changes, as shown for the ground clutter doppler frequency,

$$\begin{aligned} f_d(\phi,\theta) &= \frac{v_a \cos(\theta)\sin(\phi+\phi_{\text{crab}})}{\lambda} \\ &= \frac{v_a \cos(\theta)\sin(\phi+90^\circ)}{\lambda} \\ &= \frac{v_a \cos(\theta)\cos(\phi_{\text{fwd}})}{\lambda}, \end{aligned} \tag{2.8}$$

where ϕ is the azimuth angle and θ the elevation angle. When evaluated at array boresight, $\phi_{\text{fwd}} = 0^\circ$, the clutter doppler frequency

$$\begin{aligned} f_d(0^\circ,\theta) &= \frac{v_a \cos(\theta)\cos(0^\circ)}{\lambda} \\ &= \frac{v_a \cos(\theta)}{\lambda} \end{aligned} \tag{2.9}$$

is no longer a constant value of 0 Hz as for the side-looking array and is instead a function of elevation angle θ and subsequently range. The expression is relatively stable for small θ corresponding to far ranges and becomes more dependent as range decreases and absolute value of θ increases.

2.3.2 Forward-Looking Array Isodops. The ground clutter doppler relationship to array azimuth is important to establish since this relationship is the reason for difficulties associated with using forward-looking STAP. Given the definition of clutter doppler by Eqn. (2.8), figures can be produced to show doppler behavior around the platform.

An isodop is defined as a curve where Doppler is a constant value [15], similar to contour bars in topographical maps and isobars in weather maps. The calculation of isodops is achieved by setting a constant doppler value, allowing azimuth to vary across all 360° around the aircraft and solving for the elevation angle θ.

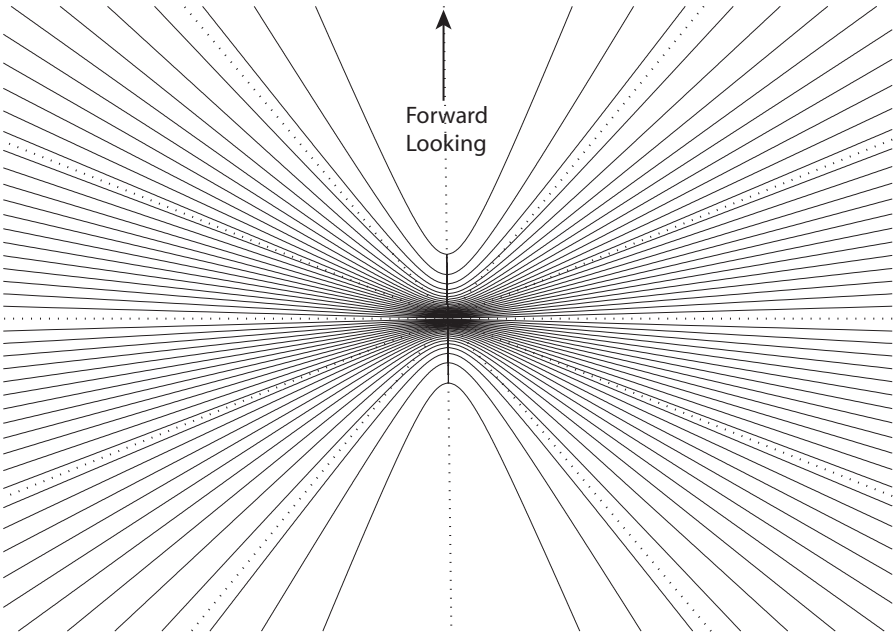

Figure 2.1: Isodops shown using spatial co-ordinates. Isodops show the greatest number of crossings by an antenna mainlobe occur for forward-looking arrays and fewest crossings occur for side-looking arrays.

The elevation angle corresponding to each azimuth for each isodop can then be used with knowledge of aircraft altitude to project the isodops onto the ground and create a 2D ground clutter map around the aircraft. The resulting pattern is typically displayed in texts [15] using a projection onto the ground with spatial co-ordinates, such as Figure 2.1.

Since the antenna pattern is typically displayed using a range and angle axis, Figure 2.1 must be modified to better show the data. To match previously published work [24], the platform altitude was defined as 3073 m to enable calculation of actual range, the converted range and angle results are shown in Figure 2.2.

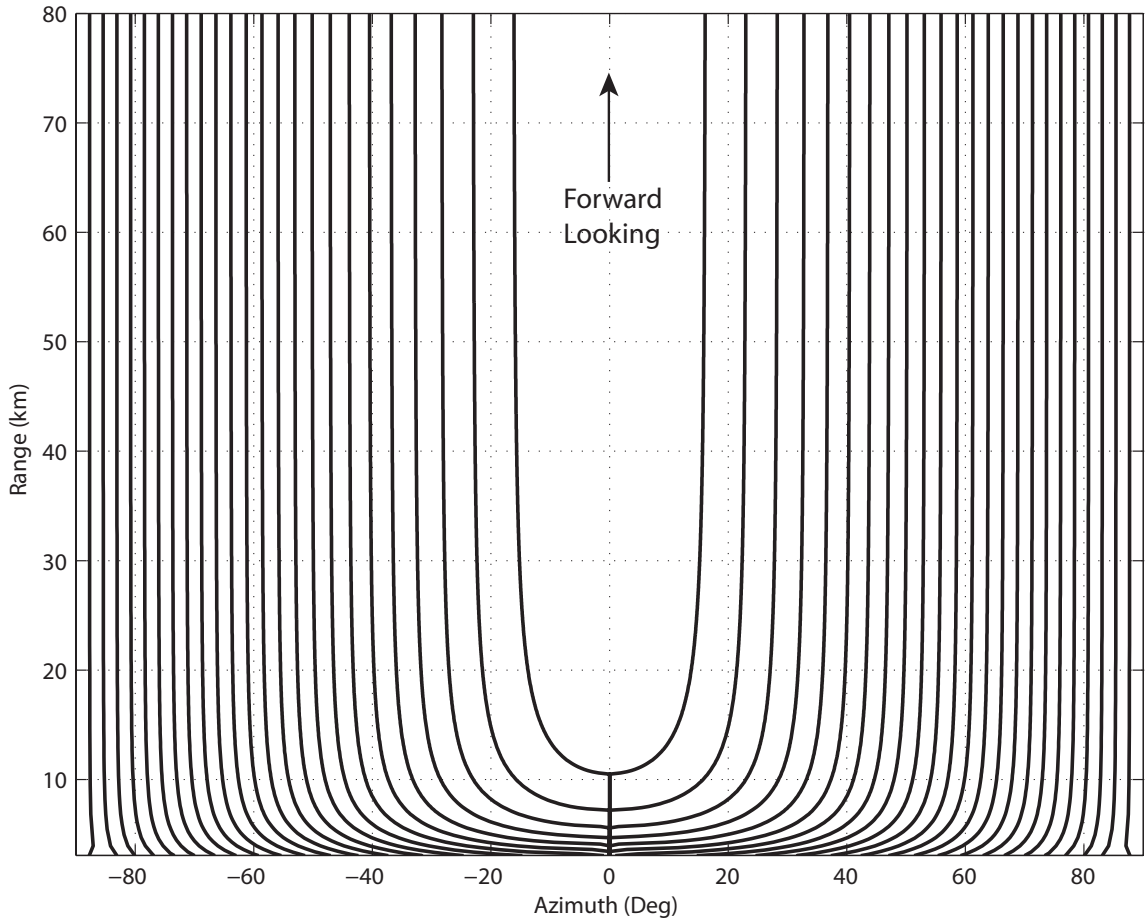

Figure 2.2: Forward-looking array isodops using a range-angular axis. The figure show the greatest number of crossings by an antenna mainlobe occur at array boresight and the result can be directly compared to the standard antenna pattern display method.

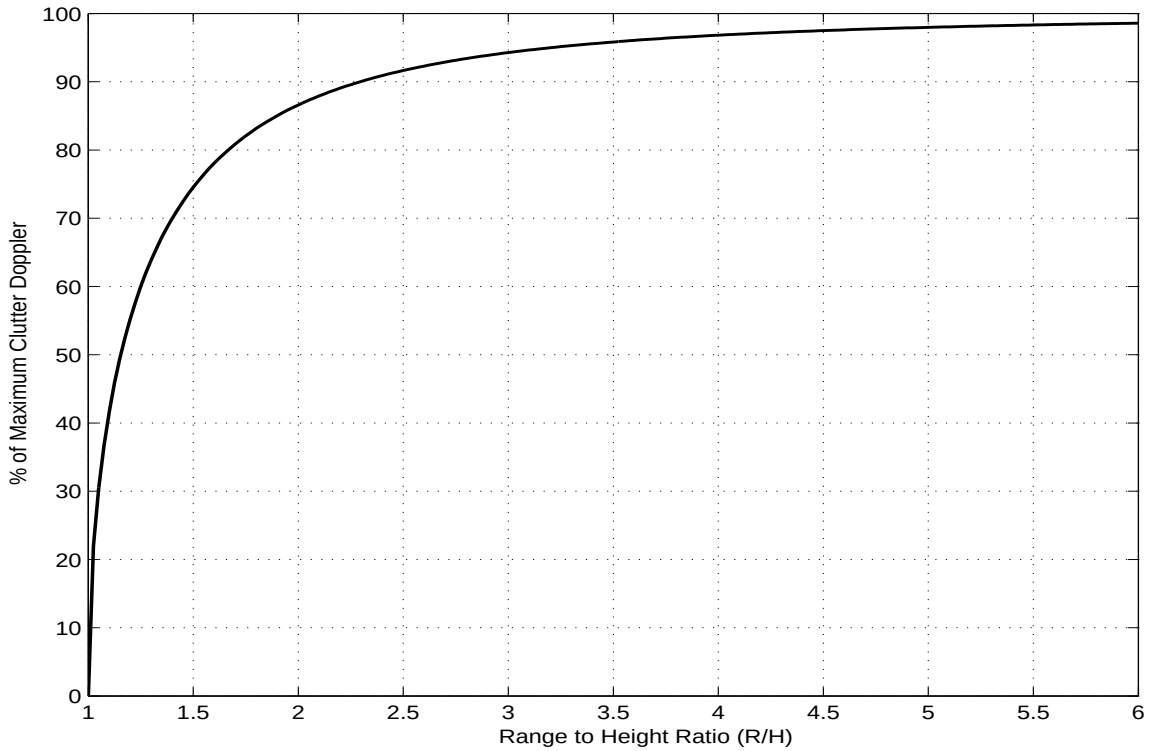

Figure 2.3: Ground clutter doppler over range for a forward-looking array showing the greatest variation occurs at small values for Range to Height, $\frac{R}{H}$ ratios. For ranges further than six times the platform altitude, there is minimal variation of ground clutter doppler.

Based on the isodop variation over range, it is seen the majority of range-doppler dependence exists at short range. The limited area of range-doppler dependence is obviously dependent on the doppler value selected, however it seems by 20 km the majority of variation is lost, yielding a Range R to Height H ratio of approximately six. The same conclusion can be found by examining the variation of clutter doppler over the range-to-height ratio $\frac{R}{H}$, as shown in Figure 2.3.

2.4 Problems of FLAR STAP

Whilst the range-doppler dependence is the major cause of performance degradation utilizing forward-looking radar, there are two distinct problems. Firstly, the clutter statistical characteristics vary significantly over range, much more so than for a side-looking array. Therefore, the filter weights must adapt to the new clutter notch

as range changes, which is well handled by using STAP. Secondly, the sample support data required to estimate covariance matrices is not iid, therefore leading to skewed clutter covariance matrix estimates and filter weights.

It is also useful to note jamming and decorrelation effects have a greater effect for a forward-looking array orientation [14]. In particular, the impact of range walk (platform movement between pulses during the collection interval) is more significant than for SLAR.

2.4.1 Range-Dependent Clutter Statistics. The range-dependence of clutter statistics has been addressed multiple times, as it is the major characteristic of forward-looking arrays. The dependence is defined in Eqn. 2.8 and also depicted in Figure 2.3, which shows the ground clutter doppler changing over range.

The impact of clutter doppler range-dependence results in a weighting vector that varies significantly across range cells for a constant transmit angle. For SLAR, since clutter doppler is range-independent along array boresight, if need be the same weighting vector can be used across a range swath since the clutter notch occurs at approximately the same $\bar{\omega}$.

The problem associated with using a constant weight vector for FLAR is shown using a series of Output SINR plots, firstly showing the difference between MF results for target ranges of 10.5 km and 66 km, in Figure 2.4. The ambiguous range doppler can be clearly shown to cause a separate clutter notch from the target range clutter notch for the 10.5 km target. At a target range of 66 km, the target range is large enough so the target range clutter doppler and ambiguous range clutter doppler are approximately the same.

It is clearly seen the clutter statistics are drastically different for the two target ranges, as denoted by the different doppler notch positions. Therefore, when there is a mismatch between the target range and the clutter statistics used to generate the weighing vector, performance degrades. Either a doppler value is nulled when there is no need as occurs using the 10.5 km weighting vector at 66 km, or alternatively, a

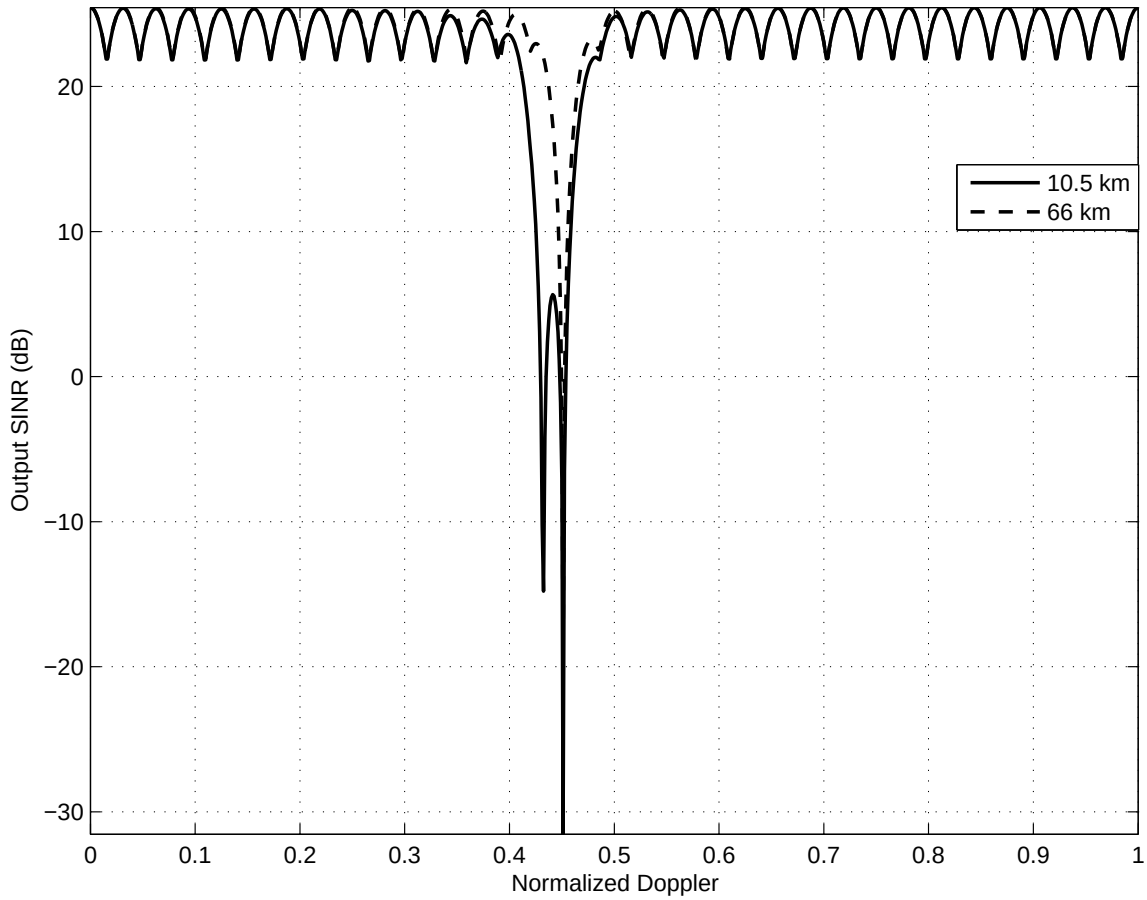

Figure 2.4: Forward-looking array MF at 10.5 km and 66 km, for a platform altitude of 3073 m. The plot shows the target range clutter doppler at 10.5 km is a different value than the range ambiguous clutter doppler, producing two distinct clutter doppler notches. At a target range of 66 km, the target range clutter doppler is the same value as the range ambiguous clutter doppler and only one clutter doppler notch occurs.

clutter doppler notch is not nulled, also leading to degradation, as would occur if the 66 km weighting vector is used for a target at 10.5 km.

As a side-note, for a target at 10.5 km there is a difference in the target range clutter notch depth and the ambiguous range clutter notch. The notch depth difference is partly an indication of contributing clutter magnitude and partly dependent on the match between the actual ground clutter doppler and the discrete normalized doppler the Output SINR is evaluated at. The closer the discrete doppler is to the actual ground clutter doppler, the deeper the notch will be, accurately representing the magnitude of competing ground clutter. Therefore, a greater sampling rate along the doppler axis can change the clutter notch relative depths as seen in Figure 2.5. The new doppler sampling rate is achieved by increasing the number of interpolations between the fixed number of doppler filters across the normalized doppler frequency axis.

2.4.1.1 Without Ambiguous Range Clutter. The inclusion of ambiguous range clutter has significant impact on weighting vector formulation since a target range of 10.5 km has a target range clutter doppler distinct from ambiguous range clutter doppler. The impact of ambiguous range clutter removal on Output SINR is seen in Figure 2.6, with the target at 10.5 km now only having one clutter notch.

However, there are again differences between the Output SINR curves and hence the FLAR weighting vectors vary significantly more than SLAR weighting vectors over the same range swath for close targets. The calculated weighting vector is based on a clutter doppler notch that varies across target range, especially for close-range targets, and hence clutter can not be effectively blocked when the weighting vector is based on clutter statistics different to the target range clutter statistics.

2.4.2 Skewed Covariance Matrix Estimation. A flow-on effect of doppler range-dependence occurs during interference covariance matrix estimation. Interference covariance matrix estimation involves using multiple sample support vectors, i.e.

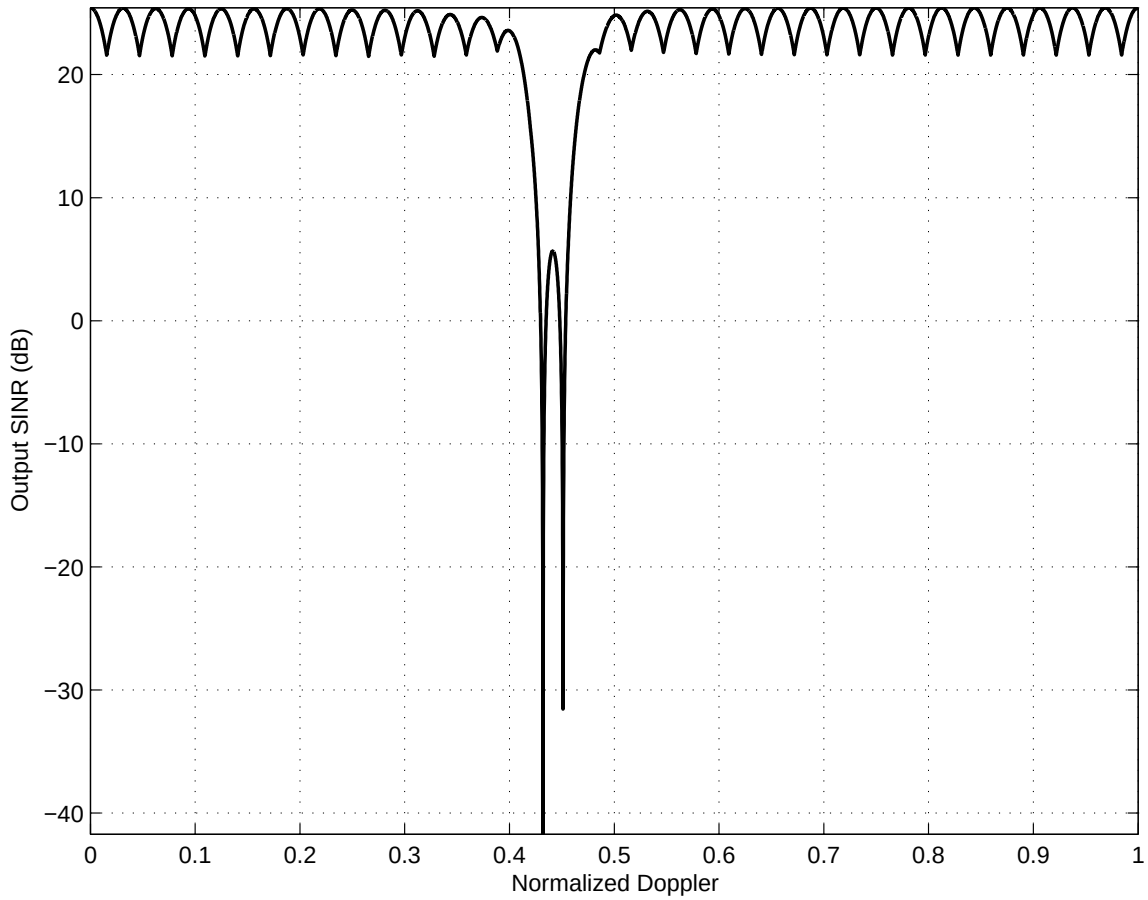

Figure 2.5: Forward-Looking Array MF at 10.5 km and platform altitude of 3073 m. The Output SINR is evaluated using a higher Doppler Axis sampling rate than the previous figure, showing the clutter doppler notch depth is affected by the error between the precise clutter doppler notch value and the closest point evaluated along the Doppler axis.

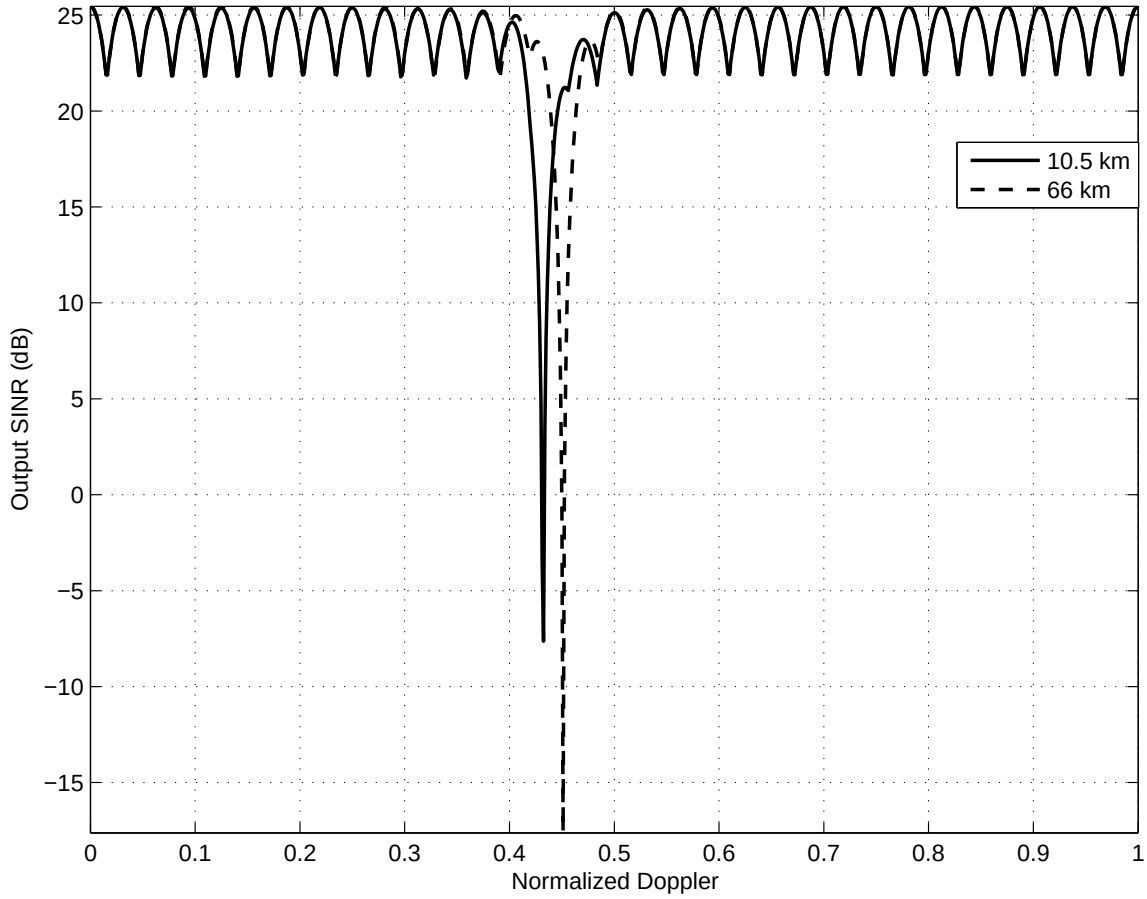

Figure 2.6: Forward-Looking Array MF without range ambiguous clutter at target ranges of 10.5 km and 66 km. The removal of range ambiguous clutter confirms the clutter doppler at 10.5 km is different to the clutter doppler at 66 km and also confirms the clutter doppler at 66 km is equal to the range ambiguous clutter doppler.

space-time snapshots, at range-cells other than the target range-cell. However, since each range-cell has a different clutter doppler value, the covariance matrix estimate has skewed clutter statistics not representative of target range-cell statistics and leads to degraded clutter suppression.

The problem is demonstrated through an Output SINR curve using weighting vectors based on estimated covariance matrices. The first estimated covariance matrix is generated *artificially* from multiple snapshot realizations of *target* range-cell statistics, whilst the second estimated covariance matrix is generated using a *swath* of range-cells *symmetric around* the target range-cell. For both estimated matrices, the AMF is used and the result averaged over 1000 realizations to reduce statistical error with the Output SINR shown in Figure 2.7.

When the sample support vectors used for matrix estimation are based on the range-cell of interest, the Output SINR is 3 dB down from the ideal condition of known covariance (MF) as predicted by Reed's Rule. The Output SINR value is lower than the preceding figures due to the lower CPI gain.

The impact of using actual sample support vectors is clearly seen and the reason for degradation at doppler below the target range doppler is caused by using the close range-cells for matrix estimation, where close is defined at ranges corresponding to $\frac{R}{H} \leq 6$. Each sample support vector closer than the target range has a clutter doppler less than the target doppler. The resulting covariance matrix estimate has clutter over the entire region $0.1 \leq \bar{\omega} \leq 0.45$, the upper limit being the ambiguous range clutter doppler.

At close target range, a STAP technique with greater sample support requirement increases covariance matrix estimation error because more sample support vectors with their own individual clutter doppler are used to generate $\hat{\mathbf{R}}$. The resulting covariance matrix estimate therefore has a larger swath of doppler values dominated by clutter.

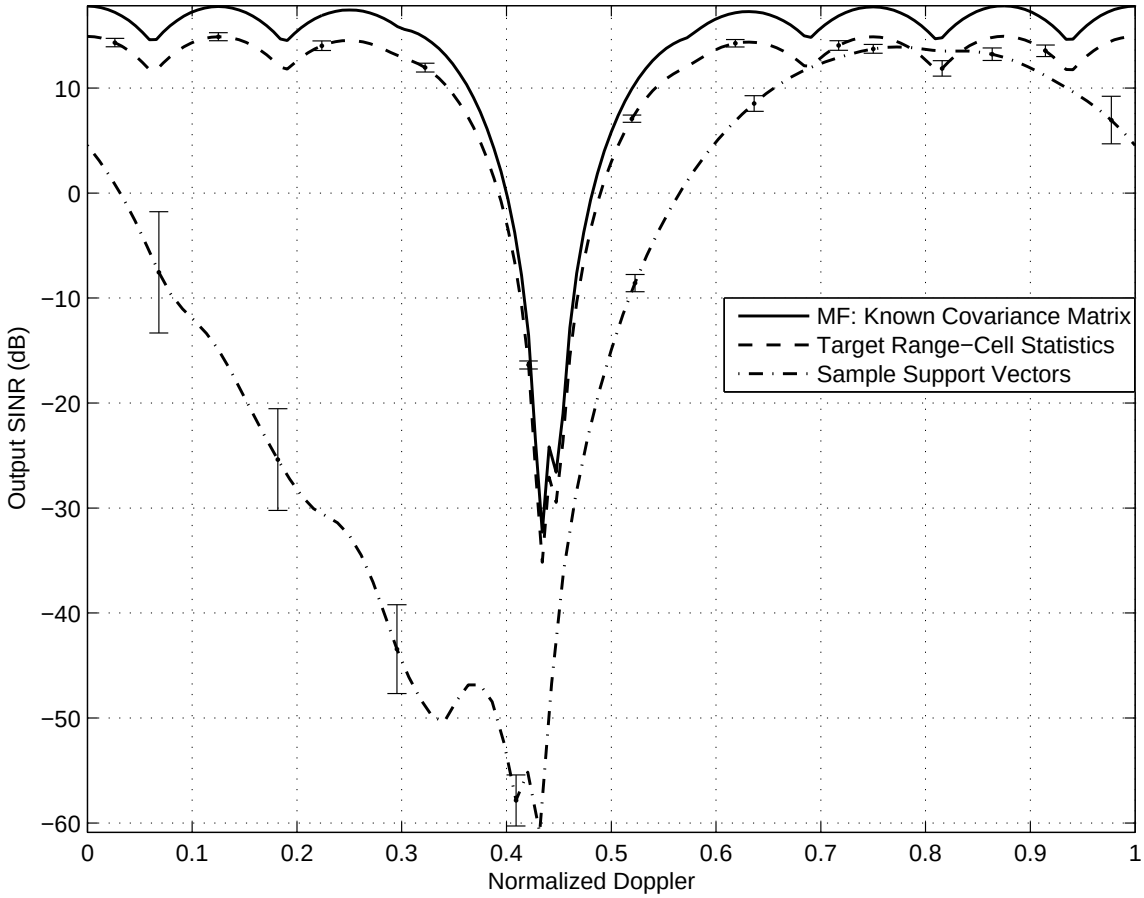

Figure 2.7: Output SINR AMF for target range of 10.5 km and platform altitude of 3073 m. Curves show difference in interference matrix estimation using 128 artificially iid sample support vectors to 128 actual symmetric sample support vectors, where both methods satisfy Reed's Rule. Output SINR curves are averaged over 1000 realizations to reduce statistical errors.

The above example is the worst case scenario for the particular target range since it included the closest range-cells available and the widest range of contributing clutter doppler values. One way to reduce degradation is to no longer select sample support vectors symmetrically, as is the standard case for SLAR, but to only select range-cells beyond the target range-cell, ensuring clutter doppler values are only going to be greater than the target range clutter doppler.

The asymmetric approach still skews the covariance matrix estimate as the sample support vectors have clutter occupying the doppler axis between the target range doppler and the ambiguous range doppler, which can be considerable at close ranges. The averaged Output SINR using asymmetric sample support vectors is seen in Figure 2.8, and whilst a marked improvement over Figure 2.7, degradation increases as the target range is reduced.

The difference between symmetric and asymmetric vectors can be observed by examining the clutter doppler values associated with the sample support vectors, shown in Figure 2.9. Both plots follow the same shape as the clutter doppler relationship across range-height ratios in Figure 2.3, however occupy a different curve region.

Using a symmetric sample support vector selection, it is observed the range of clutter doppler values used in the interference covariance matrix estimation is much larger than for asymmetric support vector selection. The plot clearly shows why there is additional degradation at low $\bar{\omega}$ values when symmetric sample support is used.

2.5 Current Forward-Looking STAP Techniques

Existing forward-looking STAP research can be split into two distinct areas: exploitation of engagement scenarios where a near-linear relationship is found to be a sufficient approximation [21] or use of doppler compensation [17].

The FDA can be considered as a type of doppler compensation. Rather than compensating for a single theoretical value, the antenna pattern is generated to accen-

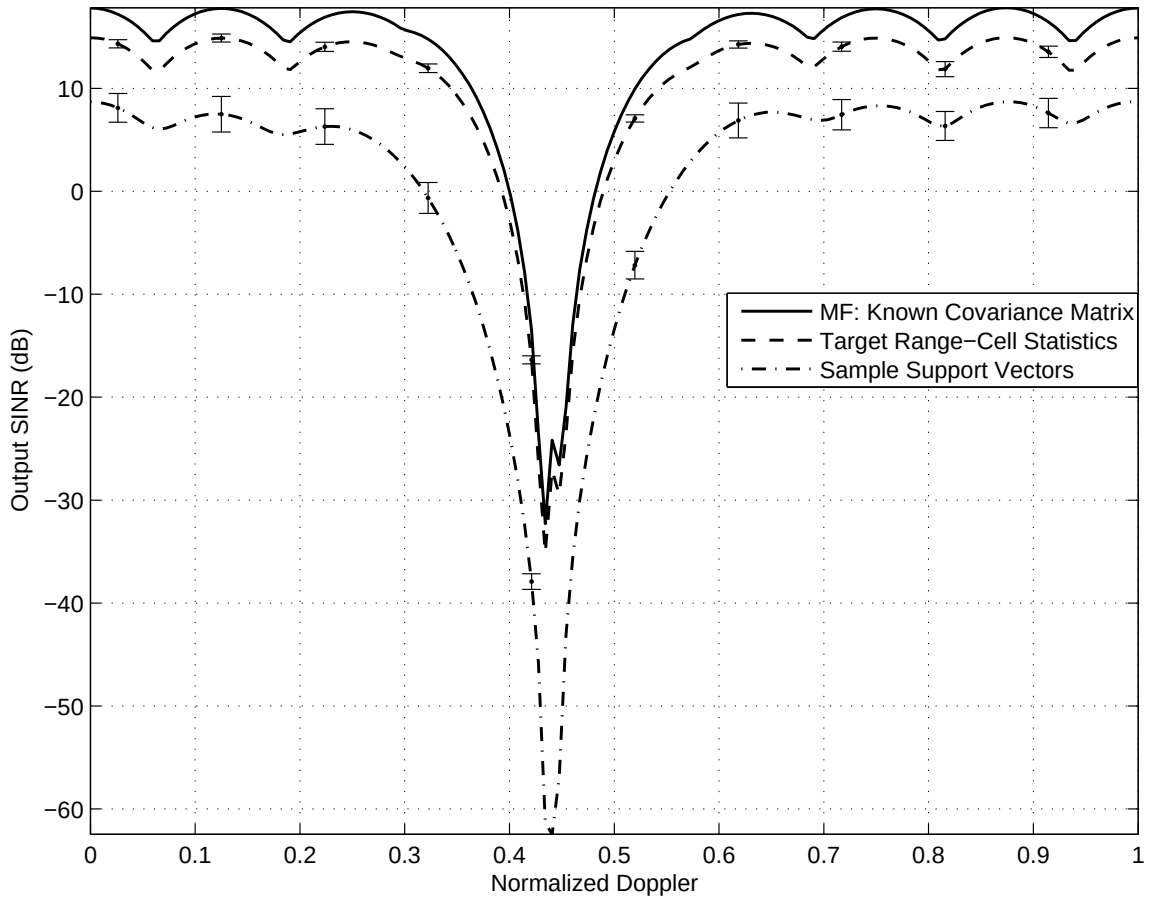

Figure 2.8: Output SINR AMF for target range of 10.5 km and platform altitude of 3073 m. Curves show difference in interference matrix estimation using 128 artificially iid sample support vectors to 128 actual asymmetric sample support vectors all chosen beyond the target range-cell, where both methods satisfy Reed's Rule. Output SINR curves are averaged over 1000 realizations to reduce statistical errors.

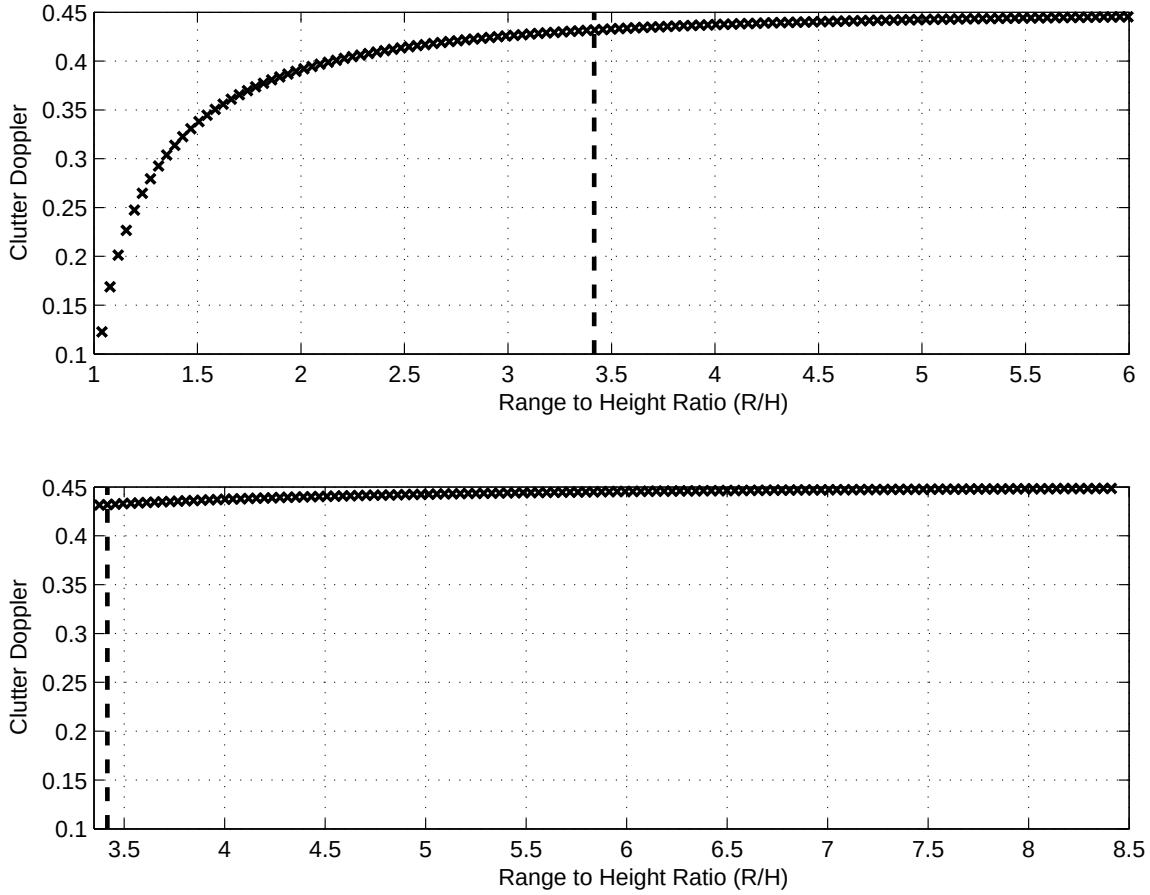

Figure 2.9: Clutter doppler associated with sample support vectors used in two previous figures. Comparison of symmetric sample support vectors (top) and asymmetric sample support vectors (bottom) shows greater variation of clutter doppler for symmetric sample support. Dashed lines indicate the target range-cell.

tuate the forward-looking isodops examined above. Additionally, the FDA approach is based on the inclusion of range ambiguous clutter, differentiating it from the current compensation approach.

2.5.1 Approximate Azimuth-Doppler Relationship. The fundamental problem with FLAR STAP is the lack of a linear inter-dependence between clutter doppler and azimuth angle. However, there is an approximate linear dependence between mainlobe clutter doppler and spatial frequency in many practical forward-looking applications [21].

The clutter surface for a forward-looking array without range ambiguous clutter is an ellipsoidal bowl [12, 20, 21], where the mainlobe clutter is a small clutter bowl section surface. When the target is distant, the mainlobe clutter is near the clutter bowl brim and scenario geometry analysis estimation enables derivation of a localized DPCA condition. The localized DPCA condition can be used as the basis of a linear doppler-angle relationship and improve low velocity target detection. However, the mainlobe clutter location moves down the bowl when the target is at close range, requiring the use of elevation DOF and resulting in a more complex relationship required to suppress the competing clutter [20].

It is noted the approach taken is concerned with mainlobe clutter and *ignores the significant effect of ambiguous range clutter.* When the target is at close range, the ambiguous clutter range rings generate additional clutter doppler values, leading to a more complex clutter surface. Therefore, the approximate relationship exploitation significantly degrades.

2.5.2 Doppler Compensation. A drastically different approach to the FLAR STAP problem is the use of doppler compensation, which attempts to regularize the data towards iid rather than finding areas where an approximate linear relationship can be exploited. Platform location and relative motion knowledge enables the calculation of theoretical clutter doppler at each range cell. Unfortunately, the limitations

of necessary measurement equipment leads to errors in the doppler estimation in particular, updating doppler estimates due to changes in aircraft flight parameters. Therefore, Fourier analysis, or more specifically the Fast Fourier Transform (FFT) is used [17]. The FFT determines the largest frequency response at each range cell, which should be the theoretical clutter doppler.

A transformation matrix operates on the original data to generate data used for STAP. The transformation matrix is block diagonal, where each channel compensates for the doppler difference between the current range cell and the range cell under test. The transformed data should therefore have only one clutter doppler value, reducing the clutter notch width to the iid sample support data notch width.

Whilst significant doppler notch width shrinkage can be experienced using doppler compensation, particularly for high resolution applications such as Synthetic Aperture Radar (SAR) [17], there is a significant limitation. As for the approximate linear relationship approach [21], the *impact of ambiguous range clutter is ignored*. Since ambiguous range clutter produces an additional clutter notch at close range, the existing FFT procedure can't be used to compensate the data.

2.6 Summary

Chapter II provided an overview of STAP with a focus on FLAR. The chapter started by providing a generic introduction to STAP in Section 2.1, including highlighting the differences between full and partial adaptivity. The metrics used to compare FDA and constant frequency array performance are introduced in Section 2.2. The remainder of the chapter focused on forward-looking array orientation with Section 2.3 showing the differences required to the side-looking data model and examining forward-looking isodops. Section 2.4 introduced the two major problems associated with FLAR STAP, whilst Section 2.5 discussed two existing approaches to minimize the aforementioned problems. With the understanding of the FLAR problem, the framework and advantages of the FDA are presented in the following chapters.

III. Frequency Diverse Array Radar Data Model

In order to assess Space-Time Adaptive Processing (STAP) techniques and compare their performance, radar test data must be available. Whilst measured radar data exists for standard constant frequency phased arrays, there are potential problems including: radar parameters not matching preferred values, collection errors and type of data environment required. To overcome these limitations, a radar data model is required to easily and quickly generate representative data. The benefit of generated radar data is the simulation parameters can be changed and enable more efficient investigation.

The situation is even more important for investigation of Frequency Diverse Array (FDA) radars since no such radar is fielded and no measured data is available. This chapter derives the radar data model for a planar FDA with generic channel frequency allocation. However, before deriving the radar data model it is useful to derive the FDA antenna pattern. The antenna pattern is the most critical difference from standard arrays and provides insight into FDA applications and performance benefits.

3.1 Frequency Diverse Array Overview

As defined previously, a FDA is an array where each channel can transmit and receive a potentially unique frequency. To simplify the analysis, an assumption is made that directly after each antenna channel there is an appropriate frequency Local Oscillator (LO), which reduces the signal down to baseband. The LO is followed by a Low Pass Filter (LPF), where it is assumed the LPF is sufficiently narrowband that *only the appropriate channel frequency is passed.* In other words, no cross-channel bleedthrough is simulated in this thesis, a critical component for the following data model derivation. The system architecture is demonstrated in Figure 3.1 for a three channel linear array.

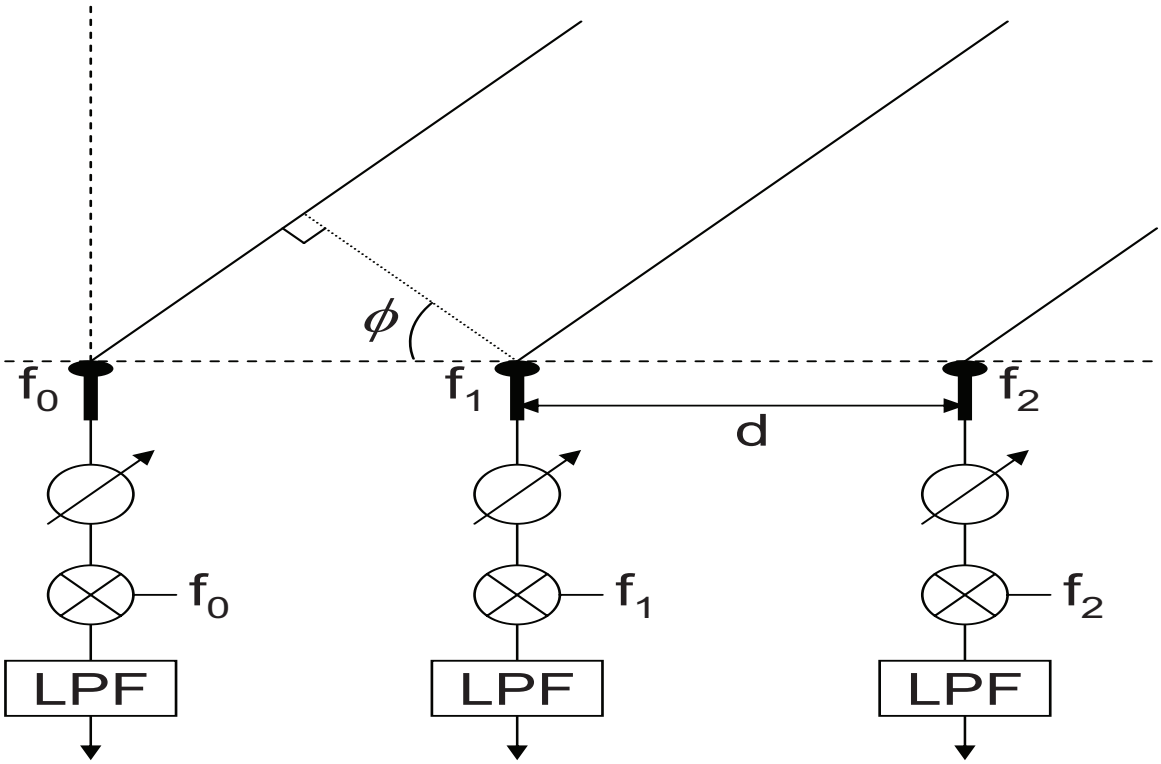

Figure 3.1: FDA system architecture showing an equally spaced array, each channel down-converted at the appropriate channel frequency followed by a Low Pass Filter (LPF).

3.2 Frequency Diverse Array Antenna Pattern Derivation

The FDA antenna pattern derivation follows the antenna pattern analysis procedure used for constant frequency array radars, in terms of breaking up the distance travelled from the target to each channel into a wavefront striking the reference channel and an incremental path length difference between the reference and all other array channels.

For a FDA, the analysis must retain the total path length from the radar to the target and back, a total distance of $2R$. Because each channel transmits a different frequency the same distance travelled contains a different number of wavelengths and hence phase progression for each channel, as shown in Figure 3.2.

The geometric basis for the antenna array pattern $W(\phi, \theta, R)$ derivation is depicted for a linear array in Figure 3.3. The figure is restricted to a horizontal linear array with the incoming signal only at a given azimuth ϕ to simplify the figure generation whilst the mathematical derivation considers a planar array and the incoming signal at an elevation θ.

The array channels are assumed equally spaced horizontally with a distance d_x and vertically with distance d_z. Assuming a radar array with N horizontal channels and P vertical channels, all channel frequencies are contained in a matrix $\mathbf{F}$, of size $N \times P$. The np^{th} channel has a frequency $\mathbf{F}[n, p] = f_{np}$ the matrix element of row n and column p. The reference channel, defined as the channel first struck by an incoming wave of positive azimuth and elevation angle, has a reference frequency $\mathbf{F}[0, 0] = f_0$.

Using basic trigonometry, the incremental phase progression $\Delta\Phi$ between the reference and np^{th} channel due to an azimuth angle ϕ and elevation angle θ is given by

$$\Delta\Phi_{np} = \frac{2\pi}{c} \left(\mathbf{F}[n, p] - f_0\right) \left(2nd_x \sin\phi \cos\theta - 2pd_z \sin\theta - 2R\right). \tag{3.1}$$

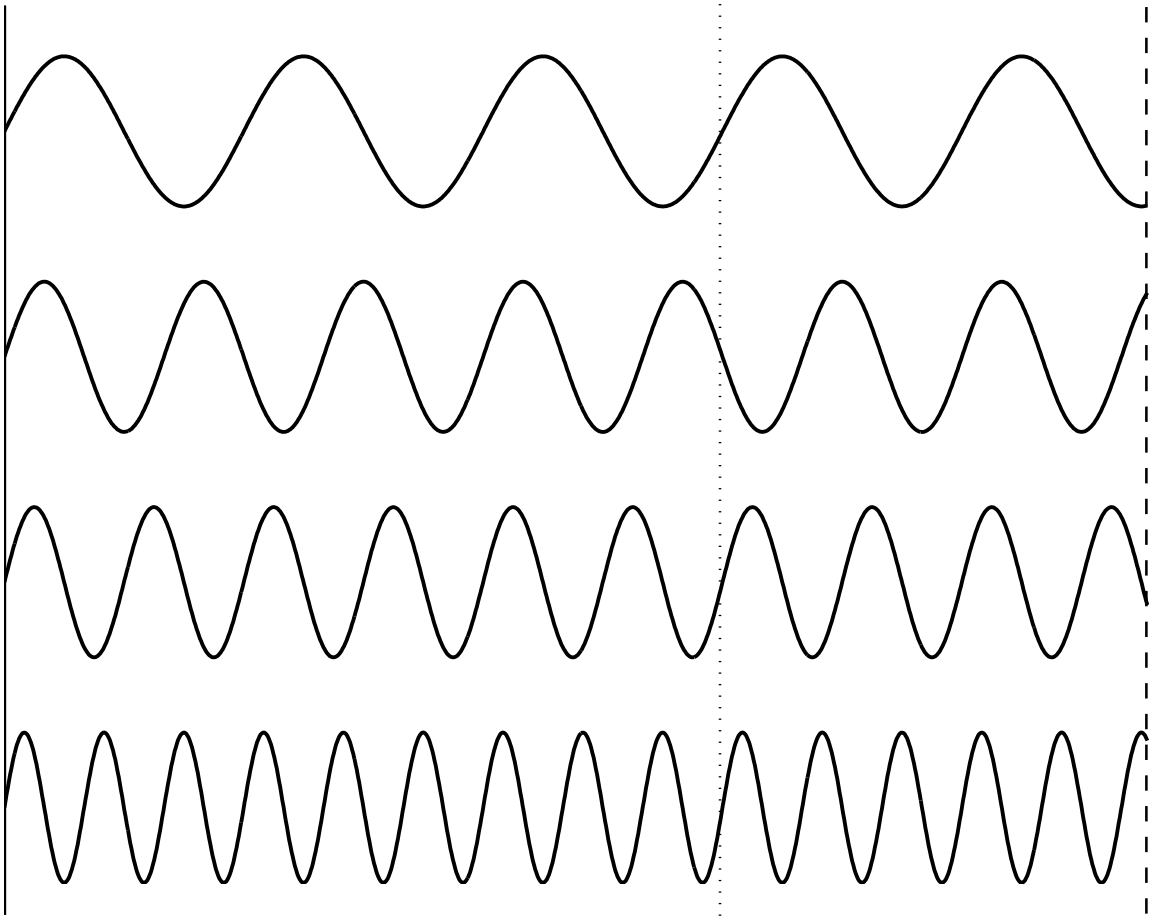

Figure 3.2: Different array channel frequencies result in different wavelength progression over the same distance travelled. The changing interference produces a range-dependent FDA antenna pattern.

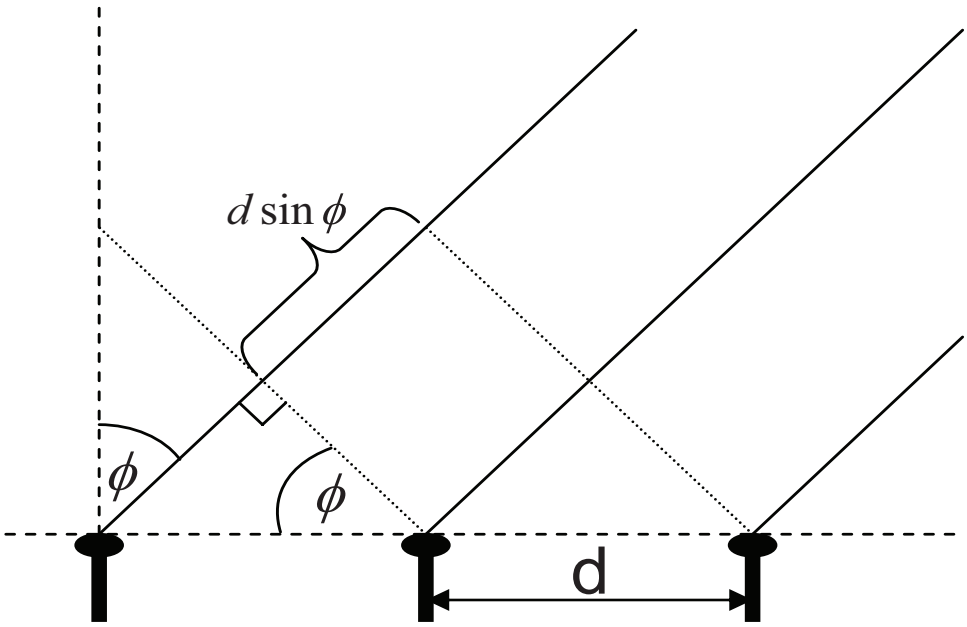

Figure 3.3: Basis for FDA antenna pattern derivation by definition of incremental path length differences with respect to the reference channel.

The antenna pattern expression can be simplified by defining matrices for the horizontal spatial frequency,

$$\boldsymbol{\Psi_x} = \frac{\mathbf{F}}{c}\left(d_x \cos\theta \sin\phi\right), \tag{3.2}$$

and the vertical spatial frequency,

$$\boldsymbol{\Psi_z} = \frac{\mathbf{F}}{c}\left(d_z \sin\theta\right). \tag{3.3}$$

For an array steered to $\theta = 0°$, $\phi = 0°$ and a range $R = 0$, the antenna pattern, $W(\theta, \phi, R)$ is defined as the summation of appropriate phase progression across all array channels. Since each channel frequency is potentially unique there is no way to factor out the horizontal and vertical channel dependency, so there is no mathematical identity that can be used to simplify the expression as for the constant frequency array. The antenna pattern is defined using the previously defined horizontal spatial frequency matrix $\boldsymbol{\Psi_x}$ and vertical spatial frequency matrix $\boldsymbol{\Psi_z}$,

$$\begin{aligned} W(\theta,\phi,R) &= \sum_{p=0}^{P-1}\sum_{n=0}^{N-1} e^{j\Delta\Phi_{np}} \\ &= \sum_{p=0}^{P-1}\sum_{n=0}^{N-1} e^{j2\pi n(d_x\cos\theta\sin\phi)\frac{\mathbf{F}[n,p]}{c}} e^{j2\pi p(d_z\sin\theta)\frac{\mathbf{F}[n,p]}{c}} e^{-j2\pi\frac{\mathbf{F}[n,p]}{c}R} \\ &= \sum_{p=0}^{P-1}\sum_{n=0}^{N-1} e^{j2\pi(n\boldsymbol{\Psi_x}[n,p]+p\boldsymbol{\Psi_z}[n,p])} e^{-j2\pi\frac{\mathbf{F}[n,p]}{c}R}. \end{aligned} \tag{3.4}$$

When the mainlobe is steered to an angle away from array boresight ϕ_0, θ_0 and to a target range of R_0, the array pattern takes on the more generic form,

$$\begin{aligned} W(\theta,\phi,R) = \sum_{p=0}^{P-1}\sum_{n=0}^{N-1} & e^{j2\pi n d_x\frac{\mathbf{F}[n,p]}{c}(\cos\theta\sin\phi-\cos\theta_0\sin\phi_0)} e^{j2\pi p d_z\frac{\mathbf{F}[n,p]}{c}(\sin\theta-\sin\theta_0)} \ \ldots \\ & e^{j2\pi\frac{\mathbf{F}[n,p]}{c}(R-R_0)}. \end{aligned} \tag{3.5}$$

3.2.1 Antenna Pattern Comparison at Target Range. It is interesting to compare the FDA antenna pattern to the range-independent constant frequency planar array pattern,

$$W_{\text{Const. Freq}}(\theta,\phi) = \sum_{p=0}^{P-1}\sum_{n=0}^{N-1} e^{j2\pi\frac{nd_x}{\lambda}(\cos\theta\sin\phi-\cos\theta_0\sin\phi_0)} e^{j2\pi\frac{pd_z}{\lambda}(\sin\theta-\sin\theta_0)}. \quad (3.6)$$

Evaluating the FDA antenna pattern at the target range $R = R_0$, the previous antenna pattern expression in Eqn. (3.5) can be simplified to

$$\begin{aligned} W(\theta,\phi,R_0) &= \sum_{p=0}^{P-1}\sum_{n=0}^{N-1} e^{j2\pi nd_x\frac{\mathbf{F}[n,p]}{c}(\cos\theta\sin\phi-\cos\theta_0\sin\phi_0)} e^{j2\pi pd_z\frac{\mathbf{F}[n,p]}{c}(\sin\theta-\sin\theta_0)} \quad (3.7)\\ &= \sum_{p=0}^{P-1}\sum_{n=0}^{N-1} e^{j2\pi n\boldsymbol{\Psi_x}[n,p]} e^{j2\pi p\boldsymbol{\Psi_z}[n,p]}. \end{aligned}$$

Except for the channel frequency dependency implicit in wavelength, the expressions for the constant frequency and FDA are now identical. Furthermore, the expected frequency diversity magnitude is known to be small compared to the reference frequency, since the use of phase-shifters is based on a narrowband radar assumption. Therefore, the additional phase attributed to each exponential due to unique channel frequencies is negligible. Hence, the FDA and constant frequency antenna patterns are effectively identical at the target range.

3.3 Generic Planar FDA Radar Data Model

A generic planar FDA enables many different frequency allocation methodologies and provides the greatest flexibility. Chapter IV considers frequency allocation limiting cases of constant frequency along vertical or horizontal channels, providing a FDA pattern along one dimension and a standard range-independent antenna pattern along the other dimension. The limiting cases can be easily collapsed into a linear FDA data model by setting the number of horizontal or vertical channels to unity.

3.3.1 Radar Geometry. The method of measuring the azimuth ϕ and elevation θ from the radar to any other point is defined as follows. Azimuth is measured from antenna boresight and is positive towards the aircraft nose. For a forward-looking array, azimuth is assumed positive counterclockwise from array boresight. Elevation is also measured from antenna boresight and is negative towards the ground. Hence, elevation is sometimes referred to as the depression angle.

Using the constant horizontal and vertical spacing defined in the antenna pattern derivation, the np^{th} channel's position $\mathbf{d}_{np}$ within the Cartesian coordinate system is defined as,

$$\mathbf{d}_{np} = -nd_x\hat{\mathbf{x}} - pd_z\hat{\mathbf{z}}. \tag{3.8}$$

The transformation vector $\hat{\mathbf{k}}$ to convert the cartesian coordinate system into the defined radar coordinate system is defined as

$$\hat{\mathbf{k}}(\theta, \phi) = \cos\theta \sin\phi\hat{\mathbf{x}} + \cos\theta\cos\phi\hat{\mathbf{y}} + \sin\theta\hat{\mathbf{z}}. \tag{3.9}$$

3.3.2 Transmitted Signal. The transmitted signal at each channel is modelled as sinusoidal. However, each channel has a different frequency because of the nature of FDA. To simplify the expressions, all channel angular frequencies are also contained within a matrix $\mathbf{\Omega}$ where

$$\mathbf{\Omega} = 2\pi\mathbf{F}. \tag{3.10}$$

Thus, the transmit signal expression for the np^{th} channel is defined by

$$s_{np}(t) = a_t u(t) e^{j(\mathbf{\Omega}[n,p]t+\psi)}, \tag{3.11}$$

where ψ is a random phase and a_t the signal amplitude. The final signal component $u(t)$ represents the envelope function or pulse train so the duration of each pulse and the time between each pulses corresponds to the radar parameters. For M pulses with

a Pulse Repetition Interval (PRI) of T_r, the pulse train is defined as a sum of delayed individual radar pulses $u_P(t)$,

$$u(t) = \sum_{m=0}^{M-1} u_P(t - mT_r). \tag{3.12}$$

To simplify the mathematics, it is useful to define the energy of a single pulse to be equal to unity when the amplitude a_t is one. Therefore, the total energy for each transmitted pulse is a_t^2.

3.3.3 Received Signal. After transmission, the electromagnetic energy strikes scattering centers and some energy is reflected back to the radar. It is important to recall the sufficiently narrow LPF assumption in Section 3.1 and therefore only have to consider the relevant channel frequency in the following derivation.

With the assumption of no atmospheric distortion, the received signal is the transmitted signal with a time delay τ_{np} and a doppler frequency shift corresponding to the scattering center or target $f_{t,np}$. The target doppler for all array channels $\mathbf{F_t}$ with a relative target velocity v_t is expressed using a matrix,

$$\mathbf{F_t} = 2v_t \frac{\mathbf{F}}{c}. \tag{3.13}$$

The channel receive expression $r_{np}(t)$ is thus

$$\begin{aligned} r_{np}(t) &= s_{np}(t - \tau_{np}) e^{j2\pi \mathbf{F_t}[n,p](t-\tau_{np})} \\ &= a_r u(t - \tau_n) e^{j2\pi \mathbf{F}[n,p](t-\tau_{np})} e^{j2\pi \mathbf{F_t}[n,p](t-\tau_{np})} e^{j\psi}. \end{aligned} \tag{3.14}$$

To simplify future results $\boldsymbol{\Upsilon'}$ a matrix containing incremental time delays relative to the reference channel τ'_{np} for all channels is defined as

$$\begin{aligned} \boldsymbol{\Upsilon}'[n,p] &= \frac{\hat{\mathbf{k}}(\theta,\phi) \bullet \mathbf{d}_{np}}{c} \\ &= \frac{-nd_x \cos\theta \sin\phi - pd_z \sin\theta}{c}, \end{aligned} \tag{3.15}$$

where $\bullet$ represents the vector dot product, also known as the inner product.

The channel phase delay $\boldsymbol{\Omega\Upsilon}'$, the product of angular frequency and channel time increment can be rewritten using the previously defined azimuth and elevation spatial frequency matrices,

$$\begin{aligned} \boldsymbol{\Omega}[n,p]\boldsymbol{\Upsilon}'[n,p] &= 2\pi\mathbf{F}[n,p]\left(\frac{-nd_x \cos\theta \sin\phi - pd_z \sin\theta}{c}\right) \\ &= -2\pi\left(n\frac{d_x \cos\theta \sin\phi \mathbf{F}[n,p]}{c} + p\frac{d_z \sin\theta \mathbf{F}[n,p]}{c}\right) \\ &= -2\pi(n\boldsymbol{\Psi}_{\boldsymbol{x}}[n,p] + p\boldsymbol{\Psi}_{\boldsymbol{z}}[n,p]). \end{aligned} \tag{3.16}$$

The above derivations for channel phase delay and the spatial frequency can be applied to simplify the received signal expression. The received signal expression in Eqn. (3.14) is first expanded to separate the two time delay components: the time from the target to the reference channel, T_R, and the channel incremental time delay τ'_{np}.

The incremental channel time delay is small and can be effectively ignored when considering the envelope in $u_p(t)$ since $T_R \gg \boldsymbol{\Upsilon}'[n,p]$. However, the incremental term can not be ignored when considering wavefront phase progression. The result of splitting the time delay is

$$\begin{aligned} r_{np}(t) &= a_r u(t - T_R - \boldsymbol{\Upsilon}'[n,p]) e^{j2\pi(\mathbf{F}[n,p]+\mathbf{F_t}[n,p])\left(t-T_R-\boldsymbol{\Upsilon}'[n,p]\right)} e^{j\psi} \\ &= a_r u(t - T_R) e^{j2\pi(\mathbf{F}[n,p]+\mathbf{F_t}[n,p])t} e^{-j2\pi(\mathbf{F}[n,p]+\mathbf{F_t}[n,p])T_R} \ldots \\ &\quad e^{-j2\pi(\mathbf{F}[n,p]+\mathbf{F_t}[n,p])\boldsymbol{\Upsilon}'[n,p]} e^{j\psi}. \end{aligned} \tag{3.17}$$

The first three exponential terms will be examined in order to simplify the final received signal expression before application of the matched filter. One simplification is achieved by noting that target velocities are small compared to the speed of light, i.e., $v_t \ll c$. Examining the second exponential shows

$$\begin{aligned} e^{-j2\pi(\mathbf{F}[n,p]+\mathbf{F_t}[n,p])T_R} &= e^{-j2\pi\left(\mathbf{F}[n,p]+\frac{2v_t\mathbf{F}[n,p]}{c}\right)T_R} \\ &= e^{-j2\pi\left(\mathbf{F}[n,p]+\frac{2v_t\mathbf{F}[n,p]}{c}\right)T_R} \\ &= e^{-j2\pi\mathbf{F}[n,p]T_R\left(1+\frac{2v_t}{c}\right)} \\ &\simeq e^{-j2\pi\mathbf{F}[n,p]T_R}. \end{aligned} \tag{3.18}$$

The third exponential term

$$\begin{aligned} e^{-j2\pi(\mathbf{F}[n,p]+\mathbf{F_t}[n,p])\boldsymbol{\Upsilon'}[n,p]} &= e^{-j\boldsymbol{\Omega}[n,p]\boldsymbol{\Upsilon'}[n,p]}e^{-j2\pi\left(\frac{2v_t\mathbf{F}[n,p]}{c}\right)\boldsymbol{\Upsilon'}[n,p]} \\ &= e^{j2\pi n\boldsymbol{\Psi_x}[n,p]}e^{j2\pi p\boldsymbol{\Psi_z}[n,p]}\ \ldots \\ &\quad e^{j2\pi\mathbf{F}[n,p]\left[\frac{(2v_t)(nd_x\cos\theta\sin\phi+pd_z\sin\theta)}{c^2}\right]} \\ &\simeq e^{j2\pi n\boldsymbol{\Psi_x}[n,p]}e^{j2\pi p\boldsymbol{\Psi_z}[n,p]}, \end{aligned} \tag{3.19}$$

is similarly simplified through spatial frequency matrix substitution and applying $v_t \ll c$.

Substituting the exponential expressions of Eqn. (3.18) and Eqn. (3.19) into Eqn. (3.17), the received signal expression is simplified to

$$\begin{aligned} r_{np}(t) &= a_r u(t-T_R)e^{j2\pi(\mathbf{F}[n,p]+\mathbf{F_t}[n,p])t}e^{-j2\pi\mathbf{F}[n,p]T_R}\ \ldots \\ &\quad e^{j2\pi(n\boldsymbol{\Psi_x}[n,p]+p\boldsymbol{\Psi_z}[n,p])}e^{j\psi}. \end{aligned} \tag{3.20}$$

The next step is downconversion to baseband through the appropriate LO *at each channel*. Following downconversion, the final received signal expression becomes

$$r_{np}(t) = a_r u(t-T_R)e^{j2\pi\mathbf{F_t}[n,p]t}e^{-j2\pi\mathbf{F}[n,p]T_R}e^{j2\pi n\boldsymbol{\Psi_x}[n,p]}e^{j2\pi p\boldsymbol{\Psi_z}[n,p]}e^{j\psi}. \tag{3.21}$$

The signal is then passed through a matched filter where the impulse response used is $h(t) = u_p^*(t)$, the conjugate of an individual radar pulse. The filter output is

$$\begin{aligned} x_{np}(t) &= \int_{-\infty}^{\infty} r_{np}(t) u_P^*(\tau - t) d\tau \qquad (3.22) \\ &= \int_{-\infty}^{\infty} a_r u(t - T_R) e^{j2\pi \mathbf{F_t}[n,p]t} e^{-j2\pi \mathbf{F}[n,p]T_R} e^{j2\pi n \mathbf{\Psi_x}[n,p]} e^{j2\pi p \mathbf{\Psi_z}[n,p]} \ \ldots \\ &\qquad e^{j\psi} u_P^*(\tau - t) d\tau \\ &= a_r e^{-j2\pi \mathbf{F}[n,p]T_R} e^{j2\pi n \mathbf{\Psi_x}[n,p]} e^{j2\pi p \mathbf{\Psi_z}[n,p]} e^{j\psi} \ \ldots \\ &\qquad \int_{-\infty}^{\infty} \sum_{m=0}^{M-1} u_P(\tau - T_R - mT_r) u_P^*(\tau - t) e^{j2\pi \mathbf{F_t}[n,p]\tau} d\tau. \end{aligned}$$

Using a change of variables by substituting $\beta = \tau - T_R - mT_r$, $d\beta = d\tau$. Therefore, matched filter output becomes

$$\begin{aligned} x_{np}(t) &= a_r e^{-j2\pi \mathbf{F}[n,p]T_R} e^{j2\pi n \mathbf{\Psi_x}[n,p]} e^{j2\pi p \mathbf{\Psi_z}[n,p]} e^{j\psi} \ \ldots \qquad (3.23) \\ &\qquad \int_{-\infty}^{\infty} \sum_{m=0}^{M-1} u_p(\beta) u_P^*(\beta + T_R + mT_r - t) e^{j2\pi \mathbf{F_t}[n,p](\beta + T_R + mT_r)} d\beta \\ &= a_r e^{-j2\pi \mathbf{F}[n,p]T_R} e^{j2\pi n \mathbf{\Psi_x}[n,p]} e^{j2\pi p \mathbf{\Psi_z}[n,p]} e^{j\psi} e^{j2\pi \mathbf{F_t}[n,p]T_R} \sum_{m=0}^{M-1} e^{j2\pi \mathbf{F_t}[n,p]mT_r} \ \ldots \\ &\qquad \int_{-\infty}^{\infty} u_P(\beta) u_P^*(\beta + T_R + mT_r - t) e^{j2\pi \mathbf{F_t}[n,p]\beta} d\beta, \end{aligned}$$

and can be simplified using common radar assumptions. These simplifications are performed next.

Based on the assumption that the individual channel frequencies are spread across a small range such that the radar is still narrowband, it is possible to approximate the Time-Frequency Auto-Correlation Function (TFACF) integral

$$\int_{-\infty}^{\infty} u_P(\beta) u_P^*(\beta + T_R + mT_r - t) e^{j2\pi \mathbf{F_t}[n,p]\beta} d\beta \ \approx 1 \qquad (3.24)$$

by assuming a doppler tolerant waveform. The normalized target doppler frequency $\bar{\mathbf{\Omega}}$ is defined as

$$\bar{\mathbf{\Omega}} = \frac{\mathbf{F_t}}{f_r} \tag{3.25}$$

and is utilized in the next step of mathematical manipulation. The matched filter output becomes

$$\begin{aligned} x_{np}(t) &= a_r e^{-j2\pi \mathbf{F}[n,p]T_R} e^{j2\pi n \mathbf{\Psi_x}[n,p]} e^{j2\pi p \mathbf{\Psi_z}[n,p]} e^{j\psi} e^{j2\pi \mathbf{F_t}[n,p]T_R} \cdots \\ &\quad \sum_{m=0}^{M-1} e^{j2\pi m \frac{\mathbf{F_t}[n,p]}{f_r}} \\ &= a_r e^{-j2\pi \mathbf{F}[n,p]T_R} e^{j2\pi n \mathbf{\Psi_x}[n,p]} e^{j2\pi p \mathbf{\Psi_z}[n,p]} e^{j\psi} e^{j2\pi \mathbf{F_t}[n,p]T_R} \cdots \\ &\quad \sum_{m=0}^{M-1} e^{j2\pi m \bar{\mathbf{\Omega}}[n,p]}. \end{aligned} \tag{3.26}$$

When a specific target range cell is selected for the m^{th} pulse, $t = T_R + mT_r$ and the summation over time is no longer applicable. Additionally, the amplitude a_r can be combined with the random phase ψ into a complex amplitude, α_t. The final result describing the voltage for a single range cell on a single pulse for a single channel is

$$\begin{aligned} x_{nmp} &= a_r e^{j\psi} e^{-j2\pi \mathbf{F}[n,p]T_R} e^{j2\pi n \mathbf{\Psi_x}[n,p]} e^{j2\pi p \mathbf{\Psi_z}[n,p]} e^{j2\pi \mathbf{F_t}[n,p]T_R} e^{j2\pi m \bar{\mathbf{\Omega}}[n,p]} \\ &= \alpha_t e^{j2\pi T_R(\mathbf{F_t}[n,p] - \mathbf{F}[n,p])} e^{j2\pi n \mathbf{\Psi_x}[n,p]} e^{j2\pi p \mathbf{\Psi_z}[n,p]} e^{j2\pi m \bar{\mathbf{\Omega}}[n,p]} \\ &= \alpha_t e^{j2\pi T_R \mathbf{F}[n,p]\left(\frac{2v_t}{c} - 1\right)} e^{j2\pi n \mathbf{\Psi_x}[n,p]} e^{j2\pi p \mathbf{\Psi_z}[n,p]} e^{j2\pi m \bar{\mathbf{\Omega}}[n,p]} \\ &\simeq \alpha_t e^{-j2\pi T_R \mathbf{F}[n,p]} e^{j2\pi n \mathbf{\Psi_x}[n,p]} e^{j2\pi p \mathbf{\Psi_z}[n,p]} e^{j2\pi m \bar{\mathbf{\Omega}}[n,p]}. \end{aligned} \tag{3.27}$$

This voltage is referred to as the per-channel, per-pulse return for a specific range cell or equivalently the voltage on the m^{th} pulse for the np^{th} channel in the array for a specific range cell where range attenuation, target reflection properties and other amplitude coefficients are contained in α_t.

3.3.4 Data Format. Due to the different frequency of each channel, both spatial frequencies and the normalized target doppler are dependent on both the horizontal and vertical channel location. It is therefore not possible to format the output in terms of a constant frequency array output expression where the azimuth spatial frequency, elevation spatial frequency, and normalized doppler are independent. An impact of interdependence between spatial and temporal domains is the inability of FDA to use Factored STAP techniques as mentioned in Section 2.1.2.1.

The implemented data format approach uses four separate steering vectors, two for the two spatial frequencies, one for the normalized doppler, and a separate term for the target range dependence with all steering vectors of size $NMP \times 1$. The steering vector expressions can be significantly simplified through the Kronecker Product $\otimes$ [8], the Hadamard product $\odot$, and the vector mathematical operator VEC [19], the last operator reshapes a matrix into a column vector. Additionally, matrices full of ones are used to match dimensions, where $\mathbf{1}_{P,Q}$ is a matrix of size $P \times Q$. The four steering vectors will now be defined starting with the azimuth spatial steering vector $\mathbf{a}(\boldsymbol{\Psi_x})$,

$$\mathbf{a}(\boldsymbol{\Psi_x}) = e^{j2\pi\left[\left(\mathbf{1}_{MP,1}\otimes(0:N-1)^T\right)\odot\mathrm{VEC}\left(\mathbf{1}_{M,1}\otimes\boldsymbol{\Psi_x}\right)\right]}, \tag{3.28}$$

and elevation spatial steering vector $\mathbf{e}(\boldsymbol{\Psi_z})$,

$$\mathbf{e}(\boldsymbol{\Psi_z}) = e^{j2\pi\left[\left((0:P-1)^T\otimes\mathbf{1}_{NM,1}\right)\odot\mathrm{VEC}\left(\mathbf{1}_{M,1}\otimes\boldsymbol{\Psi_z}\right)\right]}. \tag{3.29}$$

As mentioned above all steering vectors are the same length. Therefore, the temporal steering vector $\mathbf{b}(\bar{\boldsymbol{\Omega}})$ must also be multiplied out

$$\mathbf{b}(\bar{\boldsymbol{\Omega}}) = e^{j2\pi\left[\left(\mathbf{1}_{P,1}\otimes(0:M-1)^T\otimes\mathbf{1}_{N,1}\right)\odot\mathrm{VEC}\left(\mathbf{1}_{M,1}\otimes\bar{\boldsymbol{\Omega}}\right)\right]}. \tag{3.30}$$

Additionally, there is the target range dependent term $\mathbf{c}(\mathbf{F}, T_R)$, where the phase contribution is dependent on the channel frequency and is defined as

$$\mathbf{c}(\mathbf{F}, T_R) \;=\; e^{j2\pi T_R \mathrm{VEC}\left(\mathbf{1}_{M,1} \otimes \mathbf{F}\right)}. \tag{3.31}$$

The four steering vector format, whilst awkward due to the need of reshaping matrices corresponding to physical planar channel location, enables a neat solution for the steering vector $\mathbf{v}$ and the space-time snapshot $\boldsymbol{\chi}$. The space-time snapshot,

$$\boldsymbol{\chi} \;=\; \alpha_t \left[\mathbf{e}(\boldsymbol{\Psi}_{\boldsymbol{z}}) \odot \mathbf{b}(\bar{\boldsymbol{\Omega}}) \odot \mathbf{a}(\boldsymbol{\Psi}_{\boldsymbol{x}}) \odot \mathbf{c}(\mathbf{F}, T_R)\right] = \alpha_t \mathbf{v}, \tag{3.32}$$

is merely a scaled steering vector, itself the Hadamard product of the three spatial frequency and doppler steering vectors with the new range-frequency vector.

It is important to reinforce that the steering vector is valid for one particular azimuth, elevation and normalized doppler value out of NMP possible combinations within a Coherent Processing Interval (CPI). Additionally, the derivation is implicit for a single range-cell out of L available range-cells.

3.4 Summary

Chapter III generated the FDA antenna pattern and radar data model used in the rest of this thesis. The architecture and basic assumptions used within the derivation are examined in Section 3.1. Section 3.2 derived the antenna pattern using the same concept of a reference and incremental distance as for the constant frequency array. The FDA derivation showed the reference distance, and hence target range, must be considered since the phase progression differs across channels.

The remainder of the chapter developed the FDA radar data model, using the same procedure used by Ward [27], Jaffar [13] and Hale [10], but taking into account the effect of unique channel frequencies. Because of interdependence between the time and space domains, the resulting steering vector data format is not as simple as

for the constant frequency array. The total steering vector does not collapse into the Kronecker product of three component steering vectors and also requires definition of an additional steering vector to account for the impact of channel frequency on target range.

IV. Frequency Diverse Array Model Verification

Chapter III derived the generic planar Frequency Diverse Array (FDA) radar data model. The model now needs to be verified by setting all channel frequencies to a constant value and confirming the model collapses to the constant frequency data model.

First, the planar FDA radar data model is simplified for two limiting cases where horizontal and vertical channels have no frequency diversity. The two limiting cases easily extend into linear arrays by setting the number of horizontal channels N or vertical channels P to unity. The simplified cases modify the steering vectors and enable easier verification.

With successful verification of simplified radar data model cases, the more difficult problem of generic planar FDA verification is successfully undertaken. The increased difficulty is due to the data format manipulation required to match the constant frequency steering vectors.

4.1 Mathematical Verification of Linear FDA Data Model

The generic linear FDA radar data model can be achieved by defining the number of vertical channels P as unity for the constant vertical frequency limiting case. Alternatively, a linear FDA can be defined vertically aligned by setting the number of horizontal channels N as unity for the constant horizontal frequency limiting case. Model verification is then achieved by setting all channel frequencies to the same value and ensuring the steering vectors are identical to the linear constant frequency array format in [27].

Since this section verifies a linear FDA model, the elevation steering vector $\mathbf{e}$ is not physically required for a horizontally aligned array. Setting P equal to one ensures the exponential is unity. Similarly, the azimuth steering vector $\mathbf{a}$ is not required for a vertically aligned linear array, since setting N equal to one ensures the steering vector is unity. However, for completeness and also to build confidence in the planar FDA model verification, it is useful to examine all steering vectors.

4.1.1 Limiting Case - Constant Vertical Frequency. The first limiting case is where the planar FDA has all vertical array channels at the same frequency, i.e. frequency diversity occurs only across horizontal array channels. Therefore, the antenna pattern has range-dependence over azimuth but will be equivalent to a constant frequency array pattern over elevation.

With no vertical channel frequency dependence, the frequency matrix $\mathbf{F}$ can be fully described by a vector $\mathbf{f}$ of length N and similar argument applies for the spatial frequency and normalized doppler matrices. The flow-on effects of only requiring a vector to describe channel frequencies allows the definition of the incremental spatial vertical frequency

$$\boldsymbol{\Delta\Psi_z} \;=\; \boldsymbol{\Psi_z} - (\boldsymbol{\Psi_z}[0] \times \mathbf{1}_{N,1})\,, \tag{4.1}$$

and incremental normalized doppler

$$\boldsymbol{\Delta\bar{\Omega}} \;=\; \boldsymbol{\Omega} - (\boldsymbol{\Omega}[0] \times \mathbf{1}_{N,1})\,, \tag{4.2}$$

vectors. Defining the two incremental vectors allows the temporal and two spatial steering vectors to be written in a similar form to constant frequency planar array steering vectors. Specifically, the elevation steering vector $\mathbf{e}$ is size $P \times 1$, the azimuth steering vector $\mathbf{a}$ is size $N \times 1$, and the temporal steering vector $\mathbf{b}$ is size $M \times 1$. The frequency-range dependence can be completely encapsulated in the azimuth steering vector since all frequency variation is across horizontal channels. The fourth steering vector is now not range dependent but incorporates the two incremental vectors and is still of size $NMP \times 1$, same as the planar FDA data model.

The new azimuth steering vector contains the range dependency and is defined as

$$\mathbf{a}(\boldsymbol{\Psi_x}, \mathbf{f}, T_R) \;=\; e^{j2\pi\left[-\mathbf{f}T_R + (0:N-1)^T \odot \boldsymbol{\Psi_x}\right]}. \tag{4.3}$$

The temporal steering vector is based on the normalized doppler associated with the reference channel,

$$\mathbf{b}(\bar{\mathbf{\Omega}}[0]) \;=\; e^{j2\pi(0:M-1)^T\bar{\mathbf{\Omega}}[0]}. \tag{4.4}$$

Similarly, the elevation steering vector is also defined with a spatial frequency associated with the reference channel,

$$\mathbf{e}(\mathbf{\Psi}_{\boldsymbol{z}}[0]) \;=\; e^{j2\pi(0:P-1)^T\mathbf{\Psi}_{\boldsymbol{z}}[0]}. \tag{4.5}$$

Finally, the additional incremental vector $\mathbf{c}$ is actually composed of two different exponentials, one for each previously defined incremental vector,

$$\mathbf{c}(\mathbf{\Delta}\bar{\mathbf{\Omega}}, \mathbf{\Delta}\mathbf{\Psi}_{\boldsymbol{z}}) \;=\; e^{j2\pi\left[\mathbf{1}_{P,1}\otimes(0:M-1)^T\otimes\mathbf{\Delta}\bar{\mathbf{\Omega}}\right]} \odot e^{j2\pi\left[(0:P-1)^T\otimes\mathbf{1}_{M,1}\otimes\mathbf{\Delta}\mathbf{\Psi}_{\boldsymbol{z}}\right]}. \tag{4.6}$$

The temporal and two spatial steering vectors enable Kronecker product usage. The space-time snapshot $\boldsymbol{\chi}$ is the Hadamard product of the incremental vector and the result of the Kronecker product of the three steering vectors,

$$\boldsymbol{\chi} \;=\; \alpha_t \left\{ \left[\mathbf{e}(\mathbf{\Psi}_{\boldsymbol{z}}) \otimes \mathbf{b}(\bar{\mathbf{\Omega}}) \otimes \mathbf{a}(\mathbf{\Psi}_{\boldsymbol{x}}, \mathbf{f}, T_R)\right] \odot \mathbf{c}(\mathbf{\Delta}\bar{\mathbf{\Omega}}, \mathbf{\Delta}\mathbf{\Psi}_{\boldsymbol{z}}) \right\} = \alpha_t \mathbf{v}. \tag{4.7}$$

With a simplified FDA radar data model, the next step is to define all channel frequencies as a constant value. The first impact of defining a constant frequency is that both the incremental normalized doppler $\mathbf{\Delta}\bar{\mathbf{\Omega}}$ in Eqn. (4.2) and the incremental vertical spatial frequency $\mathbf{\Delta}\mathbf{\Psi}_{\boldsymbol{z}}$ in Eqn. (4.1) become empty vectors, vectors whose elements are all zero.

Therefore the incremental vector

$$\begin{aligned} \mathbf{c}(\mathbf{\Delta}\bar{\mathbf{\Omega}}, \mathbf{\Delta}\mathbf{\Psi}_{\boldsymbol{z}}) \;&=\; e^{j2\pi\left[\mathbf{1}_{P,1}\otimes(0:M-1)^T\otimes\mathbf{\Delta}\bar{\mathbf{\Omega}}\right]} \odot e^{j2\pi\left[(0:P-1)^T\otimes\mathbf{1}_{M,1}\otimes\mathbf{\Delta}\mathbf{\Psi}_{\boldsymbol{z}}\right]} \\ &=\; e^{\mathbf{0}_{NMP,1}} \odot e^{\mathbf{0}_{NMP,1}} = \mathbf{1}_{NMP,1} \end{aligned} \tag{4.8}$$

is seen to be unity and can be effectively ignored. Now there are only three steering vectors remaining, the same as for the constant frequency array, and each vector needs to be examined in greater detail.

The elevation steering vector $\mathbf{e}$ in Eqn. (4.5) and the temporal steering vector $\mathbf{b}$ in Eqn. (4.4), are already equivalent to those for the constant frequency array since the reference frequency f_0 is now the frequency of all array channels.

Thus, only the azimuth steering vector $\mathbf{a}$ needs to be examined to ensure it is equivalent to the constant frequency azimuth steering vector. The azimuth steering vector expression can be simplified by recognizing that the frequency vector $\mathbf{f}$ and spatial frequency vector $\boldsymbol{\Psi}_{\boldsymbol{x}}$ can be effectively replaced by scalars since the channels of each vector have the same value.

Therefore, the azimuth steering vector

$$\begin{aligned} \mathbf{a}(\boldsymbol{\Psi}_{\boldsymbol{x}}, \mathrm{f}, T_R) &= e^{j2\pi\left[-\mathbf{f}T_R + (0:N-1)^T \odot \boldsymbol{\Psi}_{\boldsymbol{x}}\right]} \\ &= e^{-j2\pi\mathbf{f}T_R} e^{j2\pi(0:N-1)^T \odot \boldsymbol{\Psi}_{\boldsymbol{x}}} \\ &= e^{-j2\pi\mathrm{f}T_R} e^{j2\pi(0:N-1)^T \Psi_x}, \end{aligned} \tag{4.9}$$

can be factored into the constant frequency array expression and a phase term dependent on the transmit frequency and target range. It is noted the above manipulation replaces the vector $\boldsymbol{\Psi}_{\boldsymbol{x}}$ by the scalar Ψ_x since all channel frequencies are set to the same value. The new phase term is constant over all array channels and can be grouped into the space-time snapshot complex amplitude α_t,

$$\begin{aligned} \mathbf{a}(\Psi_x, \mathrm{f}, T_R) &= e^{-j2\pi\mathrm{f}T_R} e^{j2\pi(0:N-1)^T \Psi_x} \\ &= e^{-j2\pi\mathrm{f}T_R} \mathbf{a}(\Psi_x). \end{aligned} \tag{4.10}$$

To summarize, the definition of all array channel frequencies to be one value led the incremental vector to become unity and the azimuth, temporal, and elevation steering vectors to correspond to the constant frequency array steering vectors [9, 10]

as shown by

$$\mathbf{a}(\Psi_x) = e^{j2\pi(0:N-1)^T\Psi_x}. \tag{4.11}$$

$$\mathbf{b}(\bar{\Omega}) = e^{j2\pi(0:M-1)^T\bar{\mathbf{\Omega}}[0]} = e^{j2\pi(0:M-1)^T\bar{\Omega}}. \tag{4.12}$$

$$\mathbf{e}(\Psi_z) = e^{j2\pi(0:P-1)^T\mathbf{\Psi_z}[0]} = e^{j2\pi(0:P-1)^T\Psi_z}. \tag{4.13}$$

$$\mathbf{v} = \mathbf{e}(\Psi_z) \otimes \mathbf{b}(\bar{\Omega}) \otimes \mathbf{a}(\Psi_x). \tag{4.14}$$

4.1.2 Limiting Case - Constant Horizontal Frequency. The other limiting case is having constant frequency across all horizontal array channels and all frequency deviation constrained to the vertical channels. The previous planar FDA matrices for frequency, target doppler, and spatial frequencies can now be reduced to vectors of length P. Analogous to the first limiting case, define incremental spatial frequency

$$\mathbf{\Delta\Psi_x} = \mathbf{\Psi_x} - (\mathbf{\Psi_x}[0] \times \mathbf{1}_{P,1}), \tag{4.15}$$

and incremental normalized doppler

$$\mathbf{\Delta\bar{\Omega}} = \mathbf{\Omega} - (\mathbf{\Omega}[0] \times \mathbf{1}_{P,1}), \tag{4.16}$$

vectors.

As for the previous constant vertical frequency case, the limiting condition enables the definition of three steering vectors with similar form to the constant frequency array, and an incremental fourth vector to simplify the generation of space-time snapshots. The azimuth spatial steering vector

$$\mathbf{a}(\mathbf{\Psi_x}[0]) = e^{j2\pi(0:N-1)^T\mathbf{\Psi_x}[0]} \tag{4.17}$$

and the temporal steering vector

$$\mathbf{b}(\bar{\mathbf{\Omega}}[0]) = e^{j2\pi(0:M-1)^T\bar{\mathbf{\Omega}}[0]} \tag{4.18}$$

are both based on the reference frequency f_0. The elevation steering vector

$$\mathbf{e}(\boldsymbol{\Psi_z}, \mathbf{f}, T_R) \;=\; e^{j2\pi\left[-\mathbf{f}T_R+(0:P-1)^T\odot\boldsymbol{\Psi_z}\right]} \tag{4.19}$$

has the varying spatial frequency along with the range dependence component since all frequency diversity is limited to elevation array channels.

The incremental vector takes on a similar form to the previous limiting case, consisting of two exponentials involving the two incremental vectors,

$$\mathbf{c}(\boldsymbol{\Delta\bar{\Omega}}, \boldsymbol{\Delta\Psi_x}) \;=\; e^{j2\pi\left\{\boldsymbol{\Delta\bar{\Omega}}\otimes\left[(0:M-1)^T\otimes\mathbf{1}_{N,1}\right]\right\}} \odot e^{j2\pi\left\{\boldsymbol{\Delta\Psi_x}\otimes\left[\mathbf{1}_{M,1}\otimes(0:N-1)^T\right]\right\}}. \tag{4.20}$$

The space-time snapshot is then calculated making use of the Kronecker and Hadamard products,

$$\boldsymbol{\chi} \;=\; \alpha_t\left\{\left[\mathbf{e}(\boldsymbol{\Psi_z}, \mathbf{f}, T_R)\otimes\mathbf{b}(\boldsymbol{\bar{\Omega}})\otimes\mathbf{a}(\boldsymbol{\Psi_x})\right]\odot\mathbf{c}(\boldsymbol{\Delta\bar{\Omega}}, \boldsymbol{\Delta\Psi_x})\right\} = \alpha_t\mathbf{v}. \tag{4.21}$$

Defining a constant frequency across array channels results in both the incremental normalized doppler $\boldsymbol{\Delta\bar{\Omega}}$ in Eqn. (4.16) and the incremental horizontal spatial frequency $\boldsymbol{\Delta\Psi_x}$ in Eqn. (4.15) becoming zero vectors.

Therefore, the incremental vector

$$\begin{aligned}\mathbf{c}(\boldsymbol{\Delta\bar{\Omega}}, \boldsymbol{\Delta\Psi_x}) \;&=\; e^{j2\pi\left\{\boldsymbol{\Delta\bar{\Omega}}\otimes\left[(0:M-1)^T\otimes\mathbf{1}_{N,1}\right]\right\}} \odot e^{j2\pi\left\{\boldsymbol{\Delta\Psi_x}\otimes\left[\mathbf{1}_{M,1}\otimes(0:N-1)^T\right]\right\}} \\ &=\; e^{\mathbf{0}_{NMP,1}} \odot e^{\mathbf{0}_{NMP,1}} = \mathbf{1}_{NMP,1},\end{aligned} \tag{4.22}$$

is unity and can be effectively ignored. The three remaining steering vectors need to be examined in greater detail.

The azimuth steering vector $\mathbf{a}$ in Eqn. (4.19) and the temporal steering vector $\mathbf{b}$ in Eqn. (4.18) are already equivalent to those for the constant frequency array, since the reference frequency f_0, is now equivalent to the array frequency. Thus only the

elevation steering vector $\mathbf{e}$ needs to be examined to ensure that it is equivalent to the constant frequency array elevation steering vector. Replacing the frequency and spatial frequency vectors with scalar values, the elevation steering vector is simplified to

$$\begin{aligned} \mathbf{e}(\boldsymbol{\Psi}_{\boldsymbol{z}}, \mathbf{f}, T_R) &= e^{j2\pi\left[-\mathbf{f}T_R+(0:P-1)^T\odot\boldsymbol{\Psi}_{\boldsymbol{z}}\right]} \\ &= e^{-j2\pi \mathrm{f} T_R} e^{j2\pi(0:P-1)^T\Psi_z} \\ &= e^{-j2\pi \mathrm{f} T_R}\mathbf{e}(\Psi_z), \end{aligned} \tag{4.23}$$

where the vector $\boldsymbol{\Psi}_{\boldsymbol{z}}$ is replaced by the scalar Ψ_z since all channel frequencies are set to the same value. The steering vector is factored into the constant frequency array elevation steering vector and a phase term dependent on transmit frequency and target range, but constant over all array channels.

Again, the definition of all channel frequencies to the be same frequency led the incremental vector to become unity, and the azimuth, temporal, and elevation steering vectors all correspond to the constant frequency array steering vectors below.

$$\mathbf{a}(\Psi_x) = e^{j2\pi(0:N-1)^T\boldsymbol{\Psi}_{\boldsymbol{x}}[0]} = e^{j2\pi(0:N-1)^T\Psi_x}. \tag{4.24}$$

$$\mathbf{b}(\bar{\Omega}) = e^{j2\pi(0:M-1)^T\bar{\boldsymbol{\Omega}}[0]} = e^{j2\pi(0:M-1)^T\bar{\Omega}}. \tag{4.25}$$

$$\mathbf{e}(\Psi_z) = e^{j2\pi(0:P-1)^T\Psi_z}. \tag{4.26}$$

$$\mathbf{v} = \mathbf{e}(\Psi_z)\otimes\mathbf{b}(\bar{\Omega})\otimes\mathbf{a}(\Psi_x). \tag{4.27}$$

The result above and in the previous subsection verifies the linear FDA radar data model is consistent with the constant frequency data model [9, 10].

4.2 Mathematical Verification of Planar FDA Data Model

With successful verification of the two limiting cases, the next step is to prove the equivalence for the planar FDA. Planar FDA verification is more difficult due to the additional array dimension involved and also the data format chosen for the

planar FDA steering vectors. It is noted that the frequency matrix $\mathbf{F}$ and the two spatial frequency matrices $\boldsymbol{\Psi_x}$ and $\boldsymbol{\Psi_z}$ can all be replaced by scalar values f, Ψ_x, and Ψ_z, respectively, when all array channels transmit and receive at the same frequency.

Applying the Vector operator [8] introduced in Chapter III, the first exponential to consider is the range dependent steering vector,

$$\begin{aligned} \mathbf{c}(\mathbf{F}, T_R) &= e^{j2\pi T_R \mathrm{VEC}\left(\mathbf{1}_{M,1} \otimes \mathbf{F}\right)} \\ &= e^{j2\pi T_R \mathrm{VEC}\left[\mathbf{1}_{M,1} \otimes \left(\mathrm{f} \times \mathbf{1}_{N,P}\right)\right]} \\ &= e^{j2\pi \mathrm{f} T_R \mathbf{1}_{NMP,1}}, \end{aligned} \tag{4.28}$$

which is now seen to be a constant phase term across all array channels. As observed during the radar data model derivation in Chapter III, a constant phase term can be effectively ignored by incorporating it into the signal complex amplitude. Being able to effectively ignore the range vector is important, as the term does not exist for the constant frequency array.

The next step is to examine the remaining three steering vectors. The argument of each exponential can be simplified by replacing the appropriate matrix with a scalar value and applying the Vector mathematical operator and Hadamard product. Additionally, the steering vectors can be further simplified by re-arranging the Kronecker product out of the exponential.

When the azimuth steering vector is simplified, the expression results in the following form,

$$\begin{aligned} \mathbf{a}(\boldsymbol{\Psi_x}) &= e^{j2\pi\left\{\left[\mathbf{1}_{MP,1} \otimes (0{:}N-1)^T\right] \odot \mathrm{VEC}\left(\mathbf{1}_{M,1} \otimes \boldsymbol{\Psi_x}\right)\right\}} \\ &= e^{j2\pi\left\{\left[\mathbf{1}_{MP,1} \otimes (0{:}N-1)^T\right] \odot \mathrm{VEC}\left[\mathbf{1}_{M,1} \otimes \left(\Psi_x \times \mathbf{1}_{N,P}\right)\right]\right\}} \\ &= e^{j2\pi\left[\mathbf{1}_{MP,1} \otimes (0{:}N-1)^T \Psi_x\right]} \\ &= \mathbf{1}_{MP,1} \otimes e^{j2\pi (0{:}N-1)^T \Psi_x} = \mathbf{1}_{MP,1} \otimes \mathbf{a}(\Psi_x). \end{aligned} \tag{4.29}$$

Undertaking the same approach for the temporal steering vector, the output is transformed to

$$\begin{aligned}
\mathbf{b}(\bar{\mathbf{\Omega}}) &= e^{j2\pi\left\{\left[\mathbf{1}_{P,1}\otimes(0:M-1)^T\otimes\mathbf{1}_{N,1}\right]\odot\mathrm{VEC}\left(\mathbf{1}_{M,1}\otimes\bar{\mathbf{\Omega}}\right)\right\}} \\
&= e^{j2\pi\left\{\left[\mathbf{1}_{P,1}\otimes(0:M-1)^T\otimes\mathbf{1}_{N,1}\right]\odot\mathrm{VEC}\left[\mathbf{1}_{M,1}\otimes\left(\bar{\Omega}\times\mathbf{1}_{N,P}\right)\right]\right\}} \\
&= e^{j2\pi\left\{\mathbf{1}_{P,1}\otimes\left[(0:M-1)^T\bar{\Omega}\right]\otimes\mathbf{1}_{N,1}\right\}} \\
&= \mathbf{1}_{P,1}\otimes e^{j2\pi(0:M-1)^T\bar{\Omega}}\otimes\mathbf{1}_{N,1} = \mathbf{1}_{P,1}\otimes\mathbf{b}(\bar{\Omega})\otimes\mathbf{1}_{N,1}.
\end{aligned} \tag{4.30}$$

The remaining vector is the elevation steering vector

$$\begin{aligned}
\mathbf{e}(\mathbf{\Psi_z}) &= e^{j2\pi\left\{\left[(0:P-1)^T\otimes\mathbf{1}_{NM,1}\right]\odot\mathrm{VEC}\left(\mathbf{1}_{M,1}\otimes\mathbf{\Psi_z}\right)\right\}} \\
&= e^{j2\pi\left\{\left[(0:P-1)^T\otimes\mathbf{1}_{NM,1}\right]\odot\mathrm{VEC}\left[\mathbf{1}_{M,1}\otimes\left(\Psi_z\times\mathbf{1}_{N,P}\right)\right]\right\}} \\
&= e^{j2\pi\left[(0:P-1)^T\Psi_z\otimes\mathbf{1}_{NM,1}\right]} \\
&= e^{j2\pi(0:P-1)^T\Psi_z}\otimes\mathbf{1}_{NM,1} = \mathbf{e}(\Psi_z)\otimes\mathbf{1}_{NM,1}.
\end{aligned} \tag{4.31}$$

Substituting the three steering vectors into the planar FDA steering vector expression,

$$\begin{aligned}
\mathbf{v} &= \mathbf{e}(\mathbf{\Psi_z})\odot\mathbf{b}(\bar{\mathbf{\Omega}})\odot\mathbf{a}(\mathbf{\Psi_x})\odot\mathbf{c}(\mathbf{F},T_R) \\
&= \left(e^{j2\pi(0:P-1)^T\Psi_z}\otimes\mathbf{1}_{NM,1}\right)\odot\left(\mathbf{1}_{P,1}\otimes e^{j2\pi(0:M-1)^T\bar{\Omega}}\otimes\mathbf{1}_{N,1}\right)\quad\cdots \\
&\quad\odot\left(\mathbf{1}_{MP,1}\otimes e^{j2\pi(0:N-1)^T\Psi_x}\right)\odot\mathbf{1}_{NMP,1},
\end{aligned} \tag{4.32}$$

can be simplified by eliminating the vectors of ones. Therefore, the three individual steering vectors can be reduced down to the equivalent steering vectors used in the constant frequency array and the total steering vector can now be calculated using the Kronecker product,

$$\begin{aligned}
\mathbf{v} &= e^{j2\pi(0:N-1)^T\Psi_x}\otimes e^{j2\pi(0:M-1)^T\bar{\Omega}}\otimes e^{j2\pi(0:P-1)^T\Psi_z} \\
&= \mathbf{e}(\Psi_z)\otimes\mathbf{b}(\bar{\Omega})\otimes\mathbf{a}(\Psi_x).
\end{aligned} \tag{4.33}$$

Thus, the planar FDA radar data model is shown to collapse down to the planar constant frequency radar data model [9, 10] when all array channels transmit and receive at the same frequency.

4.3 Summary

Chapter IV provided analytical verification of the FDA radar data model derived in Chapter III. The mathematical verification first considered the simplified linear FDA expressions based on constant vertical and horizontal frequency limiting cases extended into linear FDA data models by setting P or N to unity. Section 4.1 showed that both limiting cases collapse to the constant frequency array model when all array channel frequencies are set to a constant value.

The verification is then extended to the planar FDA data model derived in Chapter III. The equivalence of the planar FDA data model to the constant frequency model [9, 10] is contained in Section 4.2.

V. Analysis of FDA Impact on Clutter Statistics

The antenna array is analogous to the "eye" the radar uses to view the external environment. Therefore, a fundamental change in the array structure such as different channel frequencies, creates a fundamental difference in how the environment is perceived by the Frequency Diverse Array (FDA) radar.

Whilst the FDA radar data model has been verified mathematically, there are a number of impacts resulting from the utilization of FDAs requiring examination. This chapter focuses on the FDA antenna pattern, clutter spectrum, and clutter rank. Examination of topics mentioned this chapter indirectly provides some FDA simulation verification.

The beginning of the chapter is focused on the impact of a horizontally aligned linear FDA. After the impacts of a linear FDA are characterized, the same concepts are examined for a planar FDA where the analysis is complicated by the elevation dimension and the interdependence between elevation and range.

5.1 Radar Simulation Parameters

Since the Coherent Processing Interval (CPI) gain is equal to NMP and a linear array has only one vertical channel $P = 1$, care must be taken during analysis involving both linear and planar arrays. To allow fair planar array analysis, the number of vertical channels P needs to be in the same order of magnitude as the number of horizontal channels N so the total frequency diversity is the same order of magnitude.

The CPI value is fixed with the parameter values used during simulation within this chapter detailed in Table 5.1, unless otherwise noted in figure captions. The effect of keeping the CPI value fixed is a reduced number of integrated pulses M for the planar array and hence fewer doppler filters.

An important consideration when analyzing results is the platform altitude dependent effective radar horizon range. Using Multiple-Channel Airborne Radar Measurements (MCARM) radar simulation data [24], the platform altitude is 3073 m, the

Table 5.1: Chapter V Radar Simulation Parameters.

Variable	Linear FDA Comparison	Planar FDA Comparison
M (Pulses in CPI)	128	16
N (Azimuth Channels)	11	11
P (Vertical Channels)	1	8
CPI Gain	1408	1408

radar horizon is 228 km, and the Maximum Unambiguous Range (MUR) is 75 km. Therefore, depending on target range there are either 2 or 3 range ambiguous clutter rings for a total of 3 or 4 contributing clutter rings.

5.2 Frequency Allocation

Since the FDA concept is based on potentially unique array channel frequencies, it is important to consider the scope of channel frequency selection. Firstly, all derivation is based on the assumption of a narrowband radar, though unfortunately it is difficult to find definitive distinction in current literature on what constitutes narrowband and wide-band radar. A common narrow-band classification is the bandwidth (BW) is no more than 10% of the reference frequency. This limit will be applied within this thesis.

Even with the above narrow-band radar frequency limit enforcement, the scope of frequency allocation is still extremely broad. There are two fundamental considerations within the frequency allocation decision: 1) the rule determining frequency progression across array channels, i.e. sinusoidal, quadratic or logarithmic and 2) the magnitude of the frequency progressions. Mathematically, the first decision is the function to use as a channel frequency progression model and the second decision is the scaling parameter(s).

The choice of a channel frequency progression function is highly dependent on the desired FDA purpose. This thesis considers the benefits of FDAs in increasing sample-support data homogeneity for forward-looking arrays, therefore the frequency

selection needs to produce an antenna pattern to accentuate isodops. As mentioned optimal channel frequency selection is outside the scope of this thesis.

The simplest frequency progression has been selected to characterize linear FDA impact, a constant frequency increment Δf between successive array channels referred to as a constant frequency increment FDA. When the reference frequency is defined as f_0, the n^{th} channel frequency is

$$f_n = f_0 + n\Delta f, \qquad n = \{0 : N-1\}. \tag{5.1}$$

A planar FDA is more difficult to investigate since there is potential to have different frequency progressions along both horizontal and vertical dimensions. To investigate the planar FDA impact, a constant frequency increment approach is utilized, with a constant frequency increment between horizontal channels Δf_x and a separate frequency increment between vertical channels Δf_z. Thus, the np^{th} channel frequency is

$$f_{np} = f_0 + n\Delta f_x + p\Delta f_z, \quad n = \{0 : N-1\},\ p = \{0 : P-1\}. \tag{5.2}$$

With implementation of a frequency progression scheme, namely a constant frequency increment approach, scaling factor, i.e., the magnitude of Δf, Δf_x, and Δf_z are required. With the selection of a constant frequency increment, there is only one scaling factor required for a linear FDA and two scale factors for a planar FDA. The scaling factor extremes are a constant frequency array when $\Delta f = 0$, and the upper value is constrained by the narrowband assumption $N\Delta f \leq \frac{f_0}{10}$. The upper value is also constrained by the antenna pattern produced, as will be discussed when evaluating the resultant antenna pattern.

5.3 Linear FDA Antenna Pattern

The generic planar FDA antenna pattern is derived in Chapter III, specifically Eqn. (3.5). The result can be considerably simplified for a linear FDA with constant frequency increment. The simplified antenna pattern is

$$W(\phi, R) = \sum_{n=0}^{N-1} e^{j\frac{2\pi}{c}\mathbf{f}[n][2nd(\sin\phi - \sin\phi_0) - 2(R-R_0)]}, \tag{5.3}$$

where the pattern is steered to an azimuth angle of ϕ_0 and a range of R_0.

As a method to partially verify the data model, the linear FDA antenna pattern is firstly simulated using $\Delta f = 0$, the constant frequency array. The antenna pattern should have no range dependence. The antenna pattern is shown in Figure 5.1 and meets expectations by being range-independent.

The other limiting case is the selection of a large Δf value to highlight the problem of significant range aliasing taking place. The effect is shown in Figure 5.2 where $\Delta f = 25$ kHz. The antenna pattern degrades performance due to the aliasing.

For the remainder of this chapter, a frequency progression of $\Delta f = 1$ kHz is selected for the linear FDA, a compromise between the two extremes. The resulting antenna pattern is included as Figure 5.3 showing range-dependence. There is no aliasing present within the range presented. When the full radar horizon range, not just the MUR, is considered a linear FDA with $\Delta f = 1$ kHz will produce some aliasing over range as demonstrated in Figure 5.4.

5.4 Linear FDA Clutter Spectrum

A critical linear FDA impact is the change in ground clutter distribution within the azimuth-doppler domain, henceforth referred to as the clutter spectrum. The desired information on the clutter location is embedded within the space-time interference covariance matrix $\mathbf{R}$. Since the covariance matrix incorporates the antenna

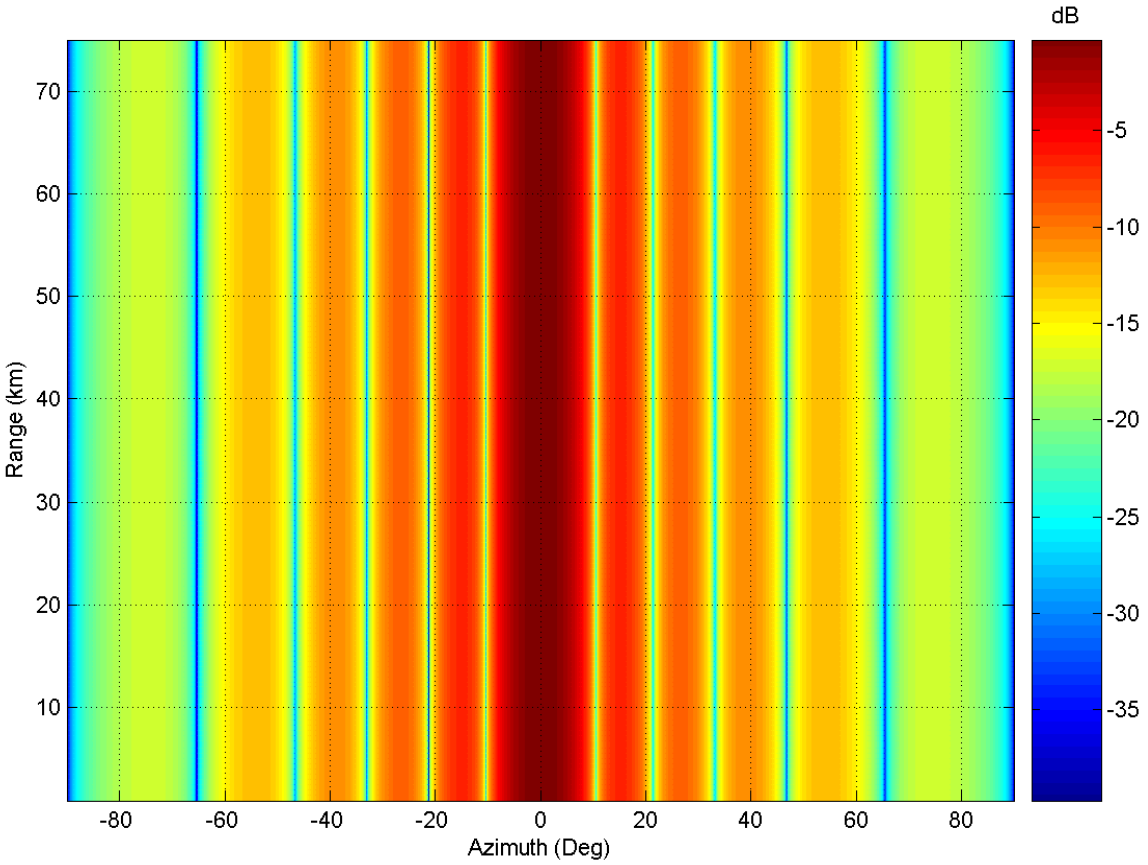

Figure 5.1: Linear FDA antenna pattern using a constant frequency increment between successive channels of $\Delta f = 0$ kHz, i.e. a constant frequency array. The antenna pattern is not range-dependent providing partial simulation verification of the FDA antenna pattern.

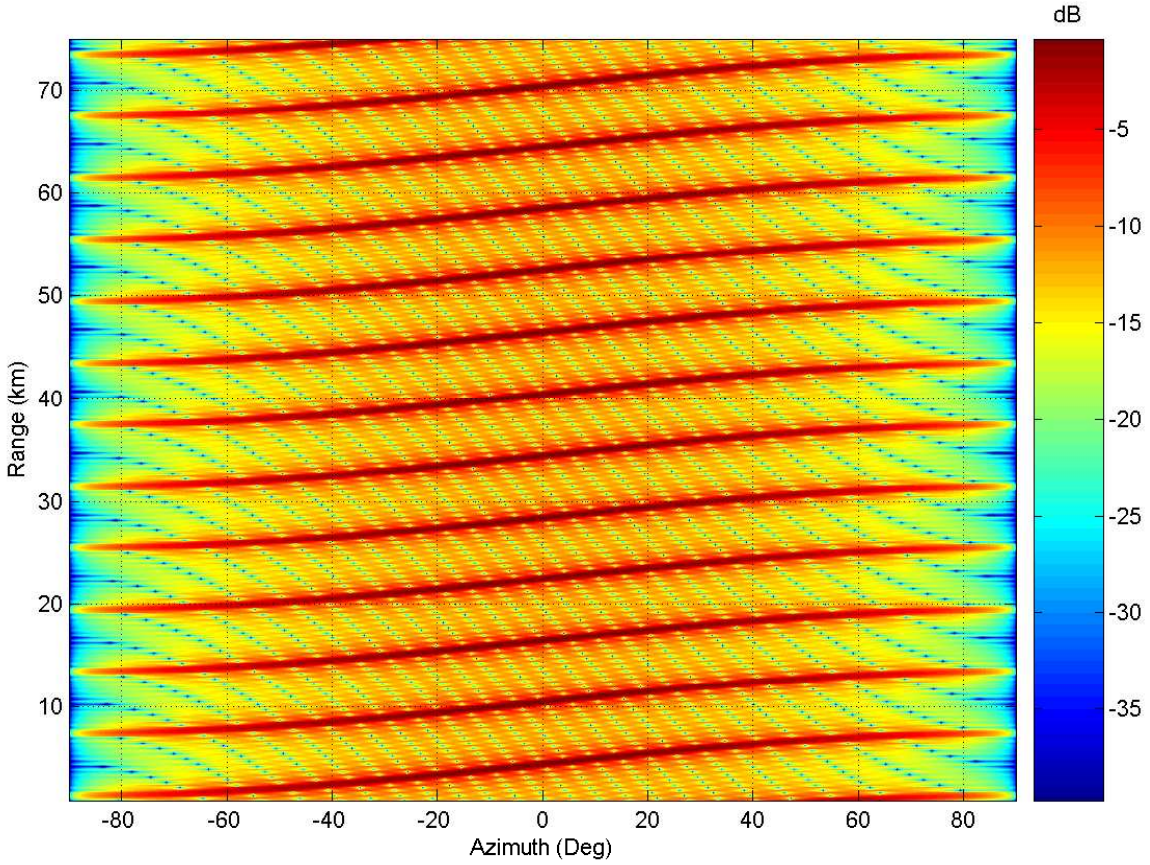

Figure 5.2: Linear FDA antenna pattern using a constant frequency increment between successive channels as $\Delta f = 25$ kHz. The FDA antenna pattern is range-dependent and also shows significant range-aliasing of the mainlobe.

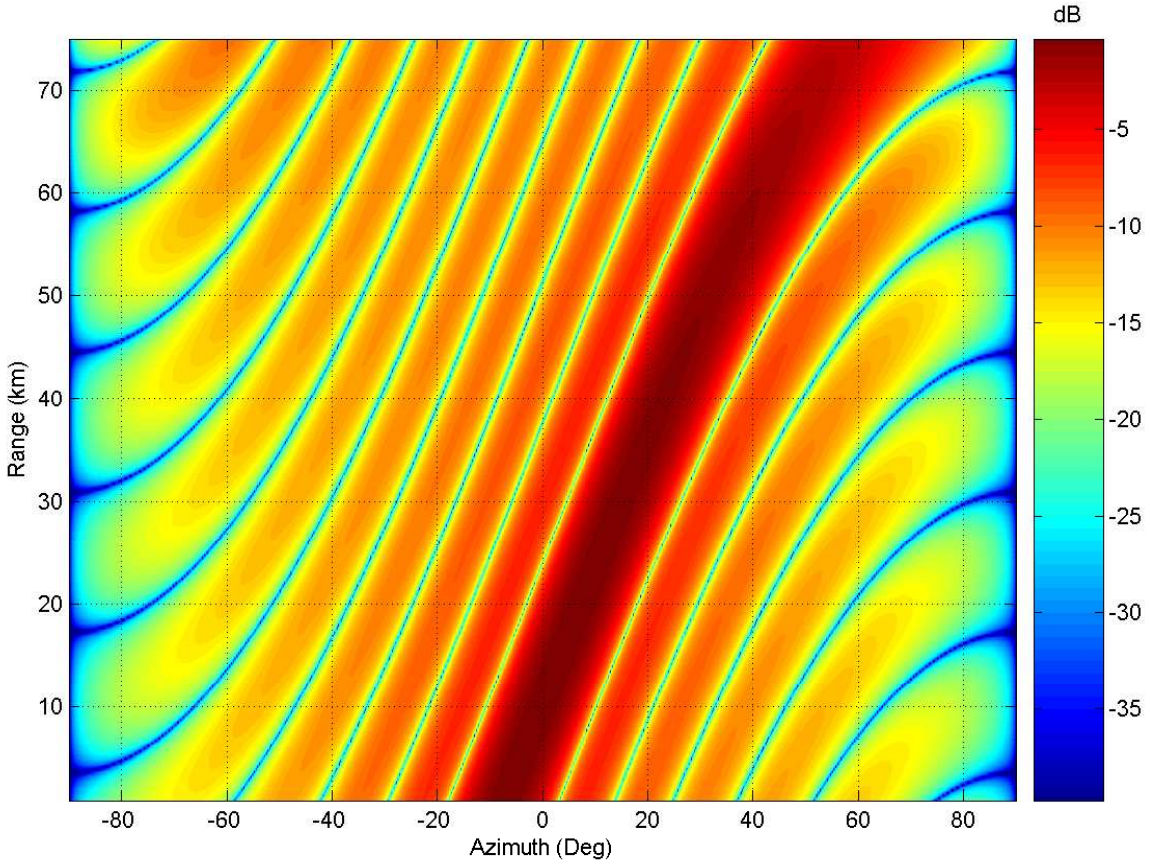

Figure 5.3: Linear FDA antenna pattern using a constant frequency increment between successive channels as $\Delta f = 1$ kHz. The FDA antenna pattern is range-dependent but does not show range-aliasing of the mainlobe.

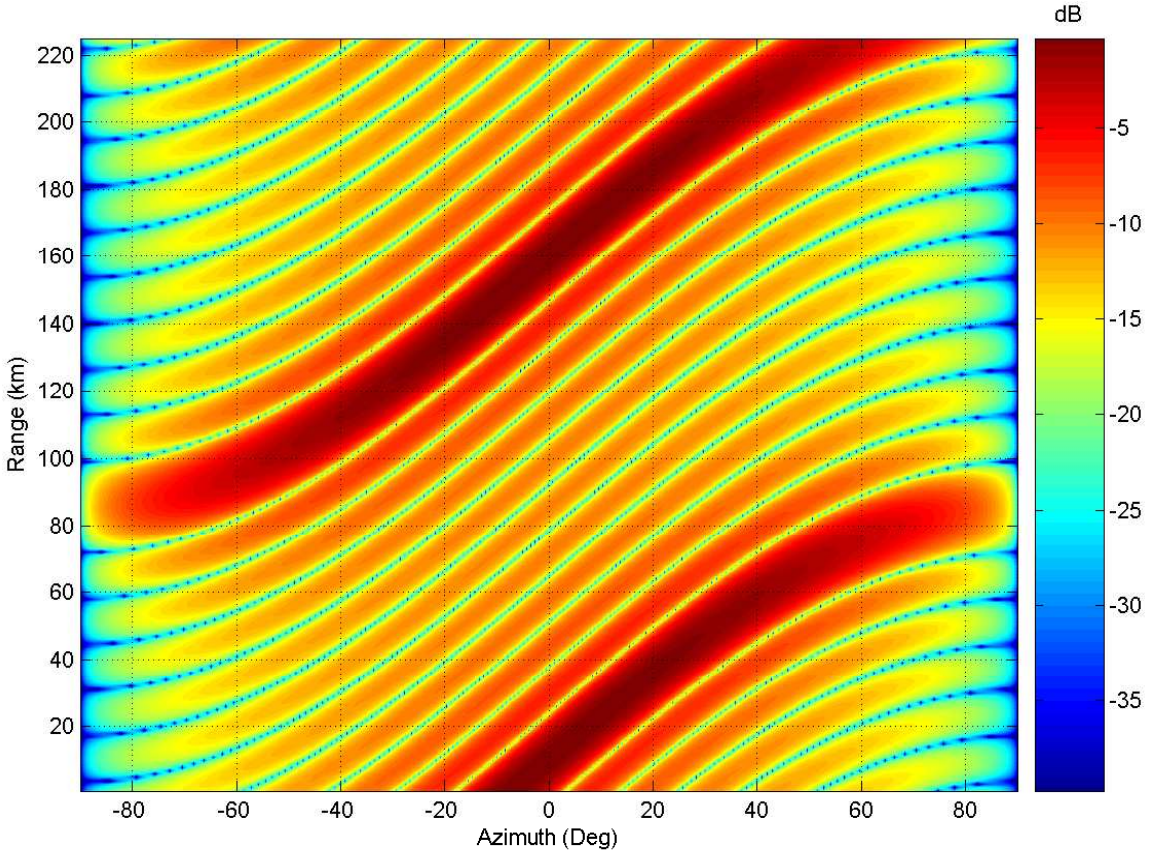

Figure 5.4: Linear FDA antenna pattern using a constant frequency increment between successive channels as $\Delta f = 1$ kHz. The FDA antenna pattern now shows some range-aliasing of the mainlobe when the radar horizon range is considered.

pattern, the FDA is expected to alter the clutter distribution within the doppler-azimuth space because of the new range-dependent antenna pattern.

One method to get accurate interference location information is through the use of a high resolution power spectral estimator, such as the Minimum Variance Estimator (MVE) [15] where

$$\text{MVE} = \mathbf{v}^H \mathbf{R}^{-1} \mathbf{v}, \tag{5.4}$$

with doppler and azimuth implicitly defined in the steering vector $\mathbf{v}$. It is often useful to also use the Improvement Factor (IF), which is equal to the MVE inverse when using the Matched Filter (MF). Where the MVE indicates clutter location by a ridge, the IF produces a plateau where optimum clutter suppression can take place and displays clutter location as a valley or notch.

5.4.1 Side-Looking FDA Clutter Spectrum. The clutter location within the azimuth-doppler domain is simple for a constant frequency linear Side-Looking Airborne Radar (SLAR). It can be predicted from the linear relationship between azimuth ϕ and doppler frequency

$$f_d = \frac{2v_r}{\lambda} \sin(\phi). \tag{5.5}$$

Since doppler frequency and azimuth angle are sinusoidally related, the clutter occupies a sinusoidal curve as seen in Figure 5.5 (a). The curve cuts through the center of the diagram, since zero azimuth corresponds to zero ground clutter doppler. If the spectrum is plotted using doppler versus sine azimuth, the spectrum would be along a straight line.

The clutter location for a linear side-looking FDA is more complex, because the antenna pattern is now range-dependent. The illumination of clutter at the target range is the same for both arrays since the antenna pattern is the same, as shown in Chapter III. However, the ambiguous range clutter rings are illuminated by a different

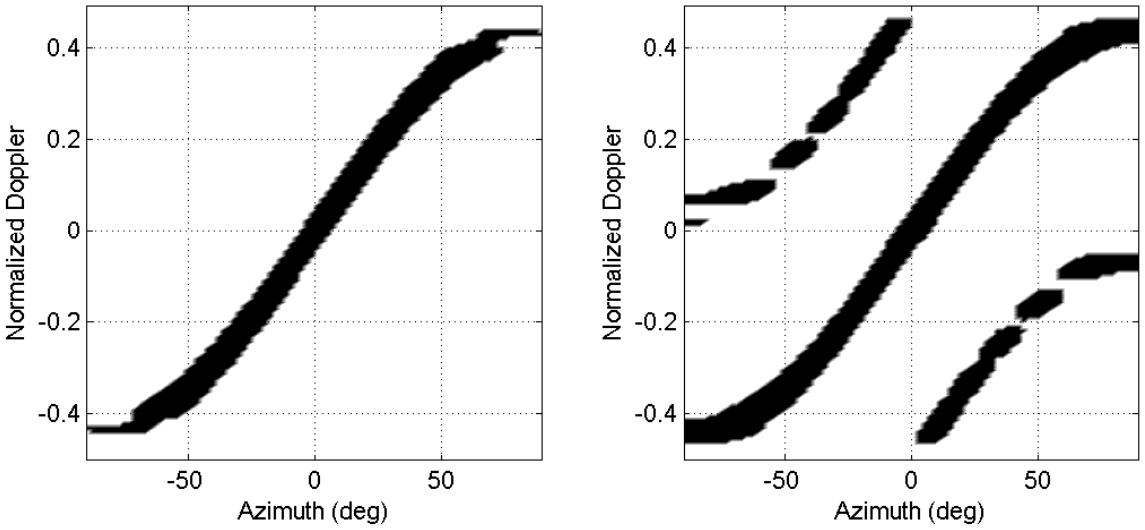

Figure 5.5: MVE for linear side-looking array. (a) Constant Frequency and (b) FDA, $\Delta f = 1$ kHz. The FDA is seen to have clutter at the same location as the constant frequency array in addition to locations not present for the constant frequency array.

cross-section of the range dependent antenna pattern, leading to multiple sinusoidal curves shown in Figure 5.5 (b).

Visual comparison of the two clutter spectra show the FDA has a larger azimuth-doppler domain proportion occupied by clutter, equivalent to an increased clutter rank as described in the next section. If the contribution from the ambiguous range clutter rings is removed, then the clutter spectra for the constant frequency and FDA SLAR are identical, since the target range terrain is illuminated identically.

5.4.2 Forward-Looking FDA Clutter Spectrum. The clutter spectrum for the linear constant frequency Forward-Looking Airborne Radar (FLAR) is more complicated than the side-looking orientation, however it can be derived from the known forward-looking doppler expression, given target range and hence elevation. The target range clutter ring produces an arc shaped clutter spectrum, since azimuth away from array boresight results in a reduced doppler value as predicted by the doppler frequency expression in Eqn. 2.8 and isodop plots in Chapter II.

Range ambiguous clutter rings produce a clutter spectrum that may be different to the target range arc, depending on the target range. At close range, within the range-doppler variation region seen in Figure 2.3, the ambiguous range clutter doppler is distinct from the target range clutter doppler and a separate arc will be produced. When the target range is sufficiently far, approximately six times the platform altitude, the ambiguous range clutter doppler approaches the target range doppler and only one arc will be present.

Additionally, only positive doppler values are represented because of back-lobe suppression implicit in the channel element pattern. The back-lobe eliminates the negative doppler values associated with clutter behind the aircraft.

The constant frequency array clutter spectrum for a target range of 10.5 km is seen in Figure 5.6 (a), where two arcs are blurred together because of insufficient doppler resolution to show the difference between normalized target range clutter doppler and normalized ambiguous range clutter doppler of $\bar{\omega} = 0.433$ and $\bar{\omega} = 0.450$, respectively. The separate arcs can be identified by the arc thickness, which is reduced when the target range clutter approaches ambiguous range clutter doppler.

As for the side-looking array, the forward-looking linear FDA clutter spectrum is identical to the constant frequency for the target range ring. However, a significantly different spectrum occurs from the ambiguous range clutter ring contribution, due to the range-dependent FDA antenna pattern. The different illumination of ambiguous range rings produces a clutter spectrum arc offset nearly 90° to the target range arcs, as seen in Figure 5.6 (b).

Again, the FDA clutter spectrum occupies a greater proportion of azimuth-doppler space than the constant frequency clutter spectrum, and therefore has increased rank. If the ambiguous range rings are removed, then the clutter spectrum is identical between the FDA and constant frequency because the target range illumination is the same.

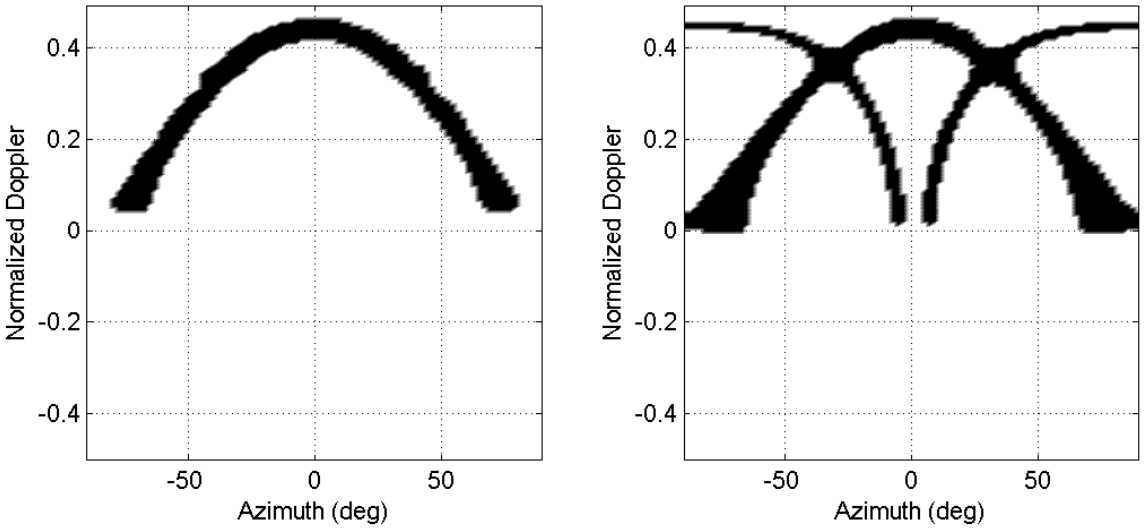

(a) (b)

Figure 5.6: MVE for Forward-Looking Array, Target Range of 10.5 km. (a) Constant Frequency and (b) FDA, $\Delta f = 1$ kHz. Similar to the side-looking array, the FDA is seen to have clutter at the same location as the constant frequency array in addition to locations not present for the constant frequency array.

5.4.3 Linear FDA Clutter Spectrum Analysis. The resulting clutter spectra for the side-looking and forward-looking linear FDAs share a striking resemblance to clutter spectra produced by spatially undersampled linear constant frequency arrays. Spatial undersampling occurs when the sensor spacing d exceeds the Nyquist frequency requirement

$$d = \frac{\lambda}{2}, \tag{5.6}$$

which is required to ensure no grating lobes exist [22]. When a sensor spacing of

$$d = \lambda \tag{5.7}$$

is selected, i.e., spatial undersampling, the resulting MVE can be observed from Figure 3.22 and Figure 3.23 for SLAR and FLAR, respectively, in [15]. Due to the graphical method selected, the comparison is easier using the IF in Figure 4.14 and Figure 4.15 of the same text.

The spatial undersampling clutter spectra referenced ignore the effect of range ambiguous clutter, which is not a problem for SLAR, and for distant targets in FLAR. Therefore, the effect of spatial undersampling for a constant frequency array with no ambiguous range clutter produces a similar clutter spectrum to FDAs when ambiguous range clutter is included. The similarity is logical since both undersampling and frequency diversity produce responses ambiguous in azimuth.

5.5 Linear FDA Clutter Rank Comparison

Space-time covariance matrix eigenvalue decomposition and analysis provides a method to quantify the difficulty of suppressing interference present. By examining the eigenvalue magnitudes, the amount of space occupied by the interference is determined. The result is equivalent to the interference scenario rank [15]. Interference scenario rank indicates the minimum Degrees of Freedom (DOF) required for any type of Space-Time Adaptive Processing (STAP) technique to fully suppress the interference and is of greatest importance when selecting partially adaptive STAP techniques. Clutter rank is another term for interference rank and is a common expression in the STAP community.

Since clutter rank is critical to the selection of appropriate STAP techniques, research has examined theoretical prediction of clutter rank from radar simulation parameters. Brennan [5] generated an expression that accurately predicts the clutter rank for constant frequency side-looking linear arrays. Currently, no equivalent expression exists for forward-looking arrays, largely due to the clutter rank being range-dependent when range ambiguous clutter is incorporated.

As briefly mentioned in the preceding clutter spectrum section, the greater the azimuth-doppler region occupied by clutter, the greater the clutter rank. The link exists because MVE is a power spectrum decomposition, whilst clutter rank calculation is an eigenvalue decomposition. Hence, both indicate the amount of clutter present.

Table 5.2: Side-Looking Array Clutter Rank Comparison.

Array Type	Range Ambiguities	No Range Ambiguities
Constant Frequency	133	133
Constant $\Delta f = 1$ kHz	389	133

5.5.1 Side-Looking Clutter Rank. A major benefit of using a constant frequency SLAR is range-independent clutter doppler along array boresight, therefore when transmitting along array boresight clutter rank remains constant whether or not range ambiguous clutter is incorporated. The clutter spectrum for the constant frequency SLAR in Figure 5.5 (a) reinforces clutter rank independence to range ambiguity inclusion.

Using Brennan's Rule [5] to predict the constant frequency array clutter rank,

$$\begin{aligned} \text{Rank} &\approx \lfloor N + (M-1)\,\beta \rfloor \\ &\approx \lfloor 11 + (128-1)\,(1) \rfloor = \lfloor 11 + 127 \rfloor = 138, \end{aligned} \tag{5.8}$$

where β is the number of inter-channel spacings crossed during a Pulse Repetition Interval (PRI) and is set to unity throughout this chapter. A comparison of SLAR clutter rank is included in Table 5.2 and there is a minor discrepancy between Brennan's Rule and the calculated clutter rank using `Matlab`®.

As predicted, Table 5.2 shows there is no difference between constant frequency and FDA when range ambiguities are not included. Also, there is no rank increase when range ambiguities are included for the constant frequency array since the azimuth transmission angle is along array boresight, $\phi = 0°$. For the side-looking FDA the range-dependent FDA antenna pattern results in range ambiguous clutter significantly increasing clutter rank.

Since there is no range dependence of ground clutter along array boresight, the SLAR clutter rank does not change based on target range for the constant frequency array when $\phi = 0°$. The FDA clutter rank has minimal dependence on target range

Table 5.3: Forward-Looking Array Clutter Rank Comparison. 10.5 km Target Range.

Array Type	Range Ambiguities	No Range Ambiguities
Constant Frequency	270	143
Constant $\Delta f = 1$ kHz	373	143

provided the FDA antenna pattern illumination of range ambiguous clutter is offset from target range illumination. With the above condition, the FDA has an almost constant clutter rank across target range because the illumination of the contributing clutter rings are effectively independent and are composed of the same number of eigenvectors.

5.5.2 Forward-Looking Clutter Rank. As observed for the forward-looking clutter spectrum, there is significant difference between the constant frequency array and FDA when ambiguous range clutter is included. However, since the antenna pattern is identical at the target range for both array types, the rank should be identical. Table 5.3 displays the difference in the clutter rank between constant frequency and FDA, both with and without ambiguous range clutter.

Since the critical characteristic of forward-looking arrays is the range-doppler dependence, the target range R or more specifically the ratio of target range to platform altitude H, impacts the clutter rank. Given a target range of 10.5 km, the $\frac{R}{H}$ ratio is approximately 3.5. Therefore, the range-doppler dependence is noticeable with distinct target and range ambiguous clutter doppler values. When the target range is increased to 66 km, a $\frac{R}{H}$ ratio of approximately 22, the target range doppler and ambiguous range doppler are near identical. The resulting clutter rank for the two different target ranges, both with and without ambiguous range clutter rings are shown in Table 5.4.

For the constant frequency array, increasing the target range to 66 km decreased the clutter rank as expected. The target range clutter doppler is now indistinct from

Table 5.4: Range Dependent Forward-Looking Array Clutter Rank Comparison.

Array Type	10.5 km	66 km
Constant Frequency (Range Ambiguities)	270	255
Constant Frequency (No Range Ambiguities)	136	143
Constant $\Delta f = 1$ kHz (Range Ambiguities)	373	395
Constant $\Delta f = 1$ kHz (No Range Ambiguities)	137	143

ambiguous range clutter doppler, equivalent to a shrinking arc width in the clutter spectrum shown in Figure 5.6 (a).

An increase in target range for the FDA showed an increase in clutter rank, the reason being the range-dependent FDA antenna pattern illuminates the ambiguous range clutter rings such that distinction between target range and range ambiguous clutter doppler is not the primary consideration. Therefore, regardless of the difference between target range and ambiguous range clutter doppler, the antenna pattern will likely result in different clutter spectrum location and hence higher clutter rank than constant frequency. Clutter rank for forward-looking FDA is relatively independent of range outside the range-doppler dependence region when ambiguous range clutter is included, as shown in Figure 5.7.

5.6 Planar FDA Antenna Pattern

The planar antenna pattern is a function of azimuth, range, and elevation, making antenna pattern magnitude visualization difficult. However, range and elevation are physically linked. Given the platform altitude, pitch, and transmit elevation angle, elevation angles can be converted into ranges and vice-versa.

5.6.1 Constant Frequency Array. A constant frequency planar array pattern is relatively easy to consider, since the antenna pattern expression does not change over range. Therefore, an azimuth versus elevation plot captures all pattern characteristics, though it is useful to convert elevation to range to examine range ambiguous impact. When the aforementioned array dimensions in Table 5.1 are used, the result-

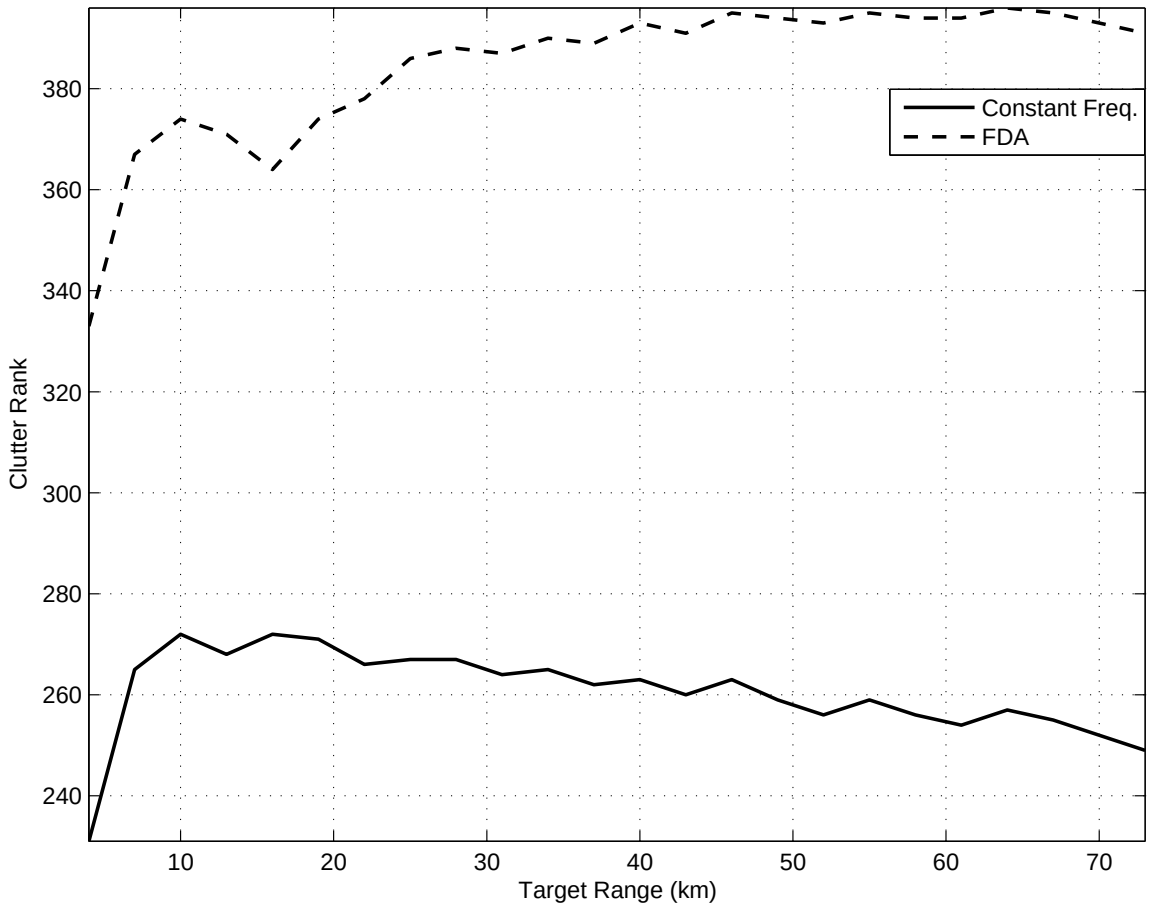

Figure 5.7: Clutter rank over target range for forward-looking linear arrays. *Beyond 30 km* the FDA clutter rank is seen to be relatively independent of target range, whilst the constant frequency array clutter rank steadily decreases as target range is increased. The decrease in constant frequency clutter rank corresponds to the reduction between target range clutter doppler and range ambiguous clutter doppler.

ing array pattern is seen in Figure 5.8 (b). The pattern is symmetric in both azimuth and elevation. However, since N and P are different, there is no central symmetry.

It is important to re-emphasize that the term elevation has already been defined in the radar data model generation. Elevation angle θ is measured from array boresight. Therefore, with a level platform, an elevation angle of 0° is aimed at the horizon. Confusion can occur when the array is steered toward the ground, since the transmitted mainbeam is at an elevation relative to the array boresight. The same azimuth-elevation pattern is used in the ground illumination scenario, however now the elevation scale needs to be shifted so the mainlobe is at the appropriate target range elevation angle rather than at 0°.

Critical to the antenna pattern analysis is the expression for the elevation angle

$$\theta = -\sin^{-1}\left[\frac{R^2 + H\left(H + 2R_{\text{eff}}\right)}{2R\left(H + R_{\text{eff}}\right)}\right], \tag{5.9}$$

where R is the range, H is the platform altitude, and R_{eff} is the effective Earth radius. The sinusoidal relationship results in a majority of ranges covering only a small elevation swath with the greatest concentration just below the horizon, $\theta = 0^\circ$.

Due to the elevation angle compression versus range, it is beneficial to analyze the antenna pattern as it is projected onto the ground, seen in Figure 5.8 (a). The image is constructed by calculating the elevation angle corresponding for each range and then including the appropriate antenna pattern cross-section response at that range. Since the constant frequency array is range-independent, only one azimuth-elevation pattern is required to build the antenna pattern ground projection image.

The limitation in displaying the elevation pattern impact over range in Figure 5.8 is the compression of elevation angles near the radar horizon. To better highlight the pattern illumination of range ambiguous clutter rings, the ground projection is recalculated using a linear range axis, out to the radar horizon of 228 km and is shown in Figure 5.9.

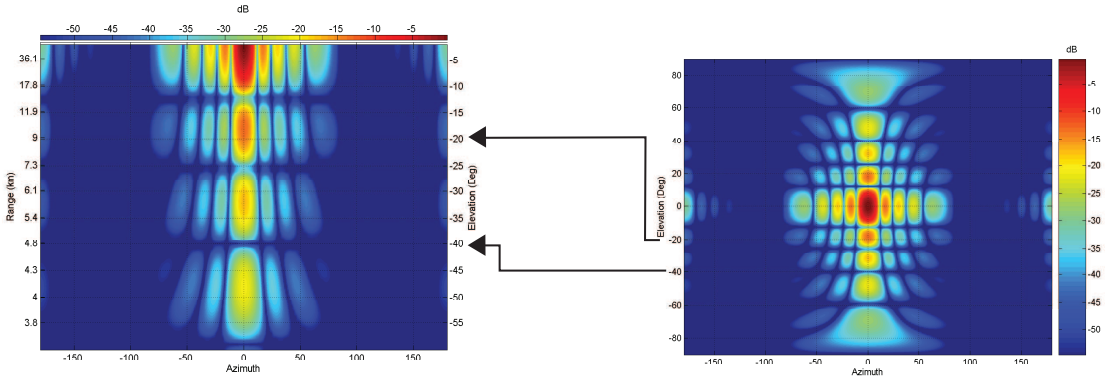

(a) (b)

Figure 5.8: Constant frequency planar array at an altitude of 3073 m and horizontal elevation transmission ($\theta = 0°$): (a) ground projection with linear elevation axis and (b) azimuth-elevation antenna pattern. The constant frequency array ground projected antenna pattern is seen to be based on one azimuth-elevation antenna pattern, with the elevation angle being transformed into appropriate range based on platform height, pitch and elevation transmit angle.

5.6.2 Planar FDA. The FDA antenna pattern has range-dependency, impacting the ability to generate the antenna pattern ground projection. In addition to determining the elevation angle corresponding to each range, the difference between the range under test and the steered to target range, $R - R_0$, must also be considered. The latter component is essential because it defines the azimuth-elevation pattern appropriate for that particular elevation, as seen from Eqn. 3.5.

Based on the above observation, the planar FDA antenna pattern is dependent on the particular platform and target parameters, compounding the difficulty of planar FDA analysis. Using an altitude of 3073 m, elevation transmit angle of 0°, i.e. horizontal elevation transmission, and target range of 10.5 km, the ground projected antenna pattern is seen in Figure 5.10 (a).

The ground projection generation relies on a unique azimuth-elevation plot at each range. At each range, the elevation is calculated and the cross-section taken from the appropriate plot, as shown in Figure 5.10 (b). Figure 5.10 highlights the azimuth-elevation pattern at the target range is identical to the constant frequency

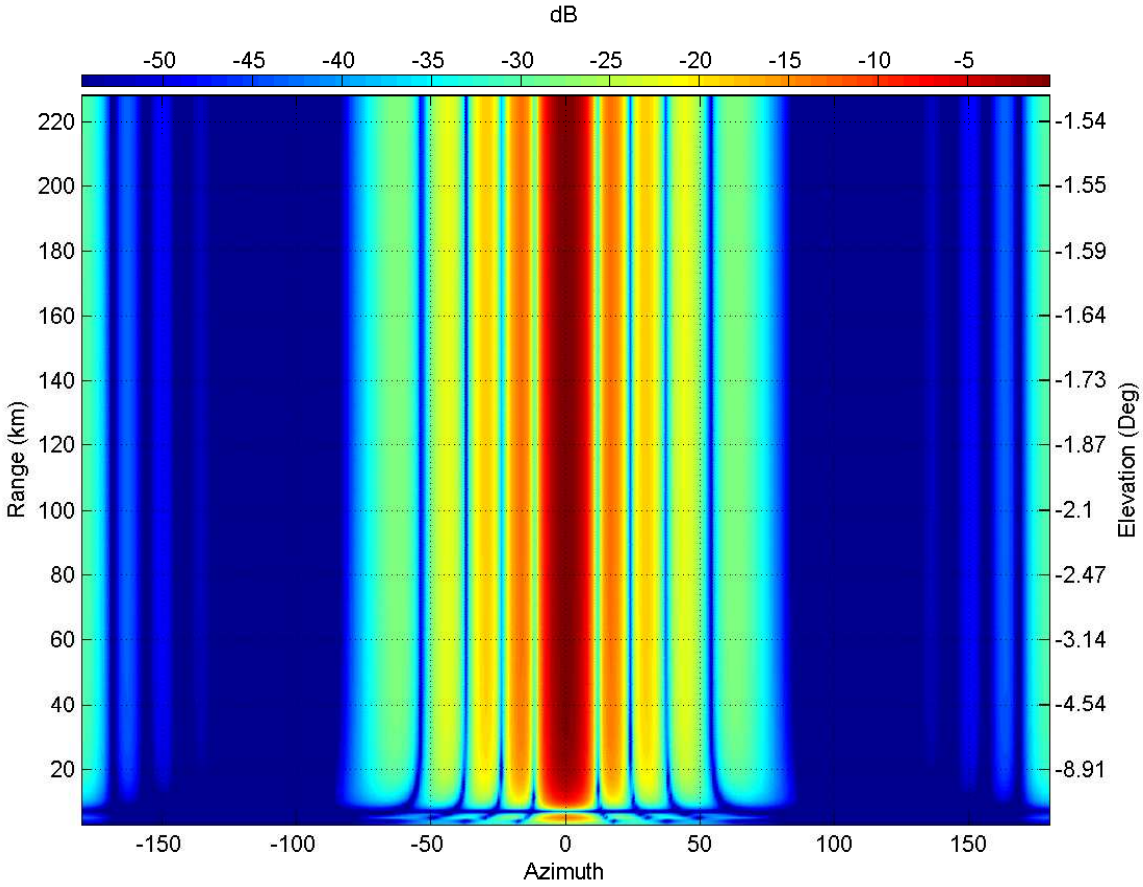

Figure 5.9: Constant frequency planar array antenna pattern ground projection using a linear range axis. When compared to the previous figure, it is seen there is a compression of elevation angles near the horizon because of the sinusoidal relationship between range and elevation angle.

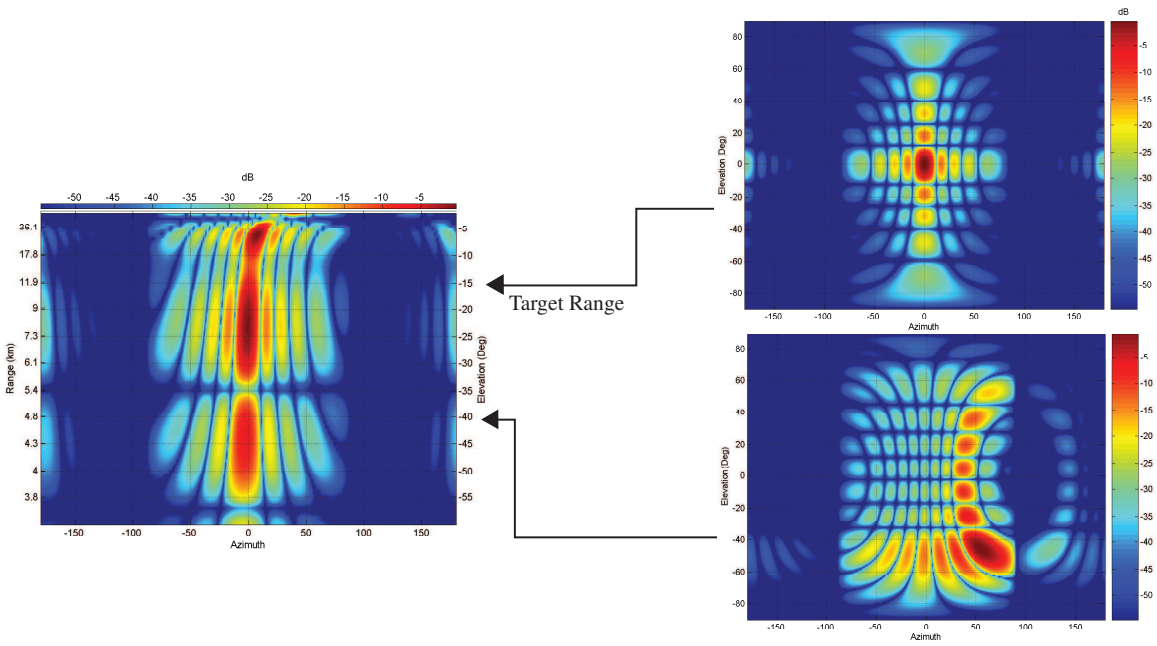

(a) (b)

Figure 5.10: Planar FDA with constant frequency increments of $\Delta f_x = 1$ kHz and $\Delta f_z = 2$ kHz. Platform altitude of 3073 m, horizontal elevation transmission and target range of 10.5 km. (a) ground projection with linear elevation axis and (b) range-dependent azimuth-elevation antenna patterns. The FDA ground projected antenna pattern is seen to be based on multiple azimuth-elevation antenna patterns, with each elevation angle transformed into a corresponding range and combined with the difference away from the target range, $R - R_0$.

array pattern, as proved in Chapter III, and also shows that at ranges away from the target range the corresponding antenna pattern can vary significantly.

Again, it is noted that the term elevation for the azimuth-elevation plots in Figure 5.10 (b) is based on angle from array boresight. If the elevation transmit angle is not 0°, then a scale offset is required. The elevation angle expression Eqn. (5.9) again produces the compression of elevation angle against range near the horizon, in addition to range difference $R - R_0$ being a non-linear function of elevation.

Additionally, to better highlight the differences between the constant frequency and planar FDA antenna patterns, the ground projection is also shown using a linear range axis out to the radar horizon shown in Figure 5.11. When compared to the constant frequency equivalent in Figure 5.9, shows antenna pattern bending in azimuth

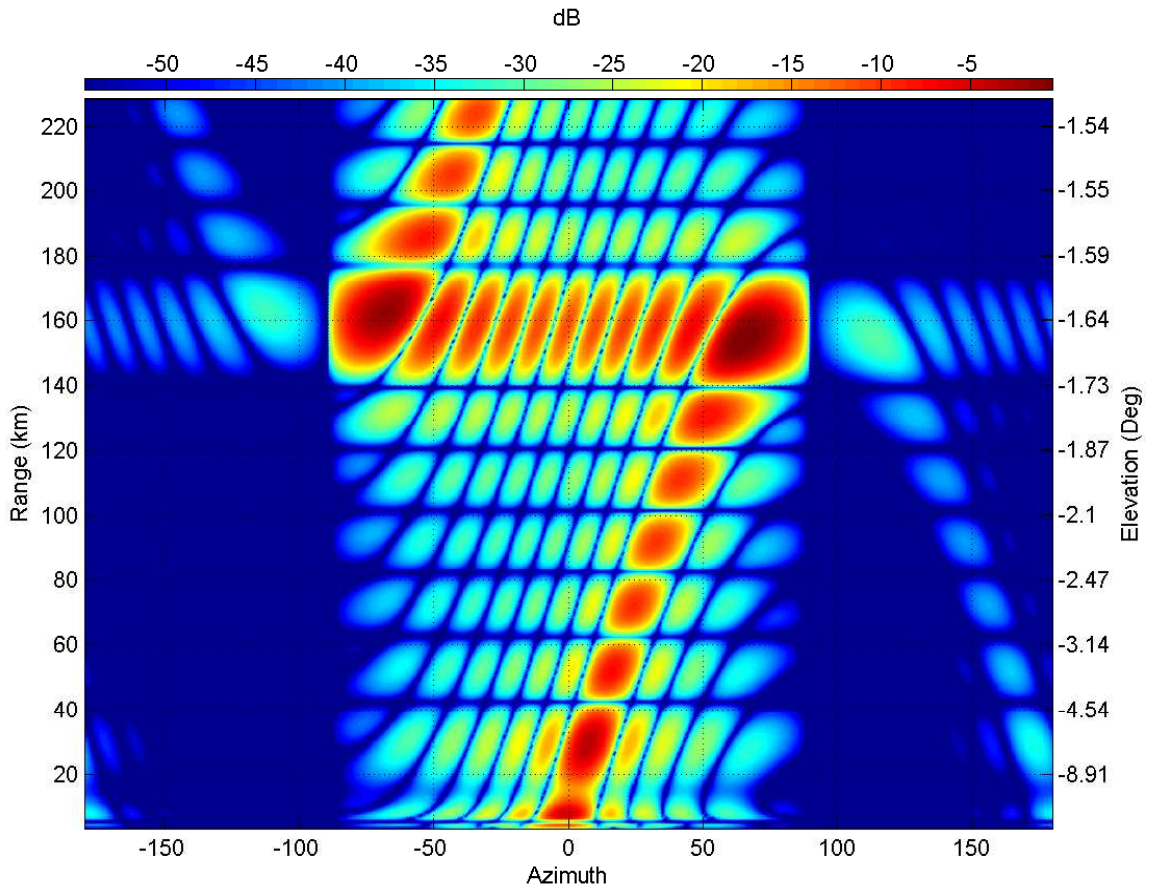

Figure 5.11: Planar FDA antenna pattern ground projection with constant frequency increments of $\Delta f_x = 1$ kHz and $\Delta f_z = 2$ kHz, platform altitude of 3073 m, horizontal elevation transmission and target range of 10.5 km. The antenna pattern ground projection using a linear range axis shows the compression of elevation angles near the horizon because of the sinusoidal relationship between range and elevation angle.

and also far range elevation null locations due to frequency diversity across vertical array channels.

5.7 Planar FDA Clutter Spectrum

There are two distinct ways to consider the clutter spectrum for a planar array. Firstly, by examining the location within the doppler, azimuth spatial frequency and elevation spatial frequency domain. The clutter location is determined by the solution

for the ground doppler relation, which for the constant frequency array is

$$f_d = \frac{2v_r}{\lambda}\sqrt{1-\cos^2(\theta)\sin^2(\phi)-\sin^2(\theta)}, \tag{5.10}$$

where v_r is the relative target velocity, λ the wavelength and the result is an ellipsoidal bowl, as mentioned in Chapter II.

The resulting ellipsoidal clutter surface is used by Richardson [20] and also Herbert [12], to analyze the effect of platform motion. Additionally, the clutter bowl offers insight to the difficulty of suppressing clutter at close target ranges, i.e., toward the base of the clutter bowl rather than the rim.

The other way to display the clutter is to consider multiple azimuth-doppler domains, each cut at a distinct elevation angle corresponding to either the target range or a range ambiguous clutter ring. Whilst there are three dimensions, the azimuth-doppler is still the most important, particularly since the range ambiguous clutter rings can now be eliminated through vertical nulling.

Although the ellipsoidal bowl is useful to highlight some features, the focus within this chapter is on the multiple elevation cross-cuts and seeing the differences between the range ambiguous clutter spectra. The focus is on ambiguous range spectrum because of identical antenna pattern illumination at the target range.

5.7.1 Planar SLAR Clutter Spectrum. The three individual azimuth-doppler cuts for the constant frequency array are shown together in Figure 5.12. It is observed that the target range clutter ring has a slightly different clutter spectrum, compared to the ambiguous range clutter rings. This effect is a byproduct of display thresholding combined with the large target range elevation angle, $\theta = -50^\circ$ impacting clutter doppler away from array boresight.

The equivalent clutter spectrum for the planar side-looking FDA, shown in Figure 5.13, is considerably different to the constant frequency array result. The

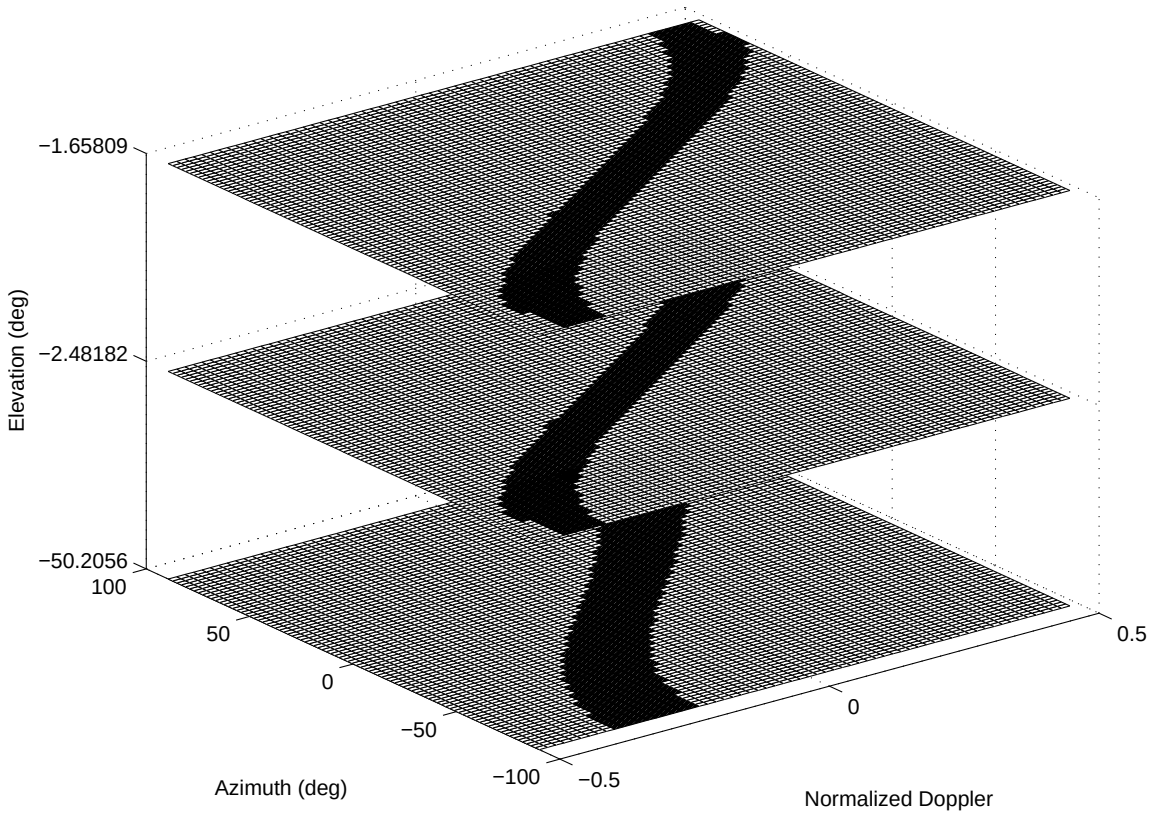

Figure 5.12: MVE for planar side-looking constant frequency array shows the clutter spectrum at the target range of 4 km (bottom surface) and the two range ambiguous clutter rings are very similar.

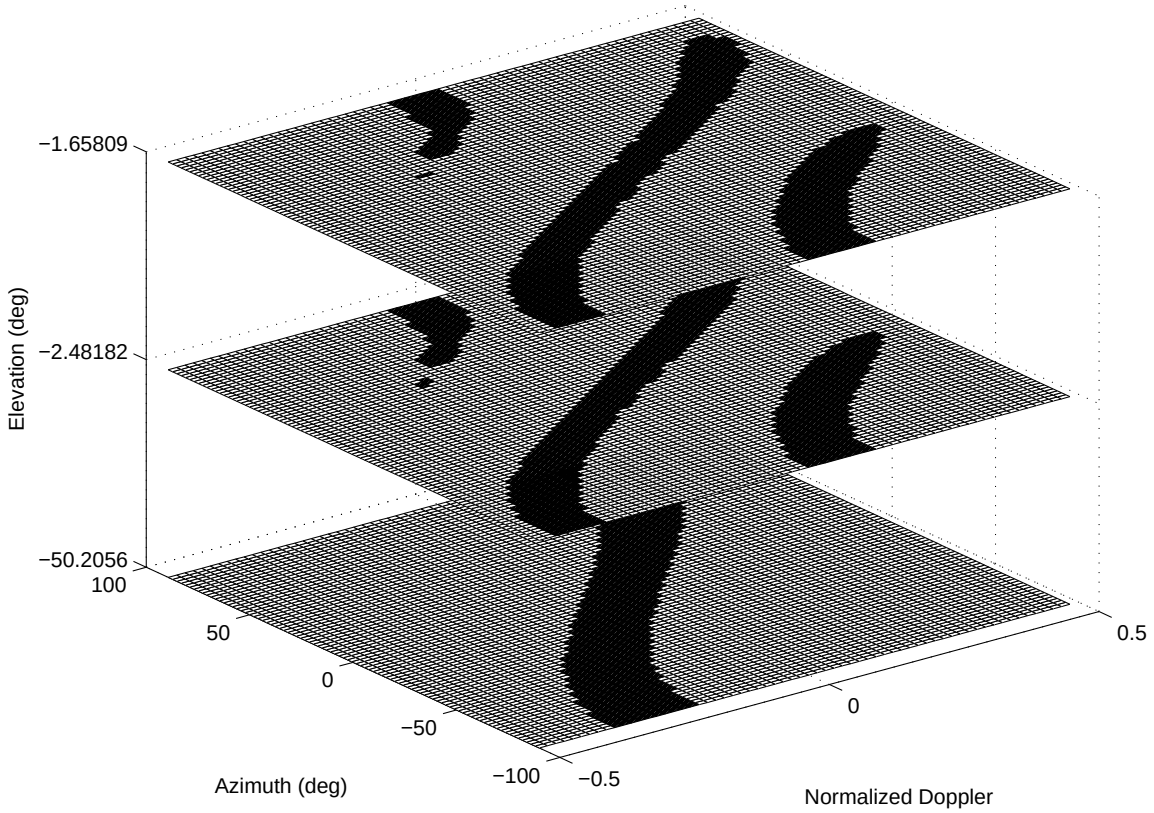

Figure 5.13: MVE for planar side-looking frequency diverse array shows the clutter spectrum at the target range of 4 km (bottom surface) differs to the two range ambiguous clutter rings. Additionally, the target range clutter spectrum is identical to the constant frequency array target range clutter spectrum.

difference is constrained to the spectrum for the range ambiguous clutter rings as expected and is due to the range-dependent FDA antenna pattern.

An important observation is the difference between the linear and planar forward-looking FDA spectra. The planar FDA does not have the additional spectra arcs fully formed because the antenna pattern illumination of range ambiguous clutter rings changes across elevation, as highlighted in Figure 5.11. Conversely, the linear FDA has the same illumination at different elevation angles without the nulls seen in Figure 5.11.

5.7.2 Planar FLAR Clutter Spectrum. When the array orientation is changed to forward-looking, the three individual azimuth-doppler plots for the constant fre-

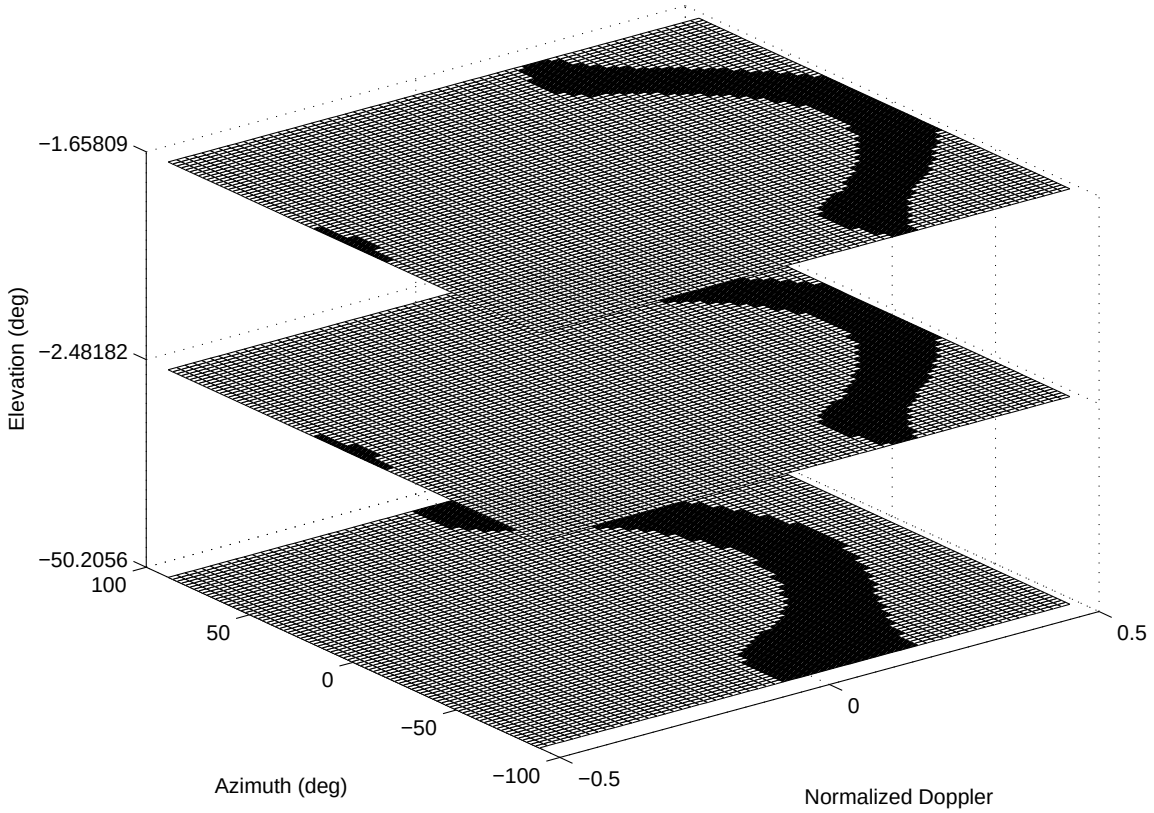

Figure 5.14: Minimum Variance Estimator for planar forward-looking constant frequency array at a target range of 4 km, showing the target range clutter spectrum (bottom surface) differs to the clutter spectrum at the two range ambiguous clutter rings. The difference in clutter spectrum is caused by the difference in target range clutter doppler and range ambiguous clutter doppler.

quency array are shown together in Figure 5.14. It is important to note that the target range is changed from 10.5 km in the linear FDA to 4 km in order to increase the clutter doppler difference between the target and range ambiguous clutter rings. Due to the reduced target range, the target range clutter ring has a different clutter spectrum compared to the two range ambiguous clutter rings spectra.

The equivalent clutter spectrum for the planar forward-looking FDA is shown in Figure 5.15. The target range is kept at 4 km to allow comparison with the constant frequency array and again the target range clutter spectrum is identical because of equal antenna pattern illumination.

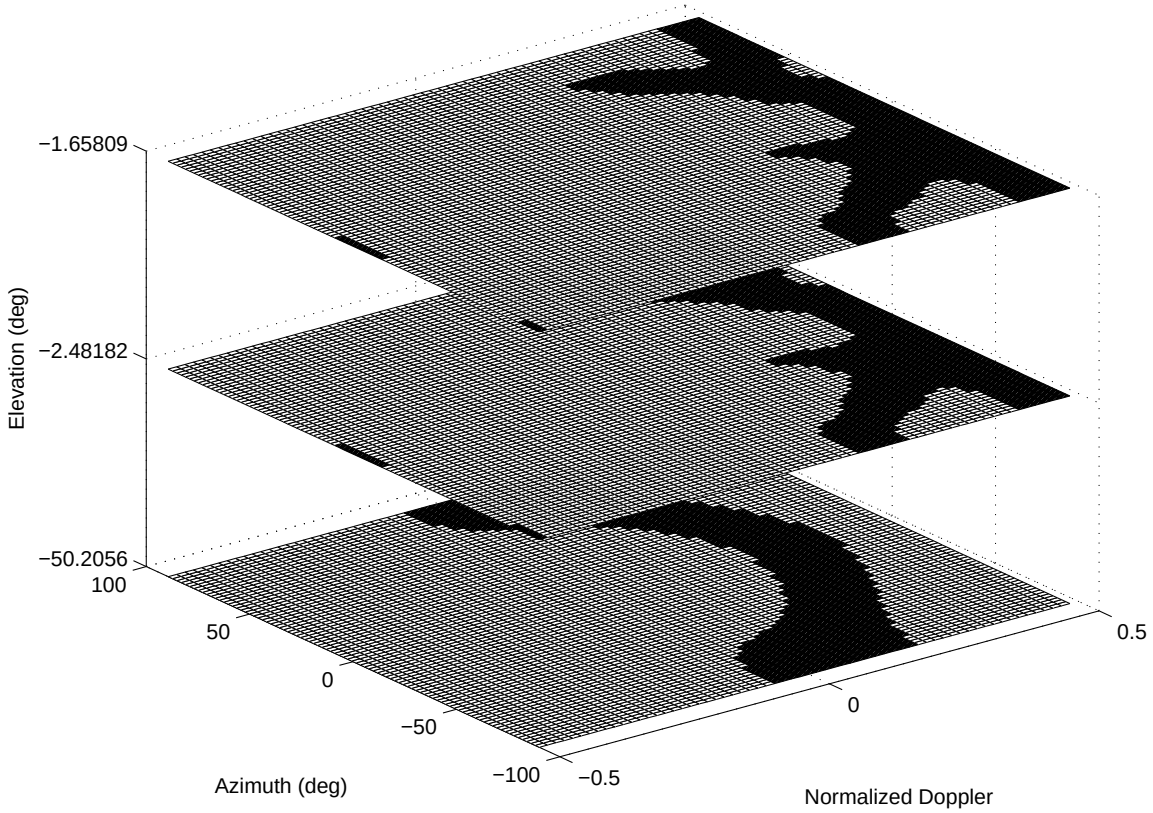

Figure 5.15: Minimum Variance Estimator for planar forward-looking FDA at a target range of 4 km, showing the target range clutter spectrum (bottom surface) differs to the clutter spectrum at the two range ambiguous clutter rings. The clutter spectrum difference is caused partly by the difference between target range clutter doppler and range ambiguous clutter doppler and also partly by the range-dependent FDA antenna pattern. Since the FDA antenna pattern is equivalent to the constant frequency antenna pattern at the target range, the target range clutter spectrum is identical to the constant frequency array target range clutter spectrum.

As for the linear FDA, the planar FDA range ambiguous clutter rings have a considerably different clutter spectra to the constant frequency planar array. Additionally, the spectra at the range ambiguous rings is different to the linear forward-looking FDA because of elevation dependent nulls. Hence, the additional arcs are not fully formed, same as for the side-looking planar FDA.

5.8 Planar FDA Clutter Rank

Brennan's Rule [5] was developed based on a linear array with only one vertical channel. Extension of clutter rank estimation for planar side-looking arrays has been proposed by Corbell [7], when β is integer. Substituting the parameter values given in Table 5.1,

$$\begin{aligned} \text{Rank} &\approx \min(P, 1+N_r)\left[\lfloor N+(M-1)\,\beta \rfloor\right] \\ &= \min(8, 1+2)\left[\lfloor 11+(16-1)\,(1) \rfloor\right] \\ &= 3\left[\lfloor 11+15 \rfloor\right] = (3)(26) = 78, \end{aligned} \tag{5.11}$$

where N_r is the number of ambiguous clutter range rings and $1+N_r$ is the total number of contributing clutter range rings.

When range ambiguities are excluded ($N_r = 0$) the expected clutter rank is

$$\begin{aligned} \text{Rank} &\approx \min(P, 1+N_r)\left[\lfloor N+(M-1)\,\beta \rfloor\right] \\ &= \min(8, 1+0)\left[\lfloor 11+(16-1)\,(1) \rfloor\right] = (1)(26) = 26, \end{aligned} \tag{5.12}$$

indicating planar array clutter rank is independent of number of vertical array channels P when range ambiguous clutter is ignored. The result is intuitive, since there is only one elevation angle corresponding to the target range ring and the number of vertical channels does not contribute.

The above clutter rank expression is only valid for SLAR and does not indicate FLAR clutter rank. Additionally, the proposed formula provides knowledge that the

Table 5.5: Side-Looking Array Clutter Rank Comparison for 10.5 km Target Range.

Array Type	Range Ambiguities	No Range Ambiguities
Constant Frequency	75	26
Constant $\Delta f_x = 1$ kHz, $\Delta f_z = 2$ kHz	78	26

SLAR clutter rank when range ambiguities clutter contributions are included will now have some range dependency because the target range can potentially impact the number of ambiguous range rings for a fixed platform altitude.

5.8.1 Planar SLAR Clutter Rank. As mentioned above, target range now has an impact on the clutter rank through the number of ambiguous range rings present. However, for a platform altitude of 3073 m, the number of ambiguous range clutter rings is the same for target ranges of 10.5 km and 66 km. Therefore, the clutter rank should be equal between the two.

The comparison of clutter rank for the selected target range of 10.5 km is shown in Table 5.5, showing that the clutter rank is accurately predicted when range ambiguous clutter rings are not considered. The inclusion of range ambiguous clutter rings resulted in a minor discrepancy between the expected rank of 78 and the `Matlab`® calculated rank of 75. The difference is small and it is expected the eigenvectors associated with ambiguous range clutter rings are not independent. Therefore, each clutter ring did not contribute a clutter rank of 26.

5.8.2 Planar FLAR Clutter Rank. Whilst there is no equivalent formula to estimate the clutter rank for forward-looking planar arrays, the same idea can be applied with regards to minimum of number of vertical channels P and total number of contributing clutter rings $1 + N_r$.

Table 5.6 shows the comparison of FLAR clutter rank at a target range of 10.5 km. It is observed the clutter rank of the two array types is equal when range ambiguous clutter is excluded. When range ambiguous clutter is included, the FDA

Table 5.6: Forward-Looking Array Clutter Rank Comparison for 10.5 km Target Range.

Array Type	Range Ambiguities	No Range Ambiguities
Constant Frequency	101	37
Constant $\Delta f_x = 1$ kHz, $\Delta f_z = 2$ kHz	99	37

Table 5.7: Range Dependent Forward-Looking Planar Array Clutter Rank Comparison.

Array Type	10.5 km	66 km
Constant Frequency (Range Ambiguities)	101	88
Constant Frequency (No Range Ambiguities)	37	37
Constant $\Delta f_x = 1$ kHz, $\Delta f_z = 2$ kHz (Range Ambiguities)	99	100
Constant $\Delta f_x = 1$ kHz, $\Delta f_z = 2$ kHz (No Range Ambiguities)	37	37

has a higher clutter rank, indicating a greater amount of competing interference caused by the additional arcs observed in Figure 5.15 compared to Figure 5.14.

The addition of range ambiguous clutter does not seem to be a multiplication of clutter rank as observed for SLAR, indicating ambiguous clutter rings do not contribute independent vectors. Since the total clutter rank is less than a multiplication by the number of contributing clutter rings, some eigenvectors associated with the range ambiguous clutter rings are common with the target range clutter.

However, it is important to check whether the planar FLAR clutter rank is target range dependent, as is found to occur for linear FLAR rank. Evaluating the clutter rank for a target range of 66 km and comparing to results achieved at 10.5 km, it is seen in Table 5.7 that some range dependence of rank exists.

It is surprising the planar FDA has a lower clutter rank than the constant frequency array at reduced target range. The reason for the reduced rank is partly attributable to the close target range having a target range clutter doppler distinct from range ambiguous clutter doppler. The other contributing reason for the clutter rank difference is the elevation dependent nulls that exist for the planar FDA but not for the constant frequency array.

For the constant frequency array, when ambiguous range clutter is not included, there is no difference in rank. When ambiguous range clutter is included, there is a noticeable rank increase for the short target range because the ambiguous range clutter rings have a different clutter doppler and hence spectrum, increasing the number of independent eigenvectors across the target and ambiguous range rings.

In contrast, the planar FDA shows minimal variation with a change in the target range. The different illumination of ambiguous range clutter rings by the FDA antenna pattern results in a total clutter rank about the same at each target range since the distinction between target range and range ambiguous clutter doppler is less important. Forward-looking FDA clutter rank has a reduced dependence on target range when range ambiguous clutter is included, as verified in Figure 5.16.

5.9 Summary

Chapter V investigated the impact of FDA use on clutter spectrum and clutter rank for both side-looking and forward-looking arrays. The radar parameters used to characterize the FDA impact are introduced in Section 5.1. Section 5.2 defined the frequency allocation across array channels, a critical component of FDA performance, with two approaches to assess frequency diversity selection detailed in Appendix A.

The next few sections focused on linear FDA impact, starting with an investigation into the antenna pattern for various frequency progressions in Section 5.3. Based on a frequency progression deemed acceptable, the impact on clutter spectrum location within the azimuth-doppler domain is shown in Section 5.4. Section 5.5 confirmed an increase in clutter location within the clutter spectrum corresponds to an increase in clutter rank.

The remainder of the chapter focused on the planar array comparison. Due to the interdependence between range and elevation, the antenna pattern is more difficult to visualize. Section 5.6 discussed these ground projected planar array pattern nuances. Section 5.7 and Section 5.8 compared the planar FDA clutter spectrum and

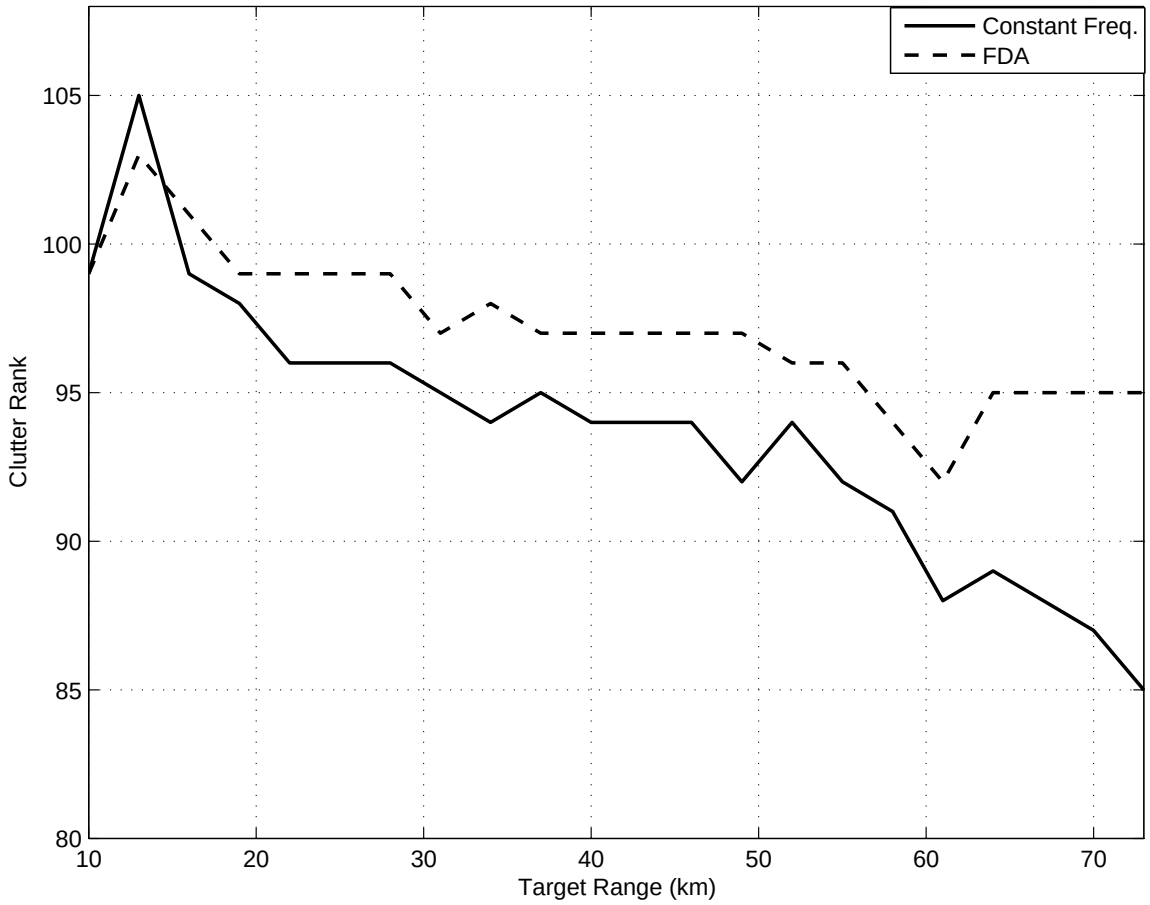

Figure 5.16: Clutter rank over target range for forward-looking planar arrays shows the constant frequency array clutter rank is more dependent on target range than the FDA, following the same trend observed for the linear array clutter rank comparison.

clutter rank, respectively, to the planar constant frequency array. The only difference from the linear results is that the clutter spectrum now has the ability to isolate the impact of each contributing clutter ring through elevation information.

VI. Linear Frequency Diverse Array Results

This chapter compares the performance of linear constant frequency and Frequency Diverse Arrays (FDAs), with focus on Forward-Looking Airborne Radar (FLAR) Space-Time Adaptive Processing (STAP). A critical aspect of performance evaluation is the selection of channel frequencies and hence FDA antenna pattern. Whilst two different approaches are proposed to evaluate selected channel frequency selection in Appendix A, there is currently no method to determine optimal channel frequencies and the same frequency progression as Chapter V is used.

Results are presented using four different engagement scenarios, with each scenario based on a physical situation of interest. The four scenarios are characterized by the combination of two critical simulation parameters; platform altitude and transmit elevation angle, with the impact of both parameters analyzed. The four physical situations are detailed in Section 6.2 and evaluated using the performance metrics introduced in Chapter II.

6.1 Radar Simulation Parameters

In order to conduct simulations, radar and target parameters need to be defined. The parameters selected for this chapter, generally follow the Multiple-Channel Airborne Radar Measurement (MCARM) program [24], with the major exception being use of one vertical channel, in order to be a linear array. The parameters used for the results contained in this chapter are summarized in Table 6.1, unless specifically noted otherwise.

It is noted that some variables included in Table 6.1 have multiple values. Different N and M values allow comparison of fully and partially adaptive STAP within sample support restrictions. Two target ranges are used to correspond to two different platform altitudes and there are multiple ground clutter doppler values to evaluate performance within appropriate clutter doppler notches. The value selected in each section is made clear within the text and the appropriate method of result presentation.

Table 6.1: Linear Array Radar Simulation Parameters.

Variable	Value
M (Pulses in CPI)	32, 8
N (Azimuth Channels)	11, 8
P (Vertical Channels)	1
Coherent Processing Interval (CPI) Gain	352, 64
f_0 (Carrier Frequency)	1240 MHz
f_r (Pulse Repetition Frequency)	1984 Hz
τ (Pulse Width)	0.8 μs
P_t (Transmit Power)	200 kW
B (Bandwidth)	800 kHz
F_n (Noise Figure)	3 dB
N_C (Azimuth Clutter Samples)	CPI
v_a (Aircraft Velocity)	$\frac{d_x f_r}{2}$
R (Target Range)	10.5 km, 8.0 km
Array Transmit Gain	18 dB
Element Pattern	Cosine
Element Gain	4 dB
Element Backlobe Level	-30 dB
d_x (Azimuth Inter-element Spacing)	0.1092 m
L_S (System Transmit Losses)	3 dB
Target ϕ	0°
Target $\bar{\omega}$	Various

It is again stressed that the frequency progression of $\Delta f = 1$ kHz between successive array channels has not been defined as an optimal selection, however it does indicate the potential benefits possible for linear FDAs.

6.2 Physical Scenario Definitions

Whilst many critical radar and target parameters are included in Table 6.1, it is important to consider the physical scenario whose performance is to be simulated. As mentioned at the start of this chapter, each physical scenario is characterized by platform altitude and elevation transmit angle.

The two platform altitudes are based on representative radar platform types, for low altitude, the platform is an Unmanned Aerial Vehicle (UAV) and for high altitude, the platform is an Airborne Early Warning And Control (AEWAC) aircraft.

The platform altitude is critical since it affects the doppler-range dependence of range-cells and hence the FDA antenna pattern required to accentuate isodops. Additionally, platform altitude determines the radar horizon range and hence the number of range ambiguous clutter rings. With an altitude of 3073 m, the radar horizon is 228 km and for nearly all target ranges there are two ambiguous range clutter rings. At an altitude of 334 m, the radar horizon drops to 75 km, which corresponds to the radar Maximum Unambiguous Range (MUR) and thus no range ambiguous clutter exists.

The second parameter is the elevation transmit angle, where the two distinct values represent airborne and ground radar modes. Firstly, for the detection of an airborne target the transmit angle is set to 0° and the beam points at the horizon, i.e. co-altitude to the radar platform. The second transmit angle applies for a ground target and therefore the specific elevation transmit angle is dependent on the platform altitude and target range. Both transmit angles assume that the array orientation is level, i.e. there is no platform pitch.

Table 6.2: Scenario Parameter Combinations.

Name	Platform Altitude (H)	Elevation Angle (θ)
AEWAC with Airborne Target	High (3073m)	0°
AEWAC with Ground Target	High (3073m)	-17.0° for 10.5 km Range
UAV with Hovering Helicopter	Low (334m)	0°
UAV with Ground Target	Low (334m)	-2.4° for 8.0 km Range

Co-altitude airborne targets will vary between each platform, for AEWACs it may be fighter aircraft, whilst for UAVs it is more likely to be hovering helicopters. The anticipated ground targets are identical for both platform types and include tanks, tracked vehicles or in the changing asymmetrical combat environment, jeeps and private motor vehicles.

The four combinations resulting from the two scenario parameters are summarized in Table 6.2. Each scenario will be discussed in greater detail, and any benefits of using a linear FDA compared to a standard constant frequency linear array reviewed.

The approach taken toward performance analysis starts with Output SINR calculation, first using the known interference covariance matrix and secondly using an estimated covariance matrix to examine the degradation using non Independent and Identically Distributed (iid) sample support vectors. The Output SINR performance across the normalized doppler range using estimated interference covariance matrices, can then be compared with Probability of Detection P_d curves at target doppler values of interest. The P_d results are based on a Probability of False Alarm P_{fa} of 0.01 and therefore each simulation involves 1000 realizations.

There are a number of considerations involved when an estimated interference covariance matrix is used. Firstly, the method of generating the matrix estimate, or more specifically the method of sample support data vector selection needs to be defined. Secondly, using the parameters in Table 6.1, the Coherent Processing Interval (CPI) gain is too large to allow sufficient sample support to meet Reed's Rule for fully

adaptive STAP. The same sample support limitation is imposed for the generation of P_d plots, since they are also based on estimated interference covariance matrices.

There are two ways to resolve the conflict between CPI gain and sample support requirements, firstly using a partial STAP technique, in this chapter using Joint Domain Localized (JDL) with a total of 64 Degrees of Freedom (DOF) of 352 DOF available. The other approach is to reduce the CPI gain size by using a smaller array, $N = 8$ and integrating fewer pulses, $M = 8$, where sufficient sample support vectors exist within the range-cells of range-doppler dependence at high platform altitude. The benefit of a reduced CPI size is the ability to assess Adaptive Matched Filter (AMF) results, which avoid any differences associated with the increased FDA clutter rank, since the clutter is not full rank.

6.3 AEWAC with Airborne Target Results

Despite recent increased interest in ground-target detection, the high-altitude platform and high-altitude target is still the most common scenario in STAP research given the historical foundation of STAP as an improvement to airborne clutter suppression. The high-altitude platform is also the approach taken in Chapter V when analyzing the FDA impact and therefore is the first scenario evaluated.

As described in the preceding section, a high platform altitude results in an increased radar horizon and hence allows contribution from range ambiguous clutter rings, leading to potentially multiple clutter doppler values. Therefore, the constant frequency array performance will vary across target range, depending on whether or not there are two distinct clutter doppler notches. Since the focus of this thesis is increasing sample-support data homogeneity and the region of greatest range-doppler dependence occurs at close range, the selected target range is 10.5 km to be within the range-doppler dependence region.

The Output SINR using a known interference covariance matrix based on the target range is seen in Figure 6.1. The results include both the Matched Filter (MF)

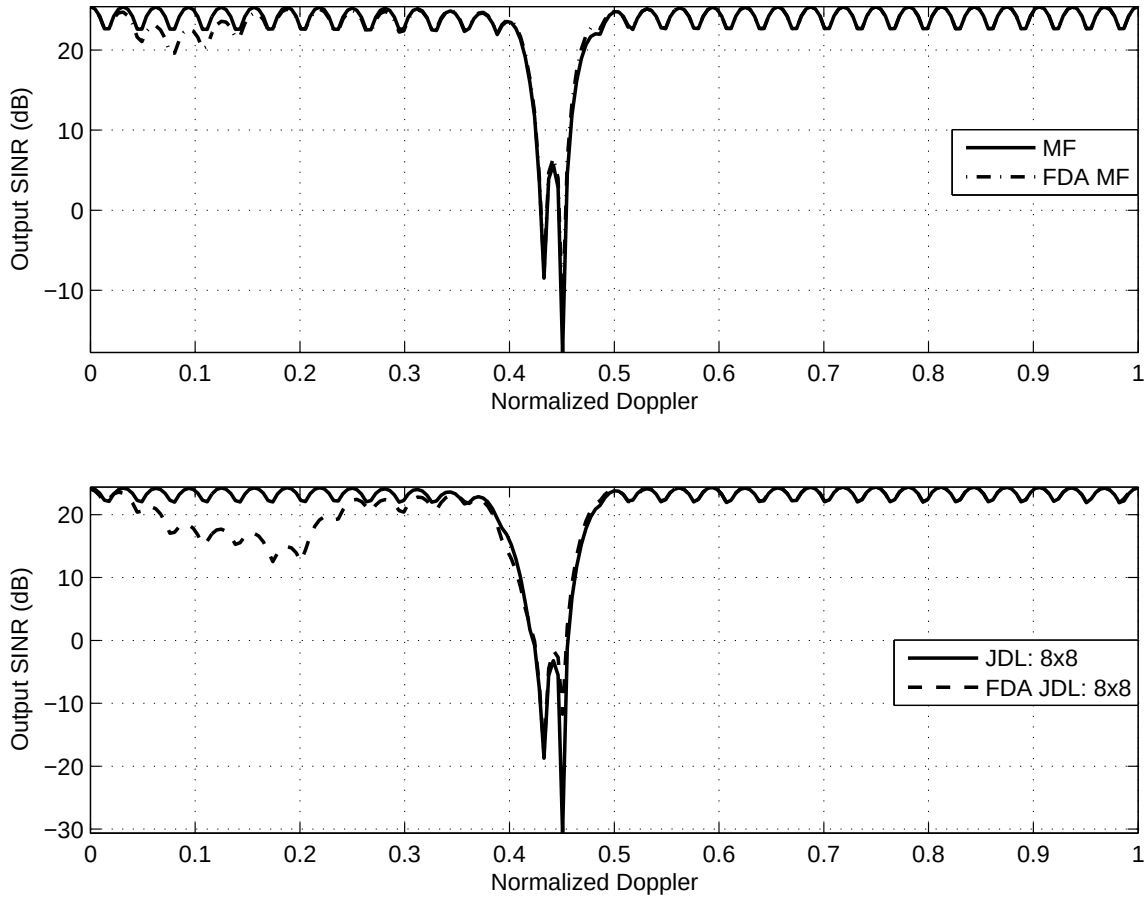

Figure 6.1: High-altitude platform, horizontal elevation transmission Output SINR using known interference covariance matrix at a target range of 10.5 km, showing two distinct clutter doppler notches. The FDA Output SINR has a reduced range ambiguous clutter ($\bar{\omega} = 0.450$) notch depth at the expense of increased degradation at other doppler values away from the clutter notch.

and partially adaptive JDL, the latter specifically to allow comparison when the interference covariance matrix is estimated. Both the constant frequency and FDA have two distinct clutter doppler notches, corresponding to target range clutter doppler $\bar{\omega} = 0.433$ and range ambiguous clutter doppler $\bar{\omega} = 0.450$.

It is noted that the FDA MF has a degradation of about 6 dB around $\bar{\omega} = 0.1$ and is caused by the FDA antenna pattern illumination of range ambiguous clutter. The degradation is minimal compared to the two clutter notch depths and is also away from the target range clutter notch, which is important for detection of low relative velocity targets. The other significant observation from the MF Output SINR is the

reduced range ambiguous clutter doppler depth at $\bar{\omega} = 0.450$ by 6 dB because the clutter is spread out by the FDA antenna pattern as evidenced by the degradation discussed above. The Output SINR curve shows an increase in clutter at one doppler value coincides with a decrease at a different doppler value.

Similar to the MF, the FDA JDL Output SINR with known covariance has the range ambiguous clutter notch depth reduced, in this case by 9.5 dB. Again, the reduced clutter at the clutter notch is counteracted by the increased clutter over $0.05 \leq \bar{\omega} \leq 0.25$. The doppler range of SINR degradation has increased because JDL is only partially adaptive and hence cannot fully suppress the clutter doppler spread caused by the FDA antenna pattern.

Using an estimated interference covariance matrix generated with symmetric sample support selection, the JDL Output SINR is seen in Figure 6.2. The result is averaged over 1000 realizations to reduce the statistical variation associated with matrix estimation and hence filter weights, as indicated by the error bars in the graph. Averaged Output SINR comparison to the known covariance Output SINR indicates the amount of degradation associated with interference matrix estimation, specifically estimation using non-iid sample support vectors.

The resulting Generalized Inner Product (GIP) comparison for the linear constant frequency and FDA for a high altitude platform is shown in Figure 6.3. The linear FDA produces a 44% reduction in GIP dynamic range and a 42% reduction in standard deviation compared to the constant frequency linear array GIP, insinuating increased sample support homogeneity. The increased sample support homogeneity is consistent with FDA outperforming in Figure 6.2 outside the clutter doppler notches.

The most noticeable differences between Output SINR using $\hat{\mathbf{R}}$ and the known covariance result is the degradation across $0.07 \leq \bar{\omega} \leq 0.45$ and a widened clutter notch. Since the sample support vectors are chosen symmetrically, the matrix estimate uses range-cells that have a maximum elevation angle of -81.6° with corresponding clutter doppler of 0.07, through to range-cells whose clutter doppler is the range am-

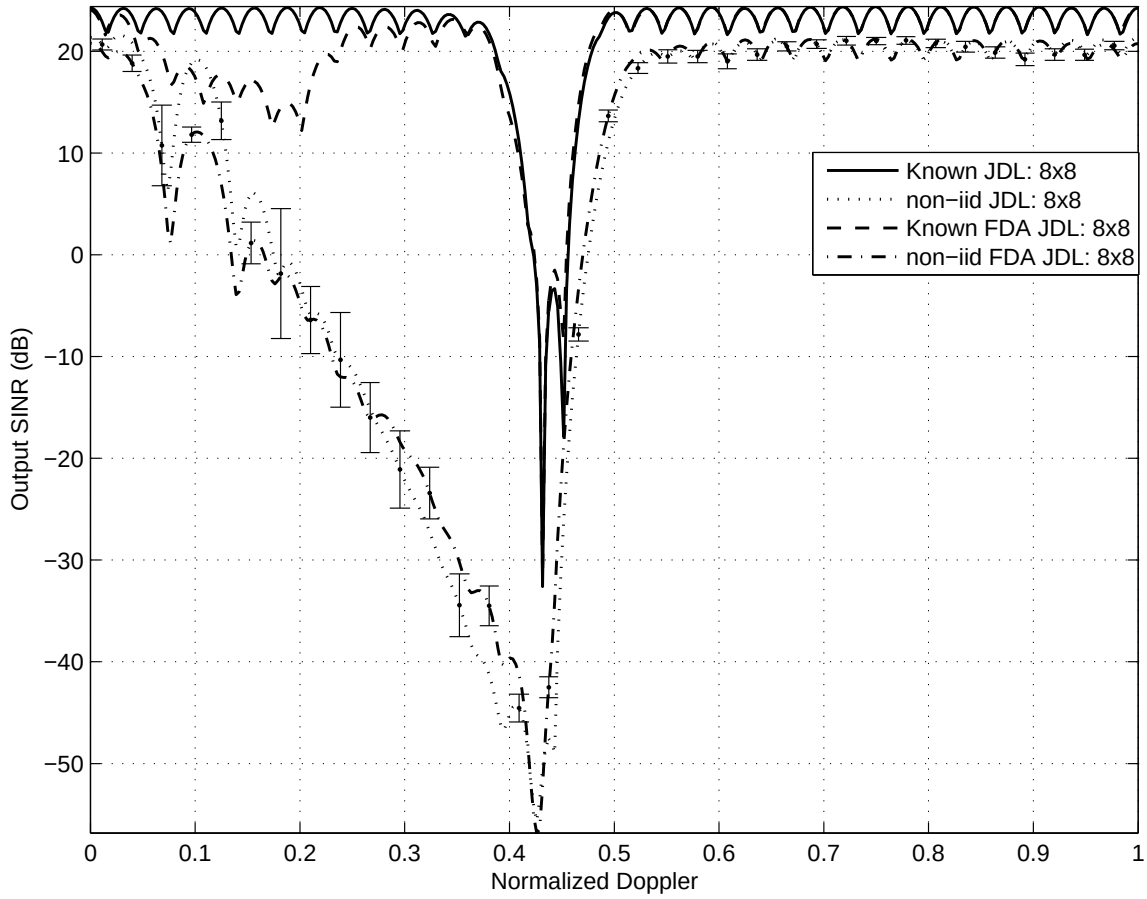

Figure 6.2: High-altitude platform with horizontal elevation transmission Output SINR. The known covariance result is compared to an estimated interference covariance matrix generated from 128 symmetrical sample support vectors. The latter curve is averaged over 1000 realizations and shows significant degradation below the target range clutter doppler due to close range-cells with different ground clutter doppler values skewing the matrix estimate.

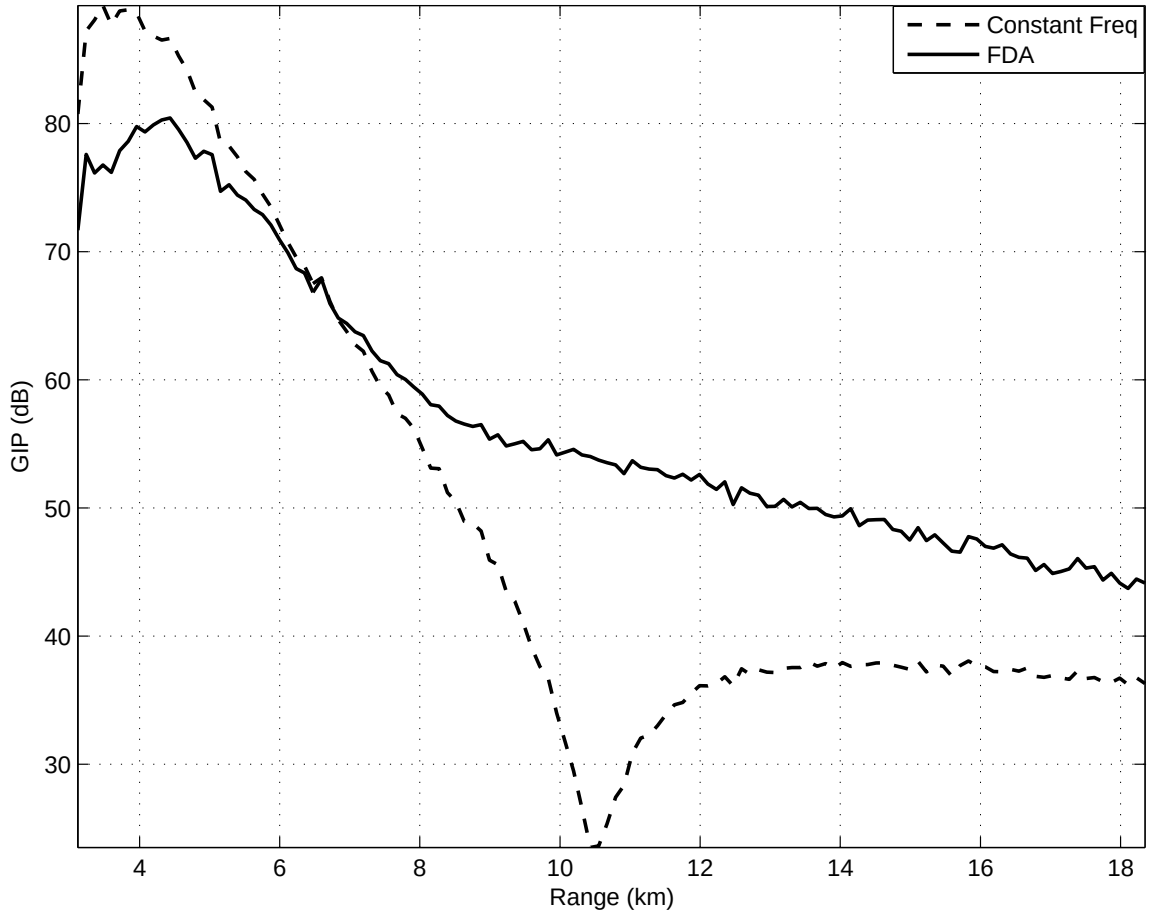

Figure 6.3: High platform altitude with airborne target GIP for forward-looking linear constant frequency array and FDA averaged over 100 runs. The FDA curve is a 44% reduction of the constant frequency GIP dynamic range, indicating the FDA sample support vectors contain fewer heterogeneities than the constant frequency array, primarily at range-cells above the target range.

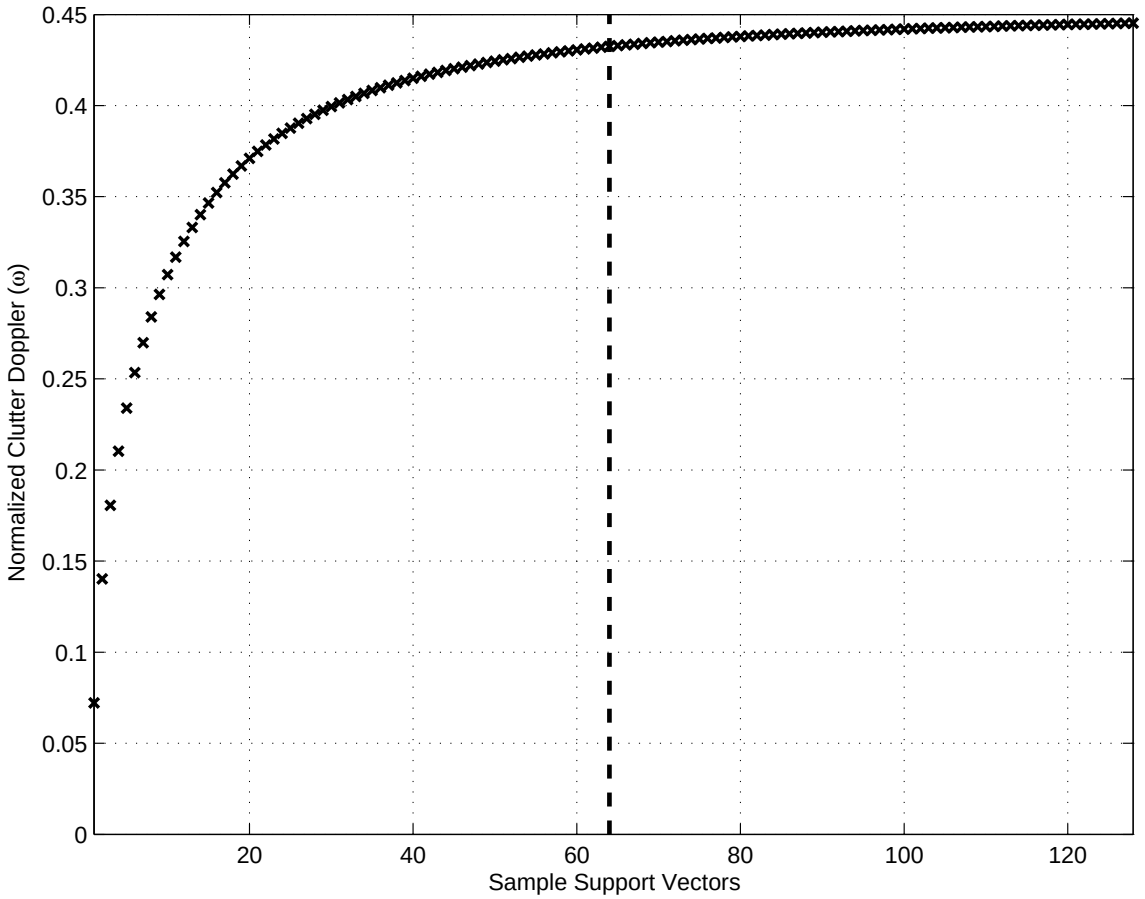

Figure 6.4: Clutter Doppler associated with high platform altitude sample support vectors used for interference matrix estimation. Dashed line indicates target range location and shows that close target range-cells have significantly different clutter doppler values that skew the matrix estimate.

biguous clutter doppler of 0.450. The distinct clutter notches at $\bar{\omega} = 0.07, 0.14, 0.18$ are caused by the clutter doppler associated with the first few range-cells used for matrix estimation, as shown in Figure 6.4. The notches are distinct because the clutter doppler difference between successive range-cells is greater at low ranges, and the value of M ensures there is sufficient sampling along the doppler axis to isolate the contribution of each close range-cell.

The generated interference matrix estimate is skewed by the range-cells whose statistics do not match the target range-cell clutter statistics. The JDL weighting vector is based on the skewed interference matrix and therefore places clutter sup-

pression over the aforementioned doppler range where no clutter exists. The greatest degradation occurs at higher $\bar{\omega}$ values, partly because the elevation angle compression versus target range given by Eqn. (5.9) leads to more range-cells contributing clutter doppler near 0.450, and partly because of the cosine elevation suppression of close range-cells by the antenna pattern element factor. It is observed in Figure 6.2 the FDA has lower degradation at normalized doppler just below the clutter doppler notch, whilst the known covariance Output SINR is the same for both array types, thereby indicating reduced degradation associated with non-iid sample support using the FDA, i.e. making sample support data more homogeneous.

Using sufficient iid sample support vectors, Reed's Rule [4] predicts an Output SINR 3 dB below the known covariance Output SINR. The iid JDL Output SINR is recalculated through artificially generating an interference matrix estimate by using snapshots based solely on the target range-cell statistics, and Figure 6.5 verifies the resultant Output SINR curve is 3 dB below the known covariance matrix result.

Using a reduced CPI the AMF Output SINR using estimated covariance matrices with non-iid sample support is seen in Figure 6.6, with the graph including the known covariance MF Output SINR, which is the upper performance limit of two-dimensional (2D) STAP for a particular CPI value. The result shows that fully adaptive STAP using non-iid sample support suffers the same type of degradation as partial STAP with a larger CPI because of skewed interference matrix estimation. The distinct clutter notches noted in Figure 6.2 are not as distinct because of the reduced number of pulses integrated and hence fewer doppler filters, grouping together clutter doppler values associated with multiple range-cells.

It is also noted that FDA AMF outperforms constant frequency AMF across the degraded $\bar{\omega}$ region, indicating less degradation caused by the skewed interference matrix when clutter rank is not ignored. The improvement is confirmed to be isolated to matrix estimation since FDA MF is inferior to constant frequency MF over the same doppler region. The result is not critical since fully adaptive STAP is typically

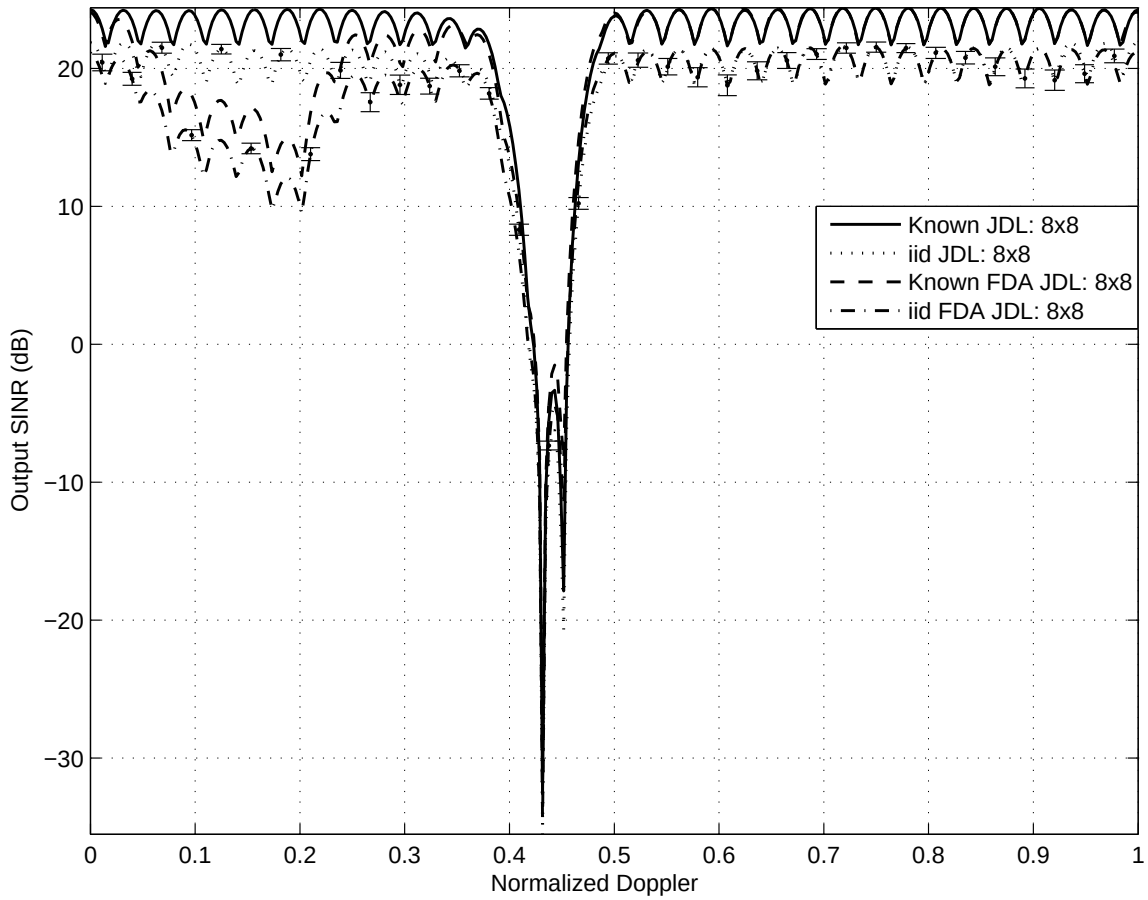

Figure 6.5: High-altitude platform horizontal elevation transmission Output SINR. The known covariance result is compared to using an estimated interference covariance matrix generated from 128 artificially iid sample support vectors. The latter curve is averaged over 1000 realizations and shows 3 dB degradation from the known covariance Output SINR across clutter doppler, consistent with Reed's Rule.

not implementable, but provides verification to the concept of FDA making sample support data more homogeneous.

Comparison between the MF and AMF in Figure 6.6 to the degradation experienced using JDL with reduced CPI in Figure 6.7, confirms the assertion in Section 2.2.3 that the greater the STAP technique DOF, the greater the degradation using forward-array sample support vectors. The reason for greater degradation with full adaptivity is because of more sample support vectors required and hence more significantly different vectors when compared to the target range-cell clutter statistics.

Based on the Output SINR results, there are two distinct clutter doppler notches critical for performance evaluation. The performance at the target range clutter doppler notch and range ambiguous clutter doppler indicate differences in sample support vector homogeneity using the FDA and represent target velocities of greatest detection difficulty.

It is important to remember that P_d plots are based on estimated covariance interference matrices, therefore the plots are constrained to partial STAP techniques for the original CPI value and the P_d results should be compared to the estimated covariance matrix Output SINR. The P_d curves use JDL with iid sample support as the upper performance limit and Non-Adaptive (NA) as a lower limit, indicating whether STAP provides any benefit over cascaded processing and is worth the additional processing overhead.

The first target doppler value to be evaluated is when the target is competing against the target range clutter doppler $\bar{\omega} = 0.433$. The P_d curve is shown in Figure 6.8 and the results are consistent with the estimated covariance matrix Output SINR in Figure 6.2.

The most obvious P_d plot feature is that there is significant degradation of approximately 18 dB between the iid and non-iid JDL results for both array types. Additionally the performance of both constant frequency and FDA JDL with actual sample support vectors is only marginally better than NA processing, the minimal

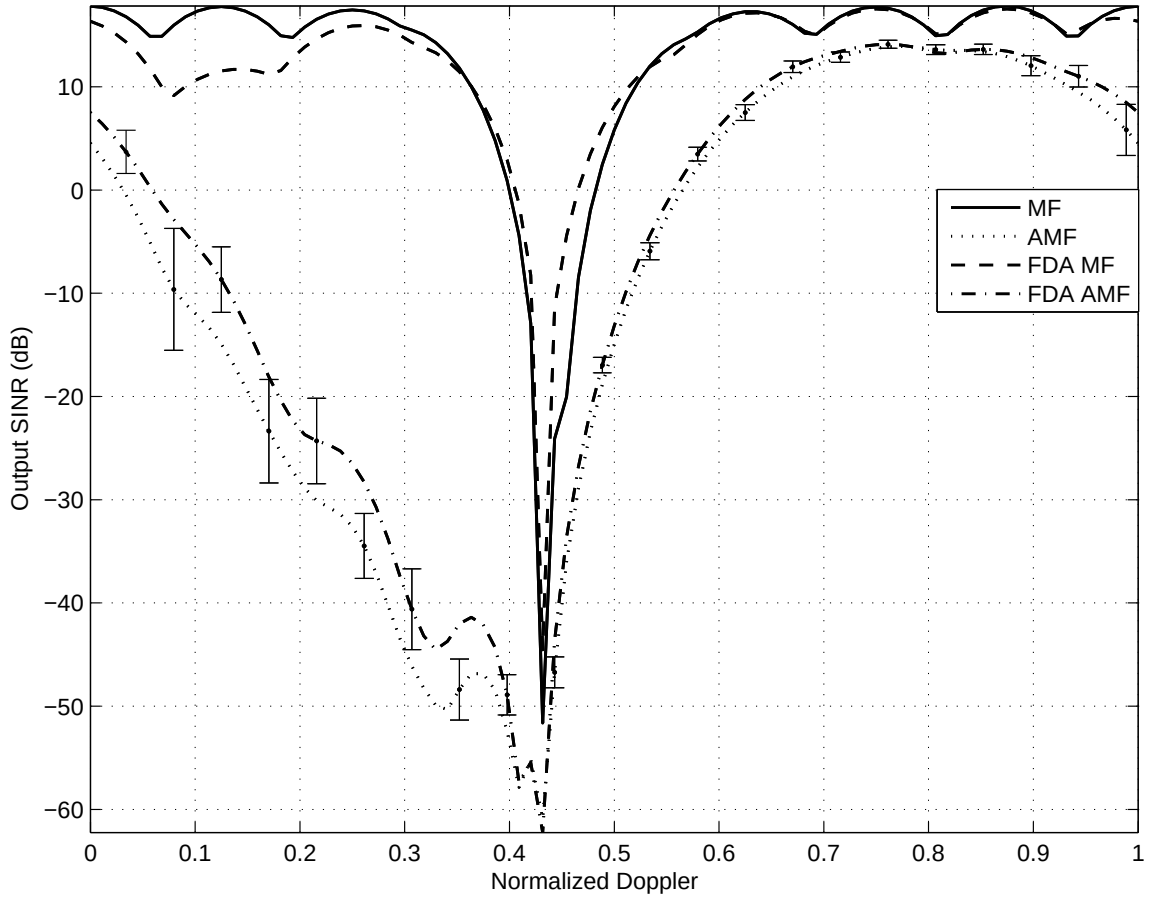

Figure 6.6: High-altitude platform horizontal elevation transmission fully adaptive Output SINR with reduced CPI values $N = 8$ and $M = 8$. Known covariance MF result is compared to AMF using an estimated interference covariance matrix generated from 128 symmetrical sample support vectors. The latter curve is averaged over 1000 realizations and shows significant degradation below the target range clutter doppler due to close range-cells with different ground clutter doppler values skewing the matrix estimate. AMF FDA is observed to outperform constant frequency AMF over the clutter doppler region of degradation.

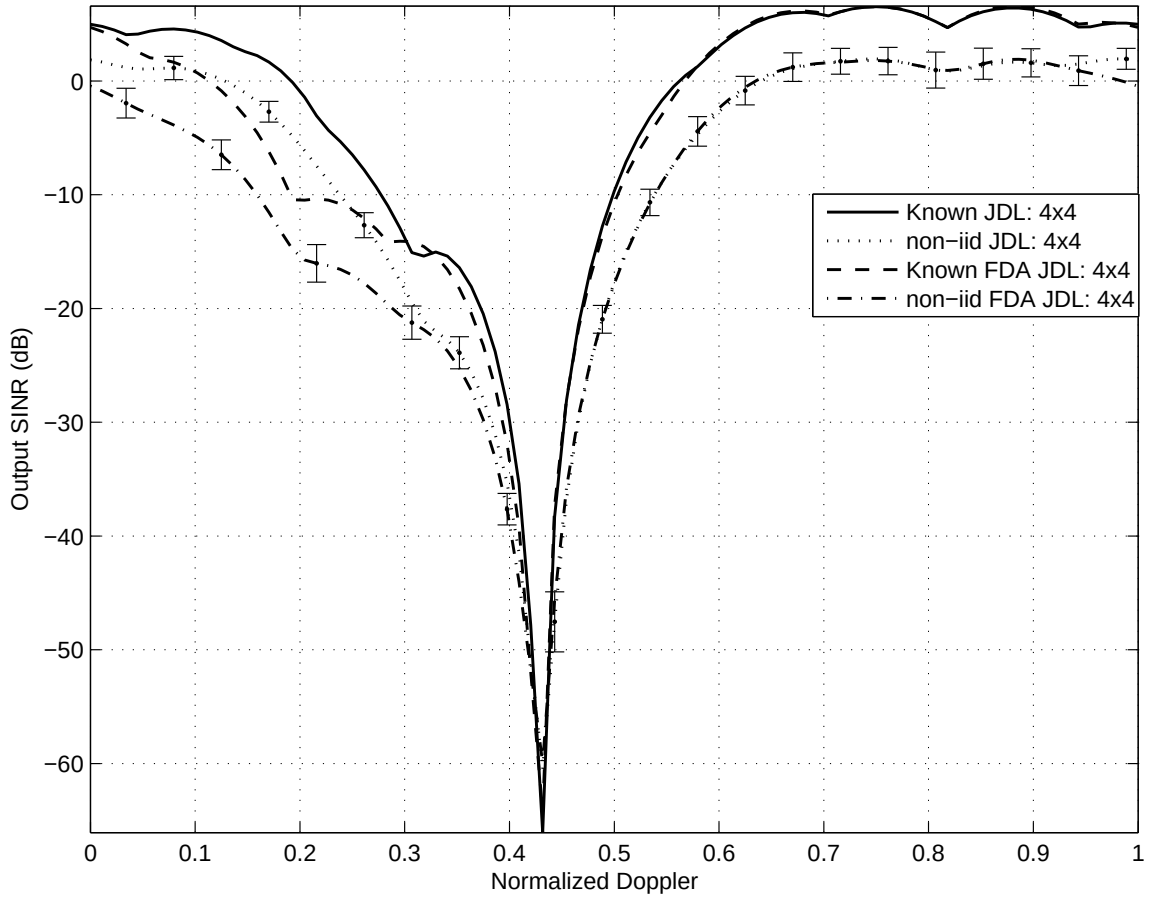

Figure 6.7: High-altitude platform horizontal elevation transmission partially adaptive Output SINR with reduced CPI values $N = 8$ and $M = 8$. Known covariance JDL result is compared to JDL using an estimated interference covariance matrix generated from 32 symmetrical sample support vectors. The latter curve is averaged over 1000 realizations and shows partial STAP degradation is less than the degradation between MF and AMF since fewer sample support vectors are used and the vectors used, are physically closer to the target range-cell and hence more representative of clutter statistics.

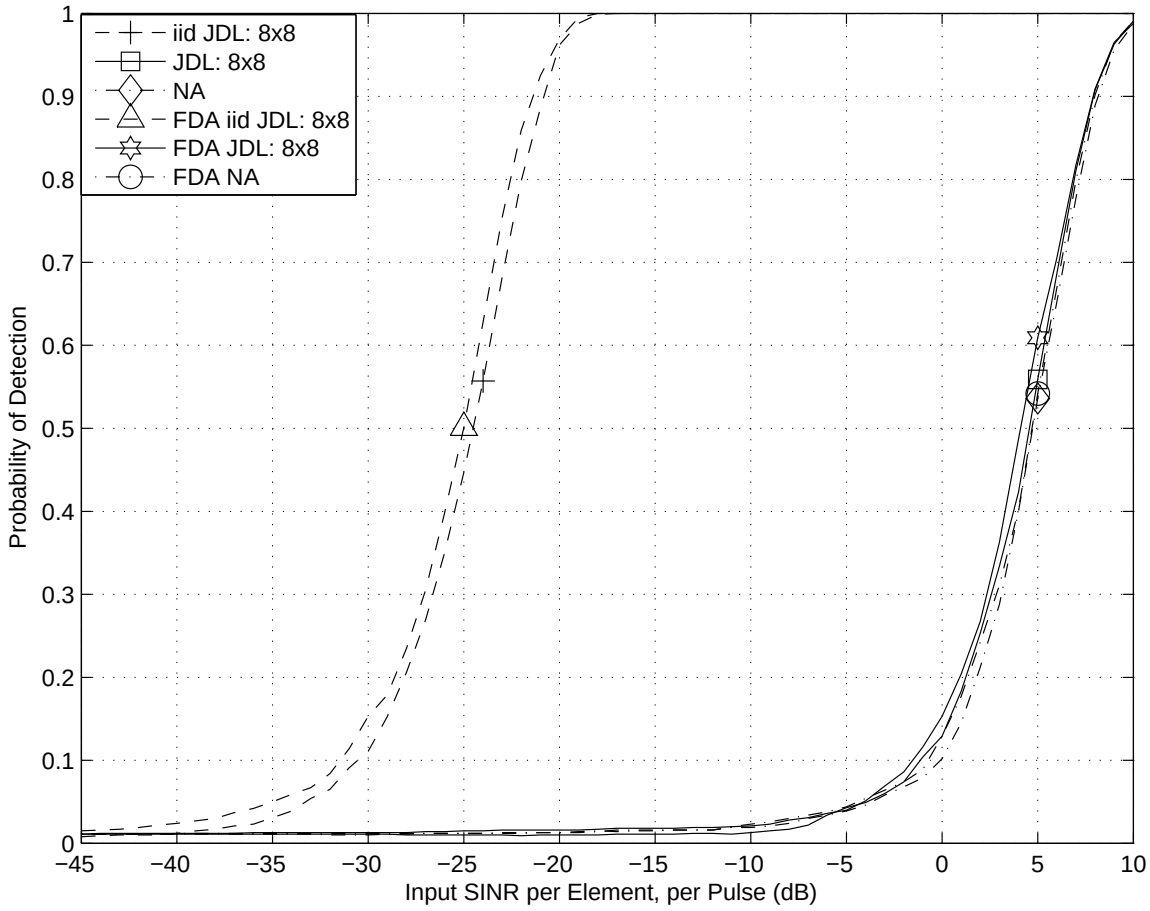

Figure 6.8: High altitude platform and horizontal elevation transmission detection curves for a target at $\bar{\omega} = 0.433$ for $P_{fa} = 0.01$. The detection curves using non-iid sample support show significant degradation for both array types and place their performance on par with non-adaptive (NA) processing.

difference indicating that at a normalized target doppler of 0.433 the additional processing associated with JDL is not worth the minimal performance gain.

The second P_d curve seen in Figure 6.9 is evaluated at a target doppler of $\bar{\omega} = 0.450$, the range ambiguous clutter doppler. The plot indicates that there is considerable performance benefit achieved by the FDA structure, specifically the illumination of range ambiguous clutter by the range-dependent antenna pattern suppressing clutter. Additionally, the performance of both array types is considerably better than the performance at $\bar{\omega} = 0.433$ in Figure 6.8 indicating that as expected there is less competing clutter from the increased attenuation from range ambiguous clutter returns.

P_d plot analysis identifies a number of salient features. The iid FDA JDL is approximately 13 dB better than the corresponding constant frequency iid sample support result. However, when actual non-iid sample support vectors are used, the difference between the two array types reduces to 10 dB, the reduction in the improvement using FDA is caused by spreading of clutter doppler by the FDA antenna pattern within the sample support vectors.

In contrast to the previous target doppler, when the target doppler is equivalent to the range ambiguous clutter notch the NA for both array types is over 16 dB below the JDL results with non-iid sample support, so the additional processing associated with STAP is of significant benefit.

Overall, the probability of detection results at the two distinct clutter doppler notches show STAP provides considerable benefit over NA processing away from the target range clutter doppler. The effect of non-iid sample support vectors is most significant at the target range clutter doppler because of the magnitude of actual clutter present combined with the skew of the estimated interference matrix. The range-dependent FDA antenna pattern results in a performance benefit at the range ambiguous clutter doppler value by suppressing the contribution of range ambiguous clutter rings.

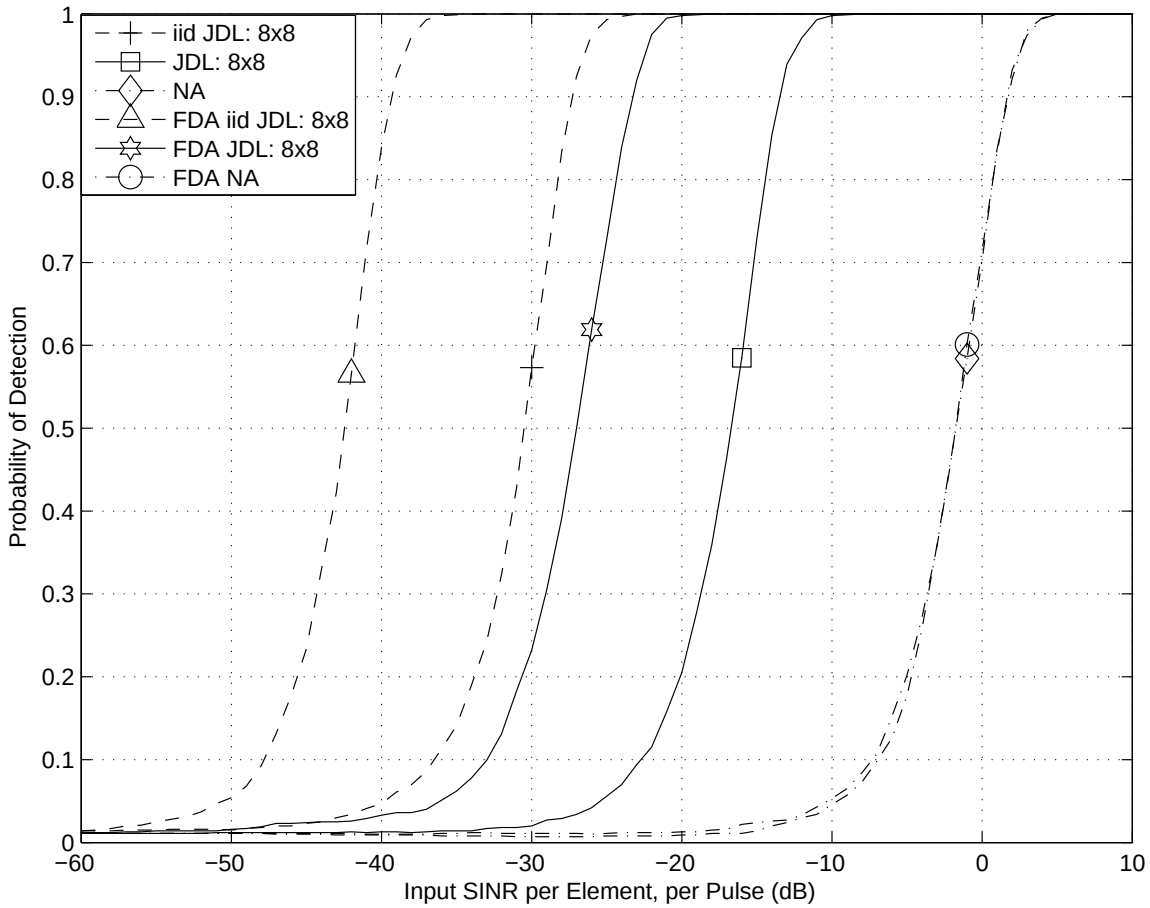

Figure 6.9: High altitude platform and horizontal elevation transmission detection curves for a target at $\bar{\omega} = 0.450$ for $P_{fa} = 0.01$. The FDA detection curves show significant performance improvement over the corresponding constant frequency array results and is attributed to suppression of range ambiguous clutter by the FDA antenna pattern.

6.4 AEWAC with Jeep Results

The next physical scenario involves changing the elevation transmit angle to correspond to the target range elevation angle, so the antenna pattern mainlobe strikes the ground. The change in elevation transmit angle from 0° to approximately -17° is of small importance for a linear array compared to a planar array because the elevation angle θ has minimal impact on the linear array antenna pattern, especially because $\cos(-17°) = 0.95$ is only marginally less than $\cos(0°) = 1$.

The known covariance Output SINR is shown in Figure 6.10 and is seen to be almost identical to the previous section despite the change in elevation transmit angle. The differences between the two elevation transmit angles is under 1 dB across the entire $\bar{\omega}$ region.

The Output SINR using estimated interference covariance matrices is shown in Figure 6.11, and again the result is near identical to the corresponding Output SINR in the preceding section. The skewed interference matrix from non-iid sample support produces the same degradation across $0.05 \leq \bar{\omega} \leq 0.45$, with FDA suffering reduced degradation near the clutter notch indicating sample support data homogeneity.

For a linear array there is minimal impact on performance when elevation transmission angles are changed. The Non-Homogeneity Detector (NHD) result is consistent with the above statement, the GIP for the new scenario is identical to Figure 6.3. The statistics are identical with FDA reducing constant frequency GIP dynamic range by 44% and reducing standard deviation by 42%. The NHD result and more homogeneous sample support is again evident by FDA outperforming constant frequency array outside the clutter doppler notches as observed in Figure 6.11.

The reduced CPI AMF Output SINR using estimated covariance matrix in Figure 6.12 is similar to the horizontal elevation transmit result in Figure 6.6. However, there is increased AMF Output SINR degradation when the elevation transmit angle is pointing at the ground. The increased degradation is caused by the reduced element factor suppression of close range-cells because of smaller elevation angle de-

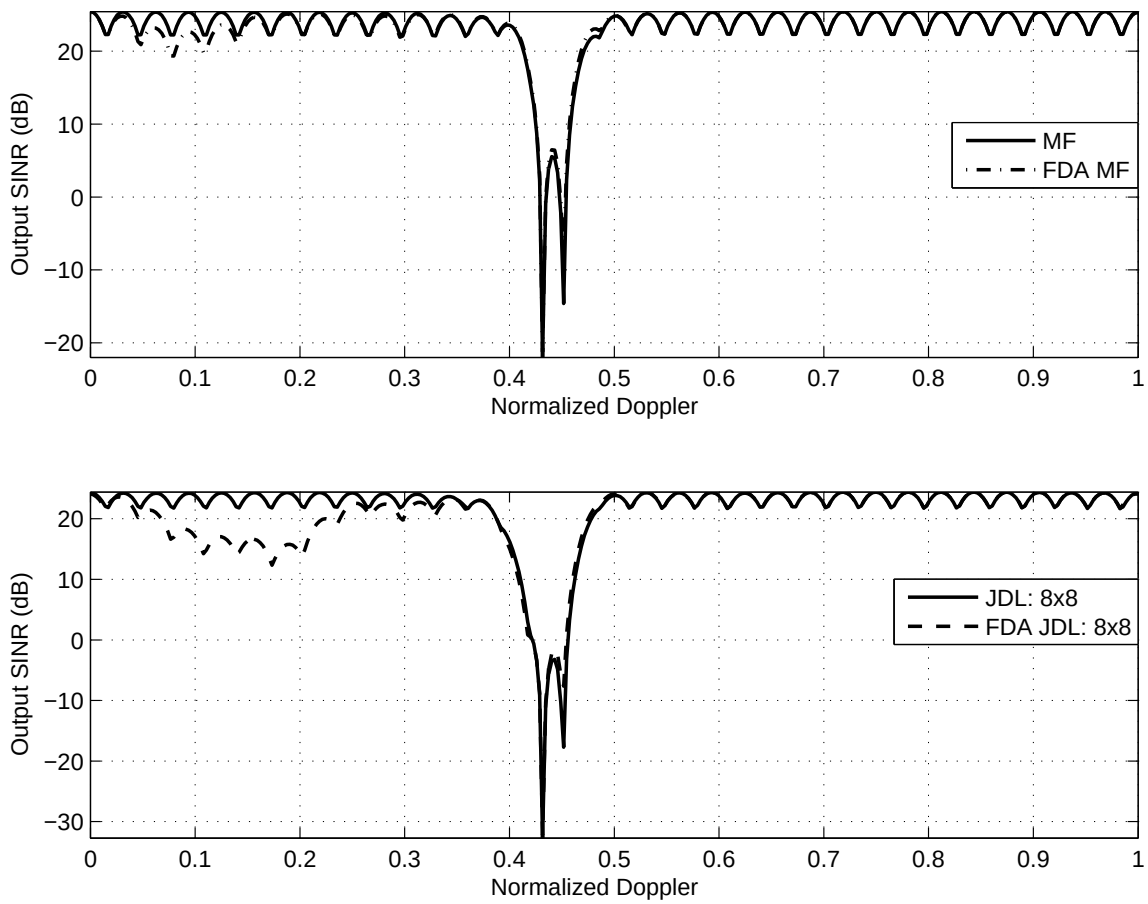

Figure 6.10: High-altitude platform, ground illumination Output SINR using known interference covariance matrix at a target range of 10.5 km. The result is nearly identical to the previous section with the change in elevation transmit angle having minimal impact. The FDA Output SINR has a reduced range ambiguous clutter notch depth at the expense of increased degradation at other doppler values away from the clutter notch.

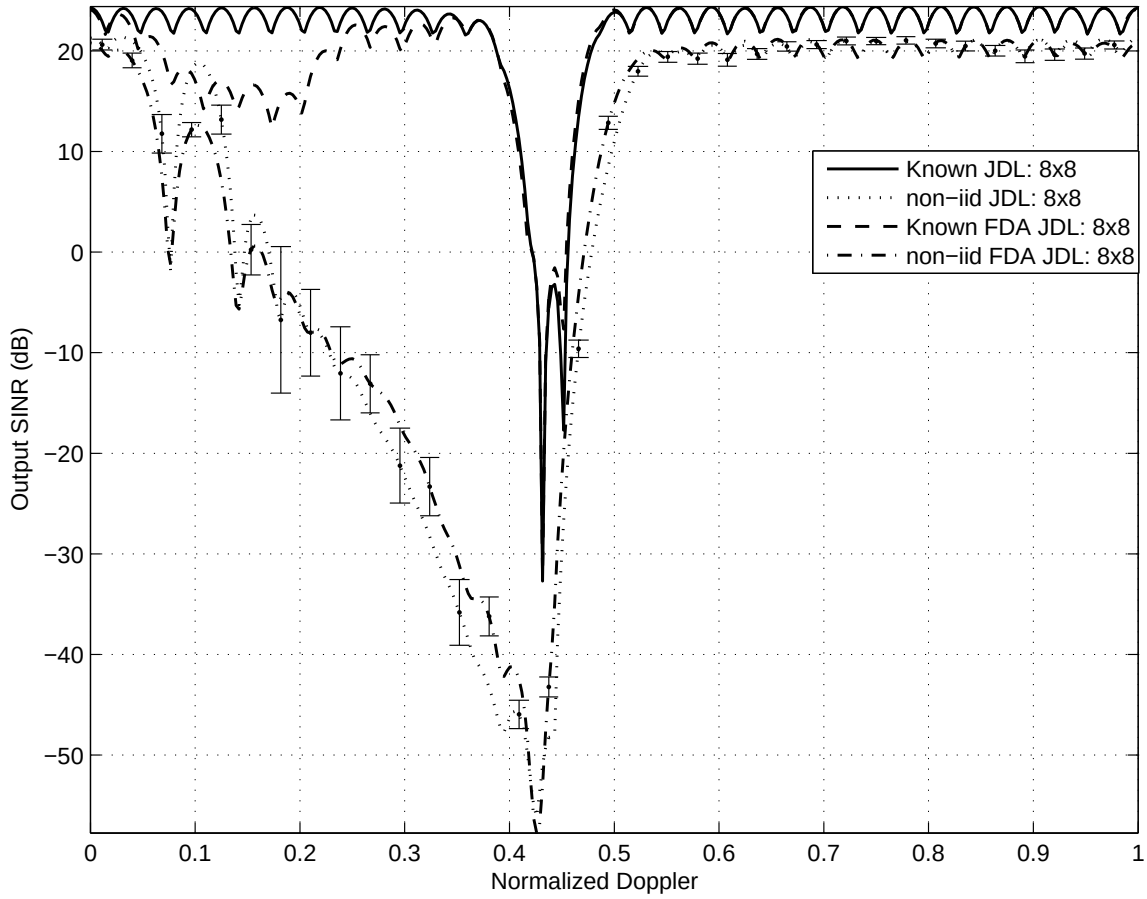

Figure 6.11: High-altitude platform with ground illumination Output SINR. Known covariance result is compared to Output SINR using an estimated interference covariance matrix generated from 128 symmetrical sample support vectors. The latter curve is averaged over 1000 realizations and shows significant degradation below the target range clutter doppler due to close range-cells with different ground clutter doppler values skewing the matrix estimate.

viation from the antenna mainlobe. The use of FDA provides greater improvement for AMF than for JDL since increased FDA clutter rank is effectively ignored when using fully adaptive processing.

When the target doppler value competes with the target range clutter doppler $\bar{\omega} = 0.433$ the P_d curve is shown in Figure 6.13. The performance is nearly identical to the corresponding detection curves for horizontal elevation transmit, with the only difference being a minimal degradation of both FDA JDL and FDA NA, on the order of 0.5 dB and within statistical error bounds.

Based on the same detection probabilities, the same conclusions can be drawn as for the preceding scenario. Firstly, significant degradation occurs from the use of non-iid sample support for both array structures and secondly, the degradation associated with the non-iid sample support reduces the performance of JDL to be approximately the same as NA processing.

For a target doppler of $\bar{\omega} = 0.450$ the target is competing against the range ambiguous clutter doppler and the detection curves are seen in Figure 6.14. There is a minor increase in the constant frequency array performance compared to the previous engagement scenario, reducing the FDA improvement to 12 dB for iid sample support and 10 dB for non-iid sample support.

The same conclusions can be drawn for the high platform altitude ground target as for the horizontal elevation transmit angle. There is minimal difference between the two scenarios because this chapter only considers linear arrays and hence elevation angle has minimal impact.

6.5 UAV with Hovering Helicopter Results

The next two engagement scenarios are based on a low platform altitude, an important side-effect of reduced altitude is no range ambiguous clutter contribution. With no range ambiguous clutter there is only one clutter doppler value for each range-cell and hence only one clutter doppler notch when using a known interference

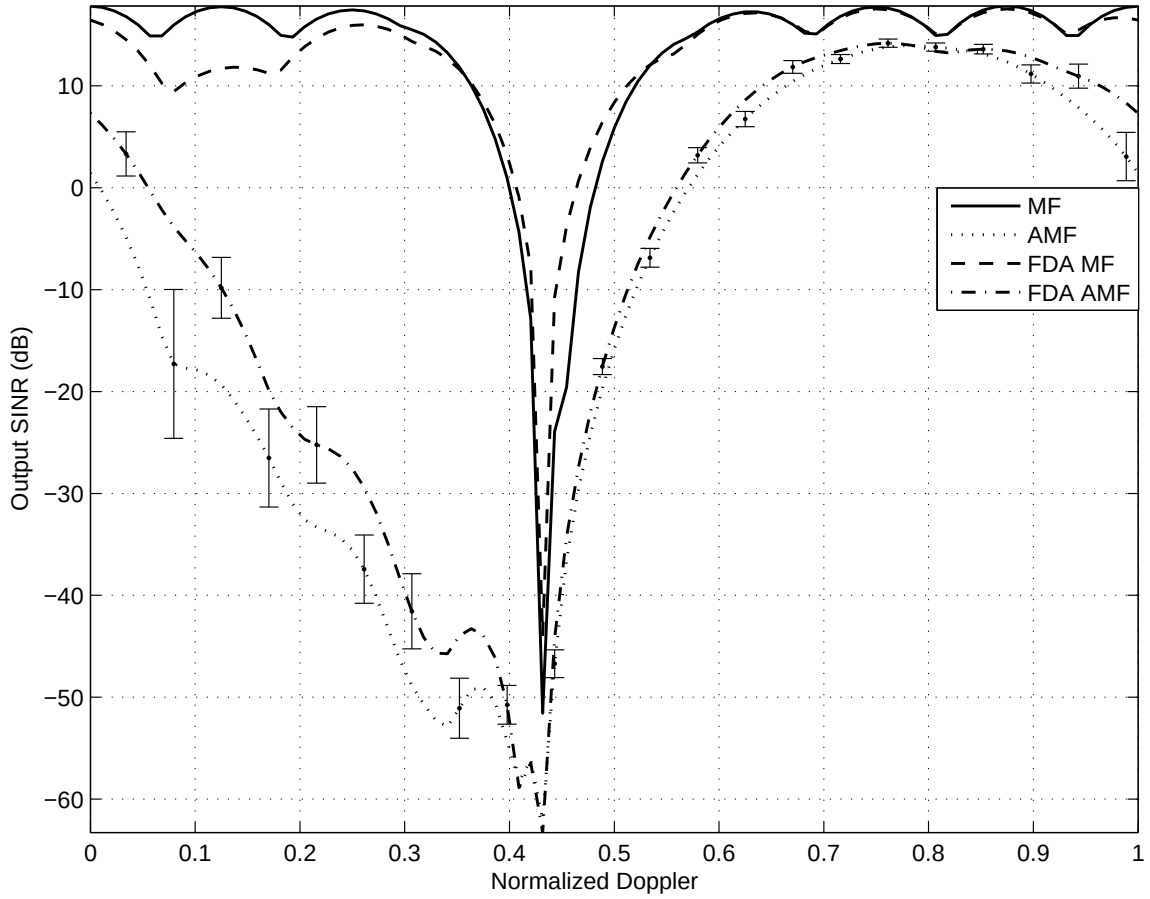

Figure 6.12: High-altitude platform with ground illumination fully adaptive Output SINR with reduced CPI values $N = 8$ and $M = 8$. Known covariance MF result is compared to AMF using an estimated interference covariance matrix generated from 128 symmetrical sample support vectors. The latter curve is averaged over 1000 realizations and shows significant degradation below the target range clutter doppler due to close range-cells with different ground clutter doppler values skewing the matrix estimate. AMF FDA is observed to outperform constant frequency AMF over the clutter doppler region of degradation.

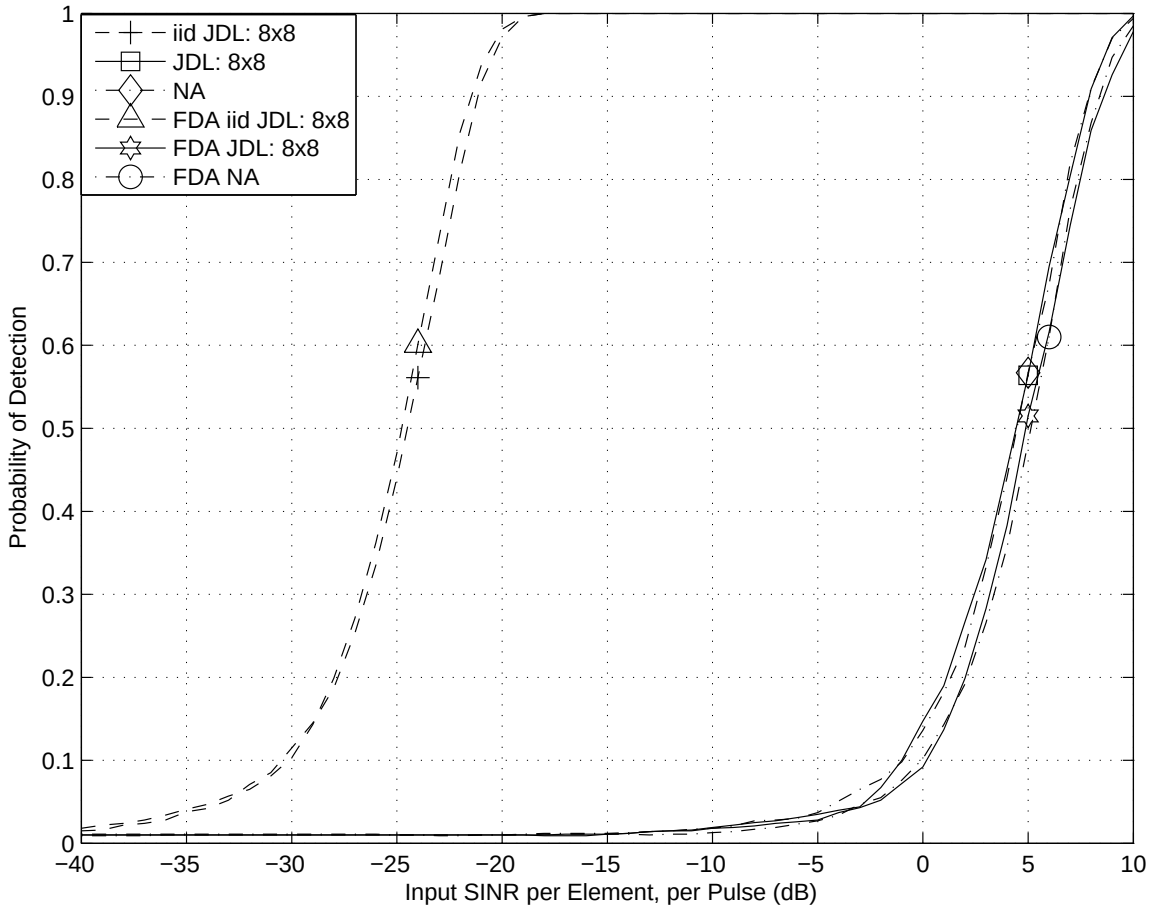

Figure 6.13: High altitude platform and ground illumination detection curves for a target at $\bar{\omega} = 0.433$ for $P_{fa} = 0.01$. The detection curves using non-iid sample support show significant degradation for both array types and place their performance on par with non-adaptive (NA) processing.

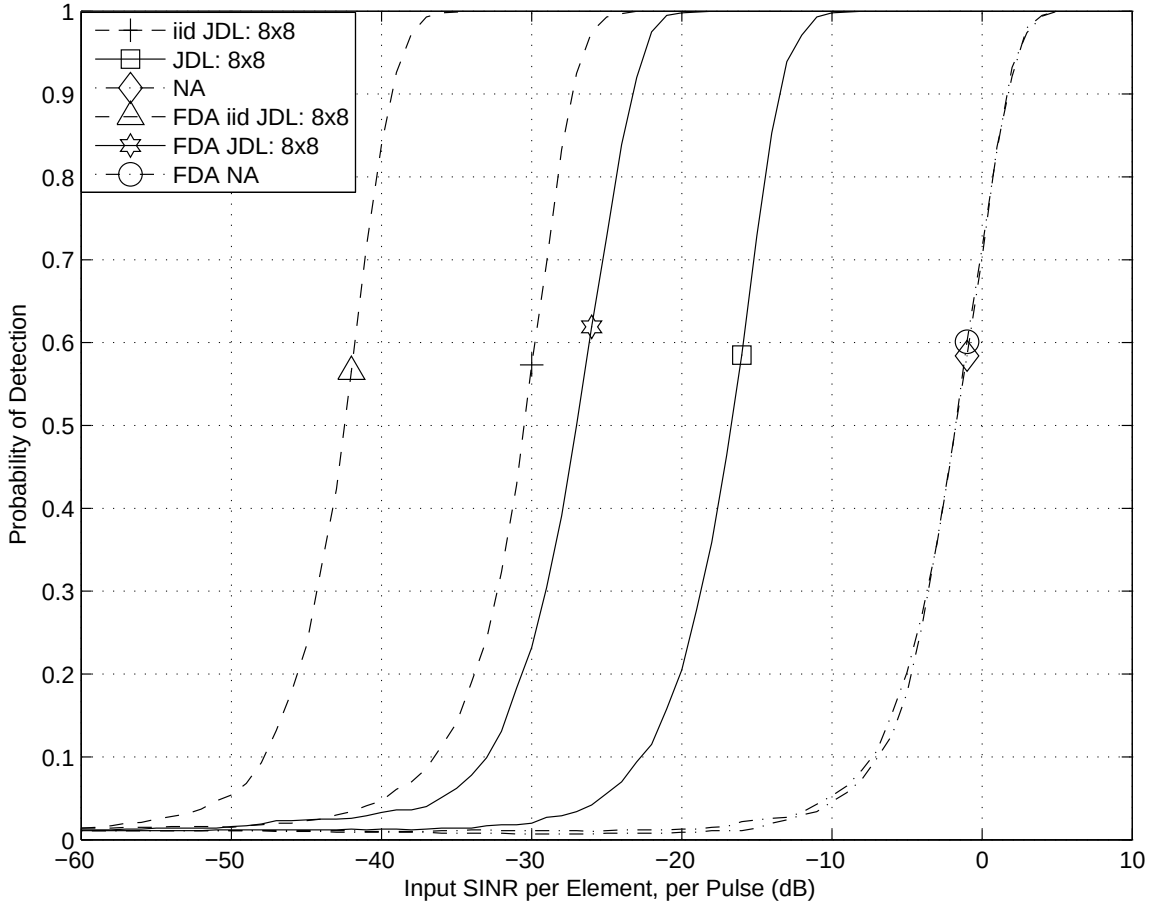

Figure 6.14: High altitude platform and ground illumination detection curves for a target at $\bar{\omega} = 0.450$ for $P_{fa} = 0.01$. FDA detection curves show 10 dB improvement over the constant frequency array results and the difference is attributed to suppression of range ambiguous clutter by the FDA antenna pattern.

covariance matrix. Another important impact of no range ambiguous clutter is equal clutter rank for the two array types as demonstrated in Chapter V.

If the same target range is used as for the previous two scenarios, the target range is now well outside the clutter range-doppler dependence region. For a high platform altitude, the sample support is limited to range-cells over $1 \leq \frac{R}{H} \leq 6$ however with the low altitude there are only 14 range-cells available within the same region, clearly an insufficient amount of sample support. The decision to use 128 sample support vectors as for the previous sections starting with the first available range-cell and selecting the target range to be symmetric within the sample swath results in a new target range is 8.0 km. The target range is outside the range-doppler dependence region since $\frac{R}{H} \approx 24$, and hence expect reduced degradation using non-iid sample support to estimate the interference covariance matrix. The expected reduced degradation can be observed by examining the sample support range-cells clutter doppler seen in Figure 6.15 and contrasting with Figure 6.4.

The Output SINR with known covariance is seen in Figure 6.16 and as predicted there is only one clutter notch. Interestingly, the clutter notch occurs at $\bar{\omega} = 0.450$ despite the reduced target range, whereas the target range doppler for 10.5 km with the high platform altitude is 0.433. The target range clutter doppler is increased because the platform altitude and hence the elevation angle has decreased from -17° to -2.4°. Additionally, because there is no range ambiguous clutter and the FDA antenna pattern is the same at the target range there is no difference between the constant frequency and FDA Output SINR curves using known covariance matrices.

When non-iid sample support is used for matrix estimation the averaged JDL Output SINR is seen in Figure 6.17. The non-iid sample support is seen to produce additional clutter doppler notches at $\bar{\omega} = 0.17$ and 0.32 corresponding to the clutter doppler at the first two range-cells used in covariance matrix estimation as shown in Figure 6.15. Degradation exists over $0.35 \leq \bar{\omega} \leq 0.45$ from the other range-cells, a smaller region of doppler degradation than for high platform altitude because the

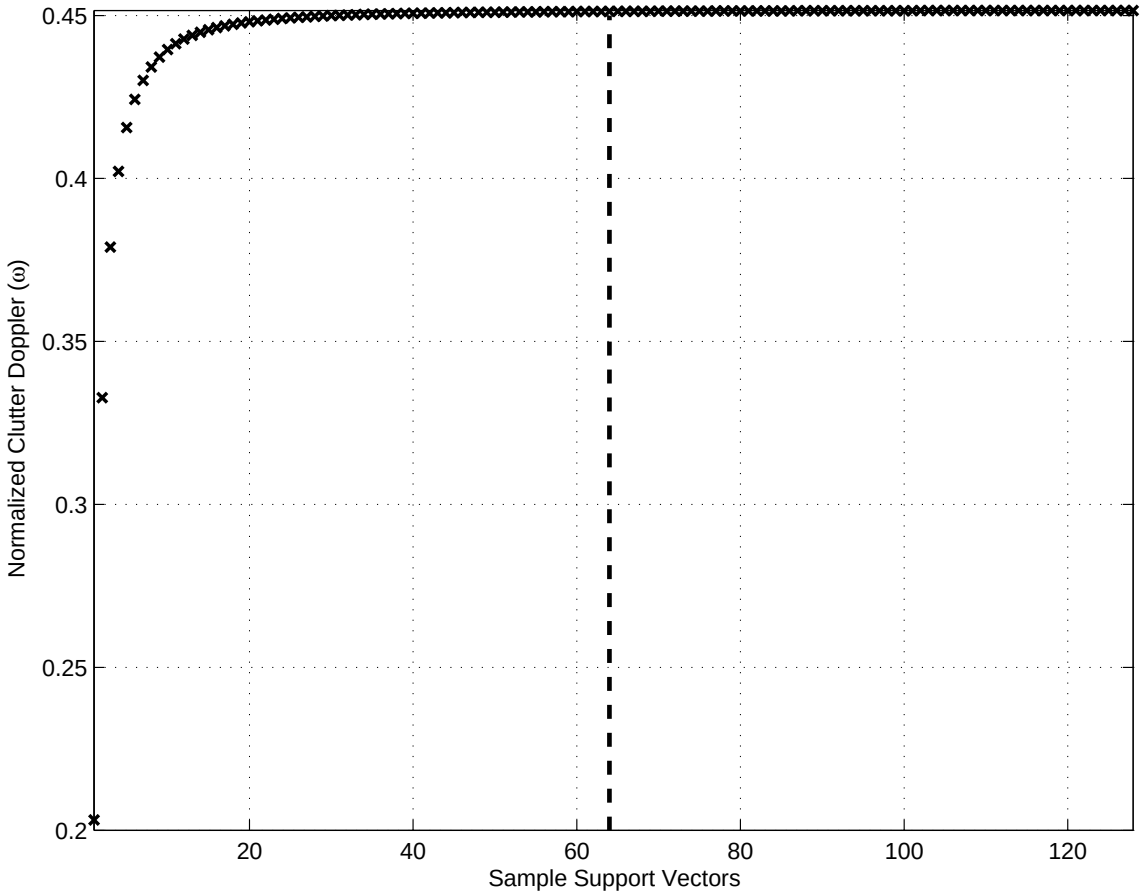

Figure 6.15: Clutter Doppler associated with low platform altitude sample support vectors used for interference matrix estimation. Dashed line indicates target range location and shows that close target range-cells have different clutter doppler values that skew the matrix estimate, but significantly less deviation than observed for the high platform altitude in Figure 6.4.

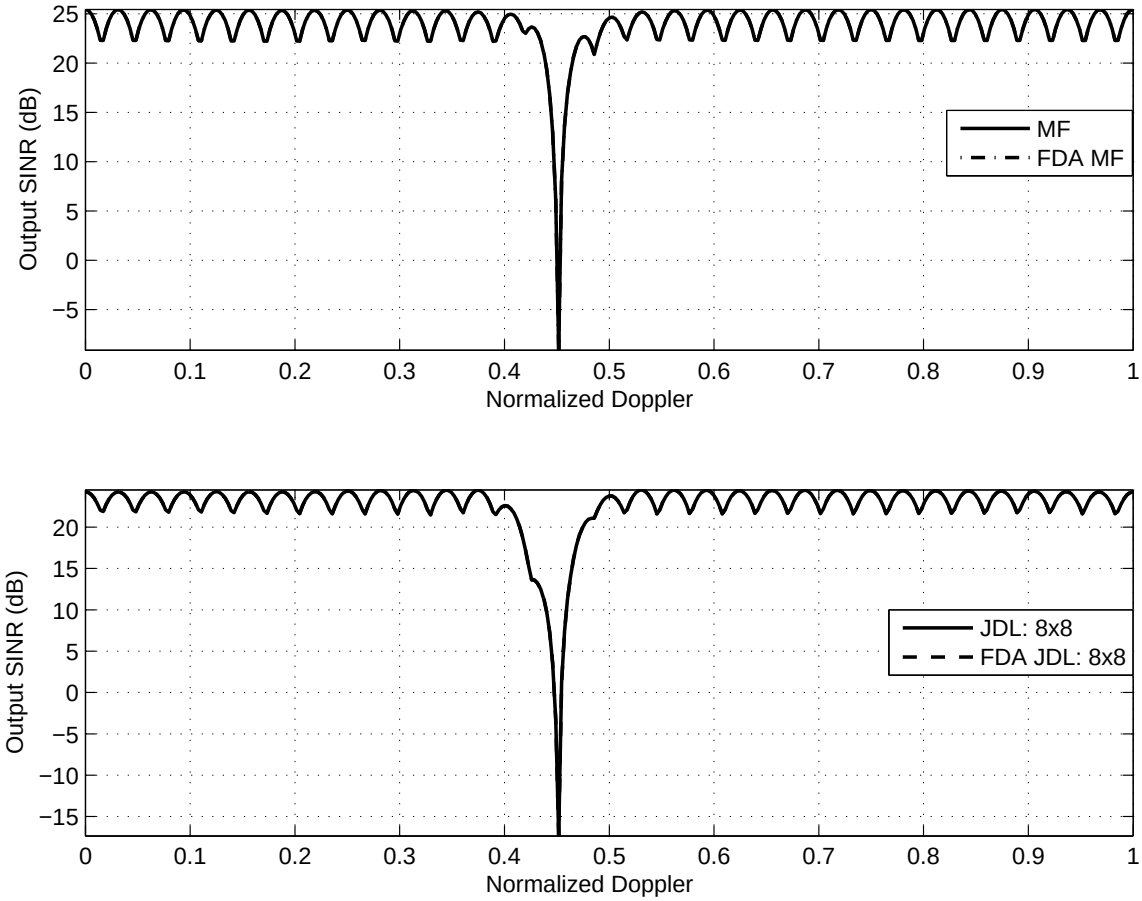

Figure 6.16: Low-altitude platform, horizontal elevation transmission Output SINR using known interference covariance matrix at a target range of 8.0 km, showing only clutter doppler notch because there is no range ambiguous clutter. The removal of the range ambiguous clutter results in the Output SINR curves being identical as opposed to the previous two scenarios.

elevation angle of range-cells is compressed by the low platform altitude. It is noted that the FDA performs slightly worse over $0.35 \leq \bar{\omega} \leq 0.4$ than the constant frequency array, however the FDA has a lower clutter notch depth, which is a more critical performance characteristic for low relative velocity targets.

The GIP for the new platform altitude is shown in Figure 6.18 and shows the GIP shape is considerably affected by the removal of range ambiguous clutter. As for the high platform altitude, the FDA improves sample support homogeneity decreasing constant frequency GIP dynamic range by 41% and standard deviation by 28%. It is noted that whilst the dynamic range reduction is of similar magnitude to the high platform altitude, the standard deviation reduction is considerably less as confirmed visually by a reduced difference between the FDA and constant frequency array at the far end of the range swath.

The AMF Output SINR using reduced CPI is shown in Figure 6.19. The Output SINR shows the additional clutter doppler notch at $\bar{\omega} = 0.17$ due to range-cells used in estimation, however the secondary notch depth is not as pronounced as for the estimated JDL Output SINR. A contributing reason for the lower secondary notch is the reduced resolution within the doppler filterbank by definition of a lower M value. The FDA provides a 3 dB improvement at the target range clutter notch indicating sample support data increase in homogeneity due to the antenna pattern.

Detection performance is only evaluated at one target doppler value, when the target competes with the target range clutter doppler $\bar{\omega} = 0.450$ and the P_d curve is shown in Figure 6.20. The performance shows significant deviation between JDL using iid sample support and non-iid sample support, on the order of 25 dB. Additionally the non-iid sample support JDL is seen to be approximately 1 dB below the NA for FDA and 2 dB for constant frequency array. Consistent to the estimated Output SINR results, using FDA also outperform the constant frequency by 2 dB, therefore FDA JDL with non-iid sample support is as good as constant frequency NA. As for

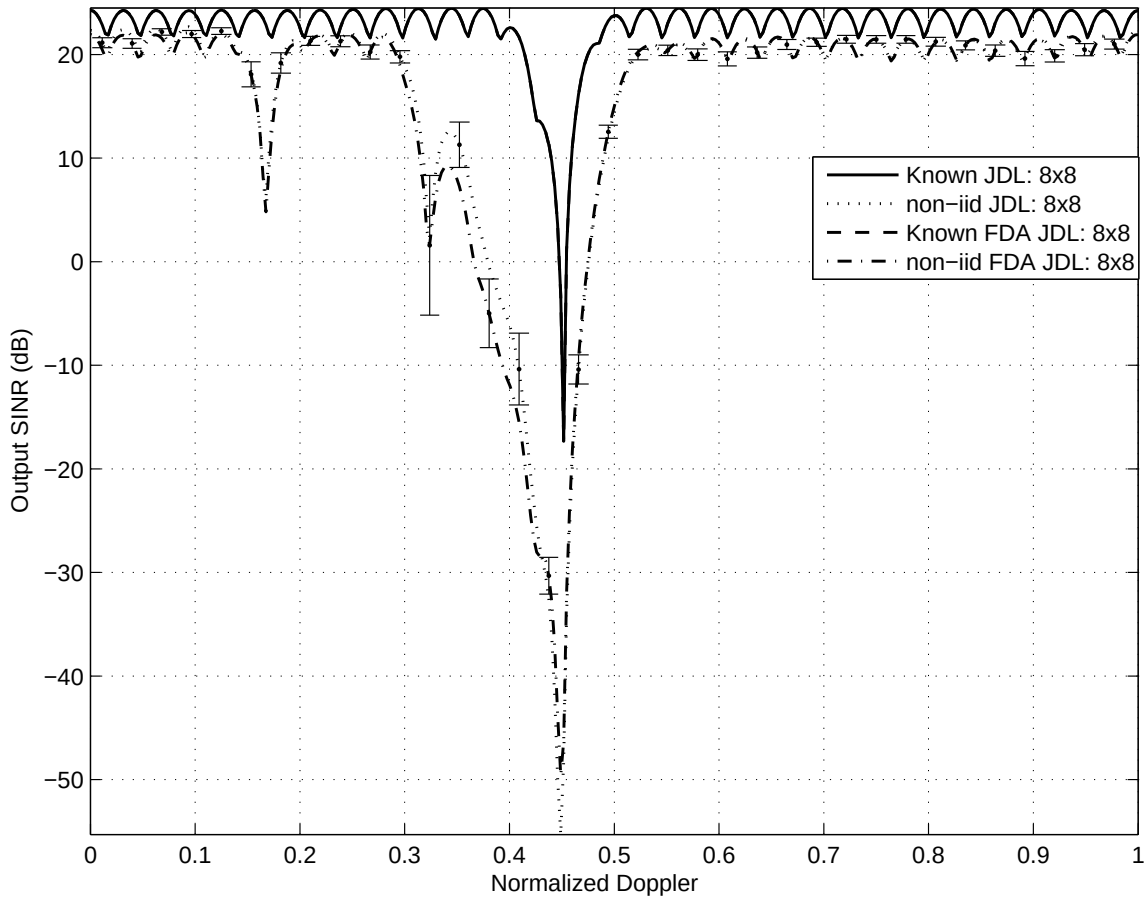

Figure 6.17: Low-altitude platform with horizontal elevation transmission Output SINR. The known covariance result is compared to using an estimated interference covariance matrix generated from 128 symmetrical sample support vectors. The latter curve is averaged over 1000 realizations and shows degradation below the target range clutter doppler due to close range-cells with different ground clutter doppler values skewing the matrix estimate. The region of degradation is less than the region experienced for the high platform altitude result, consistent with the clutter doppler associated with the range-cells used in matrix estimation.

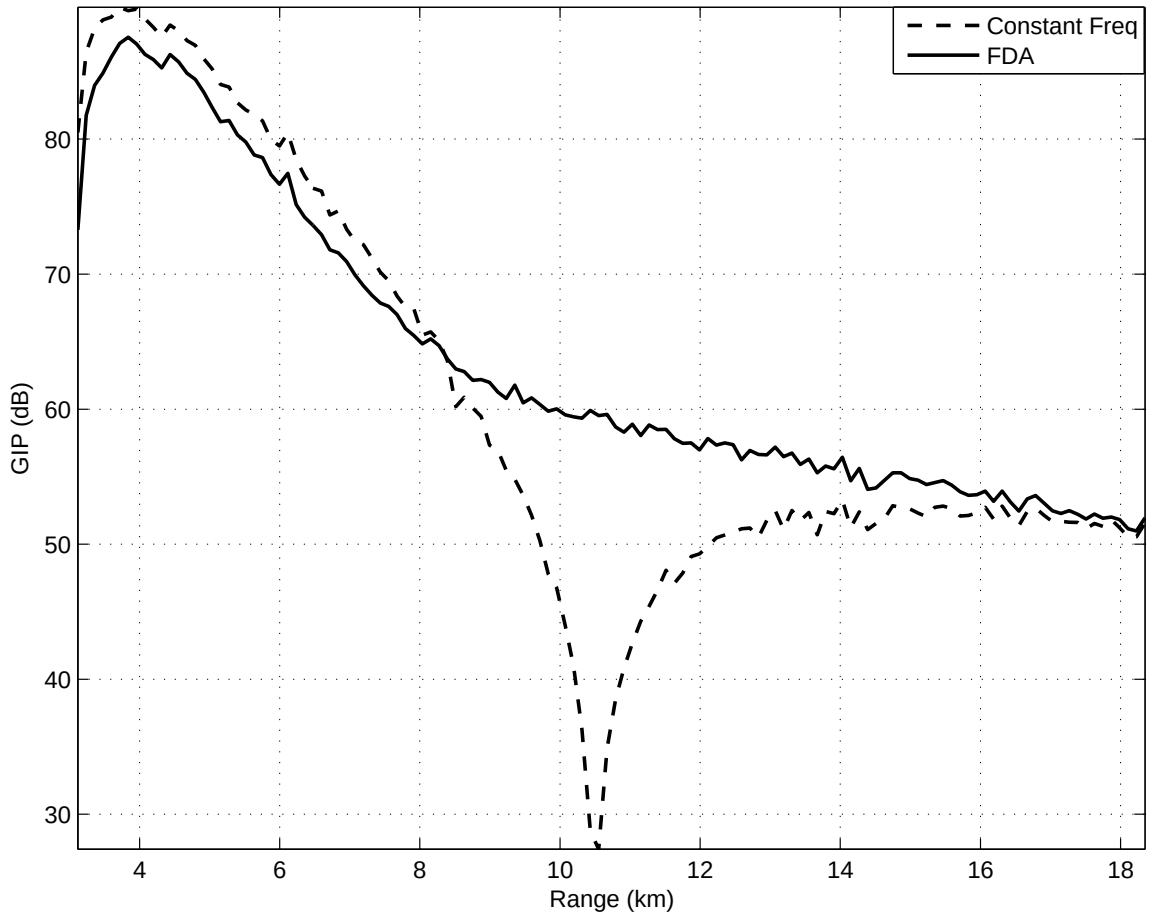

Figure 6.18: Low platform altitude with airborne target GIP for forward-looking linear constant frequency array and FDA averaged over 100 runs. The FDA curve has a marginally smaller GIP dynamic range, indicating more homogeneous sample support vectors. The difference from the previous high altitude NHD comparison is particularly evident at range-cells above the target range where there now is minimal difference between the two array types.

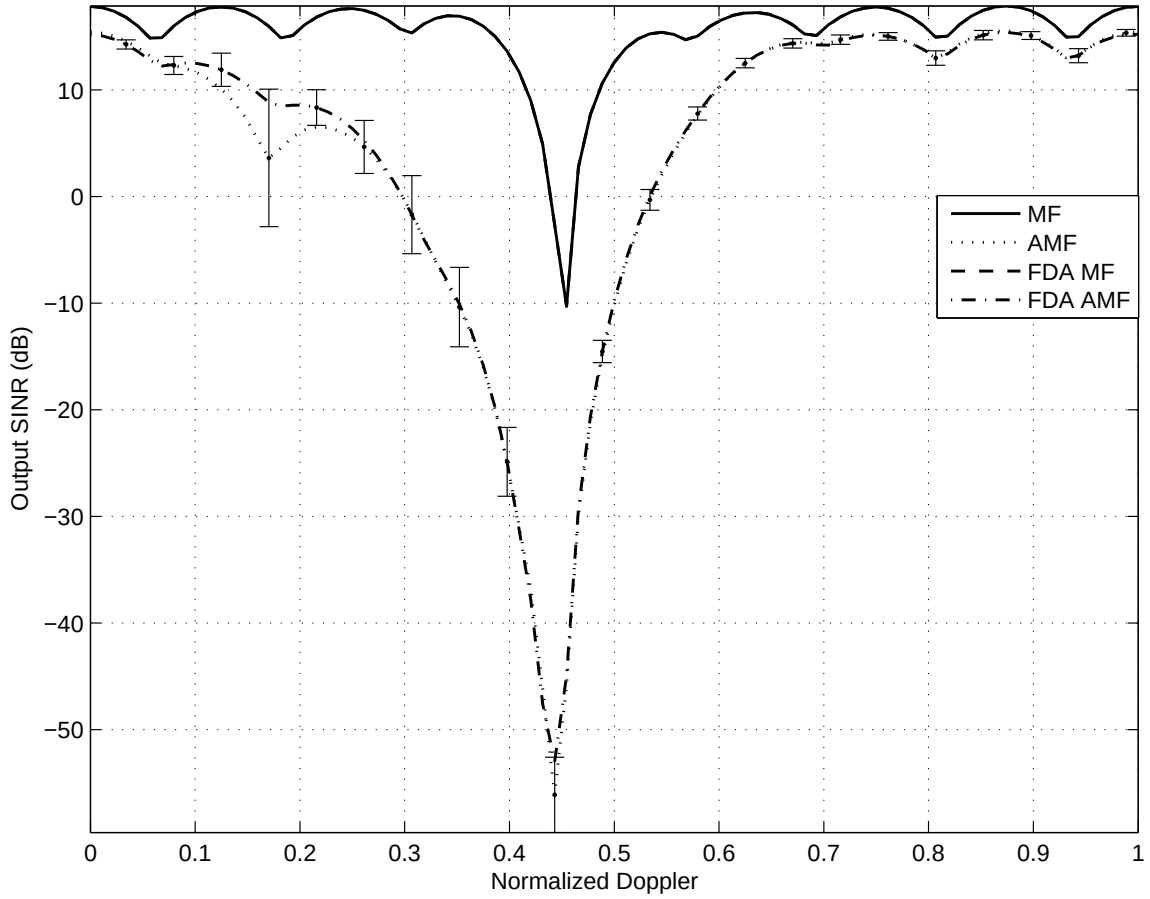

Figure 6.19: Low-altitude platform horizontal elevation transmission fully adaptive Output SINR with reduced CPI values $N = 8$ and $M = 8$. Known covariance MF result is compared to AMF using an estimated interference covariance matrix generated from 128 symmetrical sample support vectors. The latter curve is averaged over 1000 realizations and shows degradation below the target range clutter doppler due to the skewed matrix estimate. There is less degradation than the high platform altitude scenarios and the two array types are approximately equal because of the lack of range ambiguous clutter.

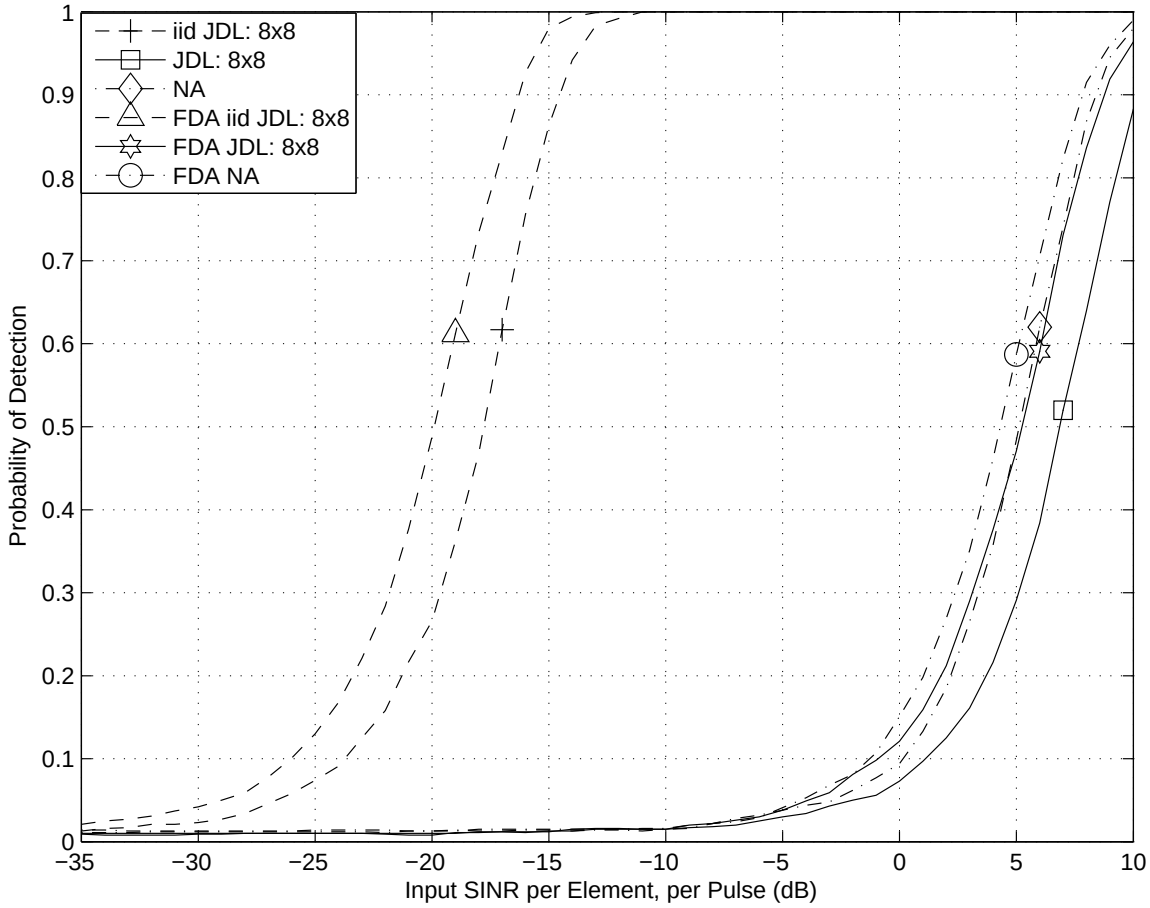

Figure 6.20: Low altitude platform and horizontal elevation transmission detection curves for a target at $\bar{\omega} = 0.450$ for $P_{fa} = 0.01$. The detection curves using non-iid sample support show significant degradation for both array types and place their performance on par with NA processing. Additionally FDA performance is seen to be approximately 1 to 2 dB above the constant frequency array for both iid and non-iid sample support, attributed to sample support increase in homogeneity.

the high platform altitude detection performance at target clutter doppler JDL with non-iid sample support performs worse than NA.

Overall, the results have shown a small but important benefit using FDA over constant frequency when the target doppler corresponds to the target range clutter doppler. Therefore the FDA antenna pattern has improved interference matrix estimation and detection performance of slow moving targets. However JDL is corrupted by non-iid sample support to a degree where it is outperformed by NA processing for both array types.

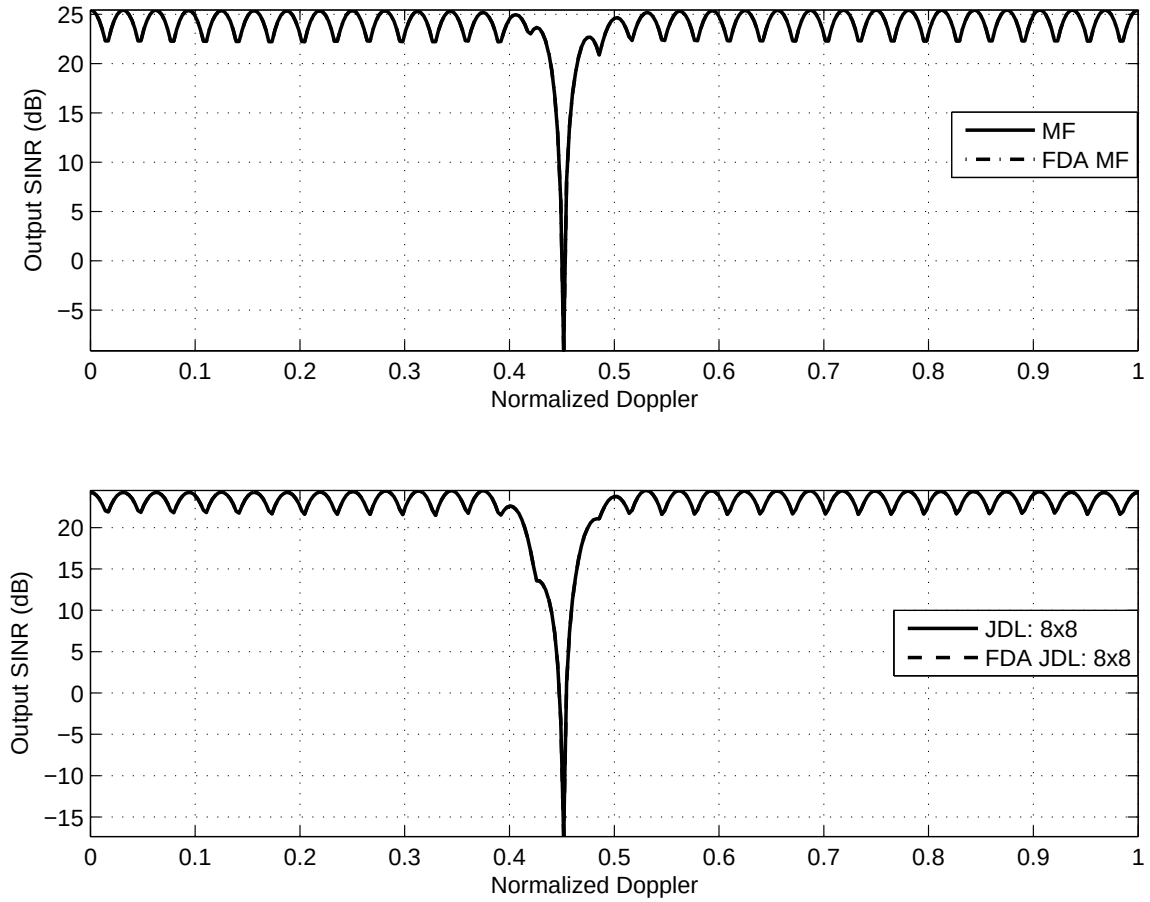

Figure 6.21: Low-altitude platform, ground illumination Output SINR using known interference covariance matrix at a target range of 8.0 km. The result is nearly identical to the previous section with the change in elevation transmit angle having minimal impact, with only one clutter doppler notch and no difference between the array types.

6.6 UAV with Jeep Results

Changing the elevation transmission angle for the low platform altitude has a minimal effect because firstly, the elevation angle changes from 0° to -2.4° and secondly, using a linear array that has minimal elevation angle dependence other than the elevation component of the antenna pattern element factor.

The Output SINR with known covariance is seen in Figure 6.21, with identical results to the horizontal elevation transmit angle, confirming the minimal impact of elevation angle definition.

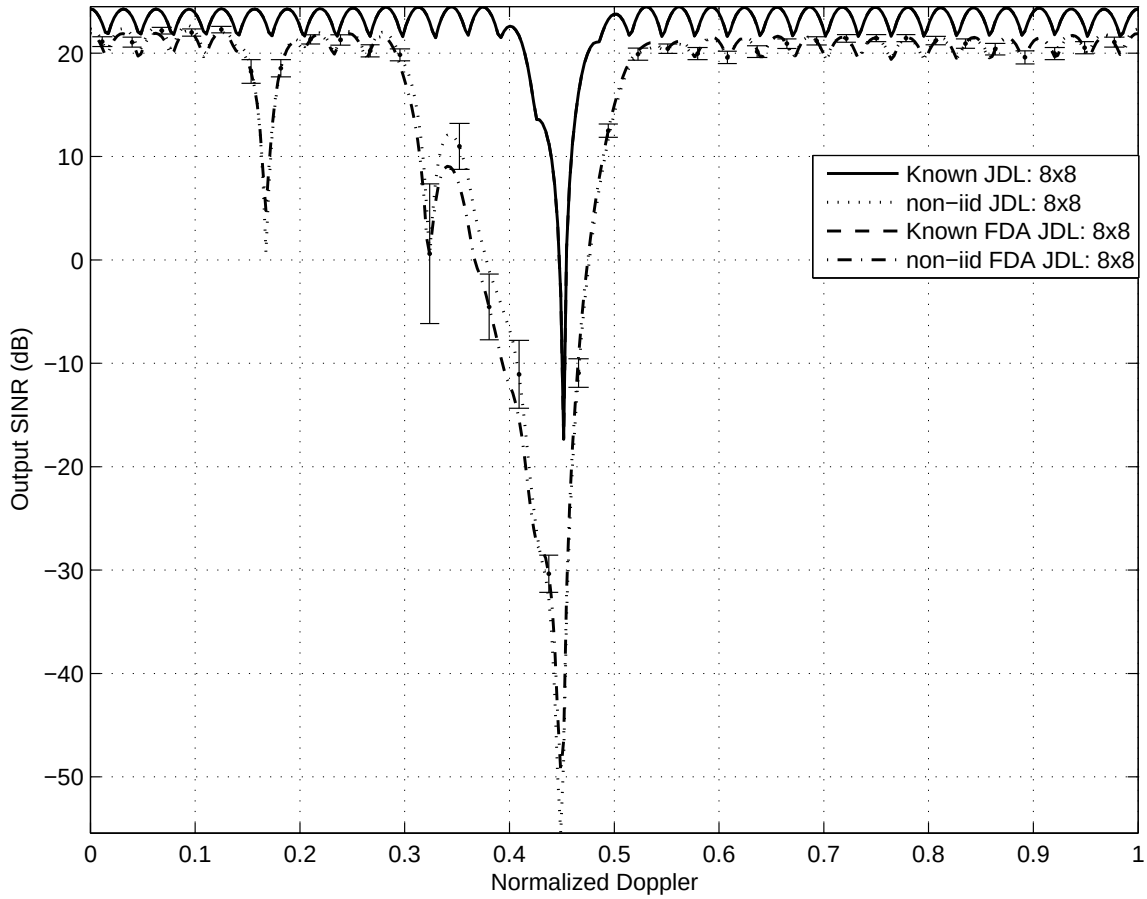

Figure 6.22: Low-altitude platform with ground illumination Output SINR. Known covariance result is compared to Output SINR using an estimated interference covariance matrix generated from 128 symmetrical sample support vectors. The latter curve is averaged over 1000 realizations and shows the same degradation as the previous scenario due to the skewed matrix estimate.

When using an estimated interference covariance matrix, the Output SINR averaged over 1000 realizations is shown in Figure 6.22, similar to the result achieved for a horizontal transmit angle with the FDA having a performance increase at the target range clutter doppler notch over the constant frequency array.

Again, the NHD result is unaltered by a change in elevation transmit angle for the linear constant frequency and FDA. The GIP result is the same as Figure 6.18, with FDA reducing constant frequency linear array GIP dynamic range by 41% and standard deviation by 28% indicating more homogeneous sample support data.

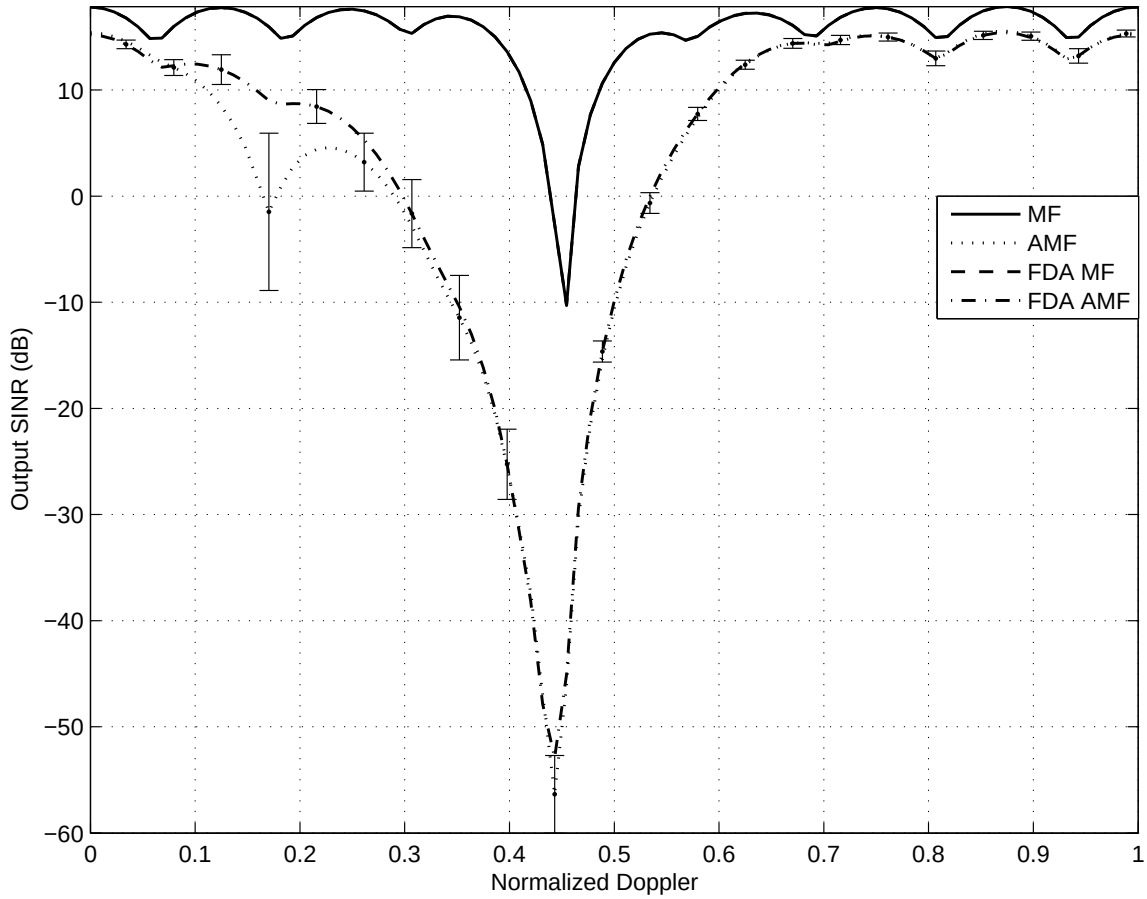

Figure 6.23: Low-altitude platform with ground illumination fully adaptive Output SINR with reduced CPI values $N = 8$ and $M = 8$. Known covariance MF result is compared to AMF using an estimated interference covariance matrix generated from 128 symmetrical sample support vectors. The latter curve is averaged over 1000 realizations and shows similar degradation to the previous scenario, indicating minimal difference caused by the change in elevation transmit angle.

When a reduced CPI is used, the AMF Output SINR is observed in Figure 6.23. The only difference noted is that the degradation around the secondary notch from non-iid sample support at $\bar{\omega} = 0.17$ is larger for the constant frequency array, which is associated with reduced suppression offered by the element factor because of a smaller angle between mainbeam and contributing range-cell.

For a target competing with the target range clutter doppler $\bar{\omega} = 0.450$ the P_d curve is shown in Figure 6.24. The performance is seen to be very similar to horizontal transmission, about 25 dB difference between iid and non-iid for both array types.

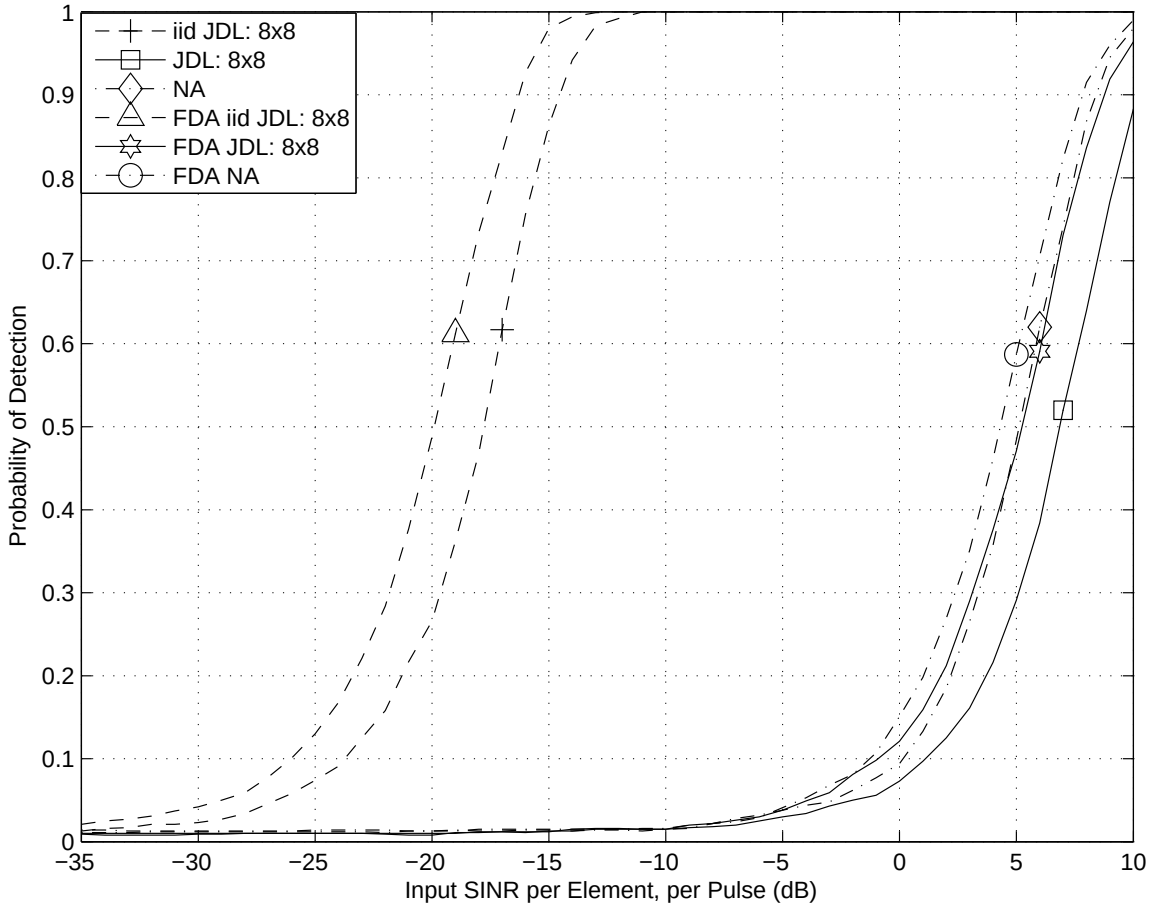

Figure 6.24: Low altitude platform and ground illumination detection curves for a target at $\bar{\omega} = 0.450$ for $P_{fa} = 0.01$. The detection curves show the same trends as the previous scenario, using non-iid sample support degrades performance to the NA processing level and FDA outperforms the constant frequency by 1 to 2 dB for both iid and non-iid sample support.

Again, the NA processing is better than the non-iid JDL, however the difference is marginally smaller by a few tenths of a decibel. The FDA improvement over constant frequency array within the target range clutter notch is preserved at approximately 2 dB.

The low platform altitude ground target results are very similar to those for the airborne target as predicted. There is improvement using FDA over constant frequency inside the clutter notch and although the magnitude is small, it supports the concept of sample support increases in homogeneity.

6.7 Linear FDA Comparison Summary

The results achieved investigating the use of a linear FDA in four different physical scenarios show that the FDA concept holds merit. The above assertion is based on benefits at particular target doppler values of interest combined with minimal or no degradation at other doppler values. To summarize, the most poignant conclusions are listed below.

- Differences in elevation transmission angle have minimal effect because the results are based on a linear array, so the only components affected are the element factor elevation component and the steering vectors.
- For a high platform altitude the greatest FDA benefit is reduced range ambiguous clutter doppler notch depth caused by the FDA range-dependent antenna pattern illumination of range ambiguous clutter rings. When target range is increased the target range and range ambiguous clutter doppler are the same and hence the sole clutter doppler notch is improved. It is important to note that increases in sample support data homogeneity is likely to contribute to the improvement at this doppler value but is not the main cause of the 10 dB detection performance increase.
- High platform altitude P_d results do not indicate more homogeneous sample support data when the target doppler corresponds to the target range clutter doppler. The magnitude of differences between the two array types are statistically insignificant so there is no indication that sample support data is degraded.
- Low platform altitude generates no range ambiguous clutter contribution and hence only one clutter notch exists. A small but consistent improvement is noted in both the estimated Output SINR and the P_d plots and the improvement of approximately 2 dB is attributed to improved sample support data homogeneity because the known Output SINR is identical. The improvement is consistent with the reduction in NHD dynamic range for both low platform altitude scenarios.

It is important to stress that the focus of this thesis is to verify the potential benefits of FDA rather than optimize results through improved channel frequency allocation. Additionally, the selection of DOF used for JDL is designed to create sample support data that had significant deviation from iid, therefore JDL performance could potentially be improved by reducing DOF and hence increasing sample support data homogeneity.

Because of the decision to select parameters that show significant degradation, the performance of JDL within the target range clutter doppler notch is outperformed by NA processing. It is noted that STAP normally provides considerable performance benefits over NA processing and also provides other benefits stemming from adaptivity to changing clutter environments.

VII. Planar Frequency Diverse Array Results

Planar arrays are used in forward-looking radar applications primarily for the ability to use elevation Degrees of Freedom (DOF) to null out range ambiguous clutter [14]. Additionally, performance improvements of two-dimensional (2D) Space-Time Adaptive Processing (STAP) techniques can be achieved through the addition of interferometric elevation processing, i.e. a factored approach and similarly, three-dimensional (3D) joint STAP techniques outperform respective joint 2D techniques [9].

The linear array results presented in Chapter VI show FDA to improve certain engagement scenarios through both suppression of range ambiguous clutter by the range-dependent antenna pattern and also sample support data homogeneity. Simulation is extended to a planar FDA to see whether similar benefits as realized over constant frequency arrays with the addition of elevation null control.

This chapter examines the benefits provided by planar FDAs based on two different channel frequency allocations and hence antenna patterns; first using frequency diversity along both array axes, and secondly, using frequency diversity only across horizontal channels. The same four physical engagement scenarios introduced in Chapter VI are used to assess the benefit of both types of planar FDAs.

7.1 Radar Simulation Parameters

The parameters used within this chapter closely follow the Multiple-Channel Airborne Radar Measurement (MCARM) program [24]. The specific radar simulation results are contained in Table 7.1 with the only significant changes from Chapter VI being an increase in the number of vertical channels P and the definition of a vertical channel spacing d_z. The parameters listed are used in all results unless specifically noted otherwise.

The same two Chapter VI Coherent Processing Interval (CPI) gain values of 352 and 64 are used, however a non-unity value for array vertical channels P means that the other CPI parameters N and M are reduced to keep CPI gain constant. The reduction of M adversely impacts the spacing between successive filters in the

Table 7.1: Planar Radar Simulation Parameters.

Variable	Value
M (Pulses in CPI)	8, 4
N (Azimuth Channels)	11, 4
$\boldsymbol{P}$ **(Vertical Channels)**	**4**
Coherent Processing Interval (CPI) Gain	352, 64
f_0 (Carrier Frequency)	1240 MHz
f_r (Pulse Repetition Frequency)	1984 Hz
τ (Pulse Width)	0.8 μs
P_t (Transmit Power)	200 kW
B (Bandwidth)	800 kHz
F_n (Noise Figure)	3 dB
N_C (Azimuth Clutter Samples)	CPI
v_a (Aircraft Velocity)	$\frac{d_x f_r}{2}$
R (Target Range)	8.0 km, 10.5 km
Array Transmit Gain	22 dB
Element Pattern	Cosine
Element Gain	4 dB
Element Backlobe Level	-30 dB
d_x (Azimuth Inter-element Spacing)	0.1092 m
$\boldsymbol{d_z}$ **(Elevation Inter-channel Spacing)**	**0.1407 m**
Transmit Taper	None
L_S (System Transmit Losses)	3 dB
Target ϕ	0°
Target $\bar{\omega}$	Various

doppler filterbank, whilst the reduction of N results in an increase in the azimuth beamwidth, the latter only occurring for the reduced CPI condition. Therefore the results achieved can not be directly compared to Chapter VI results.

7.2 Benefits of using Planar Arrays

The greatest benefit associated with the use of planar arrays is the ability to discriminate targets using elevation information in addition to azimuth and doppler information available for linear arrays. The use of elevation discrimination is particularly important for low relative velocity targets where it is difficult to discern the target using doppler and azimuth. Based on elevation discrimination and an elevation dependent antenna pattern the use of planar arrays is expected to produce considerable performance differences between airborne and ground targets, as opposed to minimum differences experienced for linear arrays in Chapter VI.

As mentioned at the start of this chapter there are two different frequency allocation schemes used, the difference being whether or not there is frequency diversity across vertical array channels. The frequency increment between successive horizontal channels has been kept as the same value used in Chapter VI, $\Delta f_x = 1$ kHz and the frequency increment between successive vertical channels is selected to be $\Delta f_z = 2$ kHz, the same value used in Chapter V.

It is also noted that under the reduced CPI condition the horizontal array length N means that the total frequency diversity across the array within this chapter is reduced compared to the diversity in Chapter VI, another reason why the results of Chapter VI and this chapter can not be directly compared.

7.3 Physical Scenario Definitions

The same four physical scenario conditions based on platform altitude and elevation transmit angle are used to assess performance, thereby allowing trends to be compared to linear array trends in Chapter VI. The parameters for the four scenarios

Table 7.2: Scenario Parameter Combinations.

Name	Platform Altitude (H)	Elevation Angle (θ)
AEWAC with Airborne Target	High (3073m)	0°
AEWAC with Ground Target	High (3073m)	-17.0° for 10.5 km Range
UAV with Hovering Helicopter	Low (334m)	0°
UAV with Ground Target	Low (334m)	-2.4° for 8.0 km Range

are reprinted in Table 7.2, and each combination will be discussed in greater detail in the relevant section.

7.4 AEWAC with Airborne Target Results

It is important to recall an impact of a high platform altitude is the inclusion of range ambiguous clutter, based on the radar horizon range and the Maximum Unambiguous Range (MUR) there are two range ambiguous clutter rings. For a close target range the clutter doppler associated with the target range will be distinct from the range ambiguous clutter doppler, producing two distinct clutter doppler notches.

The known interference covariance matrix Output SINR is seen in Figure 7.1 and is an interesting result. Firstly, there is only one clutter doppler notch as opposed to the two notches predicted. The reason why only one clutter notch is present is due to the number of pulses integrated over a CPI, $M = 8$. As only eight doppler filters are present, both the target range and range ambiguous clutter dopplers $\bar{\omega} = 0.433$ and 0.450 respectively, fall within the same doppler filter and hence the notches are not separated.

The most pertinent feature of Figure 7.1 is the performance improvement using the FDA. The difference between the array types is attributed to the improvement experienced at the range ambiguous clutter doppler, caused by the range-dependent FDA antenna pattern illumination of range ambiguous clutter rings. The reduction in notch depth is approximately 15 dB for fully adaptive processing, i.e. the Matched Filter (MF), and 20 dB for partially adaptive processing using Joint Domain Localized

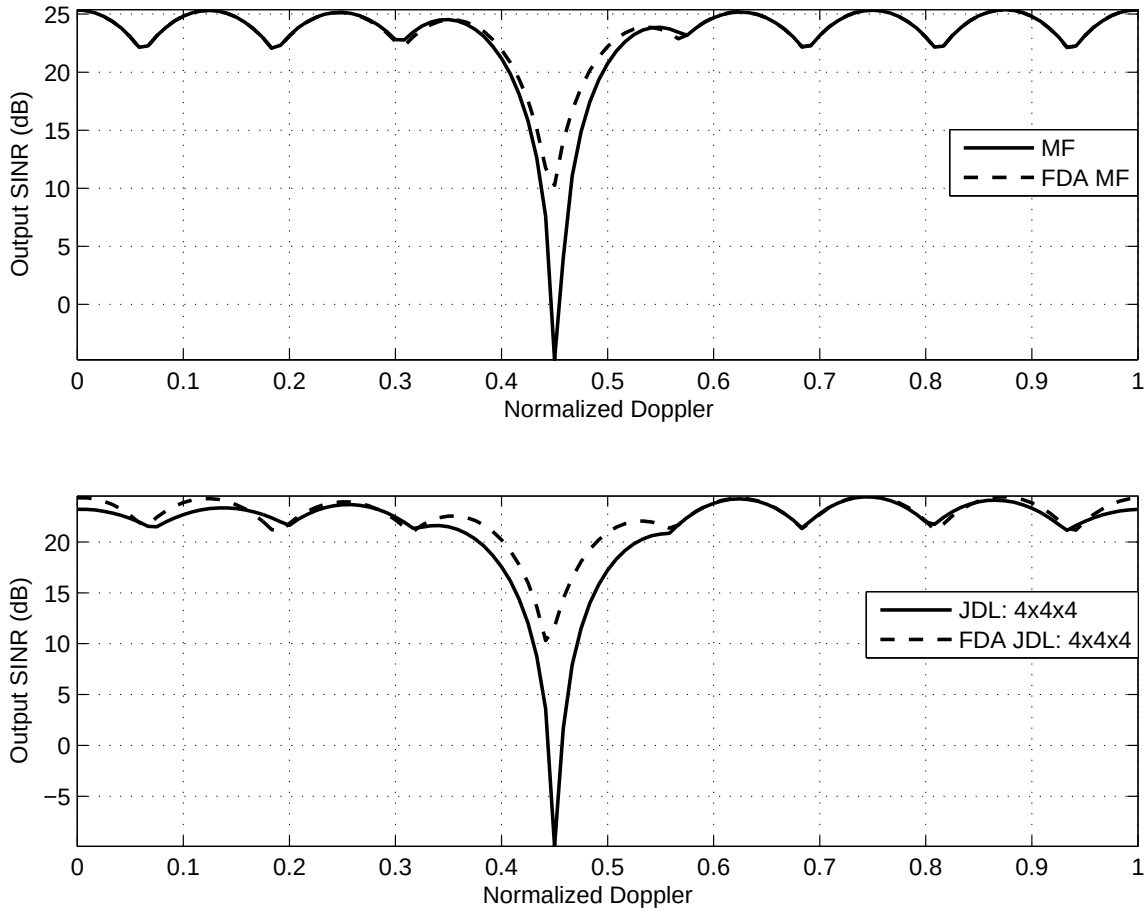

Figure 7.1: High-altitude platform, horizontal elevation transmission planar array Output SINR using known interference covariance matrix at a target range of 10.5 km. Only one distinct clutter doppler notch is observed however there are two distinct clutter doppler notch values that are not separated because of the reduced number of doppler filters. It is known there are the two distinct clutter doppler values because the FDA notch depth is decreased, as a result of the suppressed range ambiguous clutter notch.

(JDL). The use of FDA also marginally reduces the clutter notch width, particularly for partial STAP.

When the interference covariance matrix is estimated using symmetrical sample support vector selection the Output SINR is seen in Figure 7.2. As expected, there is noticeable degradation associated with the covariance matrix estimation, but the magnitude is considerably less than the degradation experienced for linear arrays. One reason for reduced degradation is greater antenna pattern suppression of range-cells further away from the target range-cell, de-emphasizing their individual clutter doppler values. The other reason is the use of elevation suppression within the JDL technique, particularly useful for high platform altitude when the target range clutter is distinct from range ambiguous clutter contributions in the elevation domain.

The other major estimated Output SINR interesting aspect is the shift in the FDA doppler notch location. The reason for the shift is because of an imbalance between the target range doppler notch depth and the range ambiguous doppler notch depth, the latter notch being mitigated by the FDA antenna pattern thereby shifting the single displayed notch left toward the target range clutter notch value. The shift is also evident using known interference covariance matrix confirming the above rationale.

The Non-Homogeneity Detector (NHD) result for the scenario parameters is shown in Figure 7.3 where the FDA increases the constant frequency array Generalized Inner Product (GIP) dynamic range by 1% and standard deviation by 10%. Whilst the GIP dynamic range is the primary statistic used for NHD analysis, standard deviation is also important as mentioned in Appendix A. The frequency diversity across vertical channels changes the GIP shape increases the difficulty in determining the FDA impact on sample support homogeneity, however, the minimal increase in GIP dynamic range and more notable increase in GIP standard deviation is consistent with the increased FDA degradation compared to the constant frequency array.

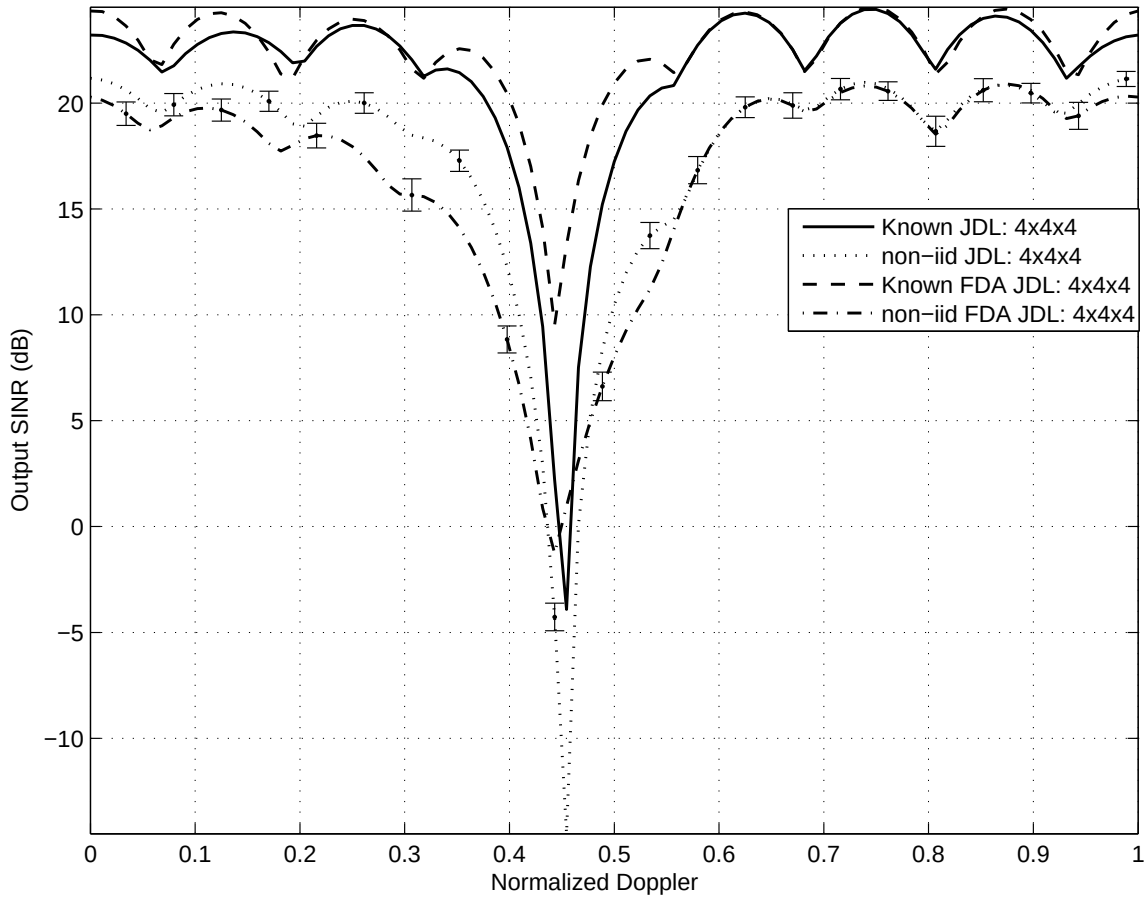

Figure 7.2: High-altitude platform with horizontal elevation transmission planar array Output SINR. The known covariance result is compared to an estimated interference covariance matrix generated from 128 symmetrical sample support vectors. The latter curve is averaged over 1000 realizations and shows degradation around the target range clutter doppler due to the skewed matrix estimate. The FDA suppression of the range ambiguous clutter is evident by the reduced notch depth and also by the shift in the FDA clutter notch doppler value to the left.

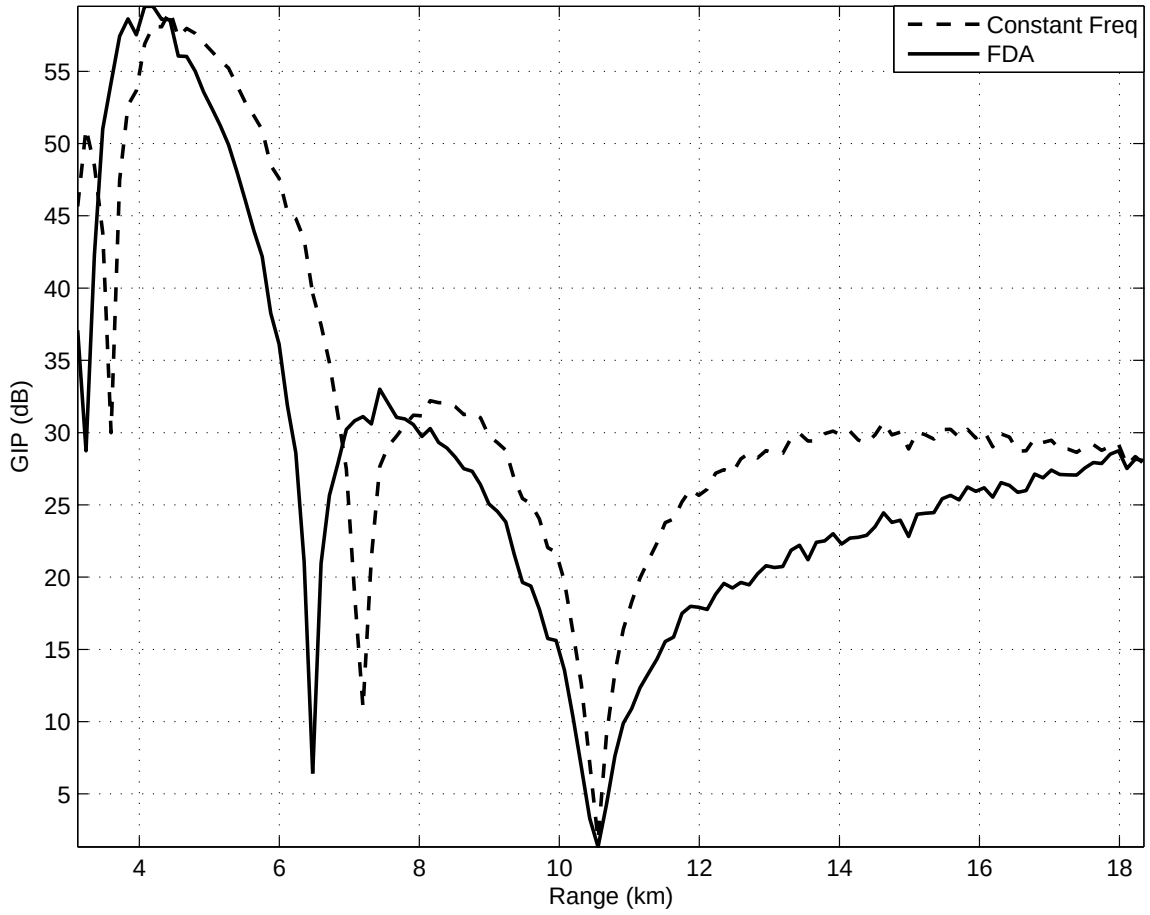

Figure 7.3: High platform altitude with airborne target GIP for forward-looking planar constant frequency array and FDA averaged over 100 runs. The major feature is the different notch locations between the two array types, corresponding to the different null locations due to frequency diversity across vertical channels impacting range ambiguous contributions. There is minimal difference in GIP dynamic range and GIP standard deviation has increased.

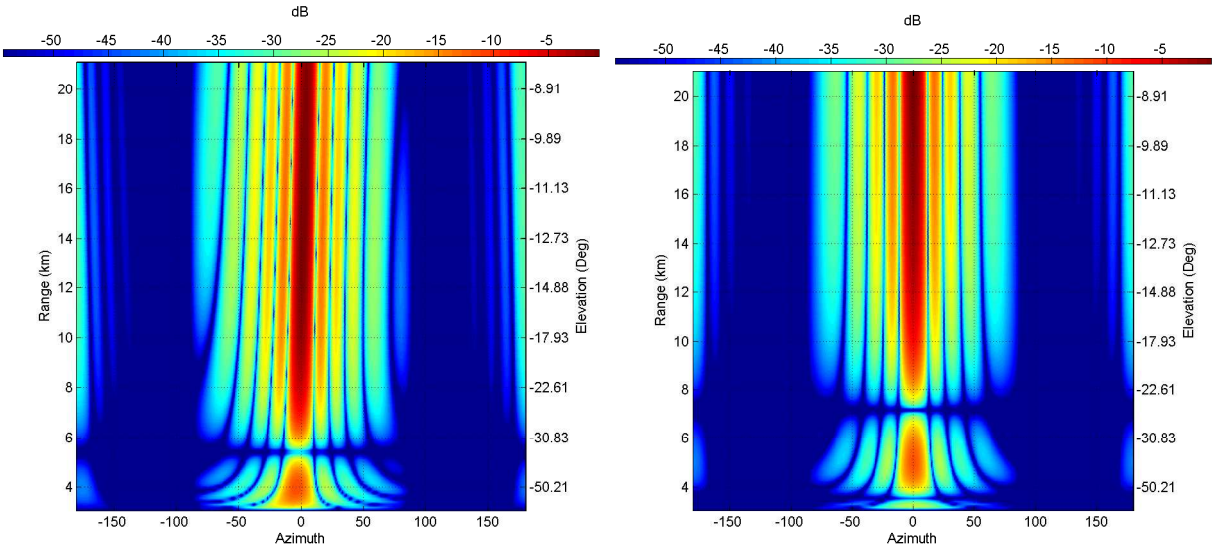

(a) (b)

Figure 7.4: Ground projected antenna pattern for high-altitude platform with 0° elevation angle, across sample support range-cells. (a) Planar FDA (b) Constant Frequency. Comparison of the two array types shows the constant frequency array has more elevation nulls close to the platform providing greater suppression of close range-cells.

The additional degradation is based on different ground projected antenna pattern illumination of close target range-cells for the two array types depicted in Figure 7.4. The FDA ground projected pattern has fewer elevation nulls at close range, therefore less suppression of close range-cells yielding an estimated interference matrix with a greater proportion of doppler dominated by clutter.

When the radar parameters are changed to generate a reduced CPI there is sufficient sample support to use fully adaptive STAP, i.e. the Adaptive Matched Filter (AMF). The difference between the MF and the AMF is shown in Figure 7.5. It is re-emphasized that the reduced values of N and M not only lowers the CPI gain, but also increases the azimuth beamwidth and increases the doppler filterbank spacing leading to a significant increase in the clutter notch width.

There is a marked difference between the MF results for the two array types, with FDA shifting the clutter doppler notch location to the left as explained previously and also providing a performance improvement of approximately 9 dB.

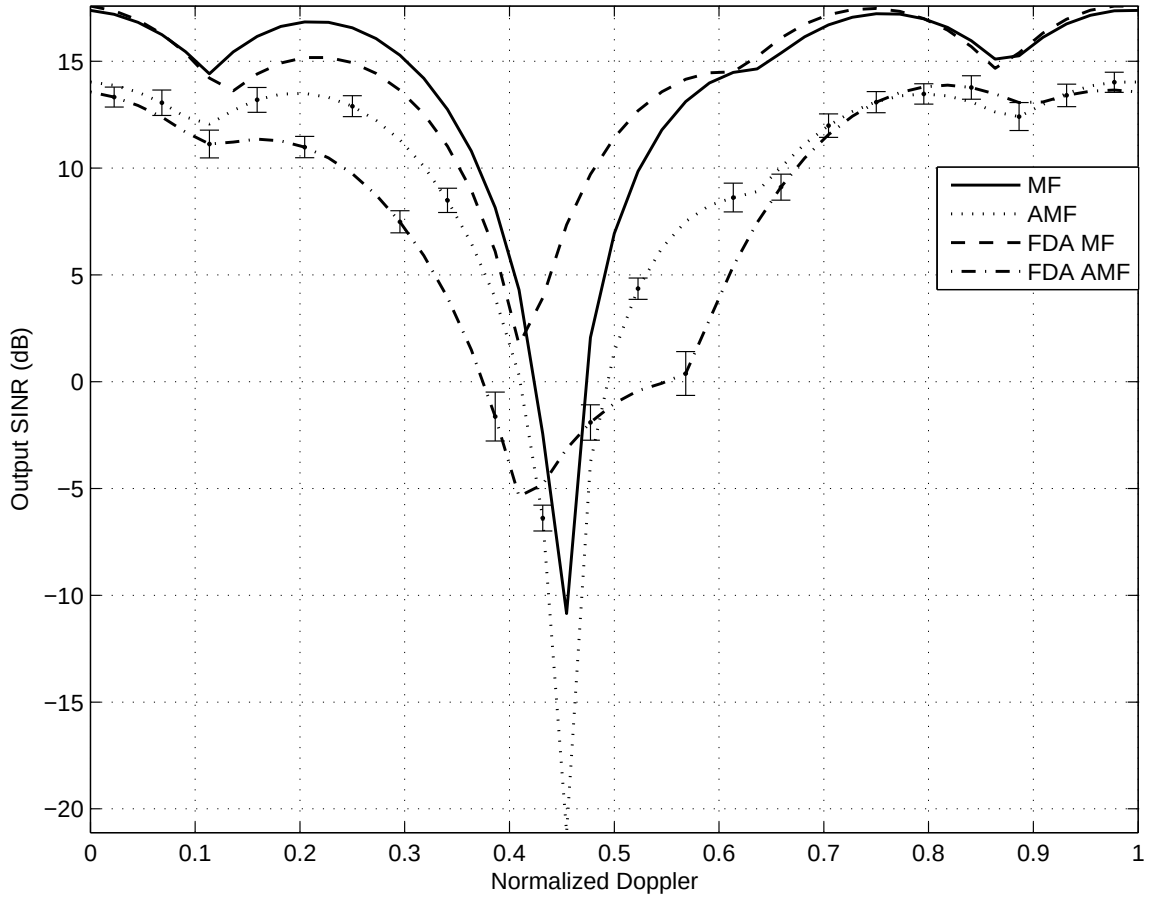

Figure 7.5: High-altitude platform horizontal elevation transmission fully adaptive Output SINR with reduced CPI values $P = 4$, $N = 4$, and $M = 4$. The MF result is compared to AMF using an estimated interference covariance matrix generated from 128 symmetrical sample support vectors. The FDA MF is seen to be considerably higher than the constant frequency array MF and also shifts the clutter notch to the left because of the FDA suppression of range ambiguous clutter. The AMF curves are averaged over 1000 realizations and show degradation, particularly for the FDA around $\bar{\omega} = 0.6$.

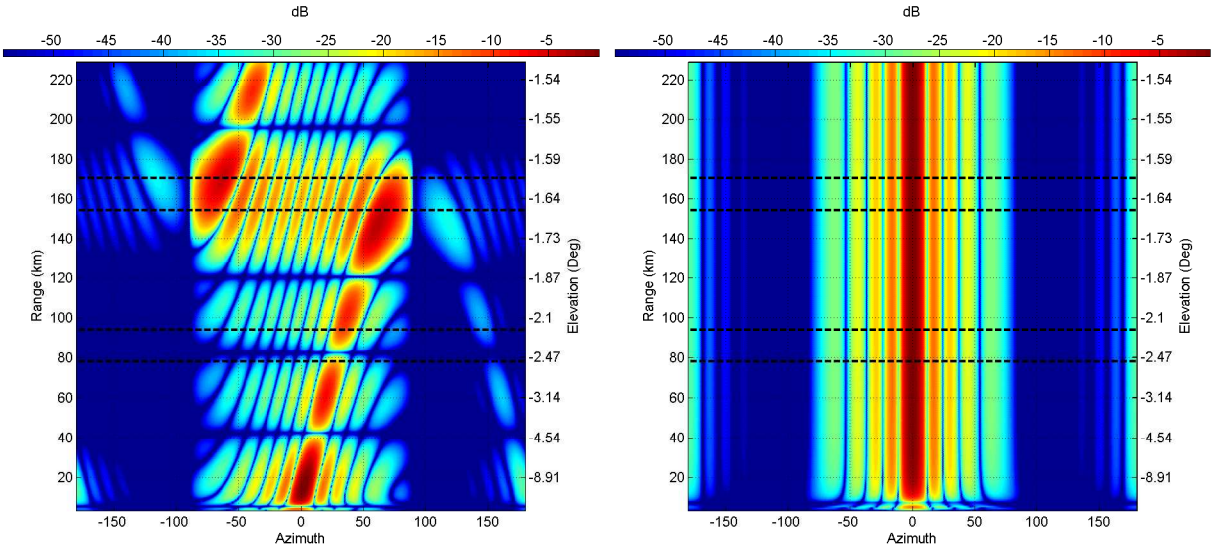

Figure 7.6: Ground projected antenna pattern for high-altitude platform with 0° elevation angle out to the radar horizon range. (a) Planar FDA (b) Constant Frequency. The dashed lines show the 1st and 2nd range ambiguous swaths corresponding to the sample support range-cells, that occur between 78-94 km and 154-170 km respectively.

Greater degradation is observed to occur for the FDA, again based on differences in the ground-projected antenna pattern over the sample support range-cells. However, the FDA improvement is not caused by the illumination of actual sample-support range-cells, but rather the illumination of range ambiguous range-cells that contribute to the aforementioned range-cells. The ground projected antenna pattern in Figure 7.6 for the two array types shows the range ambiguous contributions (occurring at 78-94 km and 154-170 km) responsible for the FDA improvement in Figure 7.2 and Figure 7.5.

Overall, the drop from known covariance to non-iid sample support increases the FDA notch depth by 7 dB and constant frequency array notch depth by 10 dB, however the FDA clutter notch width is significantly increased. The notch width increase is such that the FDA outperforms constant frequency array only within the region $0.43 \leq \bar{\omega} \leq 0.49$, making it difficult to compare sample support data homogeneity.

Following the approach taken in Chapter VI, probability of detection P_d performance is assessed at both clutter doppler notches values. Whilst the number of doppler filterbanks results in the target range and range ambiguous clutter dopplers depicted as one notch in the Output SINR, the actual amount of competing clutter and hence detection performance is different.

The detection curve using the target range clutter doppler is included as Figure 7.7 and shows a 10 dB improvement of FDA over constant frequency array using iid based sample support. When actual non-iid sample support is used the FDA improvement is reduced to 6 dB, corresponding to the above estimated Output SINR plot. The other observation is that JDL significantly outperforms NA, therefore the ability to use elevation in STAP is beneficial and as for the linear array, STAP with real sample support is less effective than NA.

A target at the range ambiguous clutter doppler has detection performance shown in Figure 7.8. The performance is seen to be different from the previous P_d curve, proving there is a significant difference despite both target doppler values being displayed within the same Output SINR doppler notch.

The improvement of FDA over the constant frequency array with iid sample support is 19 dB and the difference increases to 20 dB when actual sample support is used. The additional 1 dB increase is too small to be statistically significant, however indicates potential benefits of sample support homogeneity or at least confirms that there is no degradation.

7.5 AEWAC with Jeep Results

The next physical scenario involves changing the elevation transmit angle to correspond to the target range elevation angle so the antenna mainlobe is illuminating the ground. In contrast to the linear array results, the change in the elevation angle has a significant impact on the planar array because of explicit elevation dependence within the antenna pattern.

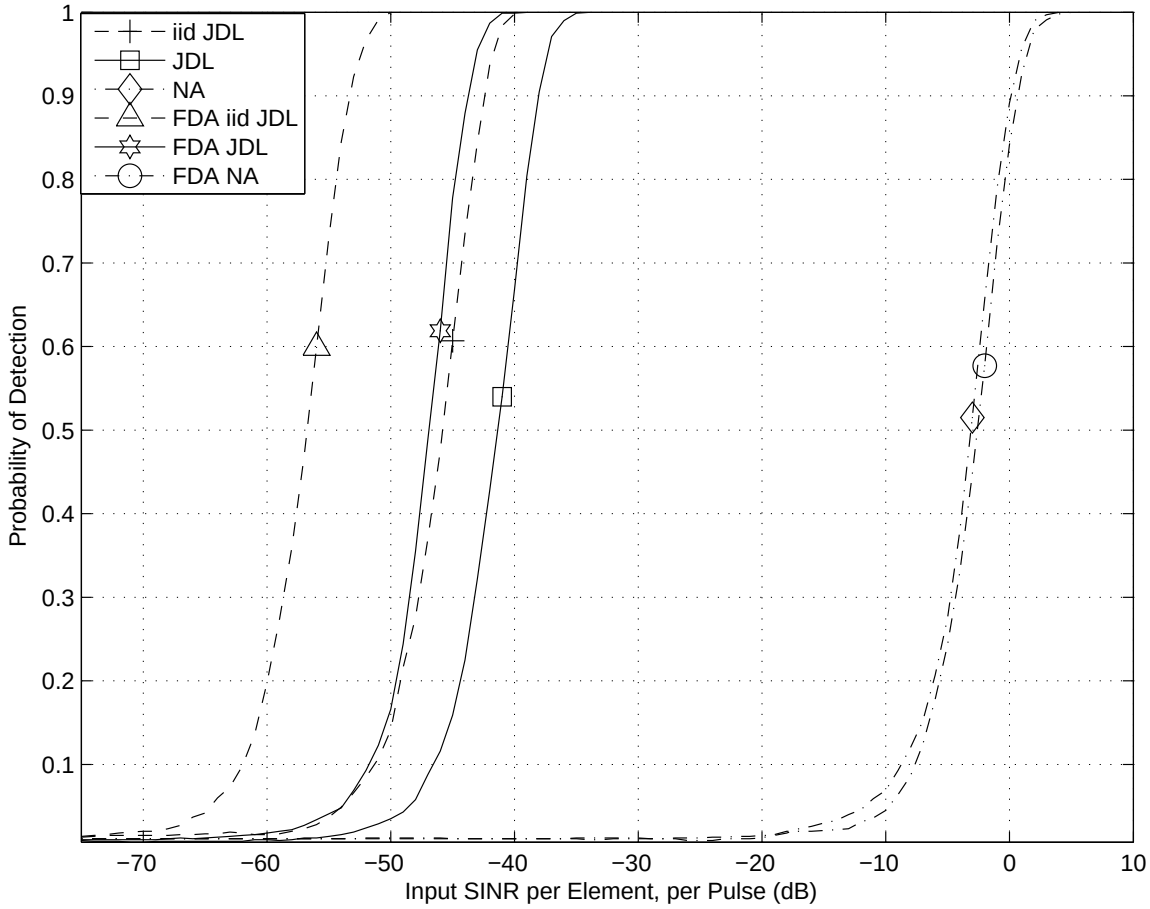

Figure 7.7: High altitude platform and horizontal elevation transmission planar array detection curves for a target at $\bar{\omega} = 0.433$ for $P_{fa} = 0.01$. The detection curves show considerable FDA performance benefits over constant frequency arrays when using both iid and non-iid sample support.

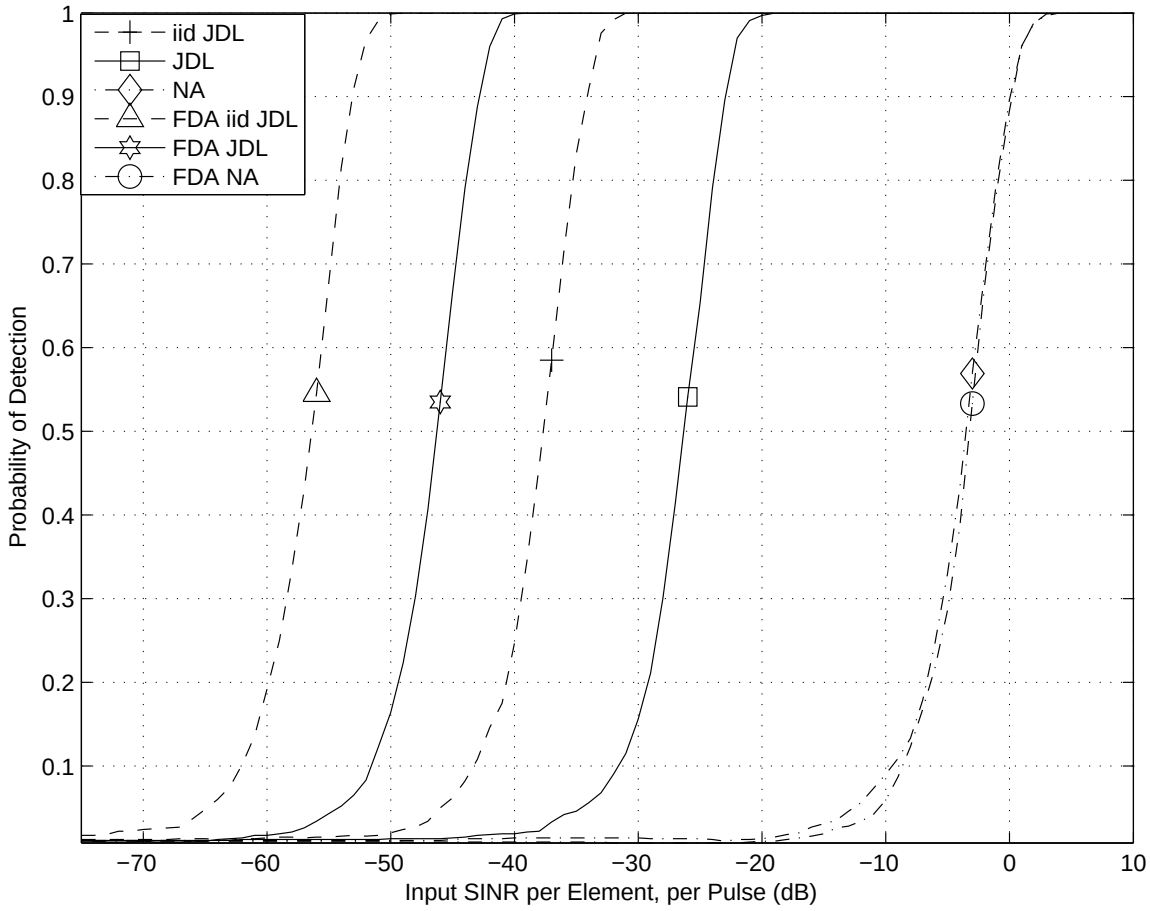

Figure 7.8: High altitude platform and horizontal elevation transmission planar array detection curves for a target at $\bar{\omega} = 0.450$ for $P_{fa} = 0.01$. The FDA detection curves show significant performance improvement of 20 dB over the corresponding constant frequency array results and is attributed to suppression of range ambiguous clutter by the FDA antenna pattern.

Using known interference covariance matrices the Output SINR seen in Figure 7.9 clearly differs from the horizontal elevation transmission Output SINR curve in Figure 7.1. There is only one clutter doppler notch despite the target range clutter doppler being distinct from the range ambiguous clutter doppler because the reduced number of doppler filterbanks as described previously, and the Output SINR magnitude shows that the clutter notch depth is considerably increased. The increase in the clutter notch depth is intuitive since the contributing clutter rings are now illuminated by the mainlobe rather than an elevation shift of -17° from mainlobe, so the clutter returns are of greater magnitude.

The most significant change observed with the new elevation angle is minimal difference between the two array types, as opposed to the airborne target where the FDA produced a considerable improvement in the range ambiguous clutter doppler notch. The lack of improvement using FDA means that the doppler notch does not shift for the FDA as is seen in the preceding section and the actual location now occurs at $\bar{\omega} = 0.433$, the target range clutter doppler. The reason for the change is the target at $\theta = -17°$ can be distinguished from the range ambiguous clutter rings at elevations of -2.5° and -1.6°, hence range ambiguous clutter shown in Figure 7.10 is suppressed. Since the target range illumination is the same at the target range the Output SINR is identical.

Using non-iid sample support to estimate the interference covariance matrices degrades the Output SINR curves seen in Figure 7.11. As for the preceding scenario, FDA shows greater degradation across $0 \leq \bar{\omega} \leq 0.6$ increasing the clutter notch width and also increasing the notch depth by 11 dB. The other observation is that the non-iid sample support for the constant frequency array has very limited degradation, showing that there is very little homogeneity in the sample support, again due to the new antenna pattern illumination of target range-cells due to the elevation angle offset.

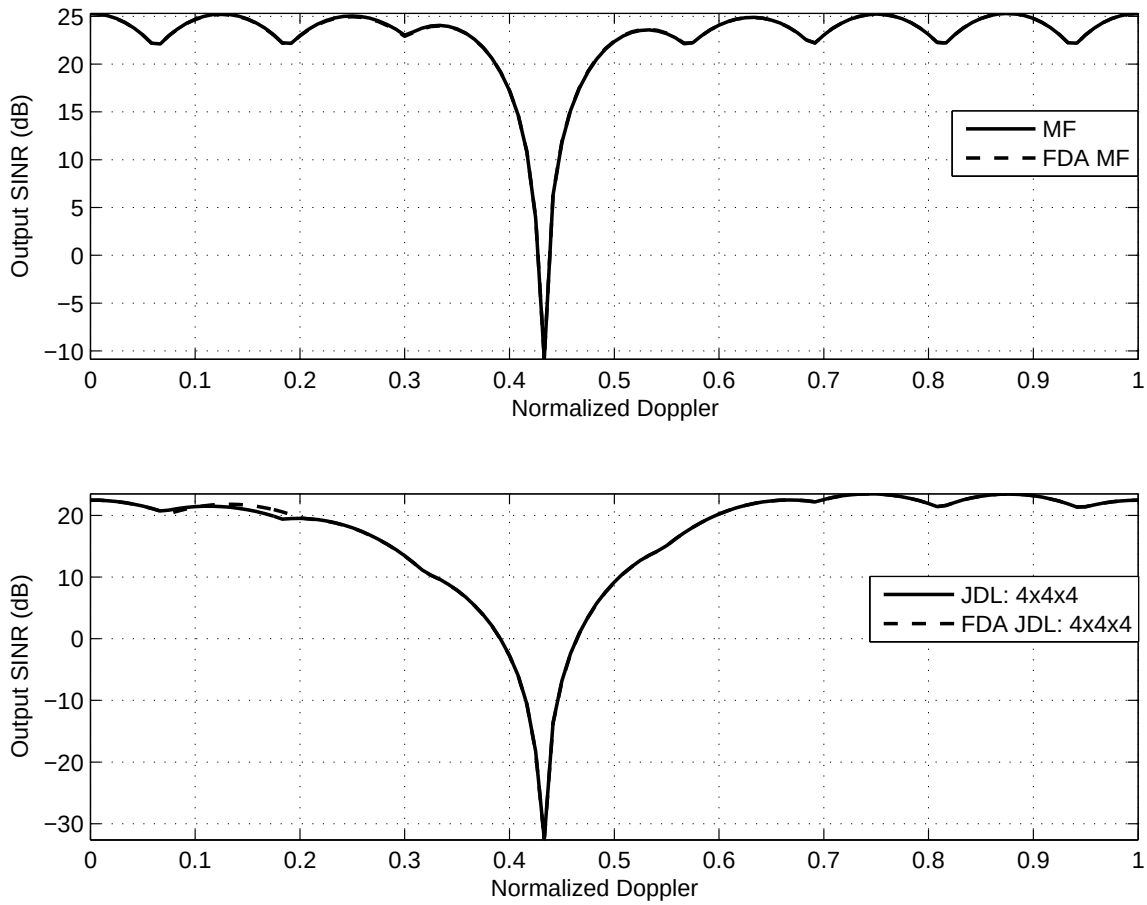

Figure 7.9: High-altitude platform, ground illumination planar array Output SINR using known interference covariance matrix at a target range of 10.5 km. Only one distinct clutter doppler notch is observed because there is sufficient elevation angle difference between the target and the range ambiguous clutter to suppress the latter, leaving only the primary target range clutter doppler. The result shows that differences in transmission elevation angle can have a large impact on planar array performance. Additionally the Output SINR scale is considerably higher than the previous scenario, indicating over 20 dB additional degradation for JDL with the change in elevation transmit angle.

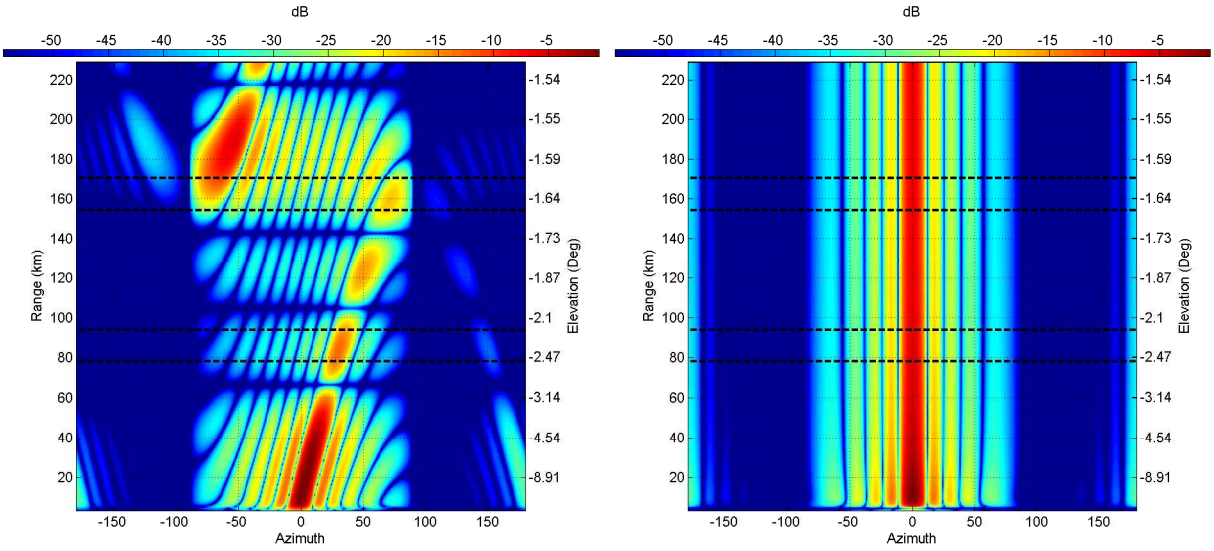

Figure 7.10: Ground projected antenna pattern for high-altitude platform with ground illumination up to the radar horizon range. (a) Planar FDA (b) Constant Frequency. The dashed lines show the 1st and 2nd range ambiguous swaths corresponding to the sample support range-cells, that occur between 78-94 km and 154-170 km respectively.

The change in elevation transmission angle from 0° to -17° has minimal effect on the NHD result. When the GIP was recalculated, the shape was identical to Figure 7.3 and the statistics were within 1 percentage point, with the FDA increasing GIP dynamic range by 1.2% and standard deviation by 11%. Therefore, the same conclusion can be drawn, frequency diversity across vertical channels changes the GIP shape and degrades sample support homogeneity.

Using reduced CPI parameters the AMF Output SINR is seen in Figure 7.12. The degradation associated with using the FDA is now increased to 20 dB at the clutter notch reinforcing the assertion in Section 2.2.3 that STAP techniques with increased DOF have greater degradation.

As for the preceding section, the increased degradation for FDA results from the FDA ground projected antenna pattern seen in Figure 7.13. The closest range-cells used for interference matrix estimation contain the smallest clutter doppler values,

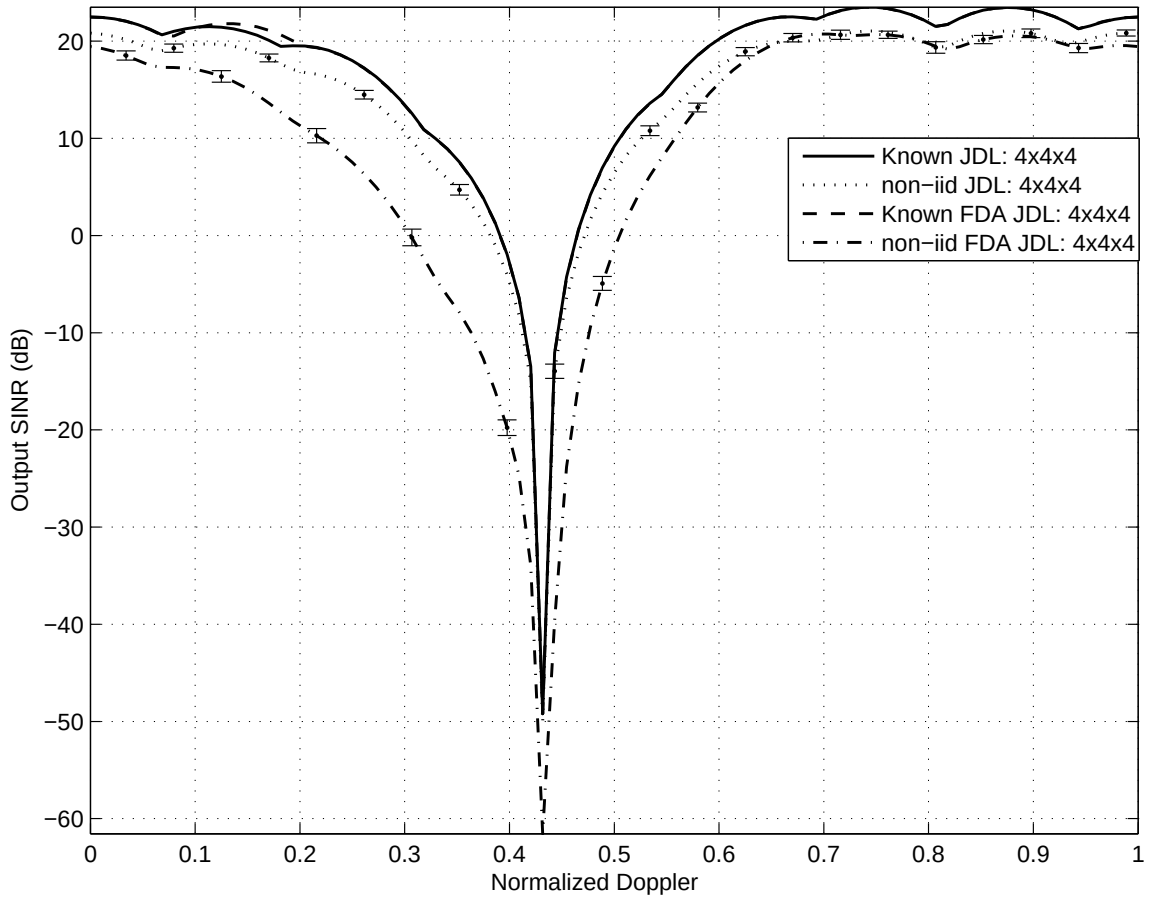

Figure 7.11: High-altitude platform with ground illumination planar array Output SINR. The known covariance result is compared to an estimated interference covariance matrix generated from 128 symmetrical sample support vectors. The latter curve is averaged over 1000 realizations and shows little degradation compared to the known covariance results because of the ability to suppress the range ambiguous contributions. The degradation caused by skewed matrix estimation is seen to have a larger impact on the FDA than for the constant frequency array.

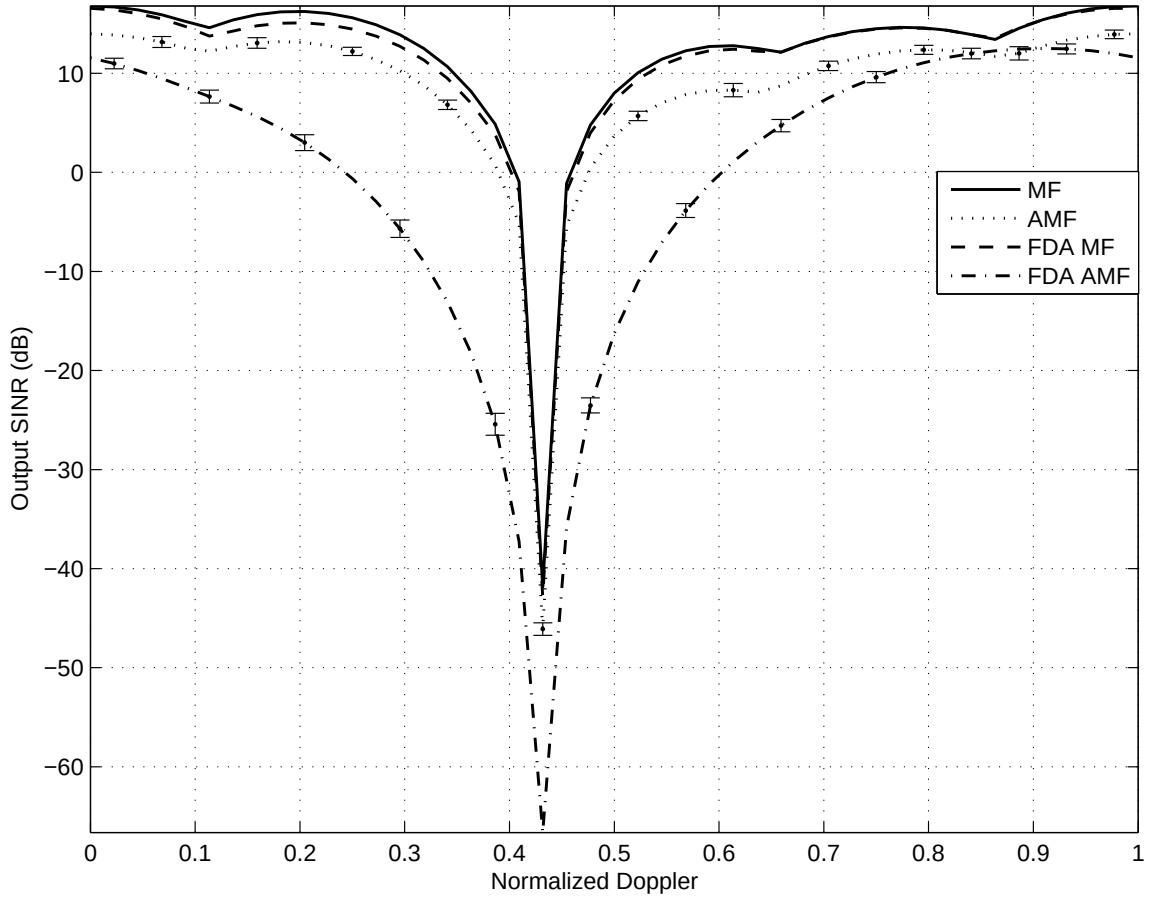

Figure 7.12: High-altitude platform horizontal elevation transmission fully adaptive Output SINR with reduced CPI values $P = 4$, $N = 4$, and $M = 4$. The MF result is compared to AMF using an estimated interference covariance matrix generated from 128 symmetrical sample support vectors. The AMF curves are averaged over 1000 realizations and similar to JDL above, the scale is considerably greater than the previous scenario however, the constant frequency degradation is small. The use of non-iid sample support for FDA is seen to considerably increase the degradation when compared to the constant frequency.

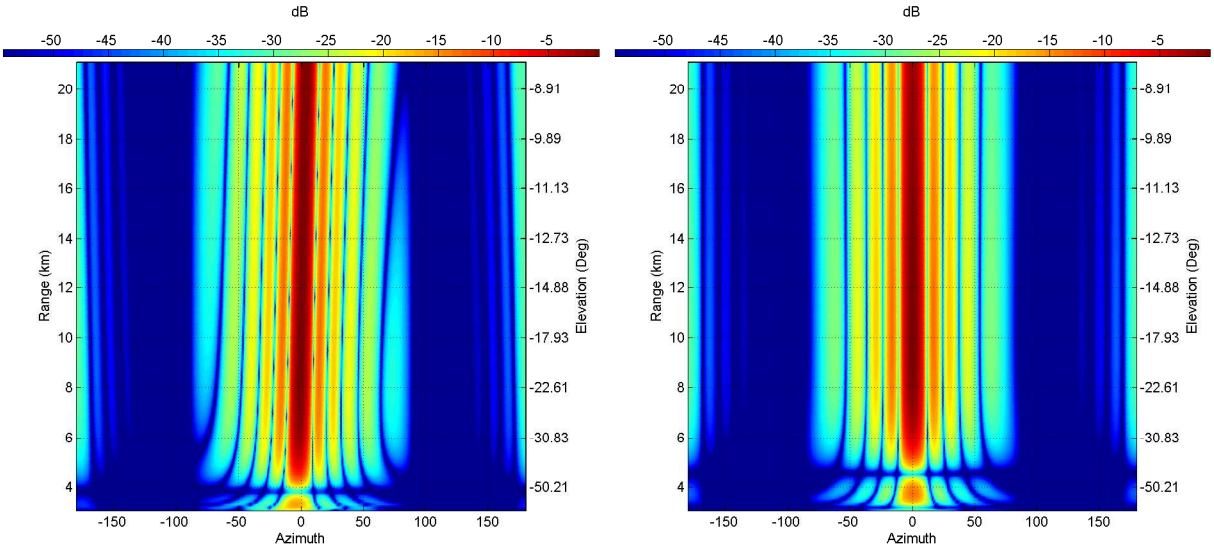

(a) (b)

Figure 7.13: Ground projected antenna pattern for high-altitude platform with ground illumination across sample support range-cells. (a) Planar FDA (b) Constant Frequency. Comparison of the two array types shows the constant frequency array has an additional elevation null very close to the platform providing greater suppression of extremely close range-cells.

and these cells have greater suppression for constant frequency array pattern skewing the weighting vector based off the estimated matrix and degrading performance.

Since the platform is still at the high altitude, detection curves are generated for two distinct target doppler values at the target range clutter doppler and the suppressed range ambiguous clutter doppler. Based on the estimated covariance matrix Output SINR, the performance at the target range clutter doppler is expected to be considerably worse than performance at the range ambiguous clutter doppler.

Using a target doppler corresponding to the target range clutter doppler the P_d curve is included as Figure 7.14. The detection curves are consistent with the averaged Output SINR with minimal difference between the two array types when using iid sample support, and approximately equal to non-iid sample support for the constant frequency array. The reason why non-iid can outperform the iid sample support is because both curves are within statistical error levels. Non-iid sample support for the FDA is seen to degrade performance by approximately 15 dB, again with the error

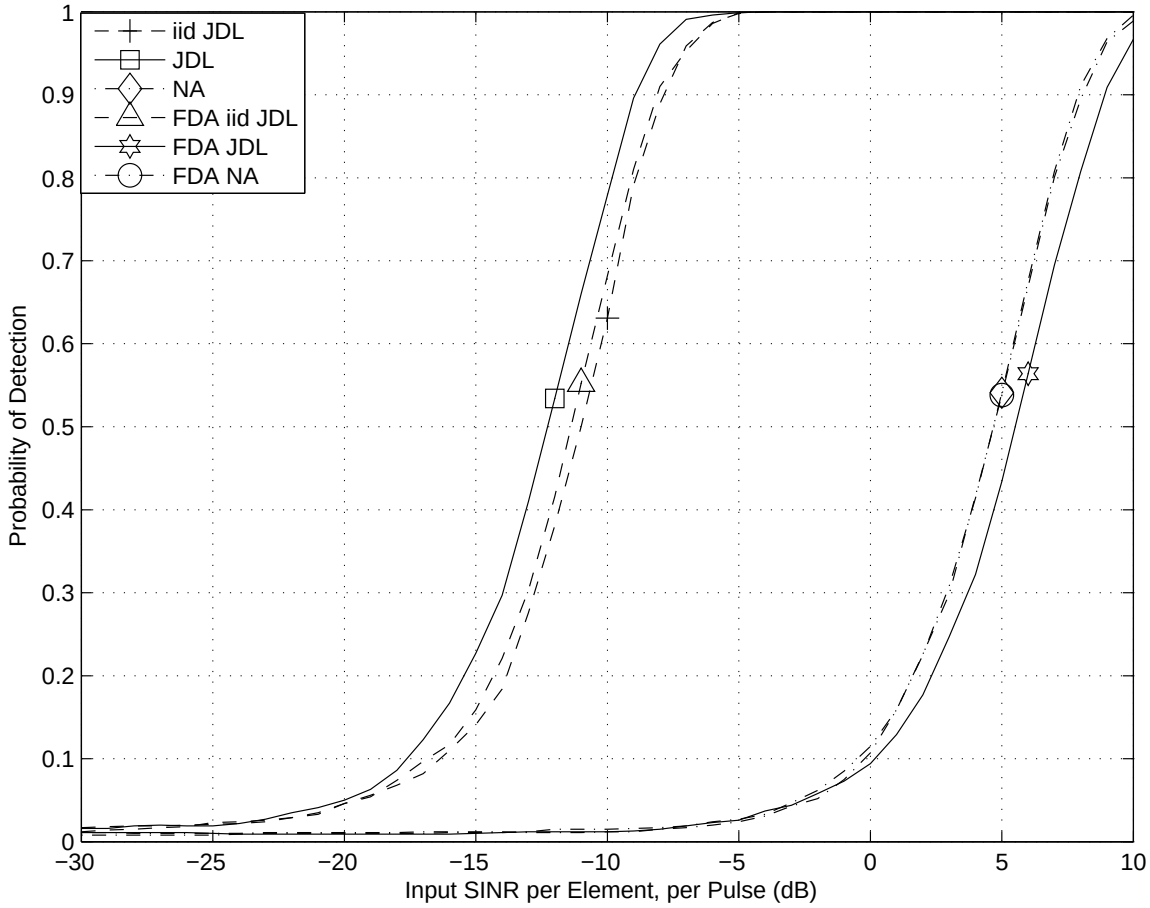

Figure 7.14: High altitude platform and ground illumination planar array detection curves for a target at $\bar{\omega} = 0.433$ for $P_{fa} = 0.01$. The detection curves show minimal difference between the iid sample support of both array types and also the constant frequency array with non-iid sample support. However there is a considerable performance degradation using non-iid sample support for the FDA, consistent with the JDL Output SINR with estimated interference matrix.

bars produced in the Output SINR and unfortunately places FDA performance at the NA processing level.

The second detection curve uses a target doppler corresponding to the suppressed range ambiguous clutter doppler $\bar{\omega} = 0.450$ with the result seen in Figure 7.15. As predicted, the performance is much better for both array types with improvements on the order of 27 dB. Again, there is no discernable degradation using non-iid sample support for the constant frequency array and approximately 15 dB for the FDA matching the Output SINR in Figure 7.11.

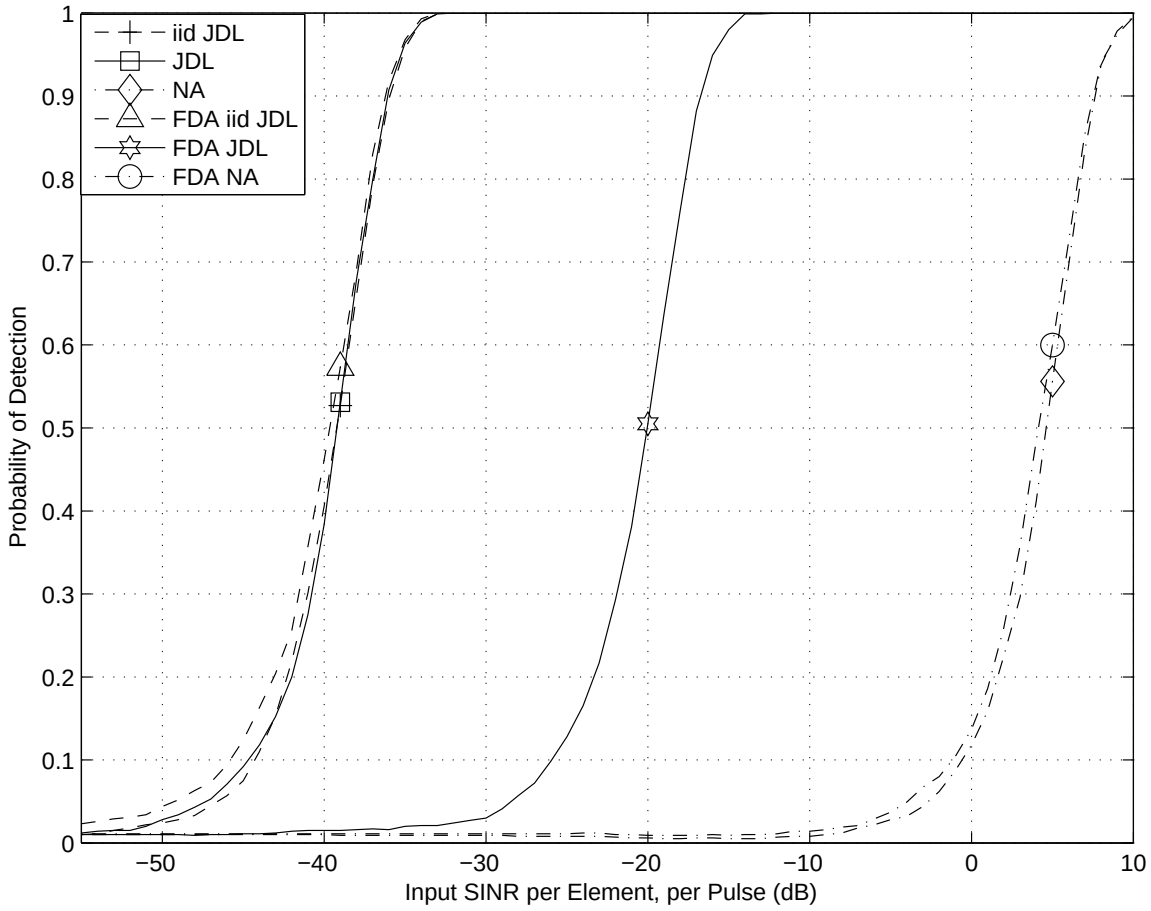

Figure 7.15: High altitude platform and ground illumination planar array detection curves for a target at $\bar{\omega} = 0.450$ for $P_{fa} = 0.01$. As for the previous target doppler value, the iid performance for both array types and the constant frequency non-iid are near identical. The FDA using non-iid is seen to suffer by 20 dB, however the performance is above NA processing.

Overall it is observed that the change in the elevation transmission angle from horizontal to ground illumination produces significant effects on the Output SINR and corresponding P_d curves. Using a known interference covariance matrix or one artificially generated by iid sample support, the range ambiguous clutter contribution is fully suppressed by the divergence in elevation angle from the target resulting in only the target range clutter doppler notch. When using non-iid sample support, FDA suffers degradation similar to the linear array result, however the constant frequency array does not suffer any notable degradation.

The two estimated interference covariance matrices are critical in determining the reason behind the degradation disparity. Since the matrices are estimated using sample support vectors meeting Reed's Rule it is not possible to determine clutter rank directly, however it is possible to generate an MVE clutter spectrum for the two array types. Whilst at high platform altitude there are range ambiguous clutter rings, they are suppressed using elevation DOF and therefore are not critical to performance. To reduce any statistical errors, multiple interference covariance matrix estimates were used, and each target range clutter spectrum image was averaged, with the final result is seen in Figure 7.16.

Comparison of the two clutter spectra confirm the constant frequency estimated interference covariance matrix array has a smaller clutter region within the azimuth-doppler domain compared to the FDA estimated interference covariance matrix. Chapter V showed the direct link between clutter spectrum and clutter rank, consistent with the degraded FDA performance. The increased clutter arc width indicates greater variation of clutter statistics across the sample support vectors used for matrix estimation.

7.6 UAV with Hovering Helicopter Results

When the scenario involves a low platform altitude there is no range ambiguous clutter contribution because the MUR is approximately the same value as the radar horizon range. As explained in Chapter VI, the lack of range ambiguous clutter

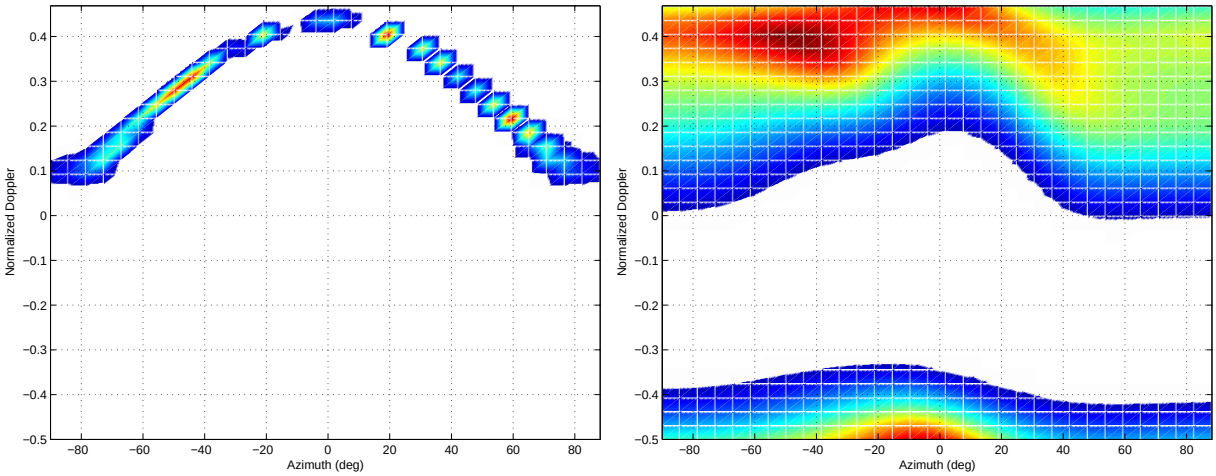

Figure 7.16: High-altitude platform and -17° elevation transmit angle, Minimum Variance Estimate clutter spectrum comparison of estimated interference covariance matrices using non-iid sample support. Using the same threshold value, it is seen that there is a drastic difference between the constant frequency array clutter (left) and the FDA (right) indicating a significant difference in clutter rank at the target range. The result is consistent with the degradation experienced using non-iid sample support in the Output SINR and both P_d plots.

produces only one clutter notch corresponding to the target range clutter doppler. The other impact of using a low platform altitude is the change of target range to 8.0 km and when combined with the platform altitude of 334 m the target range clutter doppler is 0.450.

The Output SINR with known interference covariance matrices is seen in Figure 7.17. As for the linear array, the low altitude performance is identical for both array types because the target range illumination is identical.

Additionally, when the result is compared to the high platform altitude Output SINR in Figure 7.1 it is noted that the MF is nearly identical for the constant frequency array, however for JDL there is degradation noticed at $\bar{\omega} = 0.55$. The degradation occurs because of insufficient DOF within the azimuth angular domain, recalling that the DOF is reduced from the linear results in Chapter VI. When the azimuth DOF η_a is increased the degradation is removed and when DOF is reduced, additional degradation occurs as seen in Figure 7.18, which verifies the cause as az-

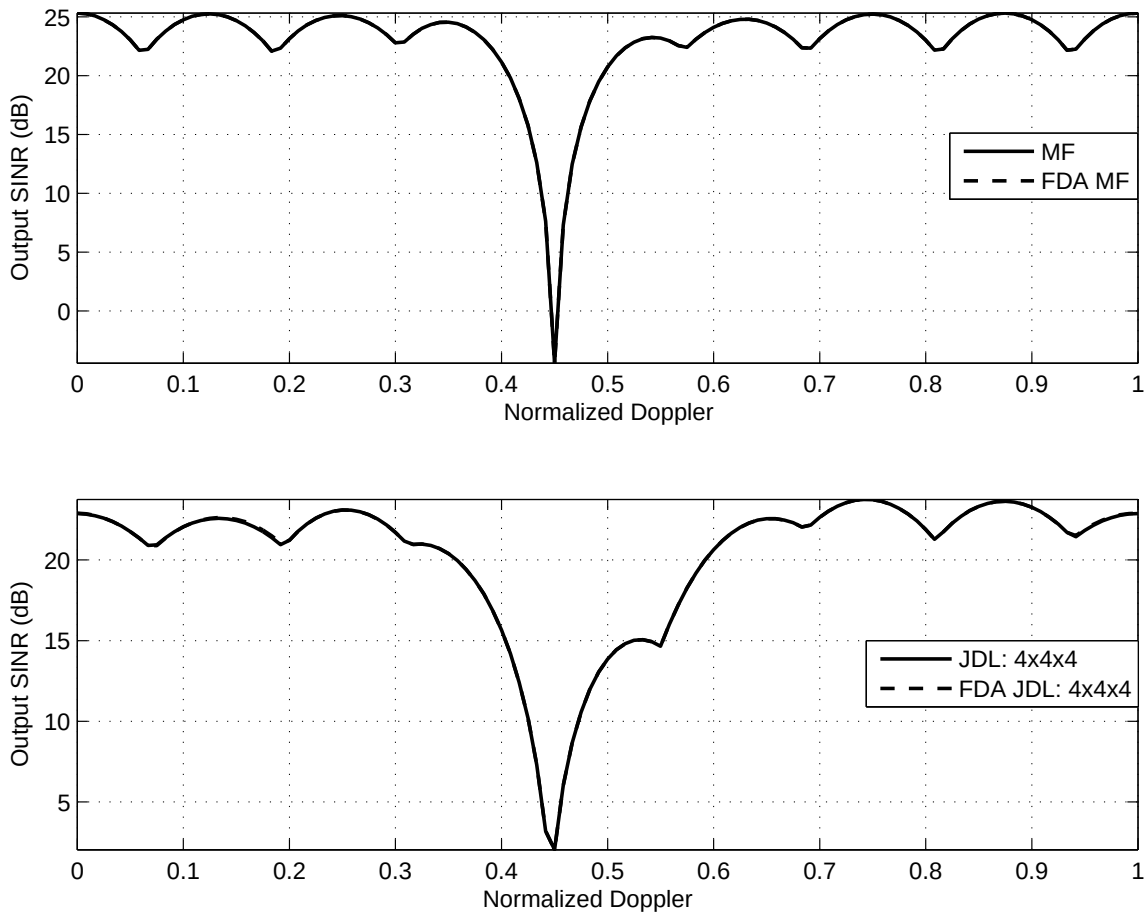

Figure 7.17: Low-altitude platform, horizontal elevation transmission planar array Output SINR using known interference covariance matrix at a target range of 8.0 km. Only one clutter doppler notch is present because there is no range ambiguous clutter at the low platform altitude. As for the linear array, the performance is identical for the two array types.

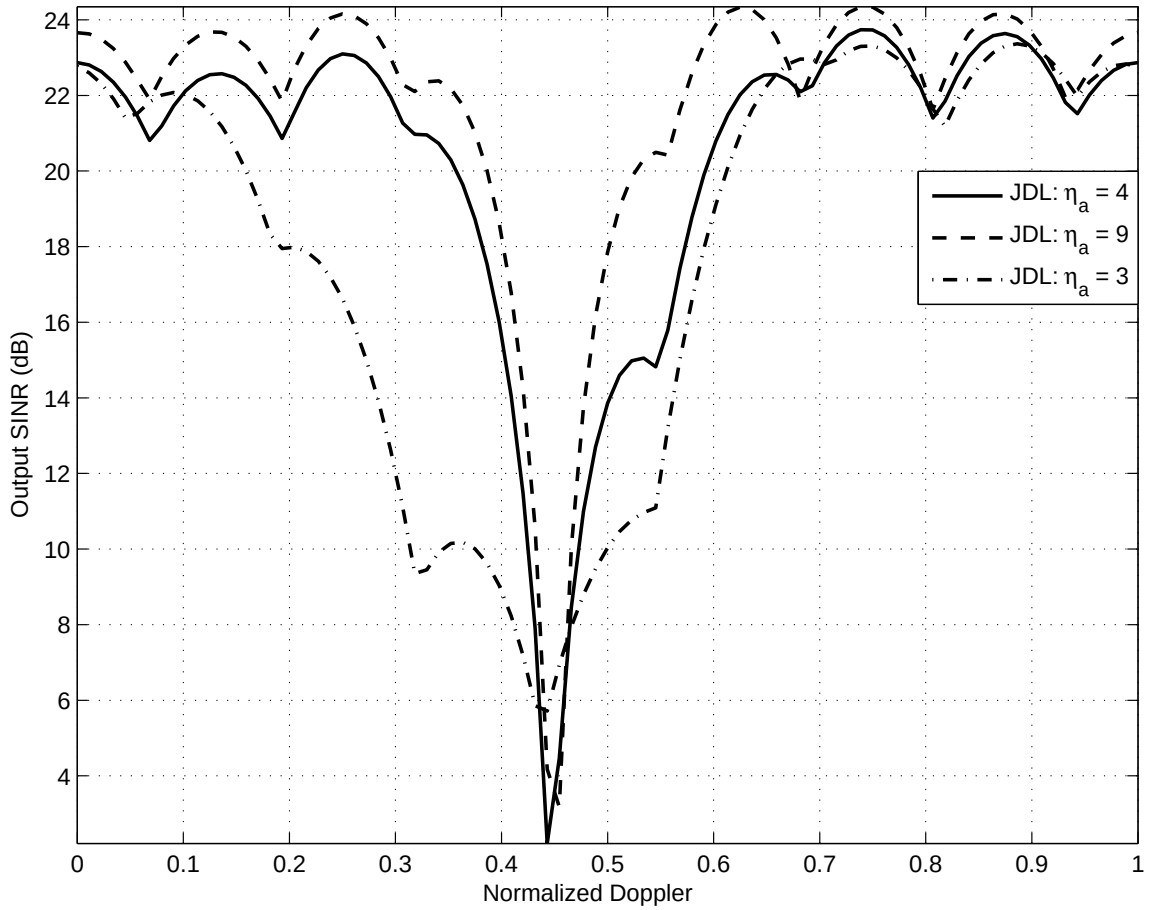

Figure 7.18: Low-altitude platform, horizontal elevation transmission planar JDL Output SINR with varying azimuth angular DOF η_a. The cause of the JDL degradation occurring at $\bar{\omega} = 0.55$ is confirmed to be insufficient azimuth DOF.

imuth DOF. It is also noted that the elevation DOF η_e is of minimal importance for low platform altitude because there is no range ambiguous clutter to suppress.

Output SINR using estimated interference covariance matrices is displayed in Figure 7.19, where the use of non-iid sample support is seen to slightly degrade the constant frequency array result and significantly degrade the FDA result. In particular, the FDA clutter notch degrades an additional 37 dB over the constant frequency array and the clutter notch considerably widened.

The change of platform altitude has a significant impact on the NHD shape as seen in Figure 7.20 and also impacts GIP first and second order statistics, primarily because the reduced altitude removes the contribution from range ambiguous clutter.

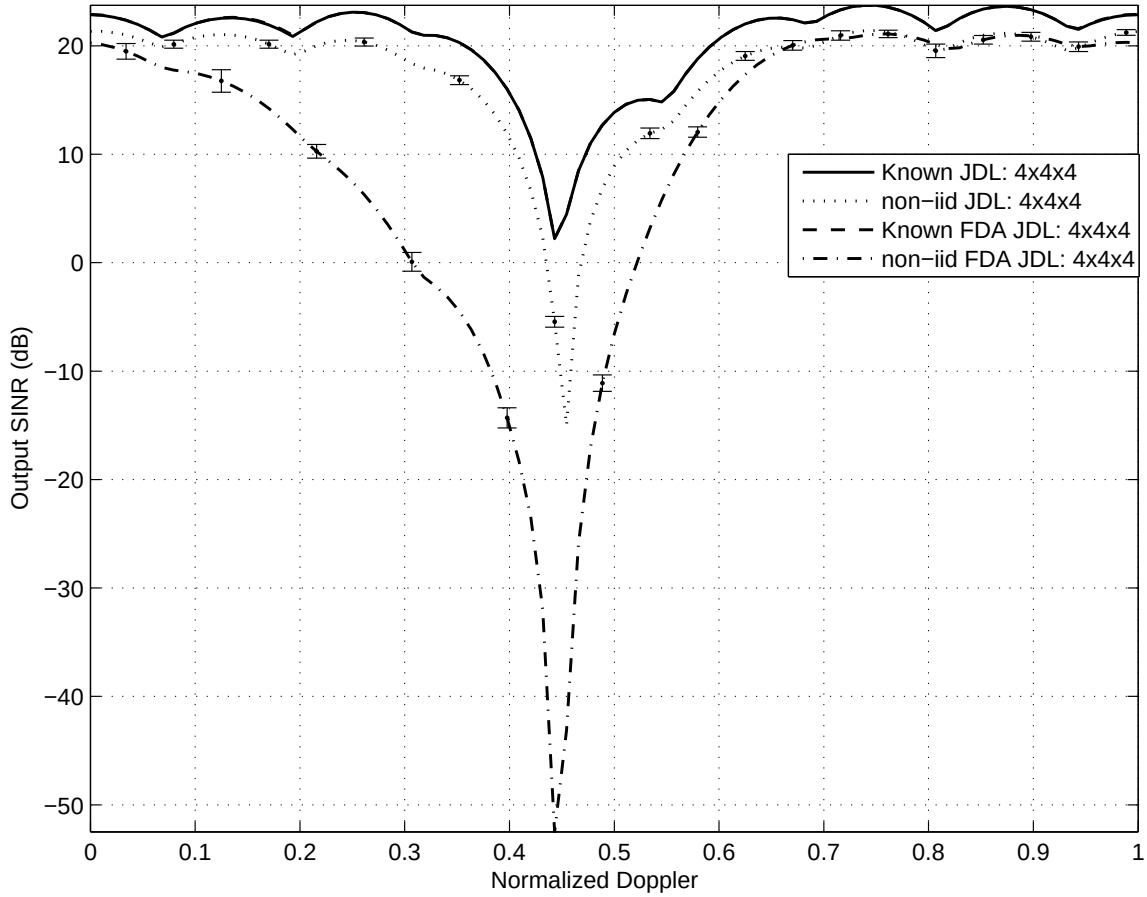

Figure 7.19: Low-altitude platform with horizontal elevation transmission planar array Output SINR. The known covariance result is compared to an estimated interference covariance matrix generated from 128 symmetrical sample support vectors. The latter curve is averaged over 1000 realizations and show medium degradation for the constant frequency array and significant degradation for the FDA. The FDA degradation is not only manifest in an increased clutter notch depth but also a widened clutter notch width.

The FDA increases the GIP dynamic range by 0.2% and reduces the standard deviation by over 29%. The decrease in standard deviation is misleading because whilst the NHD shape indicates range-cells before and after the target are more similar, they differ significantly more the target range-cell. Therefore, it is assessed the constant frequency array has greater sample support homogeneity.

The Output SINR using estimated interference covariance matrix with reduced CPI parameters is seen in Figure 7.21 and the same trends are observed for the AMF degradation as for the non-iid sample support JDL. The additional degradation associated with the FDA is reduced to 27 dB, indicating that a portion of the 37 dB difference between FDA and constant frequency JDL is due to the higher FDA clutter rank and using a partial STAP technique.

There is only one clutter notch and hence detection performance is only assessed when the target doppler value corresponds to the target range clutter doppler. The resulting detection curve is seen in Figure 7.22 and is consistent with the estimated Output SINR curve basic shape.

As expected, the two array types have identical iid performance and the degradation using non-iid sample support for the constant frequency array is 30 dB and 50 dB for the FDA. The 20 dB difference between the two array types in the P_d curve does not match the 27 dB difference in Output SINR clutter notch depth, however this is because the Output SINR clutter notches are not exactly at $\bar{\omega} = 0.450$. The clutter notch is shifted to the left for the FDA to $\bar{\omega} = 0.443$ and shifted right for the constant frequency array to $\bar{\omega} = 0.454$. The shift of $\bar{\omega} = 0.011$ is sufficient to produce the 7 dB difference, primarily in the FDA response due to the extremely steep notch depth.

The large level of degradation using non-iid sample support for the FDA is not consistent with expectations based on NHD results in Figure 7.20. The averaged MVE clutter spectrum for the two array types is seen in Figure 7.23 and confirms a performance degradation is consistent with the scenario parameters.

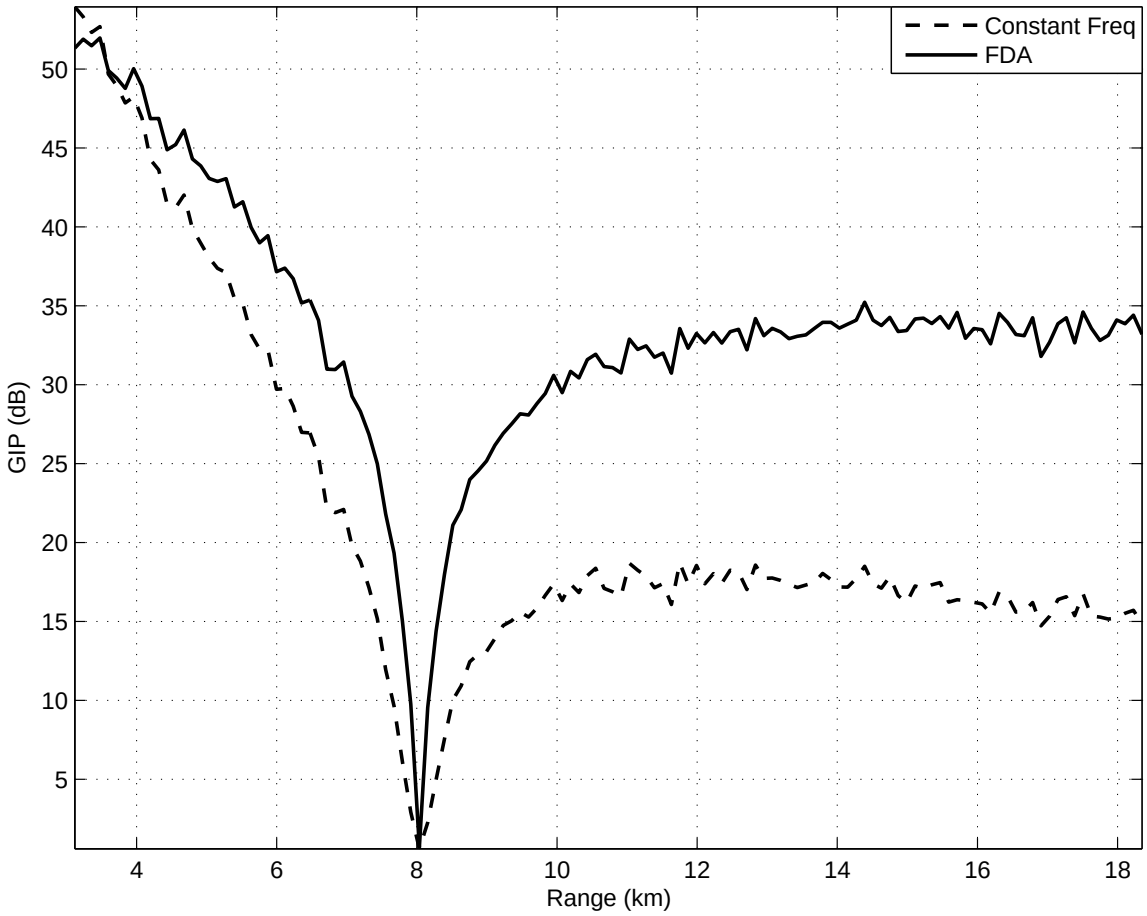

Figure 7.20: Low platform altitude with airborne target GIP for forward-looking planar constant frequency array and FDA averaged over 100 runs. The removal of range ambiguous clutter removes the multiple range notches evident in the high platform altitude NHD comparison. The FDA GIP indicates greater similarity between range-cells before and beyond the target range-cell, but both range-cell groups are considerably different than the target range-cell. The constant frequency array has a smaller dynamic range for range-cells beyond the target and expected to be of greater benefit.

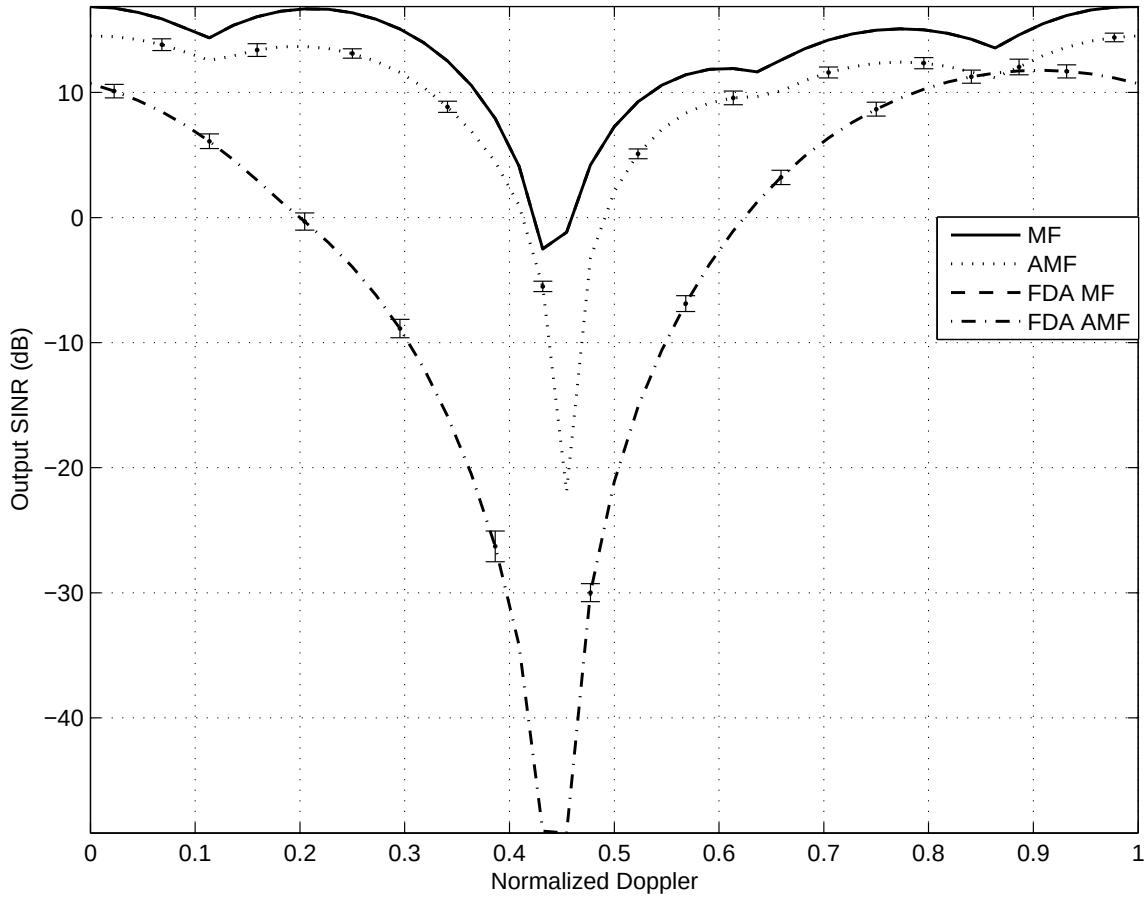

Figure 7.21: Low-altitude platform horizontal elevation transmission fully adaptive Output SINR with reduced CPI values $P = 4$, $N = 4$, and $M = 4$. The MF result is compared to AMF using an estimated interference covariance matrix generated from 128 symmetrical sample support vectors. As for the JDL above, the AMF curves averaged over 1000 realizations show considerably greater degradation for the FDA than the constant frequency array, in terms of clutter notch depth and width.

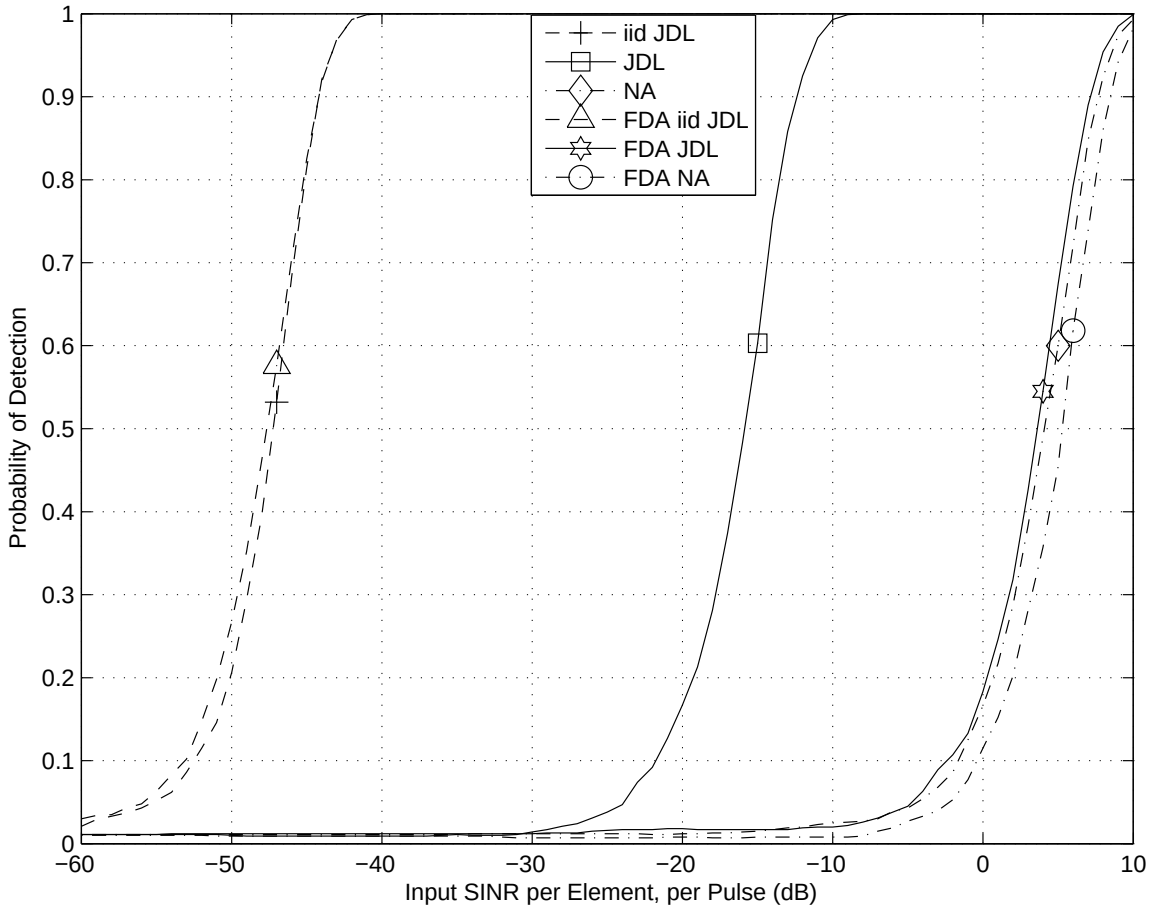

Figure 7.22: Low altitude platform and horizontal elevation transmission planar array detection curves for a target at $\bar{\omega} = 0.450$ for $P_{fa} = 0.01$. The detection curves show considerable performance degradation when using non-iid sample support for both array types, however the degradation is significantly higher for the FDA. The non-iid FDA performance is no better than NA processing, whereas the non-iid constant frequency is 20 dB better.

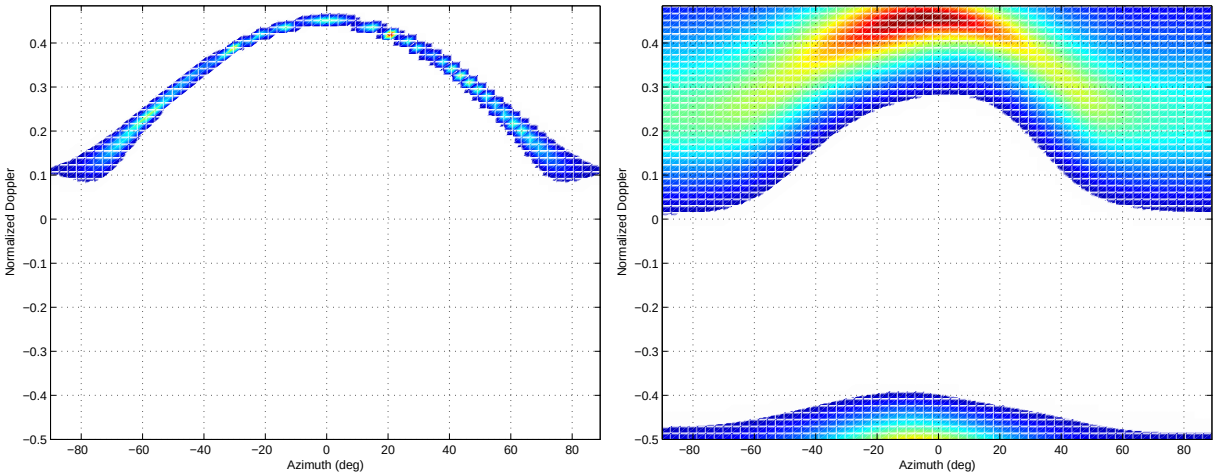

Figure 7.23: Low-altitude platform and 0° elevation transmit angle Minimum Variance Estimate clutter spectrum comparison of estimated interference covariance matrices using non-iid sample support. The constant frequency array (left) occupies a smaller space than the FDA (right) indicating the constant frequency array has a smaller clutter rank. The FDA clutter spectrum shows a considerable increase in arc width, indicating a greater degree of clutter doppler variation within the non-iid sample support.

As noted in the previous section, increases in clutter spectrum area correspond to increases in clutter rank. The constant frequency array has a smaller occupied region of the clutter spectrum compared to the FDA. The increased clutter arc width indicates greater variation of clutter statistics across the sample support vectors used for matrix estimation, i.e. FDA sample support has greater heterogeneity, more so than predicted by the NHD result.

7.7 UAV with Jeep Results

The known covariance Output SINR for a low altitude and ground target is seen in Figure 7.24 and is seen to have a similar shape to the previous scenario of low platform altitude and horizontal elevation transmission. Whilst the shape is the same the scale is not, in particular the clutter notch depth is increased by 8 dB for the MF and 15 dB for JDL, indicating that ground illumination produces more competing ground clutter.

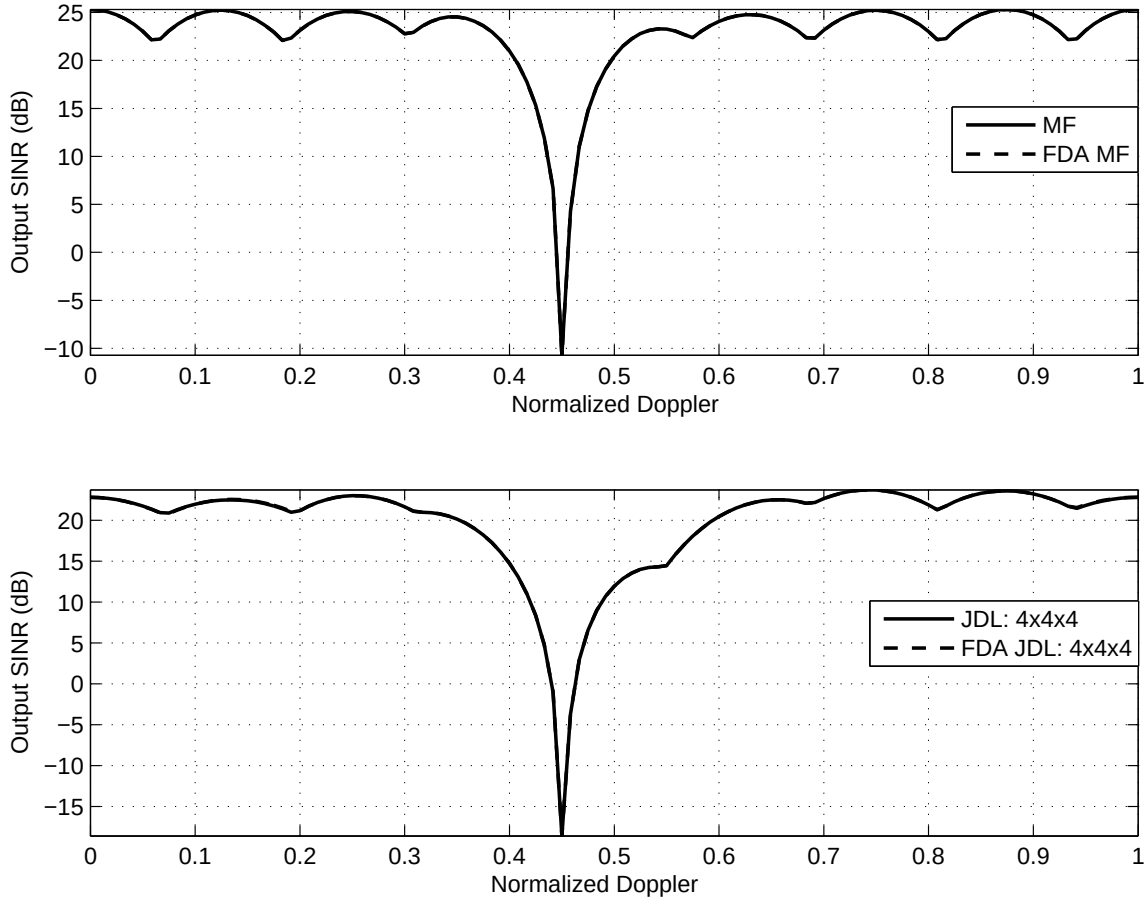

Figure 7.24: Low-altitude platform, ground illumination planar array Output SINR using known interference covariance matrix at a target range of 8.0 km. Only one clutter doppler notch is present because there is no range ambiguous clutter, the scale shows that there is a greater amount of competing clutter compared to the previous airborne target scenario.

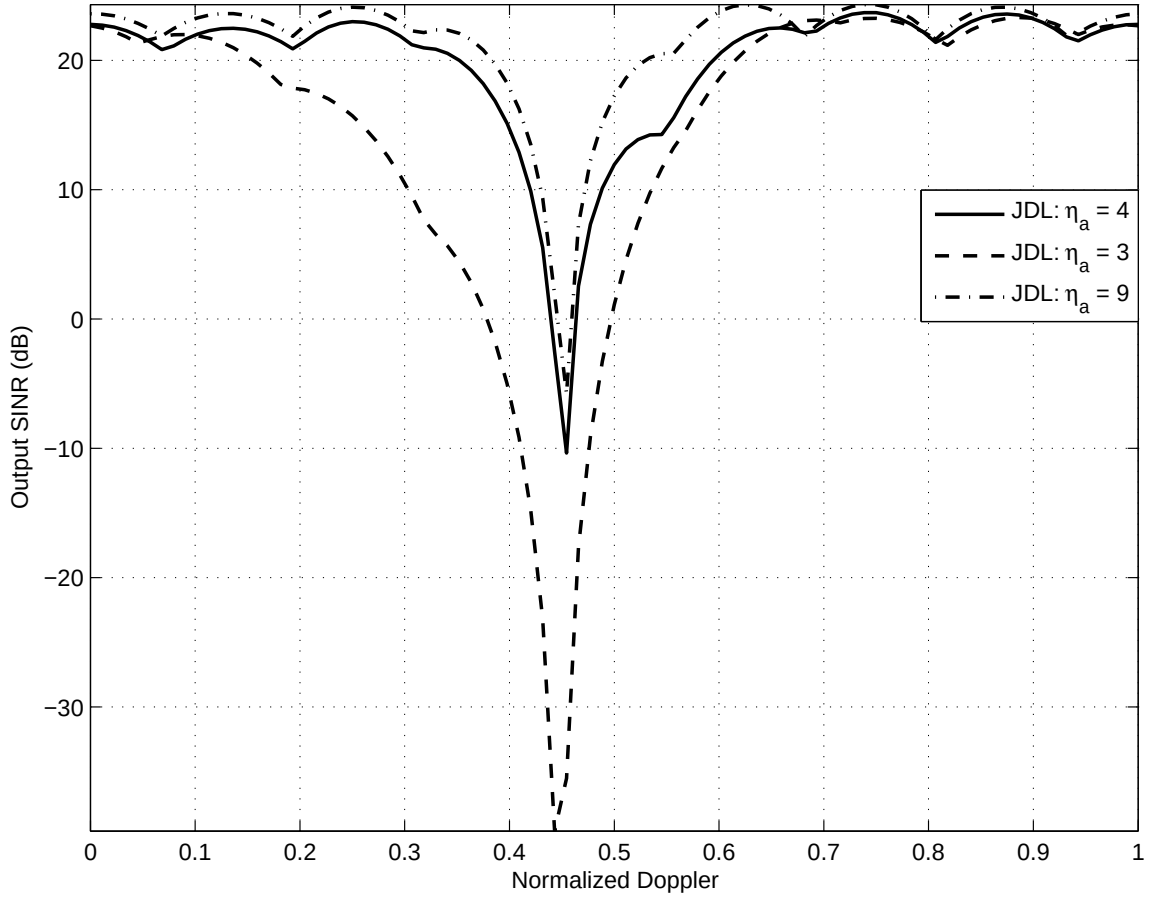

Figure 7.25: Low-altitude platform, ground illumination planar JDL Output SINR with varying azimuth angular DOF η_a. The cause of the minor JDL degradation occurring at $\bar{\omega} = 0.55$ is confirmed to be insufficient azimuth DOF.

The other noted feature is the secondary degradation for JDL at $\bar{\omega} = 0.55$. The degradation magnitude is the same as observed for the preceding horizontal transmission scenario and the reason is again the azimuth DOF η_a as verified in Figure 7.25.

When the interference matrix is estimated using non-iid sample support vectors, the resulting averaged Output SINR is shown in Figure 7.26. An interesting observation is the two array types non-iid performance is identical to the preceding section. Therefore the use of non-iid sample support vectors is seen to be independent of elevation transmission for low platform altitude, the reason is that the actual elevation angle to the target range of 8.0 km is only -2.4° producing a minimal difference in

sample support range-cell illumination. However, the minor change in elevation angle noticeably impacts the known covariance JDL Output SINR.

As for the high platform altitude, there is minimal difference in the NHD result when the elevation transmit angle is changed. For the low altitude case the change in θ is minimal going from 0° to -2.4° and the NHD result is equivalent to Figure 7.20 with minimal difference in dynamic range but FDA reducing standard deviation. As for the previous scenario, the constant frequency array has greater sample support homogeneity because the reduced standard deviation does not account for greater difference of surrounding range-cells from the target range-cell.

Using reduced CPI parameters and estimating the interference matrix, the fully adaptive Output SINR results are seen in Figure 7.27. As for the JDL section above, it is seen that the AMF results are very similar to the AMF results for horizontal elevation transmission, i.e. the non-iid results are similar but the known covariance MF results vary dependent on the elevation transmission angle.

The probability of detection curve using a target doppler value corresponding to the target range clutter doppler is seen in Figure 7.28 and there is no difference between the two array types using iid sample support. Degradation associated with using non-iid sample support is 6 dB for the constant frequency array and 18 dB for FDA, so non-iid constant outperforms non-iid FDA by 12 dB.

The change in elevation transmit angle from 0° to -2.4° has minimal impact on the FDA degradation as demonstrated by the clutter spectrum in Figure 7.29. The FDA clutter occupies a significantly increased area and hence, an increased clutter rank consistent with degraded performance.

7.8 Planar FDA Summary

The comparison of a constant frequency planar array to a planar FDA with frequency diversity along both horizontal and vertical array channels shows that there is greater variation between the four physical scenarios than seen in the linear array

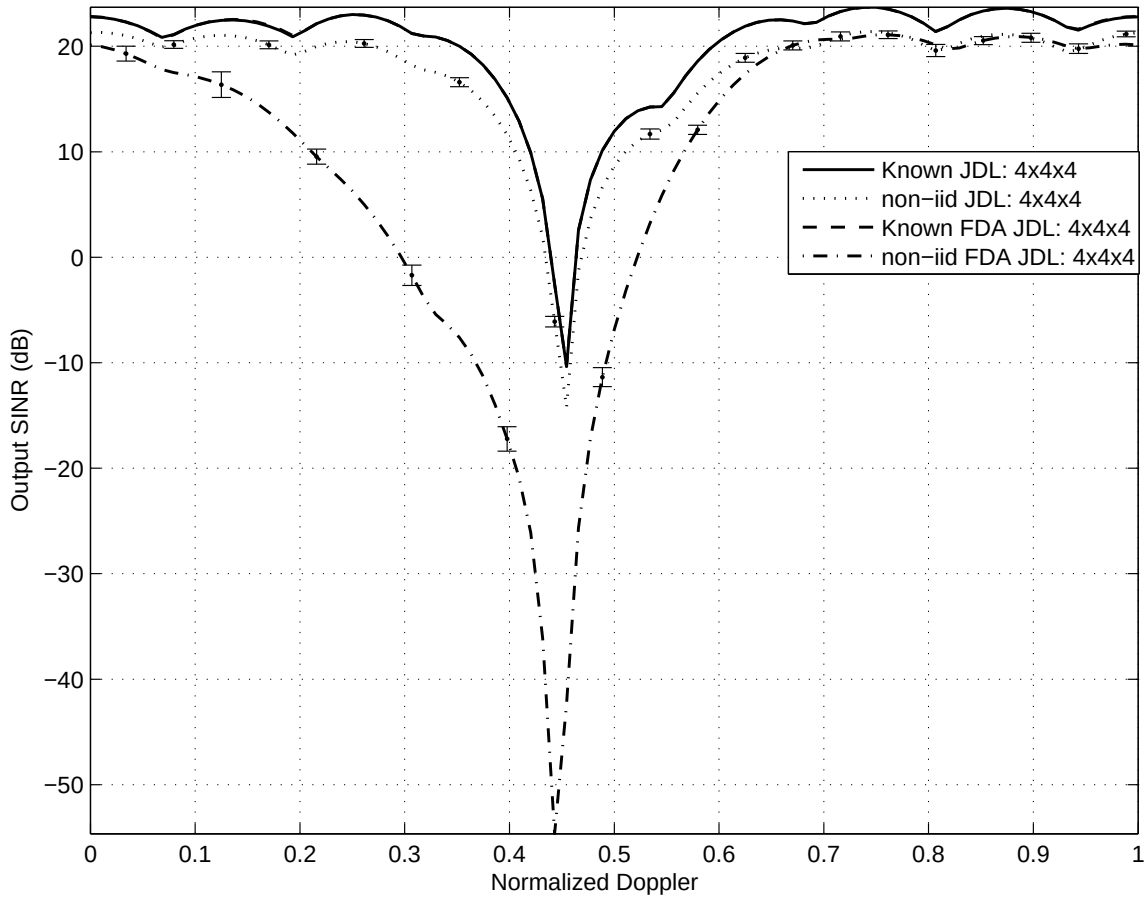

Figure 7.26: Low-altitude platform with ground illumination planar array Output SINR. The known covariance result is compared to an estimated interference covariance matrix generated from 128 symmetrical sample support vectors. The latter curve is averaged over 1000 realizations and show minimal degradation for the constant frequency array and significant degradation for the FDA. Interestingly it is the non-iid sample support JDL performance that is unchanged and the iid performance that changes when compared to the airborne target performance in the previous section.

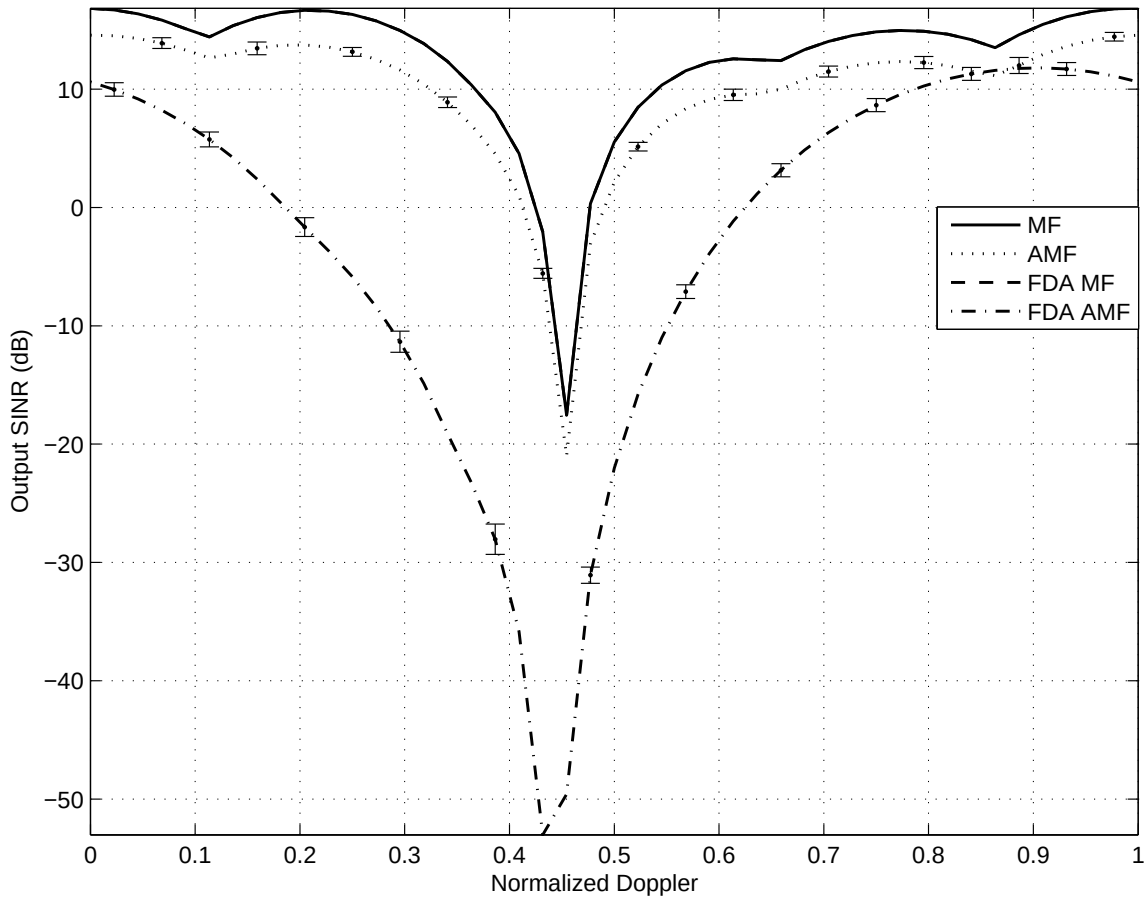

Figure 7.27: Low-altitude platform ground illumination fully adaptive Output SINR with reduced CPI values $P = 4$, $N = 4$, and $M = 4$. The MF result is compared to AMF using an estimated interference covariance matrix generated from 128 symmetrical sample support vectors. As for the JDL above, the AMF curves averaged over 1000 realizations show considerably more degradation using the FDA than the constant frequency array. Additionally the AMF results are very similar to the previous section whilst the MF results differ.

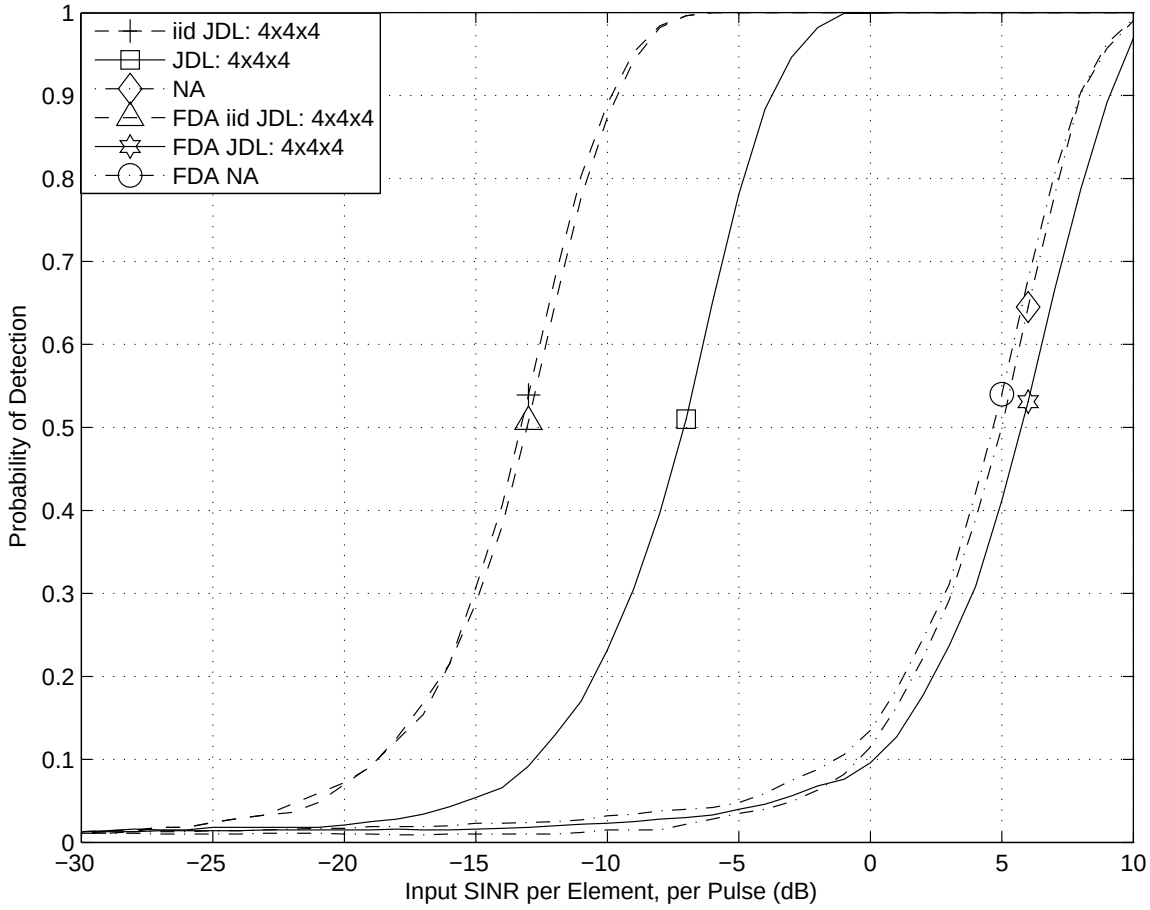

Figure 7.28: Low altitude platform and ground illumination planar array detection curves for a target at $\bar{\omega} = 0.450$ for $P_{fa} = 0.01$. The detection curves show some performance degradation when using constant frequency non-iid sample support, however considerably greater degradation for the FDA. The non-iid FDA performance is no better than NA processing, whereas the non-iid constant frequency is approximately 10 dB better. As noted above, the non-iid performance is identical and the iid performance is degraded when compared to the previous section.

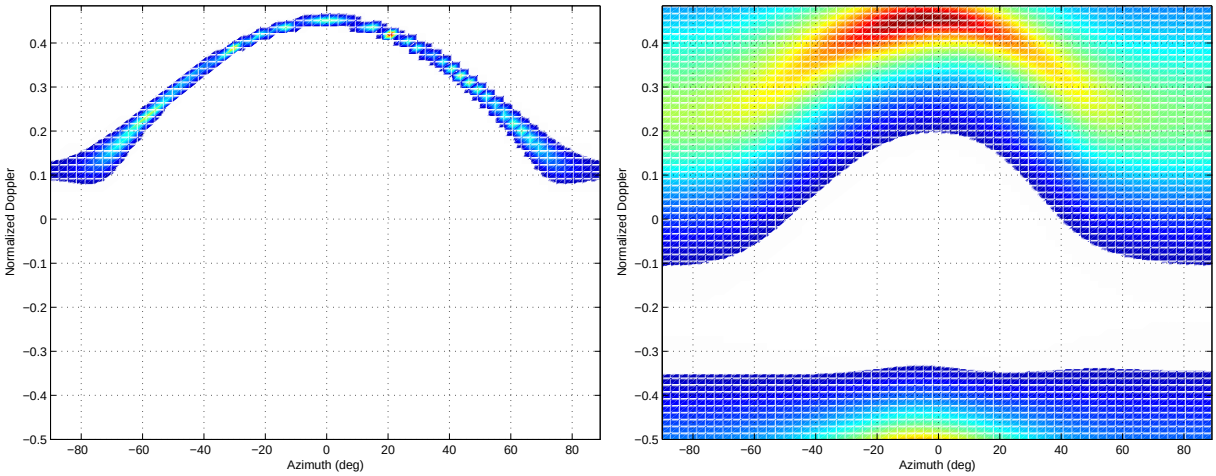

Figure 7.29: Low-altitude platform and -2.4° elevation transmit angle, Minimum Variance Estimate clutter spectrum comparison of estimated interference covariance matrices using non-iid sample support. Similar to the previous scenario, the constant frequency array clutter (left) is seen to have significantly smaller region of clutter spectrum occupied compared to the FDA (right).

comparison in Chapter VI. There is greater variation between scenarios because planar arrays increase the impact of changing the elevation transmission angle. The major features observed from the four scenarios are summarized below.

- The greatest benefit of using FDA is for a high platform altitude and airborne target, i.e. horizontal elevation transmission. The FDA illumination of range ambiguous clutter rings implicitly suppresses the range ambiguous clutter notch and therefore decreases the overall clutter notch (the lower M value results in both notches being within one doppler filter and hence are not separated). Improvements in P_d curves are consistent with the Output SINR and verify the above assessment.
- Changes in elevation transmission angle have a large impact for high platform altitudes. For a ground target, the elevation difference between target range and range ambiguous clutter rings enables suppression of range ambiguous clutter. Since there is no range ambiguous clutter for low platform altitude and the target range elevation is much smaller, the difference of changing elevation transmit angle is limited to a greater clutter notch depth.

- There is a significantly increased amount of degradation using FDA versus constant frequency non-iid sample support for low platform altitudes. The trend of increased degradation is consistent with the NHD results and whilst the level of FDA degradation is considerably higher than expected from NHD results, the degradation is representative of the comparison of the clutter spectra of the estimated interference covariance matrices. The result also highlights that the relationship between NHD dynamic range and corresponding estimated covariance matrix Output SINR changes has not been investigated.

7.9 Planar Partial Frequency Diverse Array

It is observed that the differences in the ground projected antenna pattern for a constant frequency array and FDA result in different elevation nulls that may hinder comparison of sample support homogeneity. An alternative proposed FDA structure has frequency diversity limited to horizontal array channels, hence referred to as a planar partial FDA. The new array structure ensures the elevation nulls are at the same location removing their effect from consideration, particularly helpful in the analysis of NHD results.

The same four physical scenarios are analyzed using the new planar partial FDA to determine whether FDA degradation using non-iid sample support can be reduced, particularly for low platform altitudes.

7.9.1 AEWAC with Airborne Target Results. The known covariance Output SINR is included as Figure 7.30 and shows that partial FDA performance is improved compared to the planar FDA with full frequency diversity. Because of reduced M value both the target range clutter doppler and range ambiguous clutter doppler are within one doppler filter and therefore are presented as one clutter notch. The suppression of range ambiguous clutter by the FDA antenna pattern produces a shift in the resultant single doppler notch to the left, toward the target range clutter doppler value.

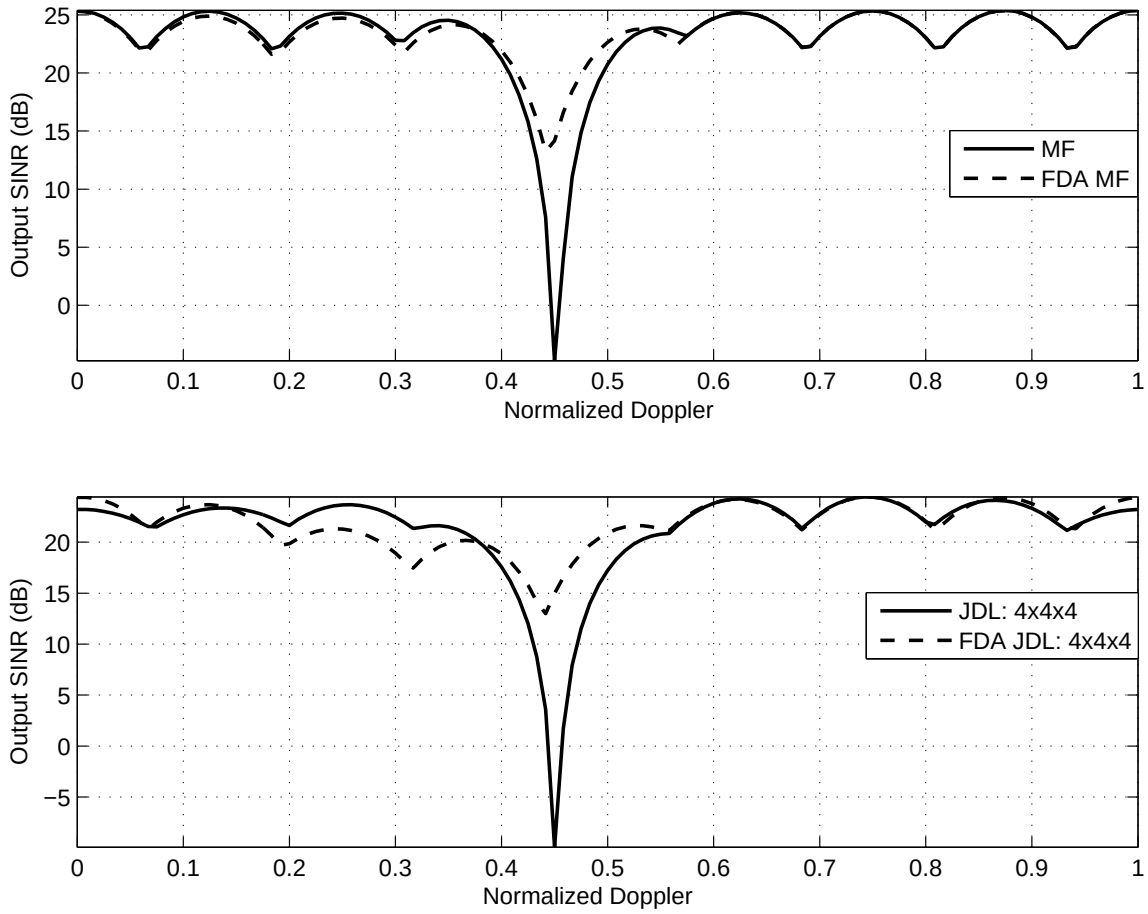

Figure 7.30: High-altitude platform, horizontal elevation transmission planar partial FDA Output SINR using known interference covariance matrix at a target range of 10.5 km. Only one distinct clutter doppler notch is observed however there are two distinct clutter doppler notch values that are not separated because of the reduced number of doppler filters. It is known there are the two distinct clutter doppler values because the FDA notch depth is decreased, as a result of the suppressed range ambiguous clutter notch.

The MF clutter notch depth for the partial FDA is reduced by 4 dB, whilst the JDL clutter notch is reduced by 3 dB compared to Section 7.4. Since the Output SINR is based on known covariance matrix, the improvement is caused by a more beneficial illumination of range ambiguous clutter. As a trade-off, it is observed that the FDA does have slightly degradation over $0.2 \leq \bar{\omega} \leq 0.35$, which is also a result from the new illumination of range ambiguous clutter and is consistent with azimuth frequency diversity producing a spread in clutter doppler from range ambiguous clutter rings.

Using non-iid sample support to estimate the interference covariance matrix, the Output SINR is seen in Figure 7.31 and shows non-iid sample support considerably increases the degradation from the known covariance, much more so than the full planar FDA.

The estimated Output SINR result indicates that the planar partial FDA sample support is worse than the planar FDA sample support, not matching the expectations of the NHD results in Figure 7.32. The GIP dynamic range is the same for both planar partial FDA and constant frequency, however, the standard deviation has been reduced by 4% indicating potential benefits or at least improvement over full planar FDA diversity. The notches corresponding to the elevation nulls and range ambiguous clutter are still present but now at the same locations, confirming vertical channel frequency diversity dominates the GIP shape more than horizontal channel frequency diversity.

However, the above NHD result highlights the increased complexity of analyzing FDA performance as both the sample support range-cells and the range ambiguous clutter contributions must be examined. Comparing the projected antenna patterns, seen in Figure 7.33 it is seen that the use of a planar FDA produces an elevation null within the first range ambiguous reducing the amount of competing clutter, whilst the partial planar FDA does not.

For reduced CPI parameters, the fully adaptive estimated Output SINR is seen in Figure 7.34 and the degradation experienced is greater for an FDA with diversity

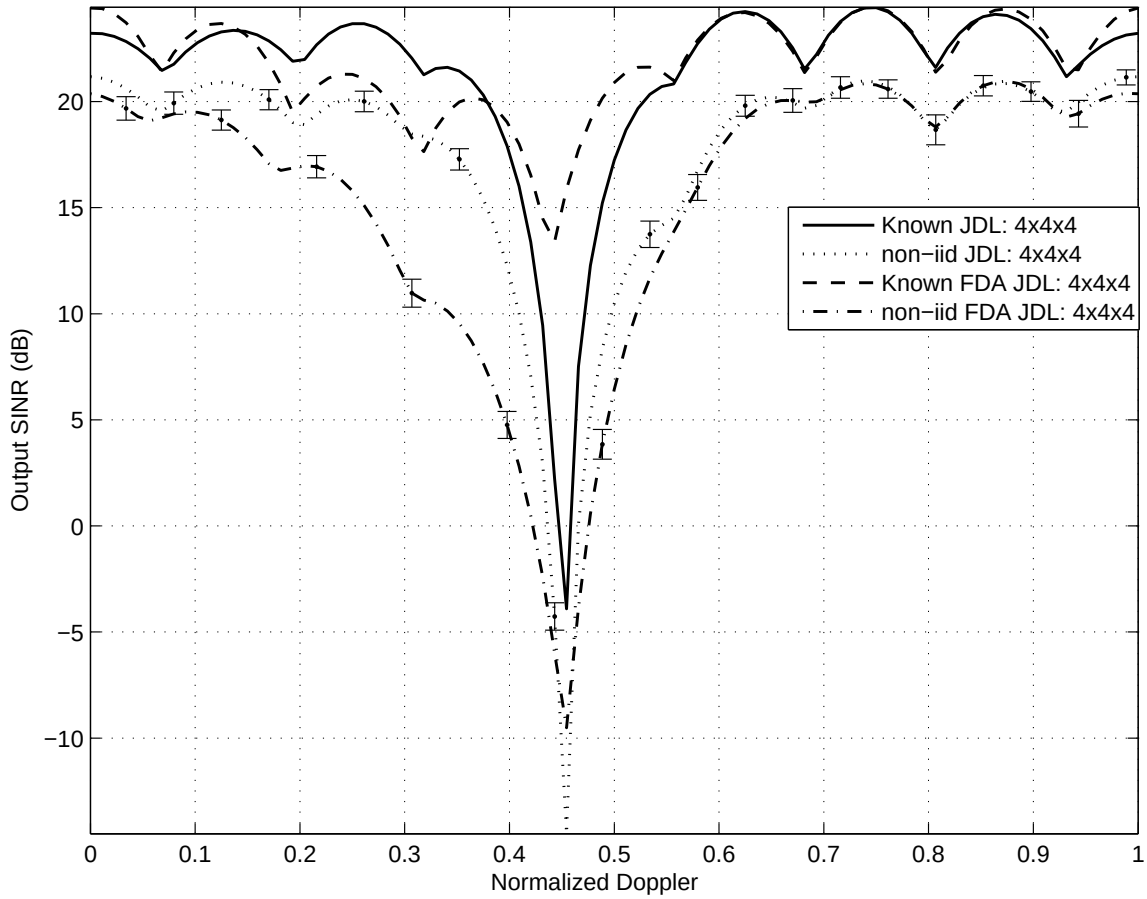

Figure 7.31: High-altitude platform with horizontal elevation transmission planar partial FDA Output SINR. The known covariance result is compared to an estimated interference covariance matrix generated from 128 symmetrical sample support vectors. The latter curve is averaged over 1000 realizations and shows degradation around the target range clutter doppler due to the skewed matrix estimate. There is significantly greater FDA degradation than the planar FDA with full frequency diversity, in notch depth and width.

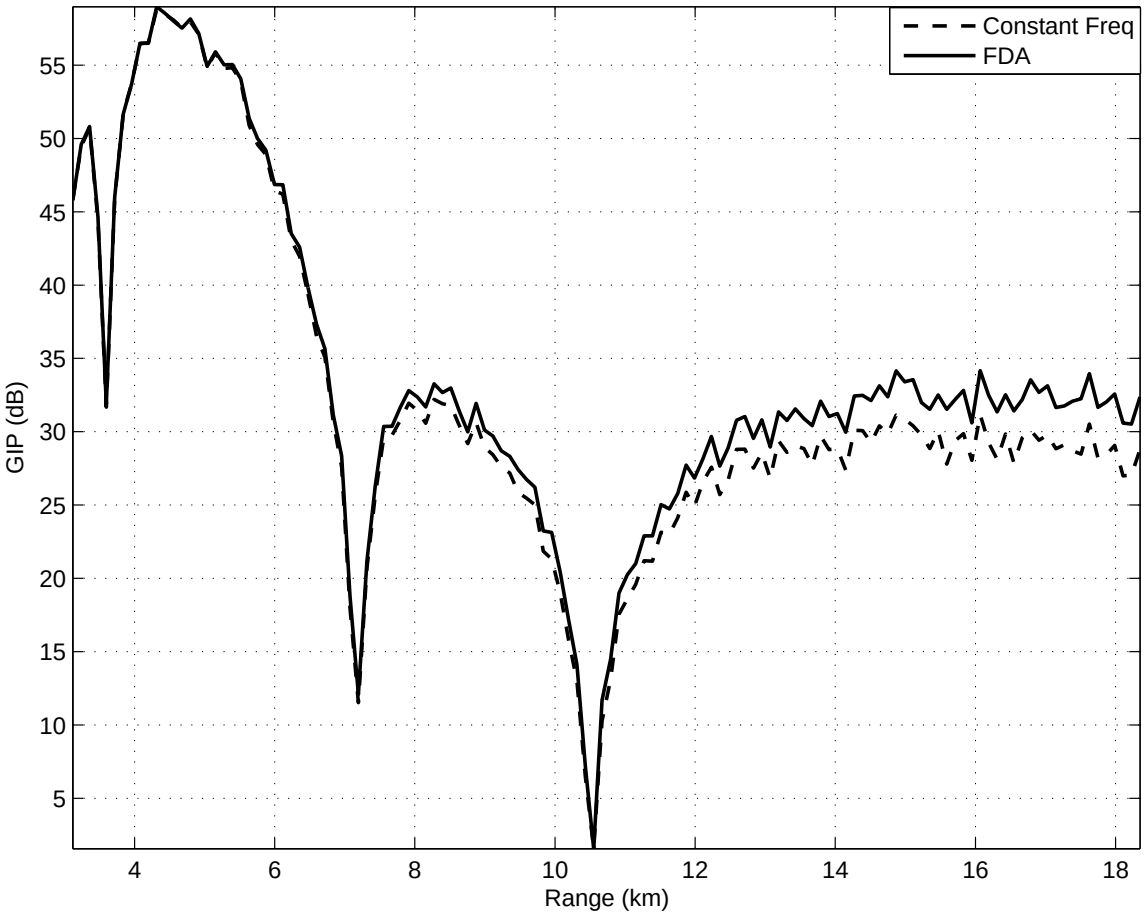

Figure 7.32: High platform altitude with airborne target GIP for forward-looking planar constant frequency array and planar partial FDA averaged over 100 runs. Limiting frequency diversity to only horizontal channels has a significant impact. The GIP notch locations are now the same for both array types and there is minimal difference between the shape of the curves, in vast contrast to the previous FDA result. Based on the minimal variation, similar non-iid sample support performance is expected with no sample support homogeneity benefits evident for array boresight targets.

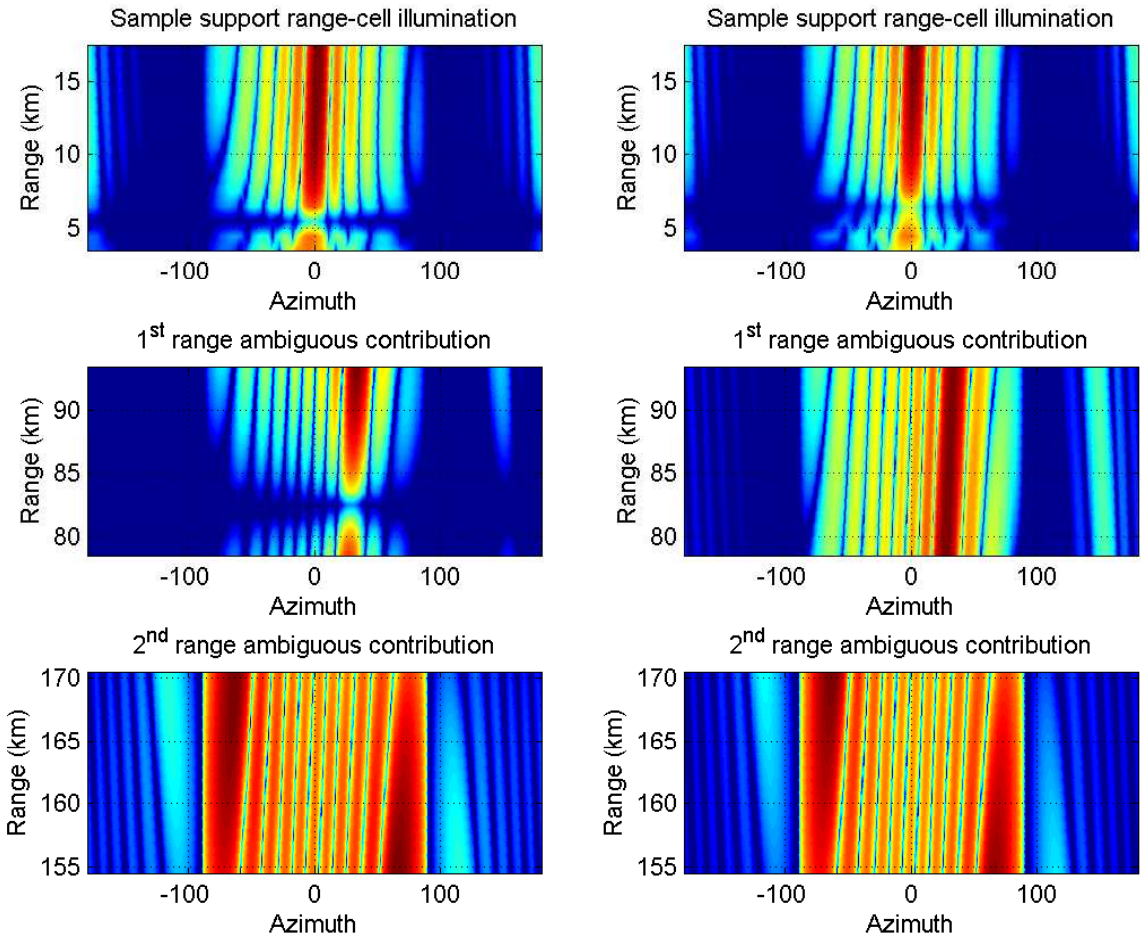

(a) (b)

Figure 7.33: Ground projected antenna pattern for high-altitude platform with 0° transmit elevation angle, across sample support range-cells and their range ambiguous contributions. (a) Planar FDA (b) Planar Partial FDA. The comparison shows that the FDA with full frequency diversity has an elevation null at the 1st range ambiguous contribution whilst the planar partial FDA does not, the reason why planar partial FDA suffers greater degradation.

limited to azimuth as opposed to the planar FDA. The same reason is described above, an elevation null placed in the first range ambiguous clutter swath of sample support vectors.

The most obvious FDA AMF feature is the degradation over $0.1 \leq \bar{\omega} \leq 0.4$. The shift in the doppler clutter notch is expected because of illumination of range ambiguous clutter reduces the range ambiguous clutter notch depth and shifting the curve to the left. The above shifting effect is compounded by the reduction of M from eight to four, increasing the doppler range that each filter covers. The range ambiguous clutter energy is spread as observed by degradation of JDL in Figure 7.30 thus leading to the unusual Output SINR shape.

With high platform altitude, there are two target doppler values at which to evaluate detection performance. The first target doppler value corresponds to the target range clutter doppler with the P_d curves in Figure 7.35, verifying the degradation of planar partial FDA compared to the planar FDA. The partial FDA non-iid sample support detection curve shifts right by 7 dB compared to the planar FDA, so that the partial FDA performance is approximately equal to the constant frequency array.

Evaluating the P_d performance with a target doppler value corresponding to the range ambiguous clutter notch doppler is shown in Figure 7.36. Again the partial FDA with non-iid sample support is worse than the previous planar FDA result, in this situation by 9 dB. Despite the degradation, there is still an improvement of 10 dB of partial FDA over the constant frequency because of FDA illumination of range ambiguous clutter.

Overall, whilst the performance is expected to improve based on removal of differing elevation nulls the planar partial FDA is seen to degrade performance, particularly in the difference between known covariance and non-iid sample support. The degradation from FDA to partial FDA is a result of range ambiguous contribution to sample support range-cells.

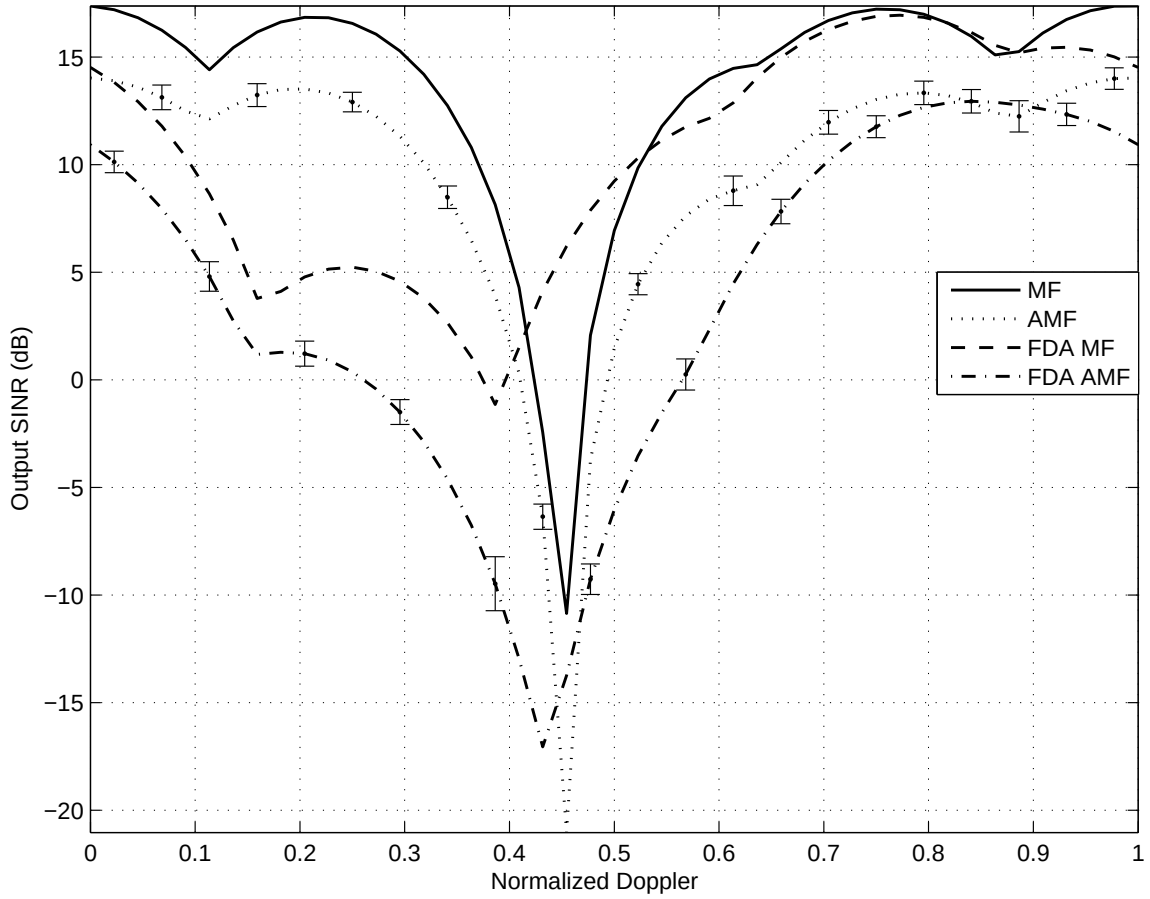

Figure 7.34: High-altitude platform horizontal elevation transmission planar partial FDA fully adaptive Output SINR with reduced CPI values $P = 4$, $N = 4$, and $M = 4$. The MF result is compared to AMF using an estimated interference covariance matrix generated from 128 symmetrical sample support vectors. The FDA MF is seen to be considerably higher than the constant frequency array MF and again shifts the clutter notch to the left. The change is the additional degradation to the left of the clutter notch, compared to the degradation to the right of the clutter notch for the planar FDA with full frequency diversity.

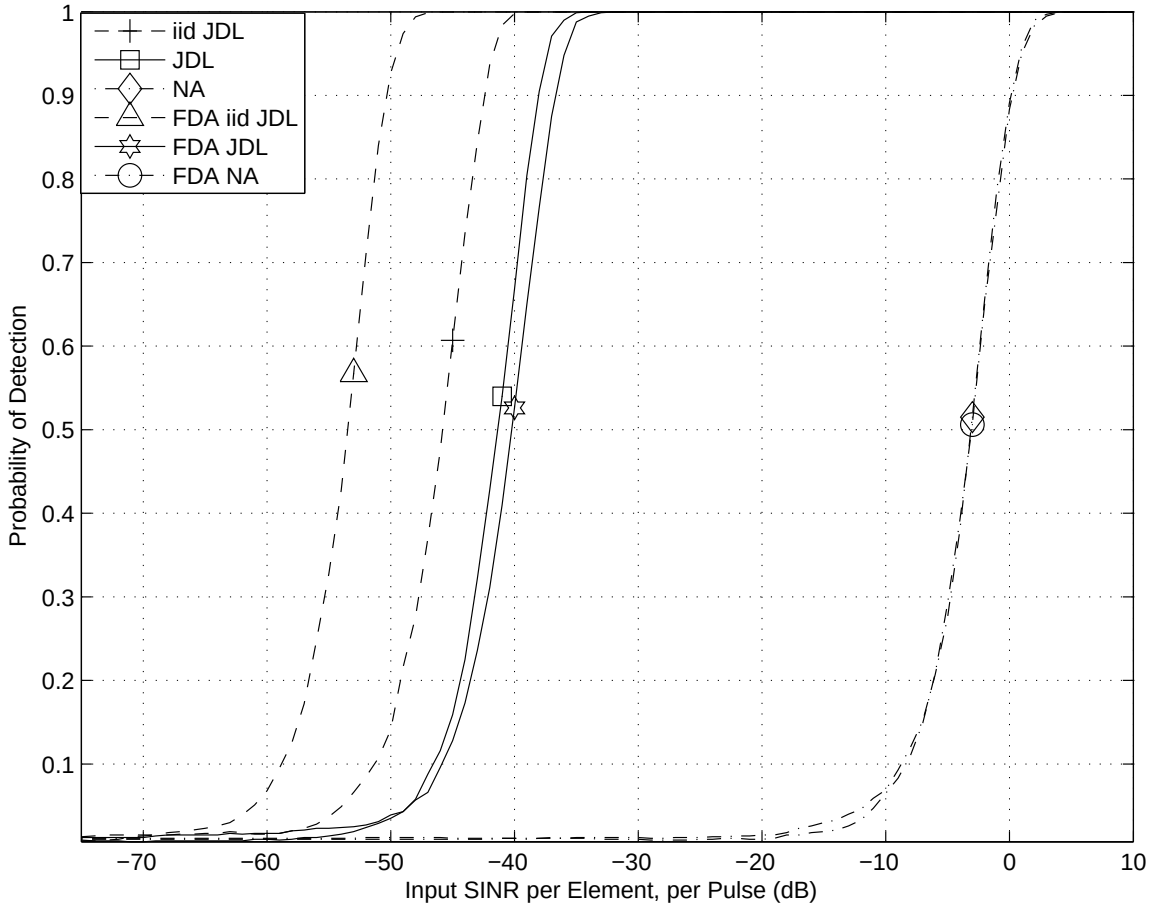

Figure 7.35: High altitude platform and horizontal elevation transmission planar partial FDA detection curves for a target at $\bar{\omega} = 0.433$ for $P_{fa} = 0.01$. The detection curves show the same FDA performance for iid sample support, however the benefit disappears when non-iid sample support is used. The degradation from the planar FDA is due to no longer having an elevation null in the first range ambiguous swath.

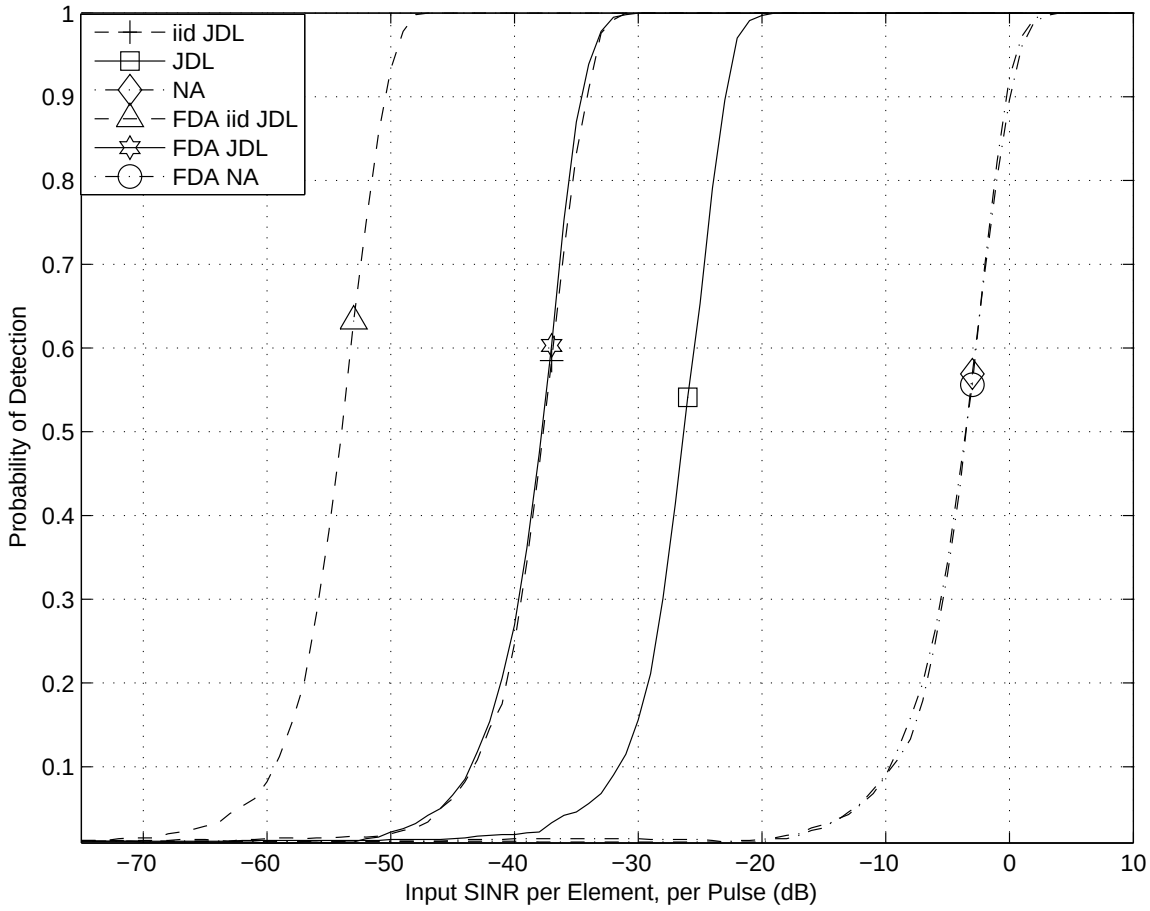

Figure 7.36: High altitude platform and horizontal elevation transmission planar partial FDA detection curves for a target at $\bar{\omega} = 0.450$ for $P_{fa} = 0.01$. Similar to above, the non-iid sample support FDA performance is seen to degrade, however there is still a 10 dB benefit over the constant frequency array, compared to the 20 dB improvement using a planar FDA.

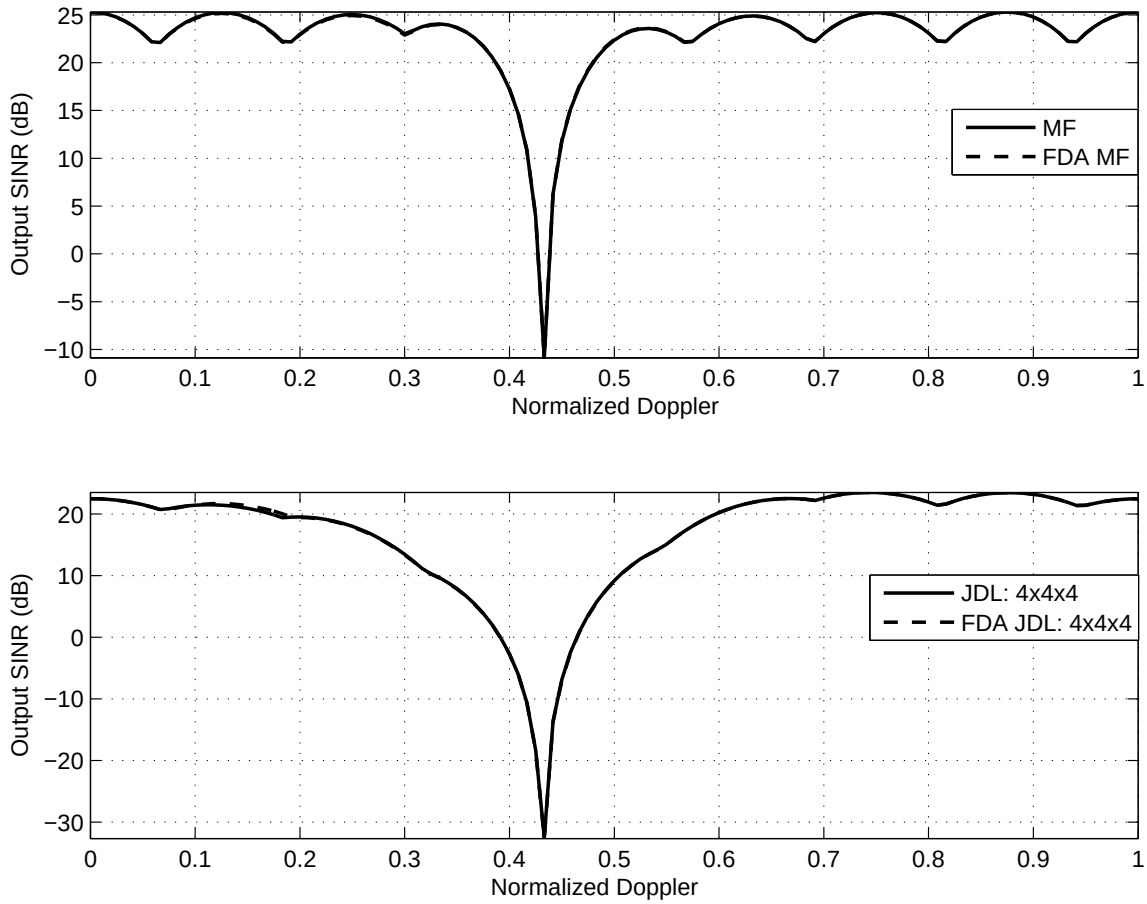

Figure 7.37: High-altitude platform, ground illumination planar partial FDA Output SINR using known interference covariance matrix at a target range of 10.5 km. Only one distinct clutter doppler notch is observed because there is sufficient elevation angle difference between the target and the range ambiguous clutter to suppress the latter, leaving only the primary target range clutter doppler.

7.9.2 AEWAC with Jeep Results. When the elevation transmit angle is changed to ground illumination, the Output SINR is seen in Figure 7.37. The partial FDA result is seen to be identical to both the planar FDA and the constant frequency array results. The lack of difference between the array types is due to suppression of range ambiguous clutter through the elevation discrimination from the ground target.

The use of non-iid sample support to estimate the interference covariance matrix produces the Output SINR seen in Figure 7.38, where the partial FDA degradation is considerably reduced compared to the planar FDA degradation. Therefore, the

limiting of frequency diversity to horizontal channels is seen to improve sample support homogeneity as predicted by NHD results.

The change in elevation transmission angle has minimal impact on planar partial FDA NHD performance, the same trend observed for the planar FDA. Therefore, the NHD analysis is same as the previous scenario and Figure 7.32.

The use of reduced CPI parameters for AMF, produces the same trend where the partial FDA reduces the non-iid degradation experienced by the FDA. Only having frequency diversity across array horizontal channels regularizes the FDA non-iid sample support as shown in Figure 7.39, however whilst the degradation is reduced, the partial FDA performance is still worse than the constant frequency array.

Detection curves for a target doppler matching the target range clutter doppler show there is minimal difference between the two array types using iid sample support and non-iid sample support, consistent with the estimated Output SINR. Therefore all four curves are within a statistically insignificant range as seen in Figure 7.40.

Using a target doppler that corresponds to the range ambiguous clutter doppler, the detection curves are seen in Figure 7.41 and as above are all effectively the same. The difference between the two array types for iid and non-iid sample support is negligible, thus partial FDA provides a 20 dB improvement over a planar FDA with full frequency diversity.

Overall, the performance is seen to improve significantly using planar partial FDA over the previous planar FDA. Limiting the frequency diversity to horizontal array channels there is minimal difference between the constant frequency and planar partial FDA as predicted the NHD results in Figure 7.32. There is also no benefit gained using azimuth frequency diversity since the range ambiguous clutter is suppressed through the target separation in elevation.

The result is consistent with the target range MVE clutter spectrum shown in Figure 7.42. When compared to the FDA with fully frequency diversity seen in Figure 7.16, the partial FDA has a significantly decreased clutter arc width and rank.

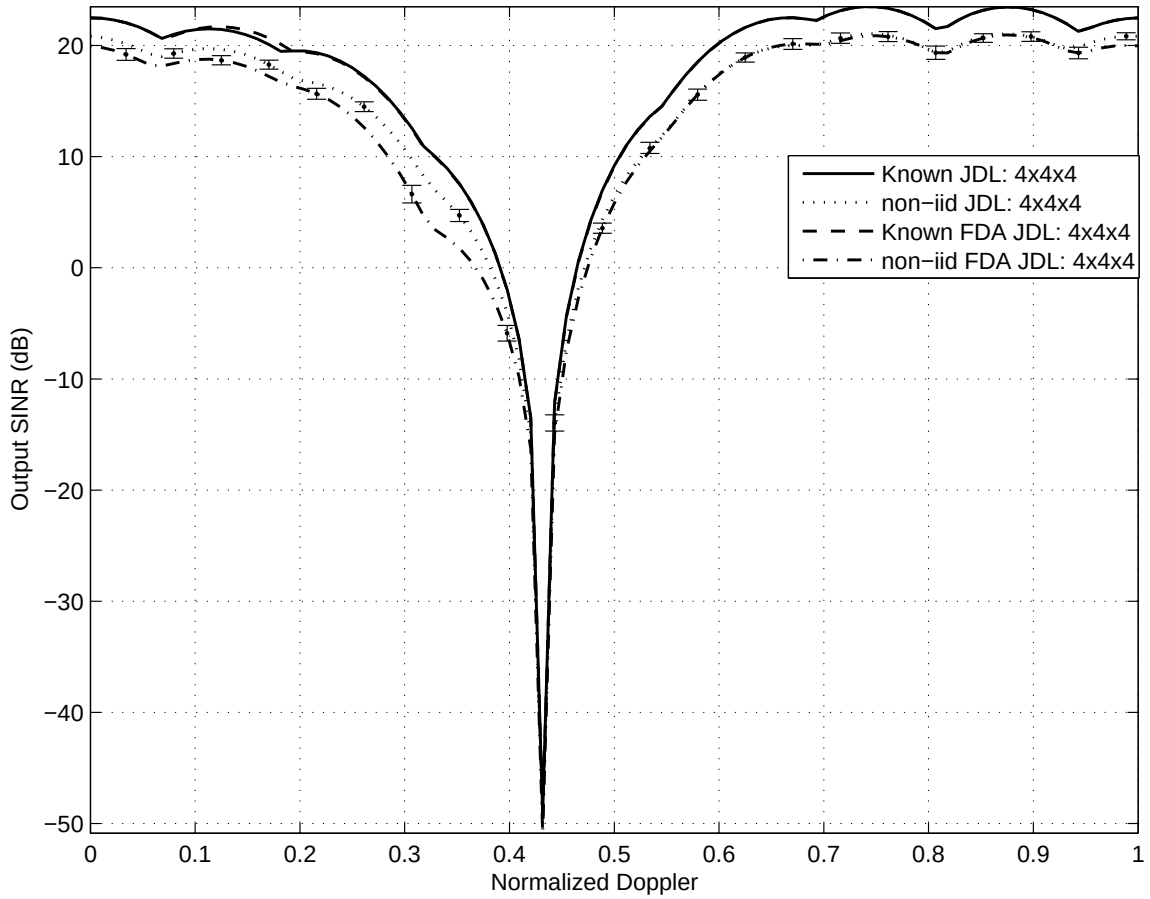

Figure 7.38: High-altitude platform with ground illumination planar partial FDA Output SINR. The known covariance result is compared to an estimated interference covariance matrix generated from 128 symmetrical sample support vectors. The latter curve is averaged over 1000 realizations and shows little degradation compared to the known covariance results because of the ability to suppress the range ambiguous contributions. The partial FDA degradation is seen to be considerably reduced when compared to the degradation experienced by the FDA with full frequency diversity. The removal of frequency diversity across vertical array channels considerably improves performance, but no better than the constant frequency array.

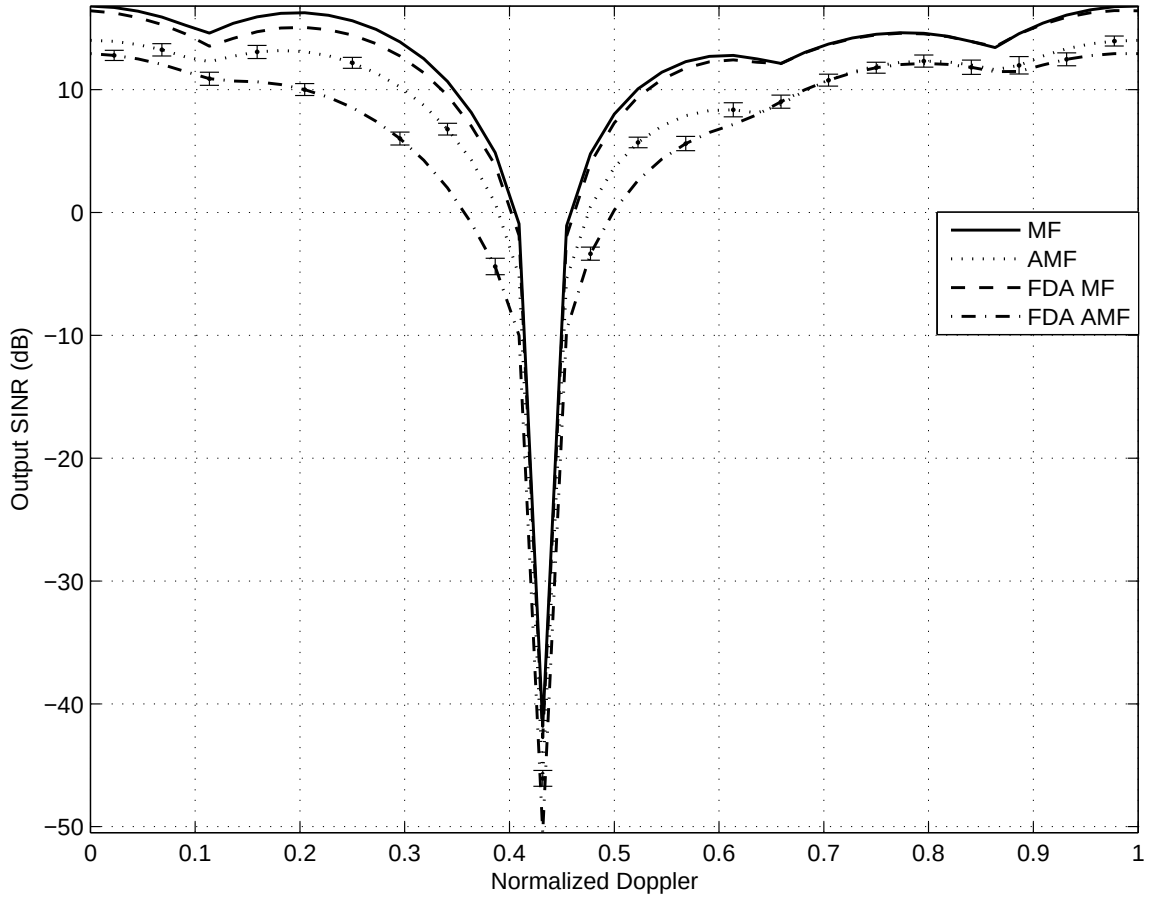

Figure 7.39: High-altitude platform horizontal elevation transmission planar partial FDA fully adaptive Output SINR with reduced CPI values $P = 4$, $N = 4$, and $M = 4$. The MF result is compared to AMF using an estimated interference covariance matrix generated from 128 symmetrical sample support vectors. The AMF curves are averaged over 1000 realizations and similar to JDL above, the partial FDA performance is considerably better than the previous FDA result, so there is minimal difference between partial FDA and the constant frequency array within the clutter notch.

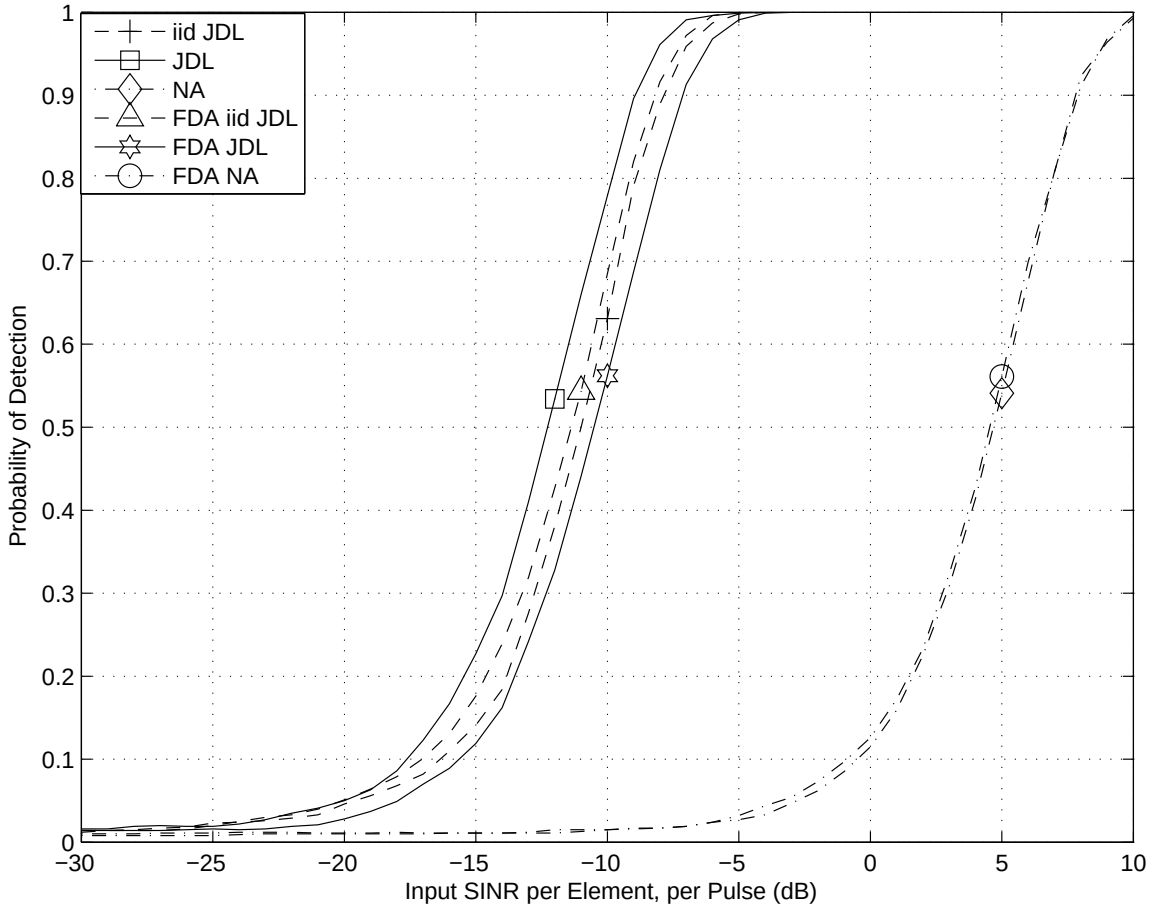

Figure 7.40: High altitude platform and ground illumination planar partial FDA detection curves for a target at $\bar{\omega} = 0.433$ for $P_{fa} = 0.01$. The detection curves now show minimal difference between iid and non-iid sample support of both array types, confirming that the partial FDA outperforms the previous FDA by over 15 dB.

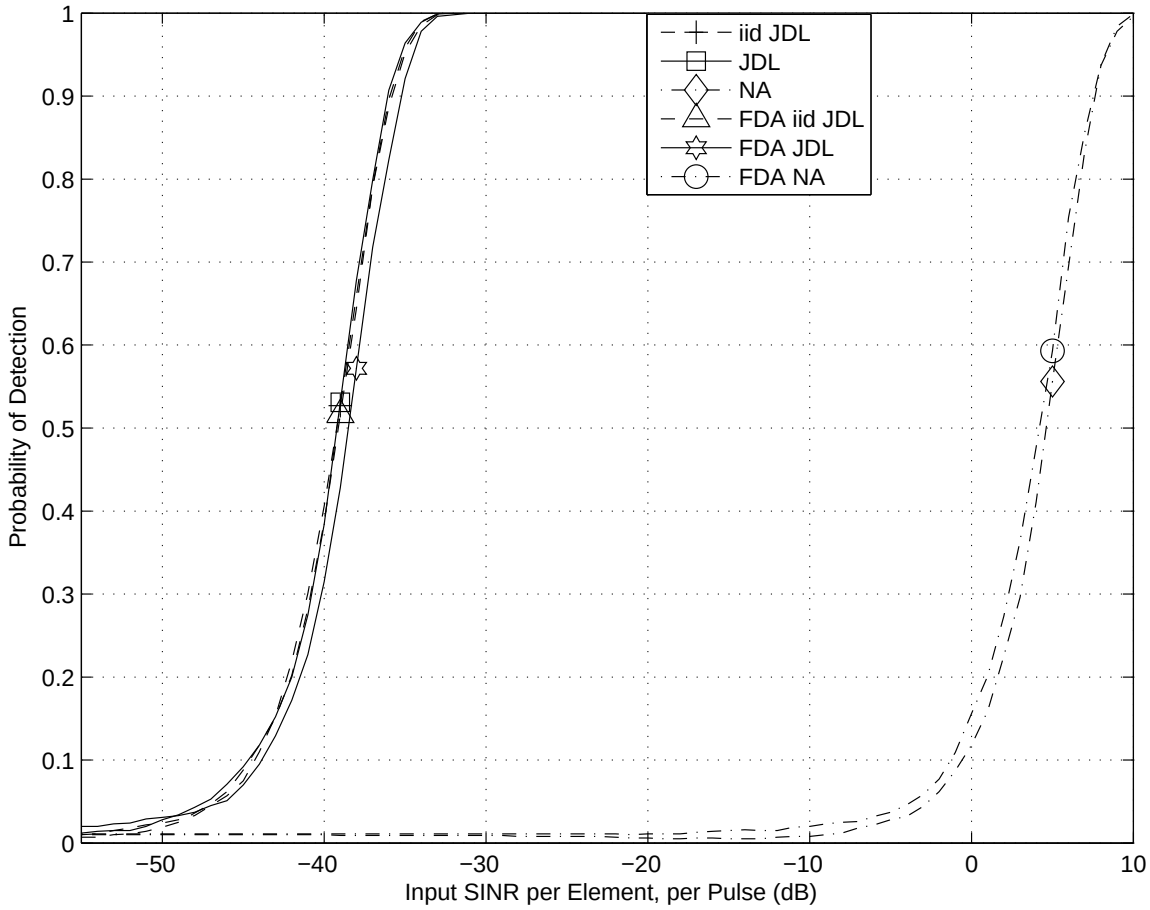

Figure 7.41: High altitude platform and ground illumination planar partial FDA detection curves for a target at $\bar{\omega} = 0.450$ for $P_{fa} = 0.01$. The detection curves now show minimal difference between iid and non-iid sample support of both array types, confirming that the partial FDA outperforms the previous FDA by approximately 20 dB.

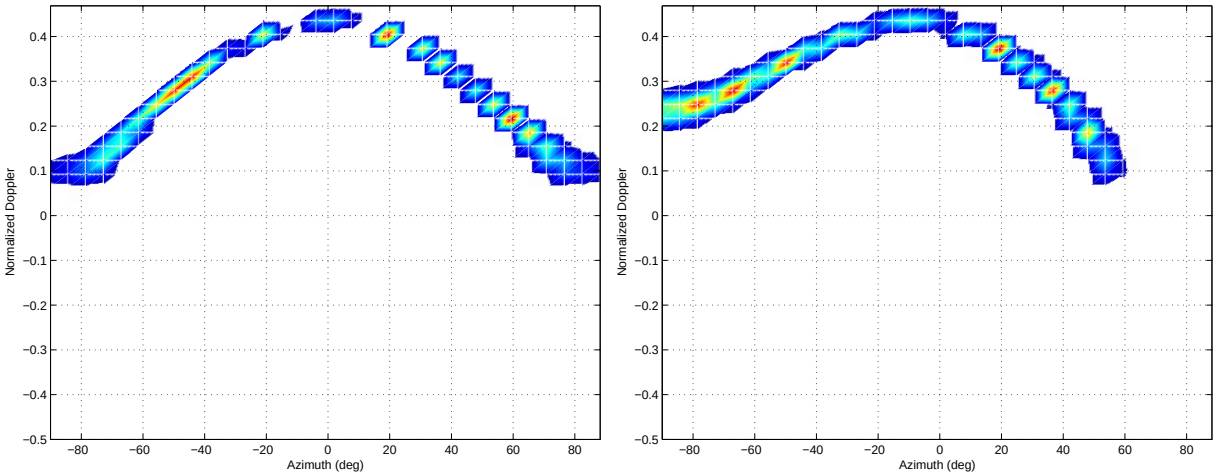

Figure 7.42: High-altitude platform and -17° elevation transmit angle, Minimum Variance Estimate clutter spectrum comparison of estimated interference covariance matrices using non-iid sample support. There is more of a shift than increase in region occupied by the constant frequency array clutter (left) and the partial FDA (right) indicating a similar clutter rank at the target range. The clutter spectra corresponding to the elevation angles at the two range ambiguous clutter rings are not included because of suppression using elevation DOF.

Now there is more of a shift in the region occupied by clutter rather than increase when comparing partial FDA and constant frequency, therefore the performance of the two array types is near identical.

7.9.3 UAV with Hovering Helicopter Results. The planar partial FDA Output SINR for a low platform altitude with horizontal elevation transmission is seen in Figure 7.43. The result is identical to the planar FDA with frequency diversity along both horizontal and vertical array channels, because there is no range ambiguous clutter and hence different elevation nulls make no difference to the clutter statistics using a known interference covariance matrix at the target range.

The use of non-iid sample support data with only horizontal frequency diversity reduces the degradation associated with using a planar FDA. The Output SINR in Figure 7.44 shows an 18 dB improvement of planar partial FDA over previous planar FDA and an associated clutter doppler notch narrowing. However, the planar par-

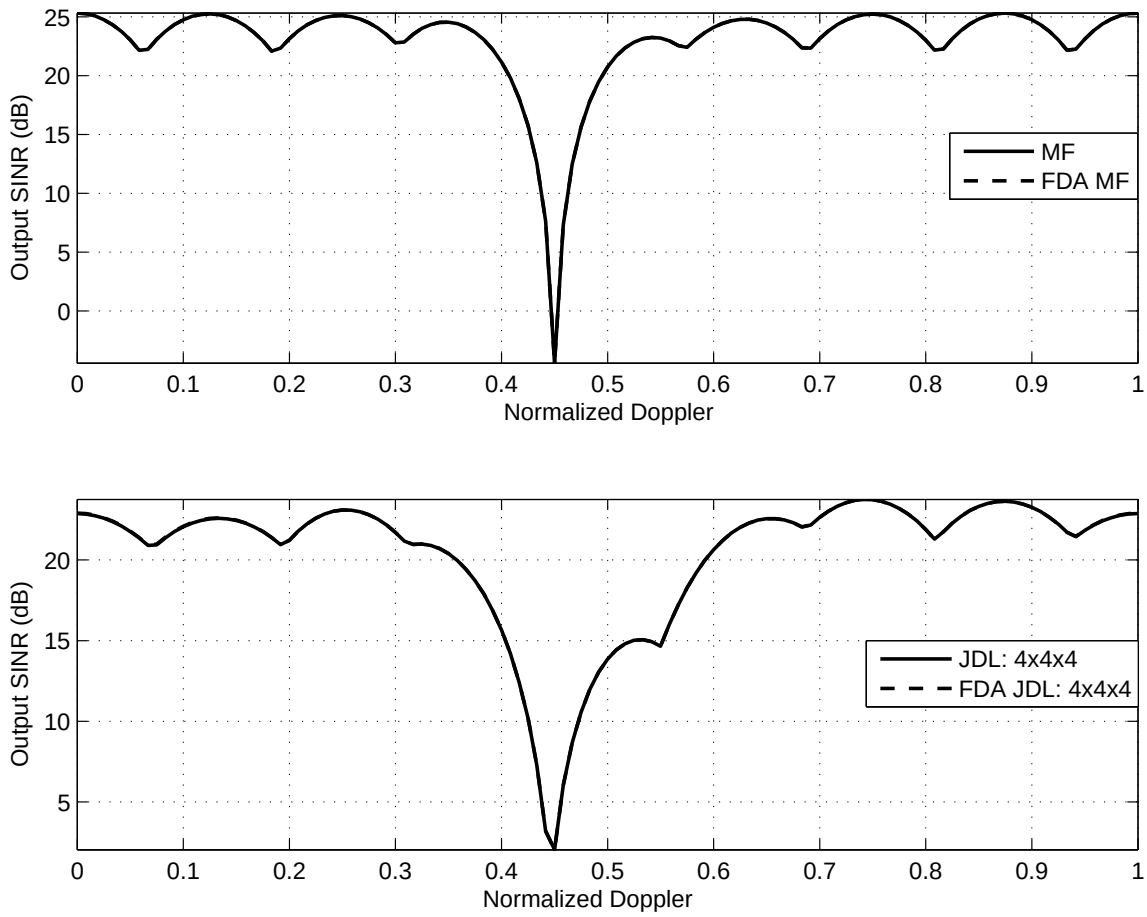

Figure 7.43: Low-altitude platform, horizontal elevation transmission planar partial FDA Output SINR using known interference covariance matrix at a target range of 8.0 km. Only one clutter doppler notch is present because there is no range ambiguous clutter at the low platform altitude and performance is identical for the two array types and to the previous FDA with full frequency diversity.

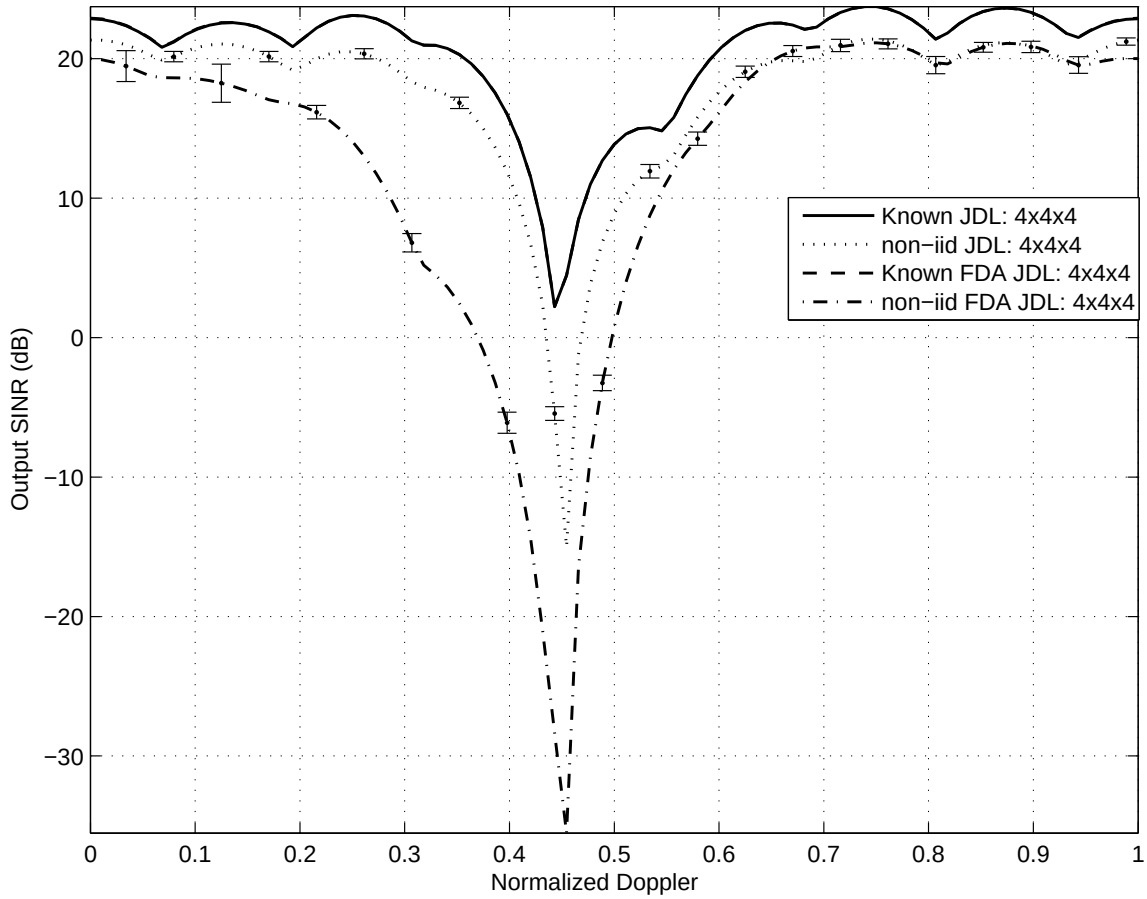

Figure 7.44: Low-altitude platform with horizontal elevation transmission planar partial FDA Output SINR. The known covariance result is compared to an estimated interference covariance matrix generated from 128 symmetrical sample support vectors. The latter curve is averaged over 1000 realizations and the partial FDA shows an 18 dB improvement over the previous FDA, however still 20 dB below the constant frequency array.

tial FDA performance is still considerably lower than the constant frequency array response.

The change in platform altitude or more specifically the removal of range ambiguous clutter contribution has a significant impact on the GIP shape as shown in Figure 7.45. Similar to the high platform altitude NHD results, the planar partial FDA is more similar to the constant frequency array than the planar FDA. The planar partial FDA has no impact on GIP dynamic range and reduces GIP standard deviation by 2.5%. Overall, the NHD results for the low-altitude partial FDA are

almost identical to the constant frequency array in terms of GIP shape and statistical criteria, indicating minimal difference in sample support data homogeneity, in contradiction to the previous Output SINR result in Figure 7.44.

For reduced CPI parameters the AMF Output SINR is seen in Figure 7.46 and the use of partial frequency diversity improves the performance relative to the planar FDA on the order of 7 dB. As expected, the improvement is less for fully adaptive processing than the partially adaptive JDL above because AMF compensates for increased FDA clutter rank, and hence previous planar AMF performance is less affected by increased sample support homogeneity than the previous planar FDA JDL.

Due to the low platform altitude only one P_d curve is assessed. The target doppler value for the detection curve is based on a target doppler value corresponding to the target range clutter doppler and the result shown in Figure 7.47. As predicted by the estimated Output SINR, the partial FDA JDL performance using non-iid sample support is improved by 16 dB over the performance experienced using planar FDA, however the constant frequency array is still performing approximately 5 dB better than the partial FDA result.

Limiting frequency diversity to only horizontal array channels is seen to considerably improve FDA performance over the full planar FDA in Section 7.6 and is consistent with the NHD results presented. Despite the 16 dB improvement in detection probability when using non-iid sample support, the planar partial FDA performance is still 5 dB worse than the constant frequency array for this scenario.

The additional degradation using non-iid sample support for the partial FDA is not consistent with NHD results that are approximately identical for both array types. However, examination of the clutter spectra of the estimated interference covariance matrices can be used to compare clutter rank, same as for the previous FDA structure. The averaged MVE result is shown in Figure 7.48.

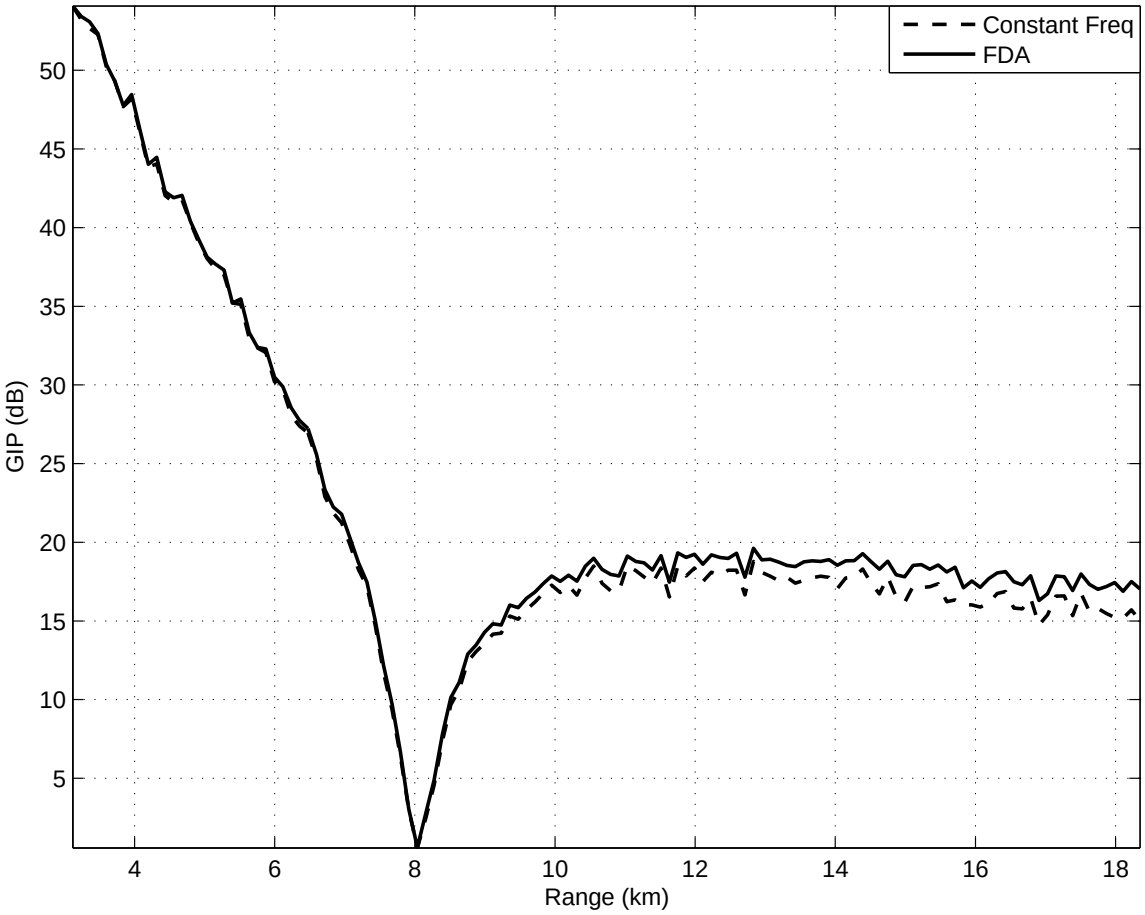

Figure 7.45: Low platform altitude with airborne target GIP for forward-looking planar constant frequency array and planar partial FDA averaged over 100 runs. As for the preceding high altitude scenario, limiting frequency diversity to only horizontal channels has a significant impact on the GIP curves, resulting in minimal difference between the two array types. Based on the minimal variation, similar non-iid sample support performance is expected with no homogeneity benefits evident for array boresight targets.

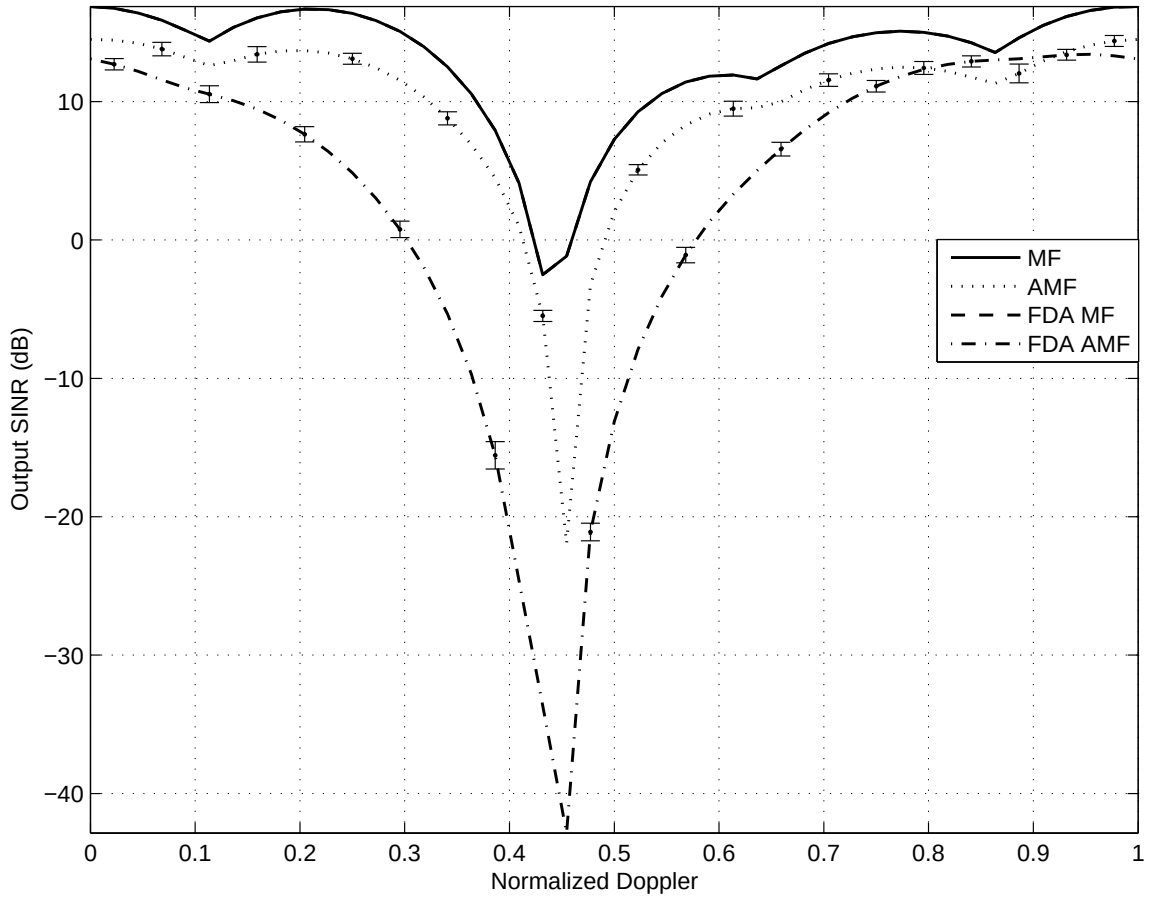

Figure 7.46: Low-altitude platform horizontal elevation transmission planar partial FDA fully adaptive Output SINR with reduced CPI values $P = 4$, $N = 4$, and $M = 4$. The MF result is compared to AMF using an estimated interference covariance matrix generated from 128 symmetrical sample support vectors. The AMF curves averaged over 1000 realizations show the partial FDA producing a 7 dB improvement over the previous FDA, however still over 20 dB below the constant frequency array.

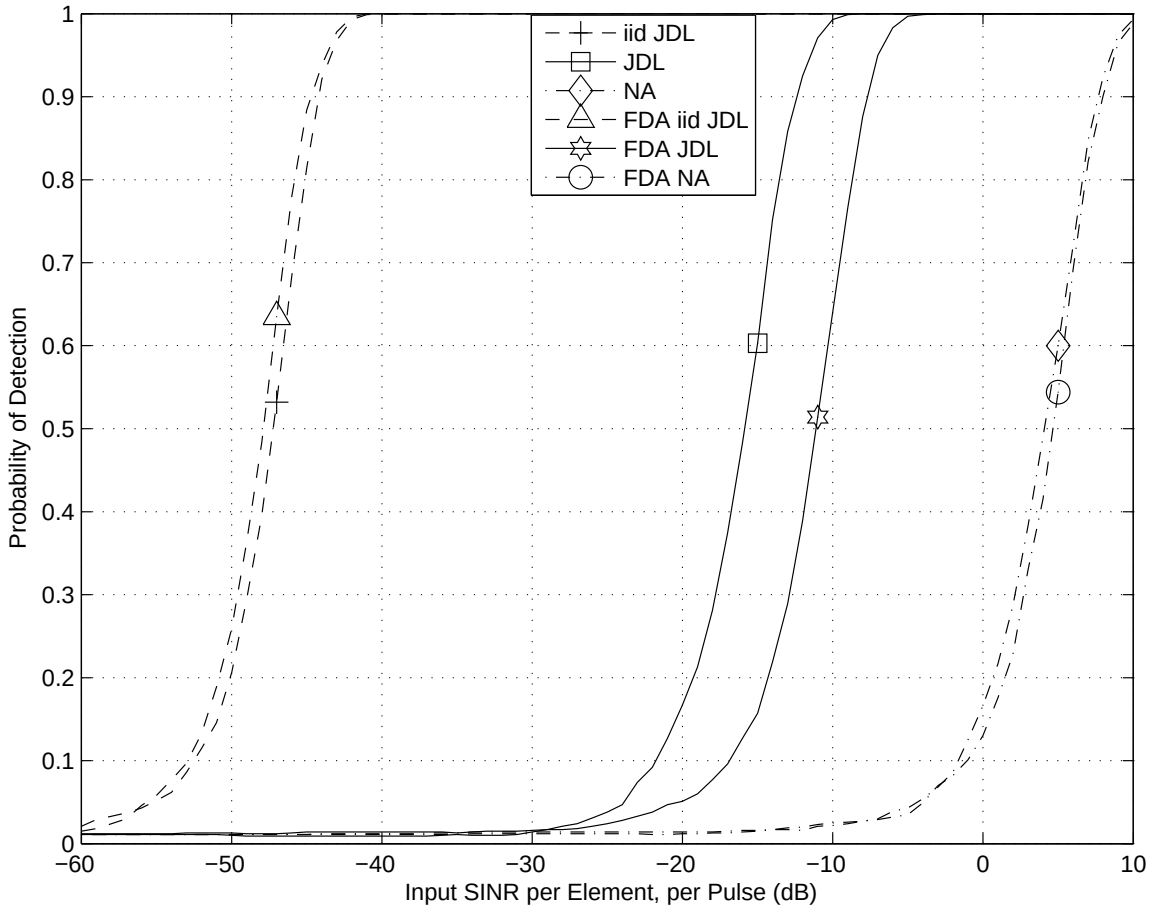

Figure 7.47: Low altitude platform and horizontal elevation transmission planar partial FDA detection curves for a target at $\bar{\omega} = 0.450$ for $P_{fa} = 0.01$. The detection curves show considerable performance degradation when using non-iid sample support for both array types, however the partial FDA degradation is reduced compared to the FDA with full frequency diversity. The non-iid partial FDA performance is better than NA processing but the non-iid constant frequency is still 5 dB better.

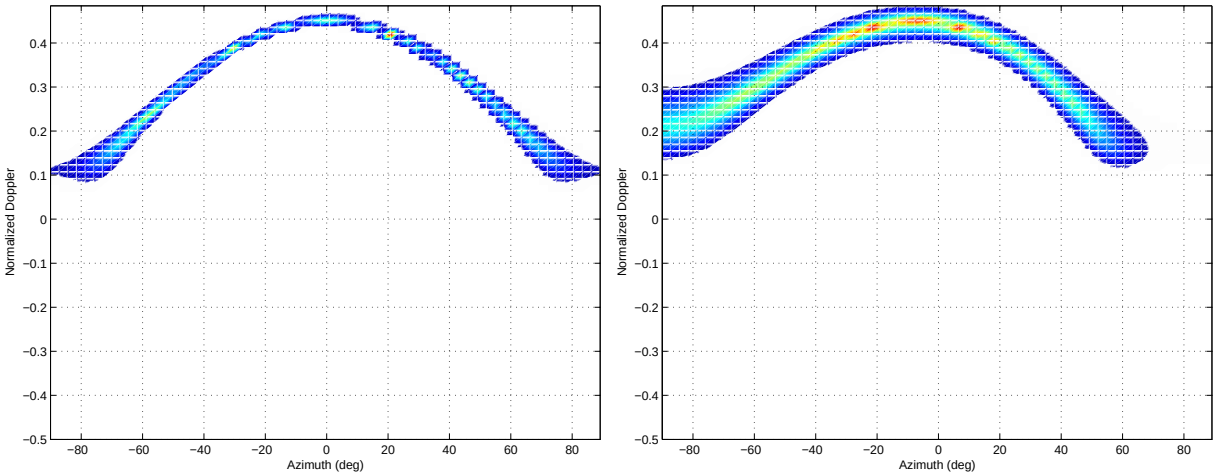

Figure 7.48: Low-altitude platform and 0° elevation transmit angle, Minimum Variance Estimate clutter spectrum comparison of estimated interference covariance matrices using non-iid sample support. The constant frequency array clutter (left) occupies a noticeably smaller region than the partial FDA (right) indicating the constant frequency array has a smaller clutter rank. The partial FDA clutter spectrum shows an increase in arc width, indicating a greater degree of variation from target-range statistics within sample support vectors.

Similar to the FDA in Section 7.6, comparison of the two clutter spectra confirm the constant frequency estimated interference covariance matrix array has a smaller clutter region within the azimuth-doppler domain compared to the partial FDA estimated interference covariance matrix. Therefore, the partial FDA estimated interference matrix has a greater clutter rank leading to degraded performance.

When compared to the FDA with fully frequency diversity seen in Figure 7.23, the partial FDA has a significantly decreased clutter arc width and rank. However, the partial FDA clutter arc width is increased compared to the constant frequency array indicating greater clutter statistics variation across the sample support vectors. Therefore partial FDA sample support has greater heterogeneity than predicted by the NHD result, which were approximately identical for the partial FDA and constant frequency.

7.9.4 UAV with Jeep Results. As for the two previous scenarios, there is no difference between the planar FDA, planar partial FDA and constant frequency array

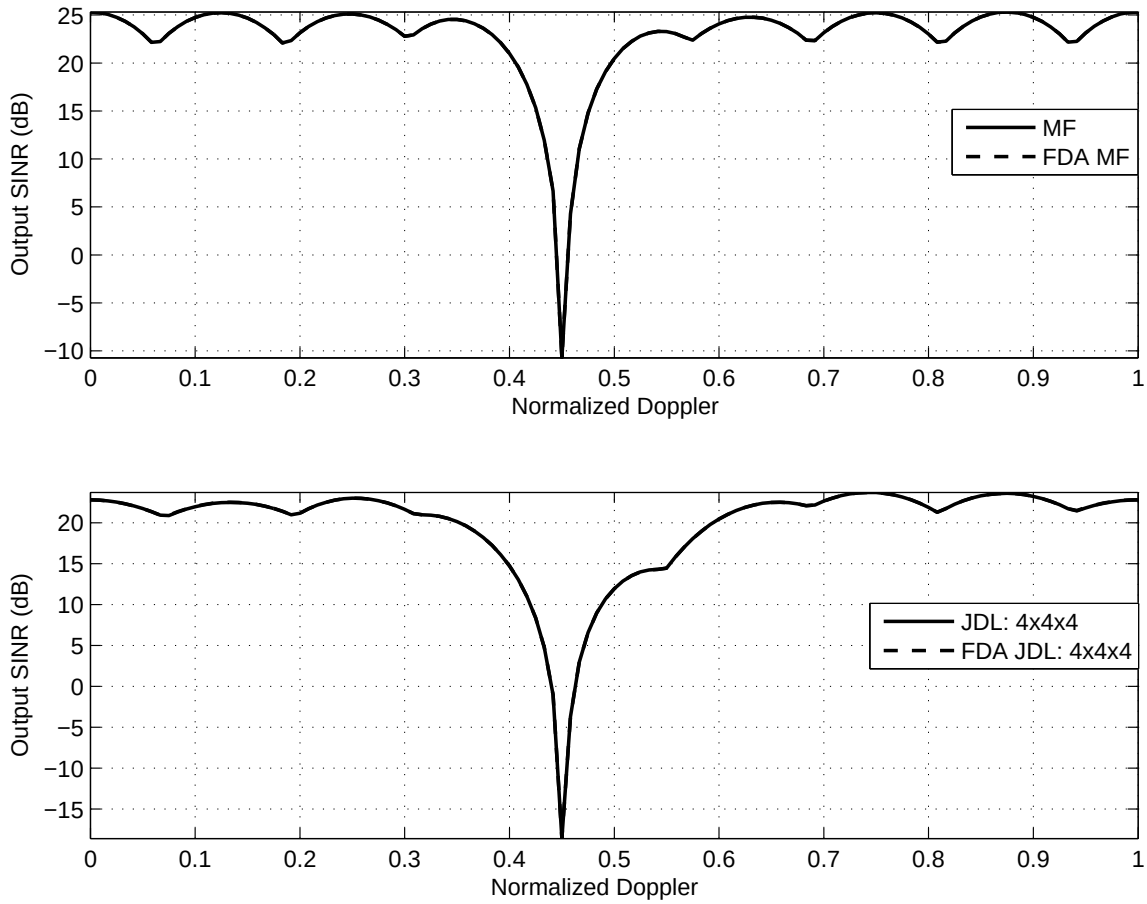

Figure 7.49: Low-altitude platform, ground illumination planar partial FDA Output SINR using known interference covariance matrix at a target range of 8.0 km. Only one clutter doppler notch is present because there is no range ambiguous clutter and the performance is identical for both array types and the FDA with full frequency diversity.

Output SINR when using known covariance as seen in Figure 7.49. The reason is the low platform altitude has no range ambiguous clutter contribution and the target range illumination is identical for all array types.

An improvement of almost 25 dB using planar partial FDA is realized using non-iid sample support over the planar FDA. The result is shown in Figure 7.50 and the planar partial FDA results in a reduction in clutter doppler notch width.

The low altitude ground target planar partial FDA NHD result is the same for the low altitude airborne target. The NHD seen in Figure 7.45 indicates that there

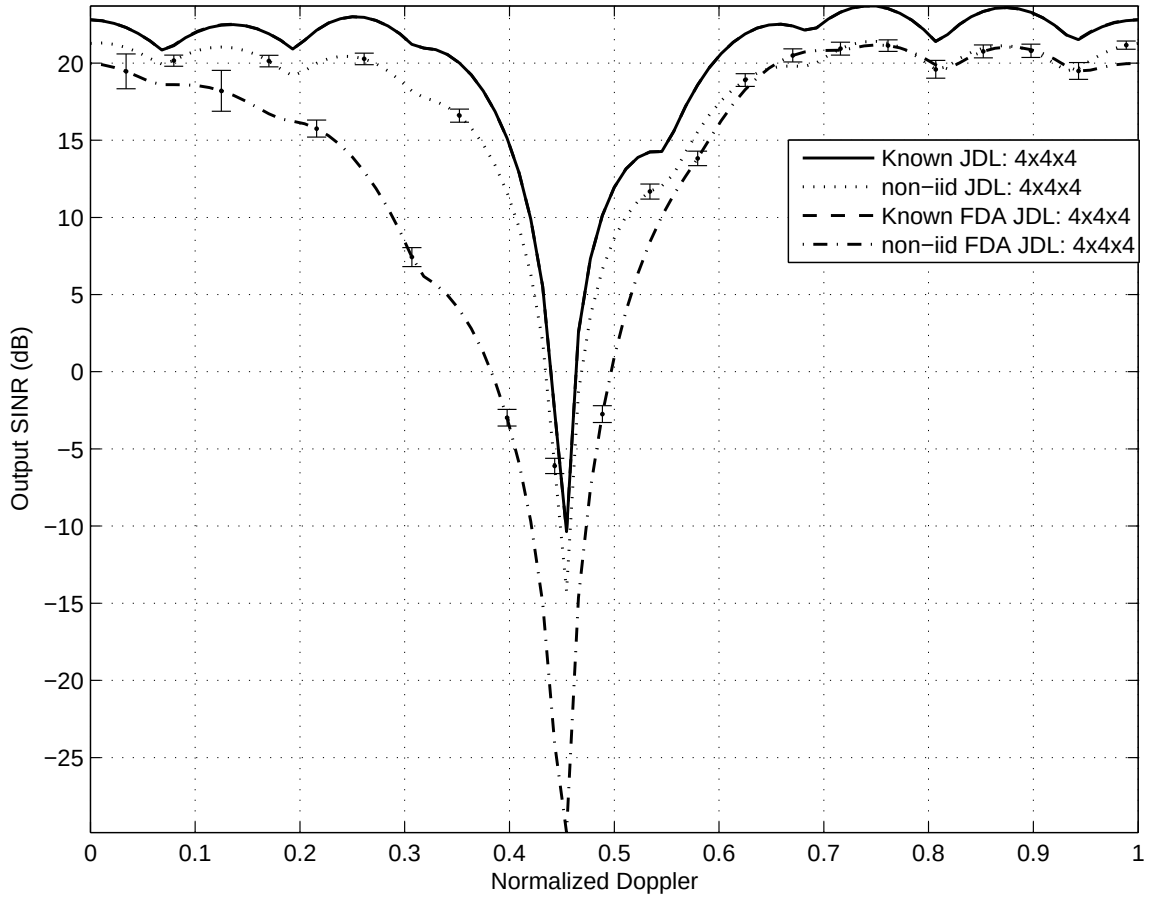

Figure 7.50: Low-altitude platform with ground illumination planar partial FDA Output SINR. The known covariance result is compared to an estimated interference covariance matrix generated from 128 symmetrical sample support vectors. The latter curve is averaged over 1000 realizations and show minimal degradation for the constant frequency array and considerable degradation for the partial FDA. The partial FDA degradation is considerably better than the degradation experienced by the previous FDA, an improvement of approximately 22 dB but still 15 dB below constant frequency array performance.

is minimal sample support data homogeneity difference between constant frequency and planar partial FDA, indicating a significant improvement of planar partial FDA over planar FDA. The result is consistent with the assertion that frequency diversity across vertical channels dominates frequency diversity across horizontal channels.

The improvement for the AMF using planar partial FDA over the planar FDA is 17 dB showing that fully adaptive processing gains are less than partially adaptive processing gains, same as for the previous low altitude scenario with an airborne target. The corresponding Output SINR plot seen in Figure 7.51 verifies that despite the benefit using partial FDA over FDA, there is still a 16 dB improvement that can be achieved by using the constant frequency array.

When the target doppler matches the target range clutter doppler, there is only a 3 dB improvement in detection performance using partial FDA with non-iid sample support over the previous planar FDA result, less than expected from Figure 7.50. As shown in Figure 7.52 the constant frequency array is still considerably better than the planar partial FDA result.

To confirm the increased clutter rank is responsible for the degradation of partial FDA compared to the constant frequency array, the MVE clutter spectra is compared in Figure 7.53. The resulting spectra are very similar to the previous scenario of the airborne target because of the minimal change in the elevation transmit angle from 0° to -2.4°.

The MVE spectra confirms partial FDA produces clutter occupying a larger proportion of the azimuth-doppler domain than the constant frequency array. Additionally, similar to the airborne target above, the clutter region is less than the FDA with fully frequency diversity.

7.9.5 Partial Frequency Diverse Planar Array Summary. It is seen that a partial FDA, one where frequency diversity is limited to horizontal array channels helps for three out of four engagement scenarios, with the exception being a high

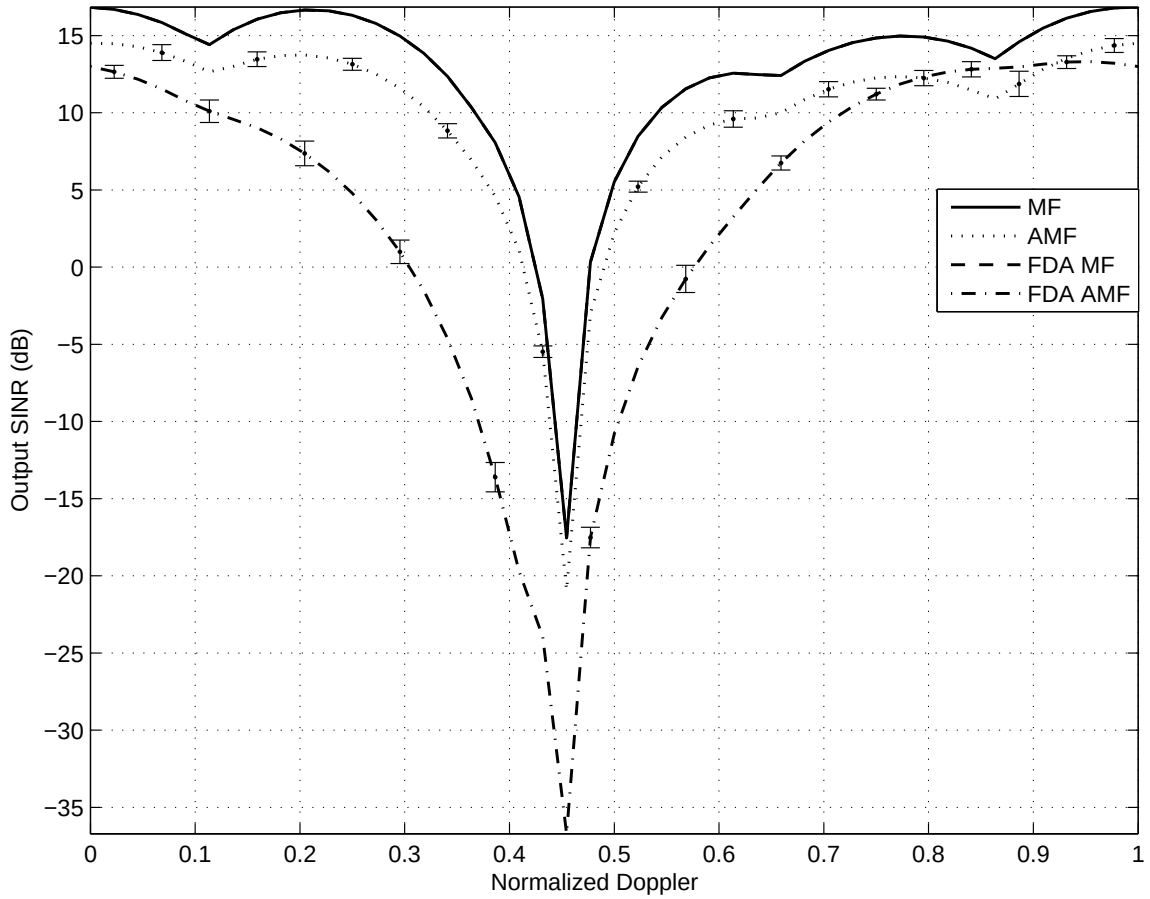

Figure 7.51: Low-altitude platform ground illumination planar partial FDA fully adaptive Output SINR with reduced CPI values $P = 4$, $N = 4$, and $M = 4$. The MF result is compared to AMF using an estimated interference covariance matrix generated from 128 symmetrical sample support vectors. The AMF curves averaged over 1000 realizations show an improvement of 17 dB of the partial FDA over the previous FDA. As for the JDL with estimated interference matrices above, the constant frequency array still outperforms the partial FDA but now by only 16 dB.

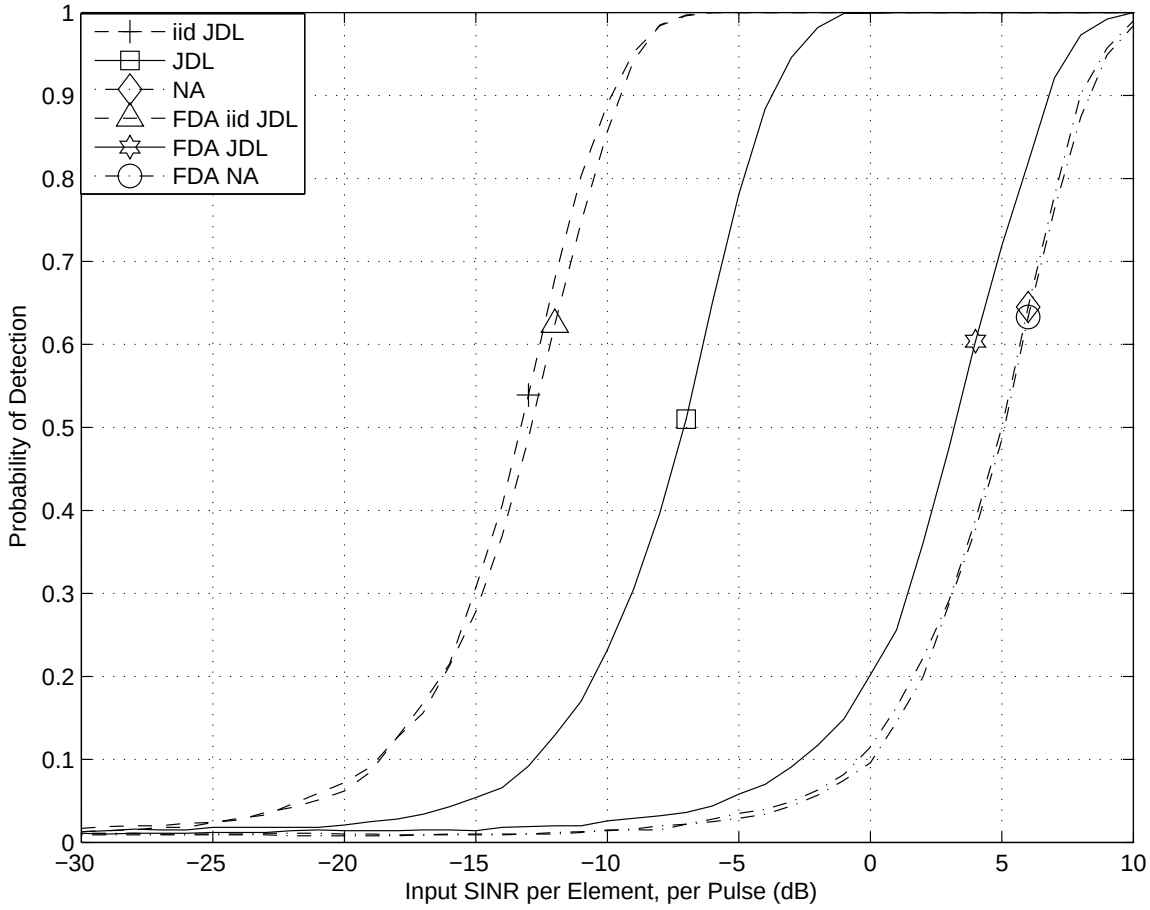

Figure 7.52: Low altitude platform and ground illumination planar partial FDA detection curves for a target at $\bar{\omega} = 0.450$ for $P_{fa} = 0.01$. The detection curves show some performance degradation when using constant frequency non-iid sample support, however considerably greater degradation for the FDA. The non-iid partial FDA performance is only marginally better than the previous FDA non-iid performance and hence also marginally better than NA processing, whereas the non-iid constant frequency is approximately 10 dB better.

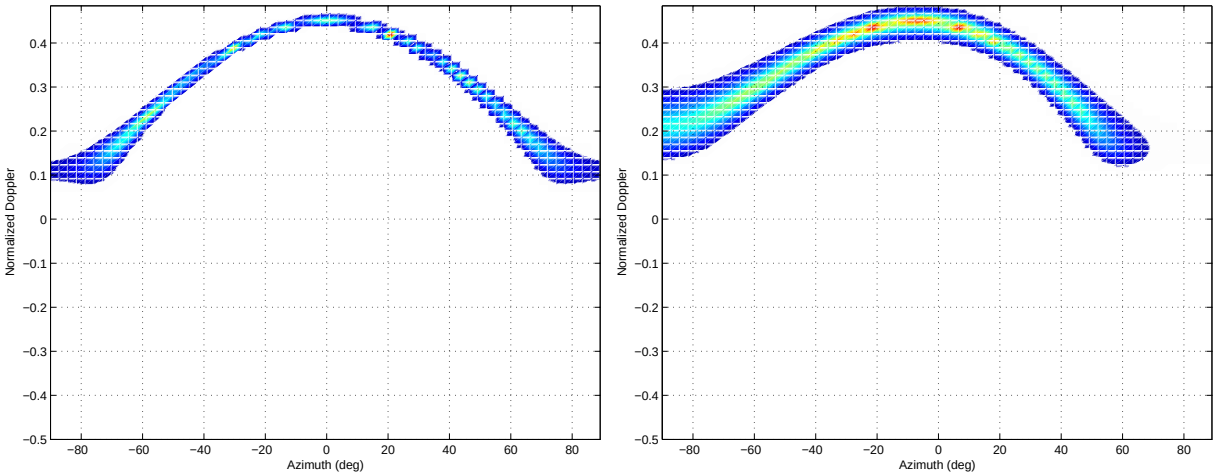

Figure 7.53: Low-altitude platform and -2.4° elevation transmit angle, Minimum Variance Estimate clutter spectrum comparison of estimated interference covariance matrices using non-iid sample support. The constant frequency array clutter (left) occupies a slightly smaller region than the partial FDA (right) indicating the constant frequency array has a smaller clutter rank. The partial FDA clutter spectrum shows an increase in arc width, indicating a greater degree of variation from target-range statistics within sample support vectors.

platform altitude and airborne target. The pertinent points from the investigation into the use of planar partial FDA are summarized below.

- The reason for the degradation in using non-iid sample support for the high platform altitude with horizontal transmission is based on the range ambiguous clutter contribution to the sample support range-cells coinciding with a planar FDA elevation null. If the target range is changed so the null is not present then partial FDA performance is better than full planar FDA.
- For both low platform altitude scenarios and the high platform altitude with ground illumination scenario, the planar partial FDA outperforms the planar FDA. Specifically, the degradation using non-iid sample support using the planar partial FDA is less than the degradation using the planar FDA, as predicted by the reduced GIP dynamic range.
- Despite the improvement achieved by removing frequency diversity from the vertical array channels, the planar partial FDA performance is still worse than the

constant frequency planar array for low platform altitude. The result does not match the NHD results where minimal difference between the two array types is expected. However, examining the estimated interference covariance matrix for both array types the clutter spectrum of the planar partial FDA is larger than the constant frequency array spectrum. The increased region of clutter corresponds to an increased clutter rank and hence degraded performance.

7.10 Planar FDA Comparison Summary

Four engagement scenarios have been considered to assess potential benefits of using a planar FDA, with both full and partial frequency diversity. The results show that whilst the FDA concept holds merit, planar frequency diversity increases degradation associated with use of non-iid sample support compared to constant frequency arrays except for high platform altitude with airborne targets. The basis for verifying and explaining the results achieved in this chapter are based on NHD results, ground projected antenna patterns and also clutter spectra of estimated interference covariance matrices.

The above assertion of planar FDA performance is based on detection curves when target doppler values match the clutter notches associated with the platform altitude. The most poignant conclusions are listed below.

- When Output SINR is evaluated using the known interference covariance matrix, with the exception of high platform altitude with horizontal elevation transmission angle scenario, there are no differences between constant frequency and both planar FDAs because of no range ambiguous clutter for low platform altitude and range ambiguous clutter suppression for a ground target at high altitude.
- For the high platform altitude and horizontal elevation transmission scenario, the range-dependent FDA antenna pattern suppresses the range ambiguous clutter that can not be separated from the target in elevation. The result is a reduced

range ambiguous clutter doppler notch when using a frequency diverse planar array, producing a detection improvement of 6 dB at the target range clutter doppler and an improvement of 20 dB for a target at the range ambiguous clutter doppler.

- For ground target performance at high platform altitude, the performance using a planar partial FDA exceeded the performance using a planar FDA by 19 dB at the range ambiguous clutter, however the response is no better than a constant frequency array. The result is consistent with the near identical NHD shape for both the constant frequency and partial FDA.
- At low platform altitude, the planar partial FDA performance is 15 dB better for airborne targets and 3 dB better for ground targets when compared to the planar FDA. However, the partial FDA performance is still 5 dB and 10 dB worse than the corresponding constant frequency array detection level. The degradation is not consistent with the low-altitude NHD predictions. However, it is consistent with the marginally increased partial FDA clutter spectrum region compared to the constant frequency array spectrum.

As noted in Chapter VI, it is important to stress that the focus of this thesis is to verify the potential benefits of FDA rather than optimize results for a given engagement scenario. Based on considerable benefits achieved in one engagement scenario, it is considered likely that through improved frequency allocation across array channels additional gain could be achieved. Additionally, exploitation of isodops to increase sample support data is easier to achieve for targets off-boresight in azimuth.

The selection of JDL DOF is designed to create sample support data that has significant deviation from iid. Therefore, the performance of STAP techniques could have been improved by reducing the DOF and hence approaching iid sample support, for example elevation DOF η_e could be reduced at low platform altitude, as there is no range ambiguous clutter that can be separated using elevation angle.

VIII. Conclusions

This thesis characterizes the concept of a Frequency Diverse Array (FDA) through derivation of a radar data model, analysis of impacts on clutter spectrum and clutter rank, and also providing sample linear and planar performance comparison using four engagement scenarios. The focus of this thesis is on the forward-looking array, where clutter doppler is dependent on elevation and hence range. It is proposed that the FDA can be beneficial through suppression of range ambiguous clutter for a linear array through the range dependent FDA antenna pattern and also in the homogeneity of sample support data where the FDA antenna pattern accentuates the forward-looking isodops.

Chapter II covered the background on Space-Time Adaptive Processing (STAP) including existing approaches taken to applying STAP for Forward-Looking Airborne Radar (FLAR). Results achieved using STAP for FLAR are not as productive as results for Side-Looking Airborne Radar (SLAR) because of range-dependent clutter doppler. To match reality and highlight these issues the interference covariance matrix estimation is done using range-cells that are not Independent and Identically Distributed (iid), breaking an assumption implicit in the foundation of STAP.

8.1 Radar Data Model

The radar data model derived in Chapter III is comparable to the physical model introduced by Ward [27]. However, the model is developed for a planar array using the approach taken by Hale [10]. Mathematical model validation is provided in Chapter IV and is achieved be setting all array channels to the same frequency, i.e. a constant frequency array.

Chapter IV also provides limiting cases by confining frequency diversity to only one array dimension. The limiting cases of constant horizontal and constant vertical frequency arrays are then collapsed to linear FDA radar data models by setting P and N, respectively, to unity. The resulting linear FDA radar data models are math-

ematically verified to be consistent with the constant frequency linear array data model.

8.2 FDA Impact Analysis on Clutter Statistics

Since the array structure is analogous to the "eye" the radar uses to view the external environment, the impact of using the FDA has to be analyzed. Using a simple channel frequency allocation scheme as an example, Chapter V examined the impact the FDA structure, specifically the range-dependent antenna pattern, has on clutter spectrum and clutter rank.

Investigation showed the FDA spreads out ground clutter within the azimuth-doppler domain because of antenna pattern variation over range. The increased region of clutter within the clutter spectrum corresponds to increased clutter rank and indicates a greater difficulty in suppressing clutter. Because of the increased clutter rank, the FDA is unlikely to provide benefits for side-looking radar applications at or near azimuth boresight. Increased clutter rank indicates However, since clutter is not full rank, the increased rank will not adversely impact FDA results using fully adaptive STAP. Unfortunately sample support requirements prohibit implementation of fully adaptive STAP and therefore, the increased clutter rank will adversely impact FDA partial adaptive STAP performance.

8.3 FDA Forward-Looking STAP

Comparison of FDA and constant frequency array results utilized four engagement scenarios, each scenario a different combination of platform altitude and the elevation transmission angle, i.e. whether an airborne or ground target. The results focused on degradation associated with using non-iid sample support and corresponding detection performance at the clutter doppler notches, i.e. low relative velocity targets. All simulations assumed boresight azimuth transmission to replicate worst case isodop conditions, reducing the magnitude of any sample support homogeneity.

8.3.1 Linear Array. The major *linear* FDA benefit is the ability to reduce the contribution of range-ambiguous clutter through the range-dependent antenna pattern. The detection of slow moving targets at far range is improved by 10 dB (see Fig. 6.14), particularly important for Ground Moving Target Indication (GMTI) applications. Additionally, FDA performance at low platform altitude where no range ambiguous clutter exists showed 1 to 2 dB (see Fig. 6.24) improvement attributed to sample support homogeneity.

8.3.2 Planar Array. The *planar* FDA and *planar partial* FDA, the latter array having frequency diversity only along horizontal array channels, did not show regularized sample support data benefits over the constant frequency array. However, similar to the linear results, both planar FDAs suppressed the range-ambiguous clutter through the range-dependent FDA antenna pattern improving detection performance by 20 dB for the high platform altitude *airborne* target (see Fig. 7.8). The high platform altitude with *ground* target is not improved since the range ambiguous clutter can be suppressed by the constant frequency array using elevation Degrees of Freedom (DOF).

With the exception of the airborne target at high platform altitude, the planar partial FDA (frequency diversity only across horizontal channels) outperformed the planar FDA, indicating frequency diversity along vertical array channels increases sample support homogeneity. The high platform altitude with airborne target is an exception because of an elevation null placed by the planar FDA over contributing range ambiguous clutter, and with a different target location the exception would not occur.

Constant frequency and planar partial FDA performance for the ground target at high altitude is identical, whilst planar partial FDA suffered degradation for both targets at low platform altitude. The reason for degraded performance at low platform altitudes is effectively explained by the clutter spectra of the estimated interference covariance matrices. The FDA with frequency diversity along both array axes has

a significantly larger region of the azimuth-doppler domain dominated by clutter, whilst the partial FDA only has a slightly greater clutter region than the constant frequency array. With the direct link between clutter spectrum area and clutter rank, the relative magnitude of degradation between the planar FDA and constant frequency array, and between the planar partial FDA and constant frequency array are consistent.

8.4 Results Contribution Summary

This thesis makes several important contributions in the adaptive interference literature realm. Firstly, this research develops and mathematically verifies the radar data model for further research into FDA and their potential applications. Secondly, this thesis analyzes the impact of using FDA on clutter spectrum and clutter rank, showing how the change in array structure effects the way clutter is perceived by the radar.

The thesis also illustrates the severe heterogeneous interference environment for forward-looking array orientation. The corresponding degradation due to non-iid sample support is compared using both linear and planar FDAs. Both fully and partially adaptive STAP is examined, with the focus on partial STAP due to the physical inability to have sufficient sample support vectors for full adaptivity.

The focus is FDA proof-of-concept for making sample support data more homogeneous, as opposed to optimization of results for a particular scenario. Therefore, the linear and planar array results for the four engagement scenarios considered are not based on optimal frequency allocation and do not necessarily represent the magnitude of benefits achievable using FDAs.

The simulation results show the FDA provides considerable benefit for low relative velocity targets, improving ground target detection for platforms such as Joint Surveillance and Target Attack Radar System (JSTARS) and Unmanned Aerial Ve-

hicles (UAV). FDAs are not a radar panacea as the performance improvements are not realized across the range of potential target velocities.

8.5 Suggested Areas for Further Research

The work thus far has produced a solid theoretical FDA foundation and identified a number of pertinent points concerning FDA application. The following paragraphs suggest a number of additional high interest research areas.

As emphasized throughout this thesis, the selection of frequency allocation across array channels has a significant impact on the array performance through the resulting FDA antenna pattern. There is potential for considerable performance improvements through different frequency allocations than those considered here. With optimum being defined as maximal Output SINR using actual sample support, it may be possible to approach the optimization as a mathematical bounded problem.

Based on the isodops observed for the forward-looking array, it is likely that the optimized frequency allocation is actually dependent on the physical scenario; primarily the target azimuth and combination of platform altitude, target range and hence elevation. It is expected the increase in sample support data homogeneity can be considerably increased for targets off-boresight in azimuth, as the isodop shape is better accentuated by the FDA antenna pattern. Further investigation is also recommended into whether adaptive frequency control benefits FDA performance and quantify any benefits.

With the noted limitations of Non-Homogeneity Detector (NHD) for underlying non-iid data, the introduction of an additional bound, or if necessary, an entirely new test metric is recommended. The modified procedure is required to enable structured choice of sample support vectors for a forward-looking array would be beneficial to both constant frequency and FDA performance for close range targets.

Finally, whilst not a critical topic, the existing FDA mathematical framework may show nuances that can be exploited in terms of either altering an existing STAP

technique or creation of a new technique. Generation of any such technique is out of scope for the current investigation, however it would be an interesting offshoot and may increase the benefits achieved by FDAs.

Appendix A. Proposed Methods to Assess Channel Frequency Diversity Impacts

As highlighted throughout the thesis, the selection of channel frequencies determines the Frequency Diverse Array (FDA) antenna pattern and frequency selection should be based on the radar's purpose. The focus of this thesis is sample support data homogeneity for forward-looking arrays. Hence, the frequency allocation should produce an antenna pattern offering properties to make sample support more homogenous.

With the goal to improve sample support data homogeneity defined, the frequency allocation is still dependent on the array size since total frequency deviation is dependent on both the magnitude of frequency diversity and the number of array channels frequency diversity exists across. Therefore, when comparing two FDAs of dissimilar array length the channel frequency allocation is critical.

There is a multitude of different schemes available to define frequency distributions across array channels. After investigation of logarithmic, polynomial, sinusoidal and random frequency distribution schemes, based on antenna pattern sidelobe levels and the desire to have a single mainlobe present across all ranges, the constant frequency increment is deemed most suitable. However, other more complex methods to assign individual channel frequencies may exist that generate improved FDA performance when compared to constant frequency increments.

Two methods are proposed to assess how a frequency allocation and resulting antenna pattern regularizes sample support data. As an initial approach, the antenna pattern can be compared to the isodop(s) to be accentuated. Alternatively, a more technical approach is to examine the Generalized Inner Product (GIP) dynamic range, commonly called the Non-Homogeneity Detector (NHD) test statistic. Both approaches are discussed below using the same simple constant frequency increments between successive array channels used in Chapter VI and Chapter VII. The qualitative approach allows prediction of any homogeneity improvements across all transmit azimuth angles, whilst the NHD is based on a specific transmit angle. In this appendix, the azimuth transmit angle ϕ is set to 0° for a worst case scenario.

A.1 Linear FDA

For the results in this section, a fixed array length of $N = 11$ and frequency increment of $\Delta f = 1$ kHz is selected to match the parameters in Chapter V and Chapter VI. Since the quantitative NHD approach is scenario parameter dependent, only one scenario will be examined to describe the NHD assessment process. Detailed NHD results and respective analysis for the four engagement scenarios are included in the relevant sections of Chapter VI.

A.1.1 Accentuation of Isodops. The accentuation of isodops is a qualitative approach providing good initial indication as to whether the antenna pattern is appropriate. The assessment is achieved by overlaying forward-array isodops on the antenna pattern as seen in Figure A.1.

It is observed the FDA antenna pattern has a range dependence resulting in the mainlobe intersecting a reduced number of isodop lines compared to the constant frequency array pattern. It is hard to change the number of crossings along array boresight because of the isodops shape, but as the beam is steered off boresight the number of crossings can be seen to reduce compared to a constant frequency array. The ideal situation is where the antenna pattern curve coincides with the isodops, as is the case for the side-looking array, and can be seen in Figure 3.3 of [15].

There are two notable limitations using isodops as an assessment criteria. Firstly, the direct link between isodop accentuation and the homogeneity of sample support data has not been mathematically proven, though the concept is intuitively sound. Secondly, the approach is qualitative and there is no mathematical criteria available in order to compare the benefit of different frequency selections with any accuracy or consistency.

A.1.2 Non-Homogeneity Detector Statistics. An alternative approach is assessing the antenna pattern through the NHD or more specifically using the GIP as a performance metric. The foundation of NHD is detecting first and second order

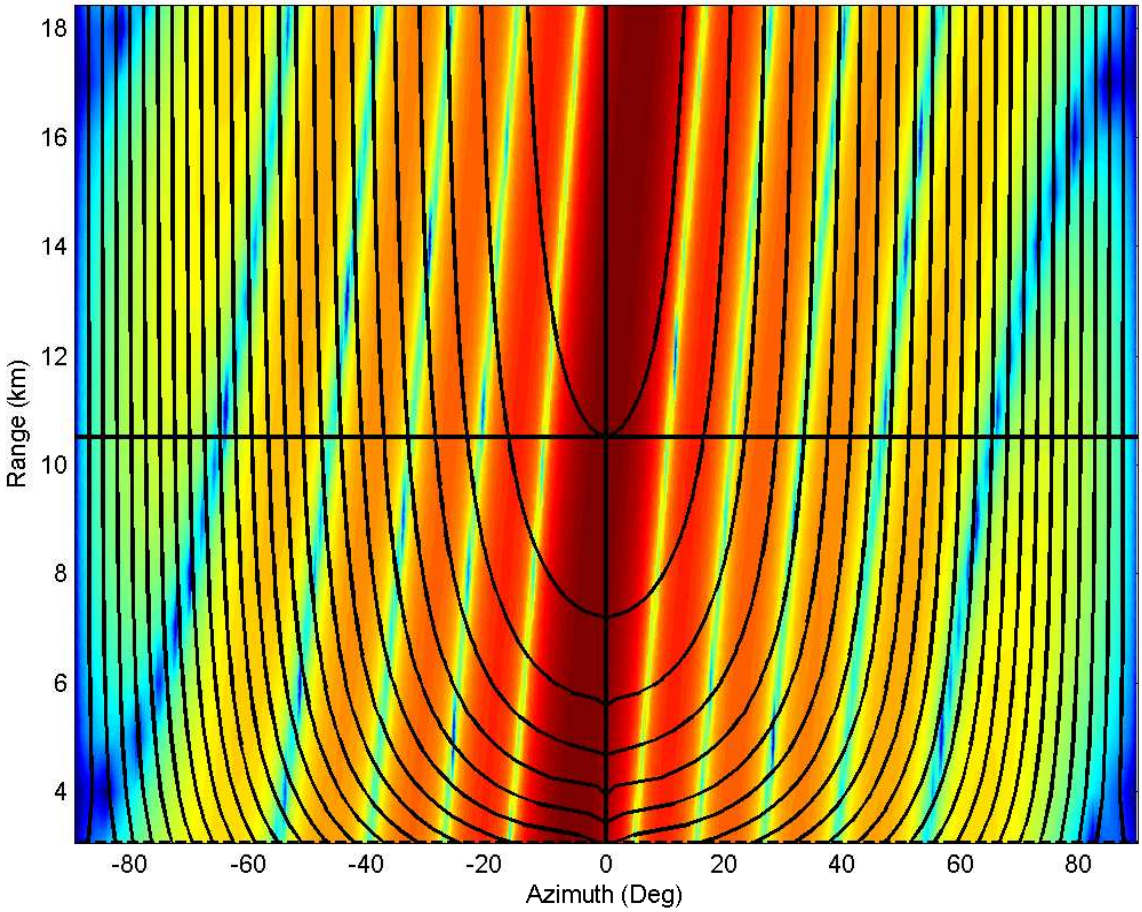

Figure A.1: Linear FDA antenna pattern, overlayed with forward-looking array isodops. Based on a platform altitude of 3073 m and 0° elevation transmit angle. The overlay shows the range-dependent FDA antenna pattern slope accentuates the isodops, reducing the number of isodop crossings.

statistic anomalies [28]. Therefore, the GIP can be used to assess how much the antenna pattern improves data homogeneity. It is proposed that the critical criteria is a reduction of GIP dynamic range, with a secondary criteria being a reduced standard deviation.

As described in Chapter II, the NHD requires a fundamental change due to the forward-looking array orientation. This orientation destroys the underlying independent and identically distributed (iid) data assumption used for the original NHD development. The change requires the initial covariance matrix $\hat{\mathbf{R}}$ represent the *target range* clutter statistics. Therefore, the estimate is artificially generated using multiple realizations based on the known covariance matrix at target range under the H_0 hypothesis. This situation cannot be repeated for measured or real world data since the target range covariance matrix is unknown. Since the NHD process relies on realizations and is statistical in nature, the NHD is averaged over 100 runs in order to improve the confidence of results.

The resulting GIP for linear constant frequency and FDA is shown in Figure A.2. The FDA under consideration produces a 44% reduction in GIP dynamic range and a 42% reduction in standard deviation, insinuating sample support homogeneity and performance increase over the corresponding linear constant frequency array.

It is important maintain physical insight of the scenario, particularly the contribution of range ambiguous clutter for high altitude platforms. Including range ambiguous clutter is critical because it has a different mainbeam clutter doppler than the target range mainbeam clutter doppler. To isolate the sample support homogeneity, other benefits such as range ambiguous clutter suppression through the range-dependent FDA antenna pattern must be addressed.

It is also important to note there is no evidence of a direct relationship between the magnitude of reductions in GIP dynamic range and standard deviation and the associated performance benefits in Output SINR and P_d. It is intuitive that larger reductions in GIP dynamic range indicate greater sample support data homogeneity,

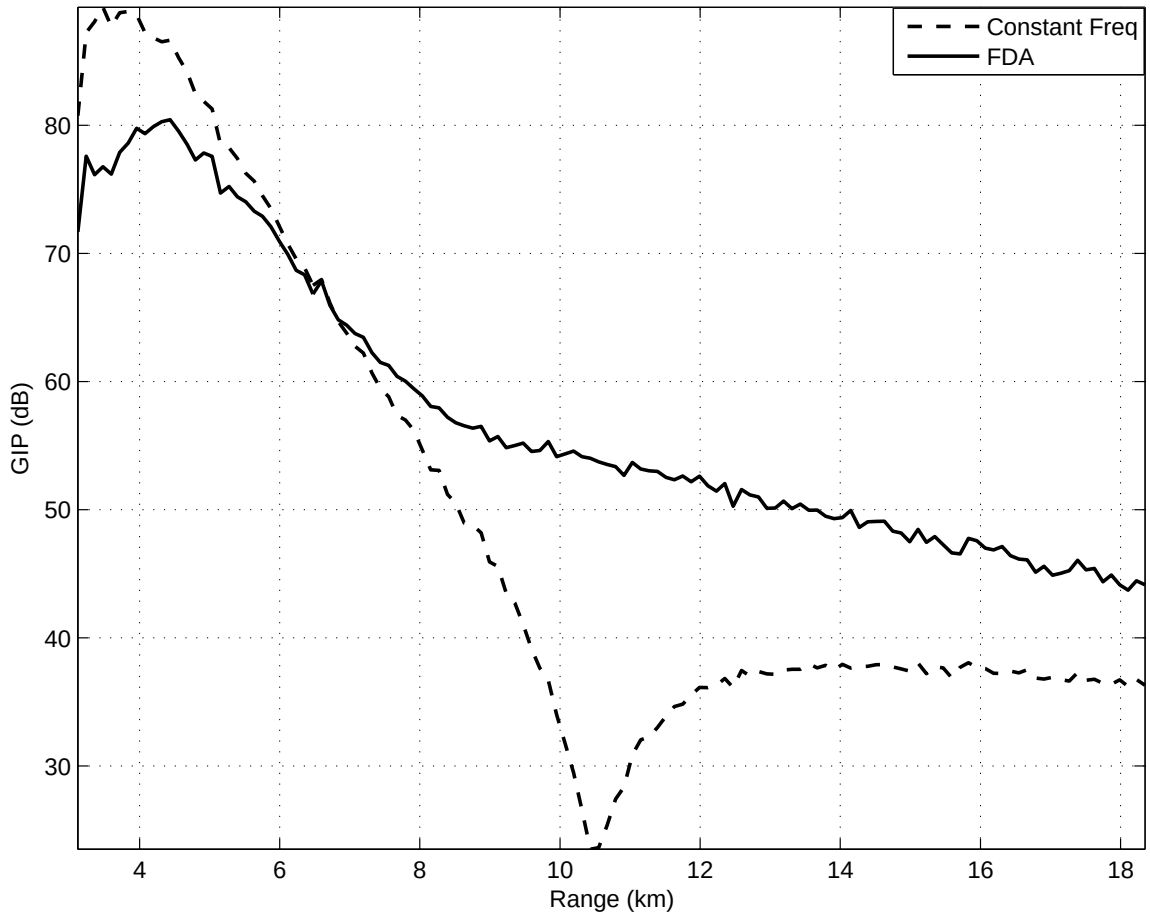

Figure A.2: Generalized Inner Product for forward-looking linear constant frequency array and FDA averaged over 100 runs. Results are based on a platform altitude of 3073 m, target range of 10.5 km and horizontal elevation transmission. The FDA curve has a smaller GIP dynamic range, indicating the FDA sample support vectors contain fewer heterogeneities than the constant frequency array, primarily at range-cells above the target range.

however, continued performance benefits with increased sample support homogeneity can not be generically quantified, i.e. the relationship may be asymptotic. Additionally, sample support homogeneity is not related to any particular clutter doppler value therefore, NHD improvements may not translate directly to P_d improvements.

A.2 Planar FDA

As seen in Chapter V, the planar array antenna pattern has an increased elevation angle dependence. Firstly, the range-elevation relationship required to generate the ground projected antenna pattern means the ground projection is reliant on the scenario parameters, particularly the platform altitude and elevation transmit angle.

The selected array parameters of $N = 11$, $P = 4$, and frequency progressions of $\Delta f_x = 1$ kHz and $\Delta f_z = 2$ kHz, correspond to parameters in Chapter V and Sections 7.4-7.7. This appendix does not consider the planar partial FDA where no frequency diversity exists across vertical channels, however NHD results for the planar partial FDA are discussed in Section 7.9.

A.2.1 Accentuation of Isodops. The overlay of isodops on the ground projected antenna pattern provides a qualitative approach to determining the frequency selection impact on sample support data homogeneity. Using the parameters defined above, the GIP is seen in Figure A.3.

It is difficult to determine qualitatively the impact of different frequency progressions partially because of elevation angle dependence, including different null locations. Therefore, NHD is of increased importance when assessing planar array frequency allocation schemes.

A.2.2 Non-Homogeneity Detector Statistics. The impact of reduced N and M values because of a non-unity P value is a reduced amount of frequency diversity along the horizontal orientation. Additionally, the azimuth beamwidth and doppler filterbank spacing is different due to the reduced parameters, and because of these

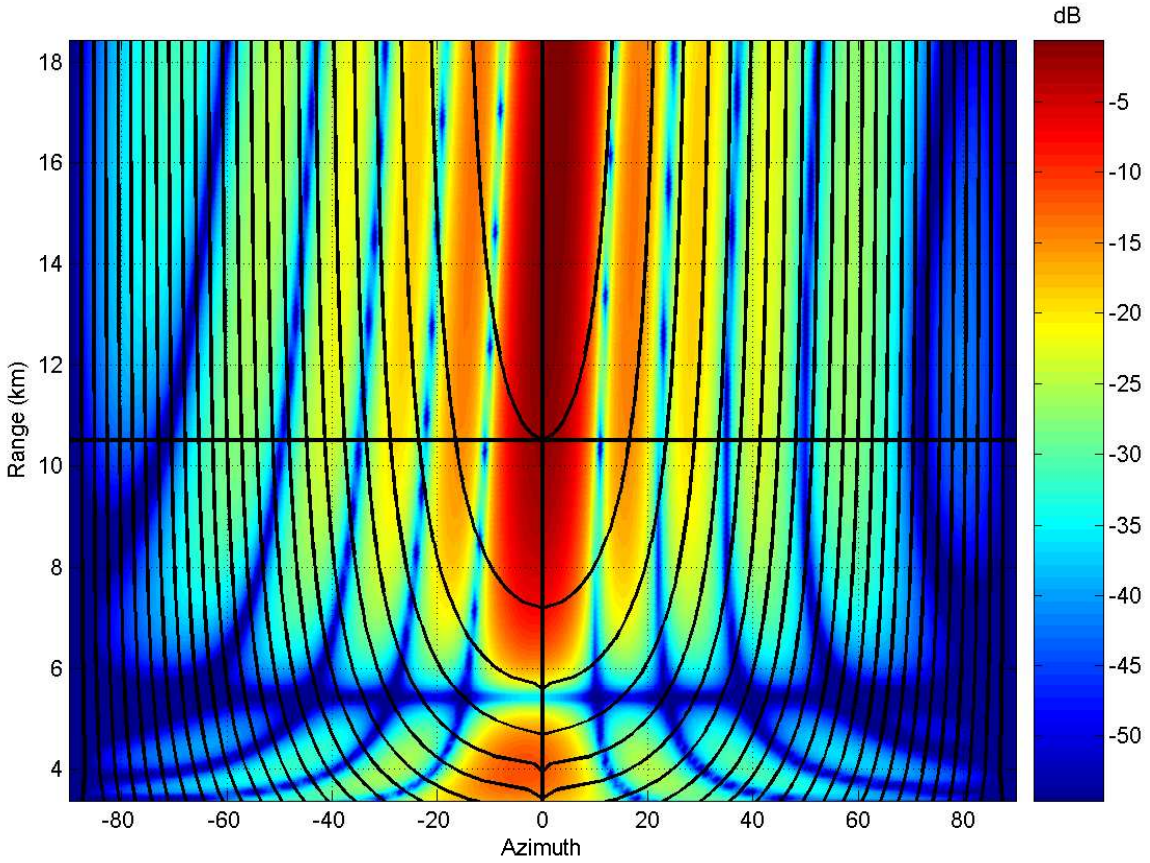

Figure A.3: Planar FDA antenna pattern, overlayed with FLAR isodops. Based on a platform altitude of 3073 m and 0° elevation transmit angle. The overlay shows the range-dependent FDA antenna pattern slope accentuates the isodops, reducing the number of isodop crossings.

changes the reduction in NHD can't be directly compared to the reductions experienced for the linear FDA.

The resulting GIP for the planar array is shown in Figure A.4. The curves are averaged over 100 realizations to smooth out statistical discrepancies. The FDA increased the dynamic range by 1% and the standard deviation by 10%.

There are two significant observations, firstly the reduced level of improvement in terms of dynamic range, and secondly the GIP shape, specifically the multiple notches. The notch at 10.5 km is expected since it corresponds to the target range and hence there is correlation between the artificially created covariance matrix estimates and the target range-cell space-time snapshots. The two other notches for each array type are caused by the antenna pattern nulls and the range ambiguous clutter contribution. The notches are offset between the two array structures because of frequency diversity along vertical array channels. The changes can be verified from the different elevation pattern nulls of Figure 5.8 and Figure 5.10.

As noted in Section A.1.2, analysis of NHD results must be done with care. In addition to the concerns raised in the previous section, the planar FDA with vertical channel frequency diversity increases NHD analysis complexity because the GIP shape is different. Therefore, the GIP dynamic range and standard deviation must be considered along with the GIP shape to predict impact on sample support homogeneity. Furthermore, it is important to remember the number of horizontal array channels N and hence total frequency diversity is reduced compared to the linear FDA NHD results, so the results between the two sections can not be directly compared.

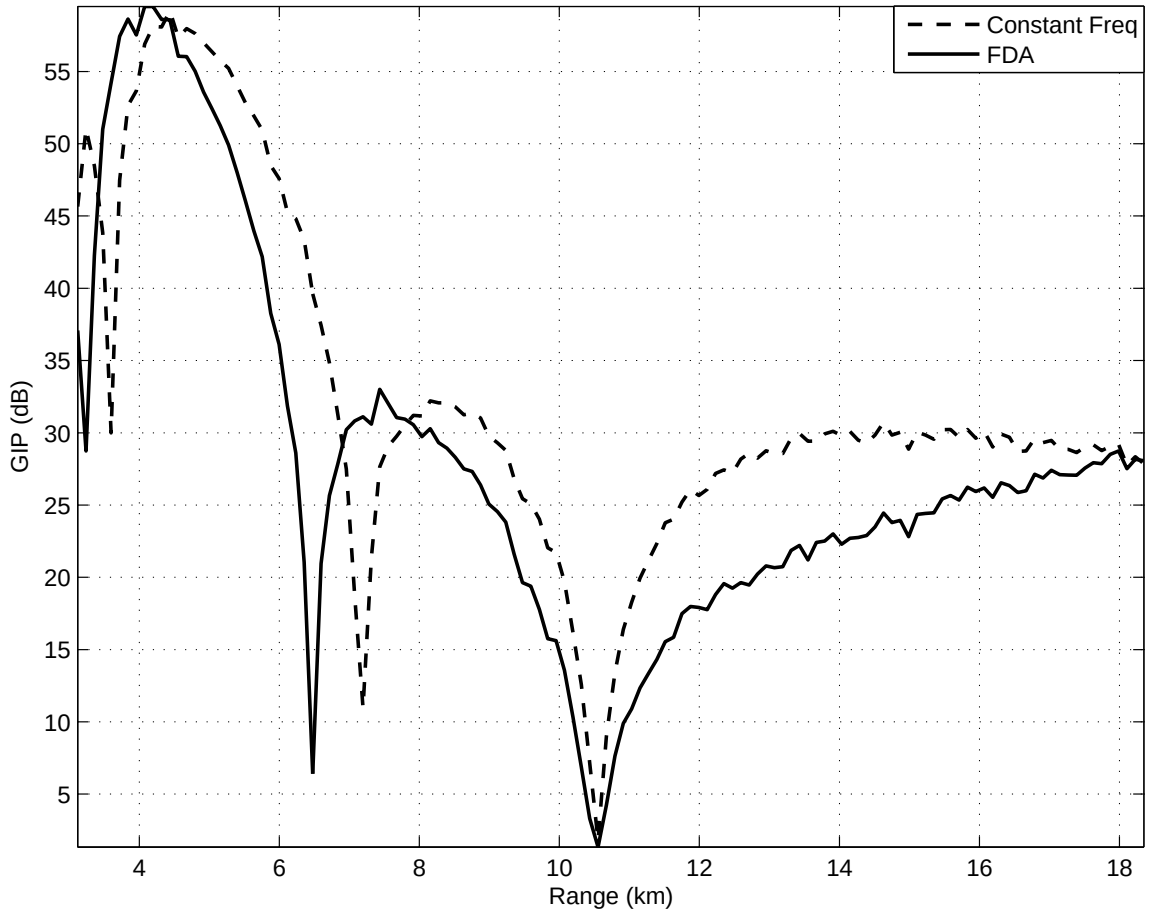

Figure A.4: Generalized Inner Product for forward-looking planar constant frequency array and FDA averaged over 100 runs. Results are based on a platform altitude of 3073 m, target range of 10.5 km and 0° elevation transmit angle. The major feature is the different notch locations between the two array types, corresponding to the different null locations due to frequency diversity across vertical channels impacting range ambiguous contributions. There is minimal difference in GIP dynamic range and it is difficult to ascertain the impact on sample support homogeneity, though the standard deviation has increased likely indicating degraded performance using the FDA.

Bibliography

1. Antonik, P. "Range-Dependent Beamforming Using Element Level Waveform Diversity". *Waveform Diversity Conference*. 2006.
2. Brennan, L. and I. Reed. "Theory of Adaptive Radar". *IEEE Transactions on Aerospace and Electronic Systems*, 9:327–252, 1973.
3. Brennan, L.E., J.D. Mallett, and I.S. Reed. "Adaptive arrays in airborne MTI". *IEEE Transactions on Antennas and Propogation*, AP-24(5):607–615, 1976.
4. Brennan, L.E., J.D. Mallett, and I.S. Reed. "Rapid Convergence Rate in Adaptive Arrays". *IEEE Transactions on Aerospace and Electronic Systems*, AES-10(6):853–863, Nov 1974.
5. Brennan, L.E. and F.M. Staudaher. *Subclutter Visiblity Demonstration*. Technical Report RL-TR-92-21, Adaptive Sensors Incorporated, March 1992.
6. Brooks, L.S. and I.S. Reed. "Equivalence of the likelihood ratio processor, the maximum signal-to-noise ratio filter, and the wiener filter". *IEEE Transactions on Aerospace and Electronic Systems*, 690–692, 1972.
7. Corbell, P.M. and T.B. Hale. "3-Dimensional STAP Performance Analysis using Cross-Spectral Metric". *2004 IEEE Radar Conference*. Philadelphia PA, USA, Apr 2004.
8. Graham, A. *Kronecker Products and Matrix Calculus with Applications*. Ellis Horwood Limited, West Sussex, England, 1981.
9. Hale, T.B. *Airborne Radar Interference Suppression using Adaptive Three-Dimensional Techniques*. Ph.D. thesis, Air Force Institute of Technology, Dayton OH, USA, May 2002.
10. Hale, T.B. "EENG668 Class Notes", 2005. AFIT.
11. Harris, F.J. "On the use of Windows for Harmnoic Analysis with the Discrete Fourier Transform". *Proc. IEEE*, 66(1):51–83, Jan, 1978.
12. Herbert, G.M. "Effects of platform rotation on STAP performance". *IEEE Proc. - Radar, Sonar Navig.*, 152(1):2–8, Feb, 2005.
13. Jaffer, A., M. Baker, W. Ballance, and J. Staub. *Adaptive space-time processing techniques for airborne radars*. Technical Report Contract F30602-89-D-0028, Hughes Aircraft Company, July 1991.
14. Klemm, R. "Adaptive Airborne MTI: Comparison of Sideways and Forward Looking Radar". *IEEE International Radar Conference*, 614–618. 1995.
15. Klemm, R. *Principles of Space-Time Adaptive Processing*. The Institution of Electrical Engineers, London, United Kingdom, 2002.

16. Klemm, R. "Adaptive Clutter Suppression for Airborne Phased Array Radar". *Proc. IEE*, 130(1):125–132, Feb, 1983.

17. Kreyenkamp, O. and R. Klemm. "Doppler compensation in forward-looking STAP radar". *IEEE Proc. - Radar, Sonar Navig.*, 148(5):253–258, Oct, 2001.

18. Michels, J.H. *Multichannel detection using the discrete-time modebased innovations approach*. Technical Report In-House Report RL-TR-91-269, Rome Laboratory, Air Force Systems Command, Griffis AFB NY 13441-5700, 1991.

19. Neudecker, H. "Some Theorems on Matrix Differentation with special reference to Kronecker Matrix Products". *Journal of the American Statistical Association*, 64:953–963, 1969.

20. Richardson, P.G. "Space-Time Adaptive Processing for Manoeuvring Airborne Radar". *IEE Electron. Commun. Eng. Journ.*, 11(1):57–63, Feb, 1999.

21. Richardson, P.G. and S.D. Hayward. "Adaptive Space Time Processing for Forward Looking Radar". *IEEE International Radar Conference*, 629–634. 1995.

22. Skolnik, M.I. *Introduction to Radar Systems, 3rd edition*. McGraw-Hill, New York, NY, 2001.

23. Skonik, M.I. *Radar Handbook*. McGraw-Hill, United States, 1990.

24. Sloper, D., D. Fenner, J. Arntz, and E. Fogle. *Multi-channel airborne radar measurement (MCARM), MCARM flight test*. Technical Report Contract F30602-92-C-0161, Westinghouse Electronic Systems, Box 1693, Baltimore MD 21203, April 1996.

25. Smith, B.E. and T.B. Hale. "An Analysis of the Effects of Windowing on Selected STAP Algorithms". *2004 IEEE Radar Conference*. Philadelphia PA, USA, Apr 2004.

26. Wang, H. and L. Cai. "On adaptive spatial-temporal processing for airborne surveillance radar systems". *IEEE Transactions on Aerospace and Electronic Systems*, 30:660–669, 1994.

27. Ward, J. *Space-time adaptive processing for airborne radar*. Technical Report Contract F19628-95-C-0002, Lincoln Laboratory, Massachusetts Institute of Technology, December 1994.

28. Wicks, M.C., W.L. Melvin, and P.Chen. "An Efficient Architecture for NonHomogeneity Detection in Space-Time Adaptive Processing Airborne Early Warning Radar". *Radar 97*.

REPORT DOCUMENTATION PAGE

Form Approved
OMB No. 0704–0188

1. REPORT DATE *(DD–MM–YYYY)*	2. REPORT TYPE	3. DATES COVERED *(From — To)*
23–03–2006	Master's Thesis	Sept 2004 — Mar 2006

4. TITLE AND SUBTITLE

Forward-looking Radar
Clutter Suppression using
Frequency Diverse Arrays

5a. CONTRACT NUMBER

5b. GRANT NUMBER

5c. PROGRAM ELEMENT NUMBER

6. AUTHOR(S)

Piotr Baizert, Flight Lieutenant, RAAF

5d. PROJECT NUMBER

5e. TASK NUMBER

5f. WORK UNIT NUMBER

7. PERFORMING ORGANIZATION NAME(S) AND ADDRESS(ES)

Air Force Institute of Technology
Graduate School of Engineering and Management (AFIT/EN)
2950 Hobson Way
WPAFB OH 45433-7765

8. PERFORMING ORGANIZATION REPORT NUMBER

AFIT/GE/ENG/06-05

9. SPONSORING / MONITORING AGENCY NAME(S) AND ADDRESS(ES)

AFMC
AFRL/SNRT
Attn: Dr. William J. Baldygo, Jr.
26 Electronic Parkway
Rome, NY 13441-4514 DSN: 587-3576

10. SPONSOR/MONITOR'S ACRONYM(S)

11. SPONSOR/MONITOR'S REPORT NUMBER(S)

12. DISTRIBUTION / AVAILABILITY STATEMENT

APPROVED FOR PUBLIC RELEASE; DISTRIBUTION UNLIMITED.

13. SUPPLEMENTARY NOTES

14. ABSTRACT

This thesis introduces a new array structure, the Frequency Diverse Array (FDA), where each channel transmits and receives at a different frequency. The resulting range-dependent FDA antenna pattern is proposed to improve forward-looking clutter suppression. The planar FDA radar data model is derived and analytically verified to be equivalent to the constant frequency data model when each element frequency is set to the same value. The linear FDA at high platform altitude provides significant benefits by reducing the range ambiguous clutter contribution, improving target detection by up to 10 dB. At low altitudes without range ambiguous clutter the linear FDA achieved a small but consistent performance improvement of 1 to 2 dB attributed to sample support data homogeneity. Planar FDA showed up to a 20 dB detection improvement for a high altitude platform with an airborne target. The simulation results show the FDA provides considerable benefit for low relative velocity targets, improving ground target detection for platforms such as Joint Surveillance and Target Attack Radar System (JSTARS) and Unmanned Aerial Vehicles (UAV).

15. SUBJECT TERMS

STAP, Forward-looking Radar, Clutter Suppression, Frequency Diverse Array, Radar

16. SECURITY CLASSIFICATION OF:			17. LIMITATION OF ABSTRACT	18. NUMBER OF PAGES	19a. NAME OF RESPONSIBLE PERSON
a. REPORT	b. ABSTRACT	c. THIS PAGE			Todd B. Hale, Major, USAF (ENG)
U	U	U	UU	240	19b. TELEPHONE NUMBER *(include area code)* (937) 255–3636, ext 4639